**AD-A268 126**

## UMENTATION PAGE

*Form Approved*
*OMB No 0704-0188*

ion is estimated to average 1 hour per response, including the time for reviewing instructions, searching existing data sources, pleting and reviewing the collection of information. Send comments regarding this burden estimate or any other aspect of this ducing this burden, to Washington Headquarters Services, Directorate for Information Operations and Reports, 1215 Jefferson and to the Office of Management and Budget, Paperwork Reduction Project (0704-0188), Washington, DC 20503.

2. REPORT DATE
1993

3. REPORT TYPE AND DATES COVERED
THESIS/~~DISSERTATION~~

4. TITLE AND SUBTITLE
Laser Photoionization Time-of-Flight Mass Spectrometry of Nitrated Polycyclic Aromatic Hydrocarbons and Nitrated Heterocyclic Compounds

5. FUNDING NUMBERS

6. AUTHOR(S)
Rae Anne Noyes

7. PERFORMING ORGANIZATION NAME(S) AND ADDRESS(ES)
AFIT Student Attending: Univ of California

8. PERFORMING ORGANIZATION REPORT NUMBER
AFIT/CI/CIA- 93-070

9. SPONSORING/MONITORING AGENCY NAME(S) AND ADDRESS(ES)
DEPARTMENT OF THE AIR FORCE
AFIT/CI
2950 P STREET
WRIGHT-PATTERSON AFB OH 45433-7765

10. SPONSORING/MONITORING AGENCY REPORT NUMBER

DTIC
S ELECTE D
AUG 1 3 1993
C

11. SUPPLEMENTARY NOTES

12a. DISTRIBUTION/AVAILABILITY STATEMENT
Approved for Public Release IAW 190-1
Distribution Unlimited
MICHAEL M. BRICKER, SMSgt, USAF
Chief Administration

12b. DISTRIBUTION CODE

13. ABSTRACT *(Maximum 200 words)*

**93-18712**

14. SUBJECT TERMS

15. NUMBER OF PAGES
269

16. PRICE CODE

| | | | |
|---|---|---|---|
| 17. SECURITY CLASSIFICATION OF REPORT | 18. SECURITY CLASSIFICATION OF THIS PAGE | 19. SECURITY CLASSIFICATION OF ABSTRACT | 20. LIMITATION OF ABSTRACT |

NSN 7540-01-280-5500

93 8 11 002

Standard Form 298 (Rev. 2-89)
Prescribed by ANSI Std Z39-18
298-102

# DISCLAIMER NOTICE

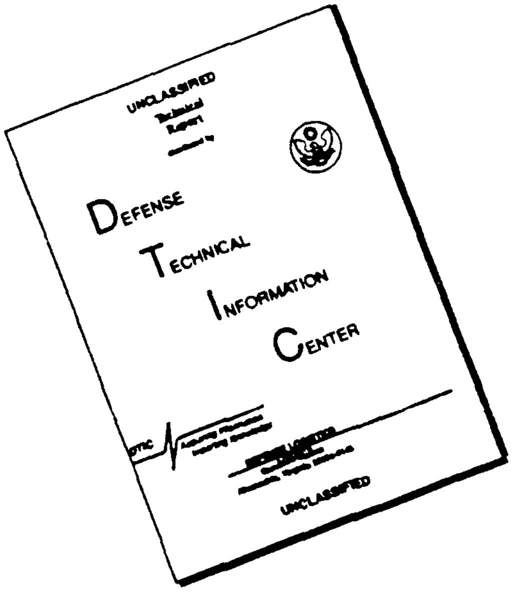

THIS DOCUMENT IS BEST QUALITY AVAILABLE. THE COPY FURNISHED TO DTIC CONTAINED A SIGNIFICANT NUMBER OF PAGES WHICH DO NOT REPRODUCE LEGIBLY.

93-070

# Laser Photoionization Time-of-Flight Mass Spectrometry of Nitrated Polycyclic Aromatic Hydrocarbons and Nitrated Heterocyclic Compounds

BY

Rae Anne Noyes
B. S. (United States Air Force Academy) 1985

THESIS

Submitted in partial satisfaction of the requirements for the degree of

MASTER OF SCIENCE

in

Chemistry

in the

OFFICE OF GRADUATE STUDIES

of the

UNIVERSITY OF CALIFORNIA

DAVIS

DTIC QUALITY INSPECTED 3

Approved:

Peter B. Kelly
Nancy S. True
Donald P. Land

Committee in Charge

1993

| | |
|---|---|
| Accesion For | |
| NTIS CRA&I | ☑ |
| DTIC TAB | ☐ |
| Unannounced | ☐ |
| Justification | |
| By | |
| Distribution / | |
| Availability Codes | |
| Dist | Avail and / or Special |
| A-1 | |

DTIC QUALITY INSPECTED 3

## TABLE OF CONTENTS

List of Tables . . . . . . . . . . . . . . . . . . . . . . . . . . . . . . . . . . . . . . . . vi

List of Figures . . . . . . . . . . . . . . . . . . . . . . . . . . . . . . . . . . . . . . . vii

Acknowledgements . . . . . . . . . . . . . . . . . . . . . . . . . . . . . . . . . . . . ix

CHAPTER 1: Introductory Discussion

1.1 Importance . . . . . . . . . . . . . . . . . . . . . . . . . . . . . . . . . . . . . . 1

1.2 Previous Investigations . . . . . . . . . . . . . . . . . . . . . . . . . . . . . . 2

1.2.1 Initial Determination of Environmental Nitro-PAH . . . . . . . . . 2

1.2.2 Photoionization of Nitro-Containing Compounds . . . . . . . . . . . 5

1.2.3 Laser Detection of PAH in Particulate . . . . . . . . . . . . . . . . 10

1.3 Motivation and Goals . . . . . . . . . . . . . . . . . . . . . . . . . . . . . . . 11

1.4 References . . . . . . . . . . . . . . . . . . . . . . . . . . . . . . . . . . . . . . 13

CHAPTER 2: Laser Desorption-Laser Photoionization Time-of-Flight Mass Spectrometry

2.1 Introduction . . . . . . . . . . . . . . . . . . . . . . . . . . . . . . . . . . . . . 17

2.2 Basic Principles of TOFMS . . . . . . . . . . . . . . . . . . . . . . . . . . . 17

2.3 Factors Affecting Flight Time . . . . . . . . . . . . . . . . . . . . . . . . . 20

2.4 Sources of Broadening . . . . . . . . . . . . . . . . . . . . . . . . . . . . . . 23

2.5 Laser Desorption . . . . . . . . . . . . . . . . . . . . . . . . . . . . . . . . . . 27

2.6 References . . . . . . . . . . . . . . . . . . . . . . . . . . . . . . . . . . . . . . 30

CHAPTER 3: Theory of Multiphoton Ionization

3.1 Introduction . . . . . . . . . . . . . . . . . . . . . . . . . . . . . . . . . . . . . 32

3.2 Application to Mass Spectrometry . . . . . . . . . . . . . . . . . . . . . . 32

3.3 Quantum Theory of MPI . . . . . . . . . . . . . . . . . . . . . . . . . . . . . 33

3.3.1 Time-Dependent Perturbation Theory . . . . . . . . . . . . . . . . . . 33
3.3.2 Time-Dependent Coefficients . . . . . . . . . . . . . . . . . . . . . . 35
3.3.3 Probability of a Two-Photon Process . . . . . . . . . . . . . . . . . . 37
3.4 MPI Fragmentation Mechanism . . . . . . . . . . . . . . . . . . . . . . . 41
3.5 Attributes of R2PI . . . . . . . . . . . . . . . . . . . . . . . . . . . . 44
3.6 References . . . . . . . . . . . . . . . . . . . . . . . . . . . . . . . . 48

CHAPTER 4: Experimental Apparatus

4.1 Introduction . . . . . . . . . . . . . . . . . . . . . . . . . . . . . . . 49
4.2 LDLPMS Instrumentation . . . . . . . . . . . . . . . . . . . . . . . . . 49
4.3 Single-Step LDLP Experiments . . . . . . . . . . . . . . . . . . . . . . 58
4.4 Two-Step LDLP Experiments . . . . . . . . . . . . . . . . . . . . . . . . 63
4.5 Mass Calibration of LDLPMS Spectra . . . . . . . . . . . . . . . . . . . 66
4.6 GC/MS Experiments . . . . . . . . . . . . . . . . . . . . . . . . . . . . 67
4.7 FAB and EI MS/MS Experiments . . . . . . . . . . . . . . . . . . . . . . 68
4.8 References . . . . . . . . . . . . . . . . . . . . . . . . . . . . . . . . 70

CHAPTER 5: Laser Photoionization Time-of-Flight Mass Spectrometry of Nitrated Polycyclic Aromatic Hydrocarbons

5.1 Abstract . . . . . . . . . . . . . . . . . . . . . . . . . . . . . . . . . 71
5.2 Introduction . . . . . . . . . . . . . . . . . . . . . . . . . . . . . . . 71
5.3 Experimental . . . . . . . . . . . . . . . . . . . . . . . . . . . . . . . 74
5.4 Results and Discussion . . . . . . . . . . . . . . . . . . . . . . . . . . 78
5.4.1 Laser Photoionization of 9-nitroanthracene & 1-nitropyrene . . 78
5.4.2 Laser Photoionization of 2-nitrofluorene & 2-nitro-9-fluorenone 90
5.5 Conclusions . . . . . . . . . . . . . . . . . . . . . . . . . . . . . . . . 98

5.6 References . . . . . . . . . . . . . . . . . . . . . . . . . . . . . . . . . . . 100

CHAPTER 6: Laser Photoionization Time-of-Flight Mass Spectrometry of Nitrobenzocoumarins and Coumarin Derivative Compounds

6.1 Abstract . . . . . . . . . . . . . . . . . . . . . . . . . . . . . . . . . . . . . 104

6.2 Introduction . . . . . . . . . . . . . . . . . . . . . . . . . . . . . . . . . . 105

6.3 Experimental . . . . . . . . . . . . . . . . . . . . . . . . . . . . . . . . . 107

6.4 Results and Discussion . . . . . . . . . . . . . . . . . . . . . . . . . . 112

6.4.1 Laser Photoionization & EI MS/MS of Nitrobenzocoumarins 112

6.4.2 Laser Photoionization of Coumarin Derivative Compounds . 118

6.5 Conclusions . . . . . . . . . . . . . . . . . . . . . . . . . . . . . . . . . . 124

6.6 References . . . . . . . . . . . . . . . . . . . . . . . . . . . . . . . . . . . 126

CHAPTER 7: Laser Photoionization Time-of-Flight Mass Spectrometry of Mixtures Containing Nitrated Polycyclic Aromatic Hydrocarbons

7.1 Abstract . . . . . . . . . . . . . . . . . . . . . . . . . . . . . . . . . . . . . 130

7.2 Introduction . . . . . . . . . . . . . . . . . . . . . . . . . . . . . . . . . . 131

7.3 Experimental . . . . . . . . . . . . . . . . . . . . . . . . . . . . . . . . . 133

7.4 Results and Discussion . . . . . . . . . . . . . . . . . . . . . . . . . . 135

7.4.1 Two-Component Mixtures of Nitro-PAH . . . . . . . . . . . . . 135

7.4.2 Six-Component PAH/nitro-PAH Mixture . . . . . . . . . . . . . 150

7.5 Conclusions . . . . . . . . . . . . . . . . . . . . . . . . . . . . . . . . . . 156

7.6 References . . . . . . . . . . . . . . . . . . . . . . . . . . . . . . . . . . . 159

CHAPTER 8: Laser Desorption-Laser Photoionization Time-of-Flight Mass Spectrometry Applied to Nitro-PAH and Diesel Particulate Matter

8.1 Abstract . . . . . . . . . . . . . . . . . . . . . . . . . . . . . . . . . . . . . 162

8.2 Introduction . . . . . . . . . . . . . . . . . . . . . . . . . . . . . . . . . . 163

8.3 Experimental . . . . . . . . . . . . . . . . . . . . . . . . . . . . . . . . . . . 165

8.4 Results and Discussion . . . . . . . . . . . . . . . . . . . . . . . . . . . . 169

8.4.1 LDLPMS of 1-nitropyrene and 2-nitrofluorene . . . . . . . . . . 169

8.4.2 LDLPMS of a Six-Component PAH/nitro-PAH Mixture . . . 173

8.4.3 LDLPMS Applied to Diesel Particulate Matter . . . . . . . . . . 176

8.5 Conclusions . . . . . . . . . . . . . . . . . . . . . . . . . . . . . . . . . . . . 182

8.6 References . . . . . . . . . . . . . . . . . . . . . . . . . . . . . . . . . . . . 184

CHAPTER 9: Conclusions

9.1 Summary . . . . . . . . . . . . . . . . . . . . . . . . . . . . . . . . . . . . . 187

9.2 Future Directions . . . . . . . . . . . . . . . . . . . . . . . . . . . . . . . . 192

9.2.1 Supplemental LDLPMS Experiments . . . . . . . . . . . . . . . . 192

9.2.2 Improvements to Instrumentation . . . . . . . . . . . . . . . . . . . 194

9.3 References . . . . . . . . . . . . . . . . . . . . . . . . . . . . . . . . . . . . 196

APPENDIX A: Calculation of Laser Power Density . . . . . . . . . . . . . . . . . . . . 197

APPENDIX B: Calibration of LDLPMS Spectra . . . . . . . . . . . . . . . . . . . . . . 200

APPENDIX C: GC/MS Spectra of Nitro-PAH & Nitrobenzocoumarin Standards 209

APPENDIX D: FAB Spectra of Nitro-PAH & Nitrobenzocoumarin Standards . . 225

APPENDIX E: EI MS/MS Spectra of Selected Nitro-Standards . . . . . . . . . . . . . 244

## LIST OF TABLES

**Table Number** **Page**

**Table 4.1** Properties of Nitro-PAH and Nitrated Heterocyclic Compounds . . . . . . 62

**Table 5.1** Properties of Nitro-PAH . . . . . . . . . . . . . . . . . . . . . . . . . . . . . . . . . . . 76

**Table 6.1** Properties of Nitrobenzocoumarins and Coumarin Derivatives . . . . . . 109

**Table 6.2** Peak Assignments for 7-nitro-3,4-benzocoumarin . . . . . . . . . . . . . . . 114

**Table 6.3** Peak Assignments for 6-nitro-3,4-benzocoumarin . . . . . . . . . . . . . . . 116

**Table 6.4** Peak Assignments for 2-nitro-6(5H)-phenanthridinone . . . . . . . . . . . . 123

**Table 7.1** Peak Assignments: 1-nitropyrene & 9-nitroanthracene . . . . . . . . . . . . 138

**Table 7.2** Peak Assignments: 1-nitropyrene & 2-nitrofluorene . . . . . . . . . . . . . . 141

**Table 7.3** Peak Assignments: 1-nitropyrene & 2-nitro-9-fluorenone . . . . . . . . . . 143

**Table 7.4** Peak Assignments: 9-nitroanthracene & 2-nitrofluorene . . . . . . . . . . . 146

**Table 7.5** Peak Assignments: 2-nitrofluorene & 2-nitro-9-fluorenone . . . . . . . . . 148

**Table 7.6** Peak Assignments: Soft Ionization of PAH/nitro-PAH Mixture . . . . . 152

## LIST OF FIGURES

**Figure Title** **Page**

**Figure 2.1** Basic Principles of Time-of Flight Mass Spectrometry . . . . . . . . . . . . 19

**Figure 2.2** Wiley-McLaren Two-Step Acceleration TOFMS . . . . . . . . . . . . . . . . 22

**Figure 3.1** R2PI and Competing Processes . . . . . . . . . . . . . . . . . . . . . . . . . . 43

**Figure 4.1** Major Components of the LDLPMS Apparatus . . . . . . . . . . . . . . . . . 51

**Figure 4.2** Detailed Side View of the TOF Mass Spectrometer . . . . . . . . . . . . . . 53

**Figure 4.3** Sequence of Events Trigger Scheme . . . . . . . . . . . . . . . . . . . . . . . 57

**Figure 4.4** Source Region for Single-Step LDLP Experiments . . . . . . . . . . . . . . 60

**Figure 4.5** Source Region for Two-Step LDLP Experiments . . . . . . . . . . . . . . . . 65

**Figure 5.1** Laser Photoionization Mass Spectra of 9-nitroanthracene . . . . . . . . . . 80

**Figure 5.2** Laser Photoionization Mass Spectra of 1-nitropyrene . . . . . . . . . . . . . 82

**Figure 5.3** Competing Photofragmentation Pathways of nitro-PAH . . . . . . . . . . . 87

**Figure 5.4** Hard Ionization of 9-nitroanthracene at 213 nm and 266 nm . . . . . . . 89

**Figure 5.5** Laser Photoionization Mass Spectra of 2-nitrofluorene . . . . . . . . . . . . 92

**Figure 5.6** Laser Photoionization Mass Spectra of 2-nitro-9-fluorenone . . . . . . . . 94

**Figure 5.7** Pathways to Major Mid-Mass Fragments in 2-nitro-9-fluorenone . . . . . 97

**Figure 6.1** Laser Photoionization Mass Spectrum: 7-nitro-3,4-benzocoumarin . . . 114

**Figure 6.2** Laser Photoionization Mass Spectrum: 6-nitro-3,4-benzocoumarin . . . 116

**Figure 6.3** Laser Photoionization Mass Spectra of Coumarin Derivatives . . . . . . 121

**Figure 6.4** Laser Photoionization Spectrum: 2-nitro-6(5H)-phenanthridinone . . . 123

**Figure 7.1** LP Mass Spectrum of 1-nitropyrene & 9-nitroanthracene . . . . . . . . . 138

**Figure 7.2** LP Mass Spectrum of 1-nitropyrene & 2-nitrofluorene . . . . . . . . . . . 141

**Figure 7.3** LP Mass Spectrum of 1-nitropyrene & 2-nitro-9-fluorenone . . . . . . . 143

**Figure 7.4** LP Mass Spectrum of 9-nitroanthracene & 2-nitrofluorene . . . . . . . . 146

**Figure 7.5** LP Mass Spectrum of 2-nitrofluorene & 2-nitro-9-fluorenone . . . . . . 148

**Figure 7.6** Soft Ionization Spectrum of PAH/nitro-PAH Mixture . . . . . . . . . . . 152

**Figure 7.7** Moderate and Hard Ionization Spectra: PAH/nitro-PAH Mixture . . . . 154

**Figure 8.1** Two-Step LDLPMS of 1-nitropyrene and 2-nitrofluorene . . . . . . . . . 171

**Figure 8.2** Two-Step LDLPMS: Six-Component PAH/nitro-PAH Mixture . . . . . 175

**Figure 8.3** Two-Step LDLPMS of Diesel Particulate & Diesel Extract . . . . . . . . 178

**Figure 8.4** Two-Step Hard Ionization and Single-Step LDLP: Diesel Extract . . . 180

**Figure B.1** Standard Pyrene Spectra for Example Calibration . . . . . . . . . . . . . . 204

**Figure B.2** Flight Time Squared and Intensity Data for Example Calibration . . . 206

**Figure B.3** Output from Calibration Program, MASS4.FOR . . . . . . . . . . . . . . . 208

**Acknowledgements**

First, I must thank my research advisor, Dr. Peter Kelly, for taking on the challenge of an Air Force pilot turned temporary chemist, with a vague memory of quantum mechanics and an ironclad 18-month deadline. The past year-and-a-half has been a tremendous learning experience and I thank you for the opportunity to work with you and become a junior "laser jockey".

Next, a big thank you to Dr. Dan Jones for setting aside so much of his precious time to run experiments, talk over data, look over papers and figures, and above all, for giving me a greater appreciation and understanding of the power of mass spectrometry.

To my "cohorts-in-crime", Cathy, James and Liu, thanks for accepting me into the group and helping me keep my sanity through what has, at times, been a very stressful journey. Cathy, I would not be where I am today had you not taken the time, and had the patience, to teach me about the mass spec, lasers, and all the associated computer programs that worked the final magic. James, your laughter and sense of humor kept the whole lab on an even keel, and you and Liu always found time to answer my questions, or at least point me in the right direction. Thank you all for your generosity and best wishes to all of you in your future pursuits.

A special thank you to Eileen, without whose help I wouldn't have survived Tinti's quantum mechanics nightmare. Also, a special thank you to Dianne for suffering through all the quantum mechanics alongside me, and for being a good friend with a comfortable couch to sleep on during those homework marathons!

To my parents, whose love and support have never failed me, even when the physical distance has been great between us. I owe the person I am today to the patience

and strength you taught me. You always let me believe that there was nothing I could not achieve with enough determination and hard work. First you helped me find my "corner of the sky", then you encouraged my return to academia in pursuit of a higher degree. Thank you for always being in my corner and for teaching me to make my own decisions. My life is a happy one because of your generosity and caring.

Many thanks to my sister, Carole, my brothers, Hal and Rich, and their families. All of you have lent me support in one way or another throughout this endeavor be it by phone calls, special cards, T-shirts, notes or pictures of the kids. A reminder that your family is thinking about you can put a rainbow into an otherwise stormy day. To my other "sister", Tina, who has been my best girlfriend since kindergarten, thanks for always listening to me, especially throughout this uncertain year. The time we've both been waiting for has arrived and I'm so glad you will be here to share it with me!

Finally, last but never least, to my soon-to-be-husband Gregg, I owe you a greater debt than I could ever possibly repay in one lifetime, but I'll give it my best shot! Thank you for taking such wonderful care of me and our home, especially the past several weeks when the back of my head, framed by a computer monitor, was your major view of me. Thanks for always being there to share a smile, a hug, or a shoulder just when I needed them most, and for standing by me through all the ups and downs of this endeavor. Gregg, your patience, caring, sense of humor, and above all, your steadfast belief in me have allowed me to achieve this goal. You've always helped me keep things in perspective, and have been there for me no matter what. I love you! This one is for US!

# CHAPTER 1

## Introductory Discussion

### 1.1 IMPORTANCE

Detection and identification of nitrated polycyclic aromatic hydrocarbons (nitro-PAH) in environmental samples is of widespread interest due to the highly mutagenic properties of this chemical class. Nitro-PAH are derivatives of PAH which are abundant in fossil fuels (e.g. coal, petroleum), and are the incomplete combustion products of organic materials. Direct emission into the atmosphere from combustion sources distributes PAH between the gas and particle phase, depending on their vapor pressure.[1] Nitro-derivatives of PAH are formed by two major mechanisms. Nitro-PAH present in direct emissions are primarily the electrophilic nitration products resulting from adsorbed-phase reactions of PAH with $NO_x$ and $HNO_3$.[2] Nitro-PAH found in the atmosphere are often the result of an atmospheric transformation of the parent PAH by the gas-phase reaction with OH radical in the presence of $NO_x$ pollutants.[2] Once formed, nitro-PAH can readily condense on respirable particulate matter.

Nitro-PAH have been determined in a variety of environmental samples including diesel exhaust,[3-9] urban and indoor air particulate,[10-13] aluminum smelter effluent,[14] coal fly ash,[15] wood and cigarette smoke condensates,[16,17] and carbon black based xerographic toners.[18] Typically, the concentration of nitro-PAH in environmental samples is one to two orders of magnitude less than that of the unsubstituted PAH present. Low concentrations coupled with the ubiquitous presence and potent direct-acting mutagenicity of nitro-PAH underscore the importance of developing highly sensitive and selective methods for their determination. This thesis presents the results of laser desorption-laser photoionization time-of-flight mass spectrometry (LDLPMS) experiments performed on four nitro-PAH and two nitrated heterocyclic compounds. Photofragmentation pathways are proposed for each of the nitro-compounds studied, and mechanisms to formation of the characteristic $NO^+$ ion peak are presented. In addition, results of LDLPMS experiments on the National Institute of Standards (NIST) standard reference material (SRM) 1650 diesel particulate material and potential for future application of the LDLPMS method to determination of nitro-PAH in environmental samples are discussed.

## 1.2 PREVIOUS INVESTIGATIONS

### 1.2.1 Initial Determinations of Environmental Nitro-PAH

The first tentative identification of a nitro-PAH in an environmental sample was reported by Cronn[19] in 1975. Direct-probe high resolution mass spectrometry (HRMS) was used to tentatively identify a nitronaphthalene in ambient air particulate. In 1978, Jäger[20] employed thin layer chromatography (TLC) and fluorescence quenching to tentatively identify 3-nitrofluoranthene and 6-nitrobenzo[a]pyrene in extracts of airborne particulate from Prague. The importance of Jäger's report was underscored by the 1978 work of Pitts et al.[21] which demonstrated that exposure of PAH adsorbed on particles to nitrogen oxides produced nitro-substituted reaction products. Of the reaction products, 1-nitropyrene and some dinitropyrenes were shown to be potent direct-acting mutagens in tests with Ames *Salmonella typhimurium* assays.

The first positive identification of a nitro-PAH in an environmental sample was reported by Schuetzle et al.[3,4] in 1980. Diesel particulate extract was subjected to normal-phase high performance liquid chromatography (HPLC) and separated into fractions for subsequent chemical analysis and bioassay tests. Positive identification of 1-nitropyrene in the moderately polar (transition) fraction was made using a combination of direct-probe HRMS and high resolution gas chromatography mass spectrometry (HRGC/MS). Thirty percent of the direct-acting mutagenicity of the total extract was attributed to the presence of 1-nitropyrene. Subsequent research by Schuetzle et al.[5,6] and Paputa-Peck et al.[7] indicated the presence of 20 nitro-PAH isomer groups containing approximately 200 nitro-PAH species in the transition fractions of diesel particulate extracts. Twenty-five of the nitro-PAH isomers were identified using low and high resolution GC/MS, and triple-stage quadrupole tandem mass spectrometry (TSQ-MS/MS).

Ambient air particulate was examined by Ramdahl et al.[10] using GC/electron ionization mass spectrometry (EI/MS) and negative ion chemical ion mass spectrometry (NICI/MS) to detect nitroaromatics in the organic extract of urban air particulate from St. Louis, MO. Compounds identified in the transition fractions included nitronaphthalene, 9-nitroanthracene, 1-nitropyrene and 3-nitrofluoranthene (later corrected to the 2-isomer).[22] The study contained the first reported mass spectrometric evidence of nitro-PAH in urban air particulate. However, the extremely complex composition of the organic particulate extracts and limitations of the fractionation and analysis techniques precluded more complete characterization of the samples.

The powerful technique of bioassay-directed fractionation was applied by Nishioka et al.[11] to the problem of detecting nitro-PAH in ambient air particulate extracts. The process involves sequential fractionation of increasing chromatographic resolution with the ultimate goal of reducing the complexity of the original fraction so that most chromatographic peaks contain a single component. Fractions are tested at each step to direct continued fractionation of the most mutagenic subfractions. Using bioassay-directed fractionation coupled with EI/MS and NICI/MS , Nishioka et al. reported the first identification of mutagenic hydroxylated nitro-PAH in a neutral polar fraction of ambient air particulate extract in 1986.[11] Subsequently in 1988, Nishioka et al. reported the first mass spectrometric evidence for hydroxylated nitro-PAH and hydroxylated nitro-polycyclic aromatic ketones (nitro-PAK) in polar fractions of ambient air particulate extract.[23]

Arey et al.[24] applied the method of bioassay-directed fractionation to identify the major mutagenic fractions of ambient air particulate extracts, which contained compounds more polar than the nitro-PAH. In fact, while nitro-PAH (particularly 1-nitropyrene) contribute significantly to the direct-acting mutagenicity of diesel exhaust extracts, the nitro-PAH compounds have been reported to contribute less than 10% of the overall direct-acting mutagenicity of ambient air particulate extracts. In 1992, Arey et al.[12] reported the identification of nitrophenanthrene lactones (nitro-6H-dibenzo[b,d]pyran-6-ones) in the most mutagenic fraction from the environmental chamber reaction of phenanthrene with OH radical in the presence of $NO_x$. In a subsequent study, Helmig et al.[25] identified 2-nitro-6H-dibenzo[b,d]pyran-6-one (6-nitro-3,4-benzocoumarin) as the most mutagenic isomer and quantified its presence in southern California ambient air samples, NIST SRM 1649 urban dust, and NIST SRM 1650 diesel particulate matter. Experimental results attributed up to 45% of the direct-acting mutagenicity of ambient air particulate extract to the nitrated heterocyclic compound.[25]

### 1.2.2 Photoionization of Nitro-Containing Compounds

All of the reported identifications of nitro-PAH discussed have a common bond. Each determination generally involved extraction of the sample, followed by a chromatographic separation (TLC,HPLC,GC), fractionation, and finally, mass spectrometric detection to confirm identification. Attempts have also been made to derivatise the non-fluorescent nitro-PAH to highly fluorescent amino-PAH for fluorescence and electro-chemical detection,[26] or to pentafluoropropyl amides for subsequent nitrogen-selective thermionic and flame ionization detection[27] with some success. However, all of the procedures discussed thus far are time-consuming, labor-intensive and expensive. Laser photoionization mass spectrometry offers potential as an inexpensive quick screening process for the presence of nitro-containing compounds, as well as the possibility of sensitive, isomer selective detection of nitro-PAH compounds in a mixture.

Laser photoionization of nitro-containing compounds is a challenge because they are labile and tend to predissociate upon exposure to ultraviolet (UV) irradiation. The two-photon photodissociation dynamics of $NO_2$ were examined in-depth by Morrison et al.[28,29] over the wavelength range 425 nm to 520 nm, by recording the multiphoton ionization (MPI) spectrum of the photolysis product NO. They concluded that the course of ionization for NO was dominated by predissociation of $NO_2$ at the level of the second photon, i.e. within the $B^2B_2$ state of $NO_2$. Data suggested that the high energy pathway

$$NO_2 \rightarrow NO\,(X^2\pi) + O\,(^1D)$$

became important soon after it became energetically accessible (< 475 nm). Another interesting observation was an anomaly in the MPI spectrum at 427 nm which suggested that the two-photon excitation accessed a high-lying linear state of $NO_2$ ... probably $(...1\pi_g^{\ 4}\ 5\sigma_g)^2\Sigma_g^{\ +}$ predicted by theory.

A photodissociation dynamics study of nitromethane was conducted by Moss et al.[30] using ArF excimer laser excitation. The study concluded that the primary 193 nm photofragmentation products of nitromethane are $CH_3$ and $NO_2$. Secondary products, NO and O are produced through subsequent unimolecular decomposition of the $NO_2$ fragment. Two photodissociation channels were proposed:

Major channel

$$\begin{aligned} CH_3NO_2 + h\nu &\rightarrow CH_3 + NO_2\,(1^2B_2) \\ &\rightarrow CH_3 + NO\,(X^2\pi) + O\,(^3P) \end{aligned}$$

Minor channel

$$\begin{aligned} CH_3NO_2 + h\nu &\rightarrow CH_3 + NO_2^{**}\,(2^2B_2) \\ + h\nu &\rightarrow CH_3 + NO\,(A^2\Sigma^+) + O\,(^3P) \end{aligned}$$

Two recent studies of dimethylnitramine (DMNA) aimed at understanding ignition and combustion pathways of propellants and explosives offer conflicting opinions. Sausa et al.[31] concluded from their photodissociation study of DMNA at 248 nm that the unimolecular formation of NO was not important to decomposition. In contrast, Stewart et al.[32] suggest from results of a low pressure homogenous pyrolysis study of DMNA that a nitro-nitrite rearrangement followed by scission of the NO-NO bond may be an important decomposition pathway. The pathway is illustrated by the reaction:

$$(CH_3)_2NNO_2 \rightarrow (CH_3)_2NO\text{-}NO \rightarrow (CH_3)_2NO + NO$$

The nitro-nitrite rearrangement mechanism involves an isomerization from $-NO_2$ to $-ONO$ at the carbon to which the nitro group was originally attached. Bowie et al.[33]

proposed the nitrite intermediate to explain the appearance of the $[M\text{-}NO]^-$ anion peak in the negative ion mass spectra of nitroaniline derivatives. Budzikiewicz[34] refers to the isomerization of nitrobenzene to the nitrite form prior to fragmentation to account for appearance of the phenoxy cation $(C_6H_5O)^+$ in the EI mass spectrum of nitrobenzene.

Perhaps the most intriguing evidence for the nitro-nitrite rearrangement was presented by Ioki[35] in reporting the e.s.r. detection of several aryloxyl radicals obtained after UV illumination of nitro-containing compounds. In particular, the e.s.r. spectrum of 6-nitrobenzo[a]pyrene upon illumination with UV light in degassed benzene solution at room temperature, showed hyperfine structure identical to the e.s.r. spectrum of the benzo[a]pyren-6-oxyl radical produced by abstracting a proton from benzo[a]pyren-6-ol in benzene solution. Ioki concludes that formation of the oxyl radical in 6-nitrobenzo[a]pyrene is a consequence of the photorearrangement of its nitro group. He adds that the choice of highly conjugated aromatic compounds, which stabilize the free radical by delocalizing the unpaired electron, may have contributed to successful observation of the aryloxyl radical hyperfine structure.

A number of relevant studies have been conducted on the laser photoionization of nitrobenzene. Apel and Nogar[36] obtained MPI mass spectra of nitrobenzene using 248 nm (KrF) and 193 nm (ArF) laser excitation. The highest weight ion occurred at a mass-to-charge ratio (m/z) of 93 amu, corresponding to loss of NO from the parent ion $[M\text{-}NO]^+$. The base peak at m/z 77 corresponded to $[M\text{-}NO_2]^+$ ion. No molecular ion was observed, but the strong $NO^+$ signal was attributed to photodissociation of the parent to produce $NO_2$ and subsequent dissociation/MPI of $NO_2$ to produce $NO^+$.

Lubman et al.[37] performed resonant two-photon ionization (R2PI) of several substituted nitrobenzenes at atmospheric pressure with helium bath gas, and under vacuum conditions in a comparative investigation. Generally, molecular ions were not observed in spectra obtained under vacuum conditions. Extensive fragmentation occurred in all the nitro-compounds under vacuum conditions with 266 nm and 213 nm excitation. However, R2PI at 1 atm in He often produced "soft" ionization (little fragmentation), even at power densities comparable to the vacuum condition experiments, and molecular ions were frequently observed. Lubman credits the successful soft ionization of the very fragile nitro-molecules to the moderating effect of He background gas, which has a low collisional effectiveness.

Marshall et al.[38,39] carried out in-depth research of laser dissociation, ionization and fragmentation processes in single-ring nitroaromatic molecules over the wavelength range 232.5 nm to 260 nm. Numerous spectra were recorded at various wavelengths and power densities to deduce the wavelength and power dependence of the carbon fragment patterns and the often dominant $NO^+$ ion signal. Five possible routes to the formation of the $NO^+$ ion in nitrobenzene and o-nitrotoluene were proposed and compared with experimental data. Based on experimental observations, the major $NO^+$ ion formation mechanism was identified as predissociation of the parent to lose $NO_2$, then predissociation of $NO_2$ and subsequent two-photon ionization of the NO fragment (IP 9.25 eV):[40]

$$M + h\nu \rightarrow (M\text{-}NO_2) + NO_2$$

$$NO_2 + h\nu \rightarrow NO + O$$

$$NO + 2h\nu \rightarrow NO^+ + e^-$$

Marshall et al. discounted the direct formation of $NO^+$ by predissociation of the parent to lose NO as a major dissociation route for nitrobenzenes. However, the direct production of NO from the parent is of interest to the current research on nitro-PAH. The production of $NO^+$ directly from the parent molecule is a two-step process:

$$M + h\nu \rightarrow (M\text{-}NO) + NO$$

$$NO + 2h\nu \rightarrow NO^+ + e^-$$

Marshall's principal objection to the direct production route was the absence of an $[M\text{-}NO]^+$ ion peak in all of the spectra, while the $[M\text{-}NO_2]^+$ ion peak was prominent in the spectra of nitrobenzene.

Just when the question of $NO^+$ ion production in nitro-compounds appeared settled, Huey et al.[41] conducted a new study on the photodissociation of nitrobenzene. Photolysis of nitrobenzene was performed at 240, 260, 280 and 313 nm, and the photofragments were subsequently entrained in a molecular beam and ionized by VUV 125 nm photons. Three primary photodissociation pathways were observed for nitrobenzene:

1. $C_6H_5NO_2 \rightarrow C_6H_5 + NO_2$
2. $C_6H_5NO_2 \rightarrow C_6H_5NO + O$
3. $C_6H_5NO_2 \rightarrow C_6H_5O + NO$

   $(\text{or} \rightarrow C_5H_5 + CO + NO)$

with both stepwise and concerted mechanisms for producing $C_5H_5$ in step (3) being energetically feasible at the wavelengths employed. Results allowed the possibility of a nitro-nitrite rearrangement as consistent with observed competition between production of NO and $NO_2$ (for $\lambda \geq$ 280 nm), as both products could be formed through a common nitrite transition state.

### 1.2.3 Laser Detection of PAH in Particulate

The application of laser photoionization mass spectrometry to the *in situ* characterization of PAH and PAH derivatives on particulate has been very limited. Two recent studies have involved the use of laser microprobe analysis to examine various particulate samples. The investigation by Sine et al.[42] in 1984 employed a LAMMA-500 laser microprobe mass analyzer to characterize soot from an experimental oil shale retort. The Sine group objective was to evaluate the capability of LAMMA in analyzing carbonaceous environmental samples. Both positive and negative ion mass spectra of the soot sample were collected. The negative ion mass spectrum was dominated by carbon cluster ions, $C_nH_x$ with up to 25 carbons and zero to two hydrogens. The positive ion mass spectrum contained a combination of inorganic and organic information. Organic compounds identified in the soot included twenty-five unsubstituted PAH from m/z 252 to m/z 620. Twenty of the PAH identities were confirmed by HPLC, GC/MS and/or direct insertion EI/MS and CI/MS analysis. Though the technique correctly identified several PAH by *in situ* analysis, the results were not quantifiable other than for semi-quantitative comparison of relative intensities between various samples.

Another study by Delmas and Muller[43] examined the use of Fourier transform mass spectrometry (FTMS) laser microprobe for the *in situ* characterization of nitro-PAH adsorbed to two carriers, activated charcoal and silica gel. The PAH-doped particles were analyzed before and after exposure to a gaseous $NO_2/HNO_3$ mixture. Ionization was performed by an ArF excimer laser (193 nm) and irradiance of approximately $9 \times 10^6$ W/cm$^2$, which provides soft ionization for most PAH and derivatives. The positive ion FTMS laser microprobe spectrum taken before $NO_2/HNO_3$ exposure showed abundant molecular ion for each PAH standard. Degradation products were studied in negative ion mode, with ejection of ions with m/z < 150amu to improve mass resolution. Fragments corresponding to the $[M\text{-}NO]^-$ anion of three nitro-PAH were identified in the resulting spectrum and application of the FTMS laser microprobe method to environmental particles was proposed for future work.

## 1.3 MOTIVATION AND GOALS

Despite extensive research on the photoionization of nitrobenzene and derivatives, the photochemistry of nitro-PAH has remained relatively unexplored. One goal of the current study is to obtain and interpret characteristic photofragmentation patterns of representative nitro-PAH and nitrated heterocyclic compounds. Gaseous $NO_x$ is a prevalent air pollutant emitted from such fossil fuel combustion sources as utilities, vehicles, and industrial waste incinerators.[44] Arey et al.[2] demonstrated that nitro-PAH may form in the atmosphere by gas-phase reactions of PAH with the OH radical, predominantly during daylight hours. Examination of the photoionization products of nitro-PAH and derivatives have significant implications for the atmospheric formation and transformation reactions of this mutagenic chemical class.

Acquisition of representative photoionization spectra and identification of characteristic photofragments of nitro-PAH are prerequisites for application of laser photoionization to determine their presence in environmental samples. Comparison of experimental data from an environmental sample to known properties of reference compounds is an often-used method to confirm the identification of a particular species in the complex sample matrix. The second objective of the present research is to investigate the application of laser desorption-laser photoionization time-of-flight mass spectrometry (LDLPMS) to the direct analysis of particulate matter. The potential exists to directly determine the presence of nitro-PAH and nitrated heterocyclic compounds in environmental samples, without costly extraction and separation steps, by using LDLPMS.

In the current study, laser photoionization mass spectra are obtained for four nitro-PAH : 9-nitroanthracene, 1-nitropyrene, 2-nitro-9-fluorenone and 2-nitrofluorene. Each of these nitro-PAH were previously identified in diesel exhaust particulate.[3-7] Laser photoionization mass spectra are also obtained for the isomers 2- and 3-nitro-6H-dibenzo[b,d]pyran-6-one (a.k.a. 6- and 7-nitro-3,4-benzocoumarin). The 2- and 4-nitro-dibenzopyranone isomers were recently identified by Arey et al.[12] and Helmig et al.[25] in the most mutagenic fraction of ambient air particulate extracts. Mixtures of the nitro-PAH standards as well as mixtures of PAH standards with nitro-PAH are also examined by LDLPMS. Spectra obtained from the reference compounds encouraged the examination of the NIST SRM 1650 diesel particulate matter. The LDLPMS spectra acquired for the NIST standard are also presented and discussed.

## 1.4 REFERENCES

1. Helmig, D.; Arey, J.; Atkinson, R.; Harger, W. P.; McElroy, P. A. *Atmos. Environ.* **1992,** *26A*, 1735.

2. Arey, J.; Zielinska, B.; Atkinson, R.; Aschmann, S. M. *Int. J. Chem. Kinet.* **1989,** *21*, 775.

3. Schuetzle, D.; Lee, F. S. C.; Prater, T. J.; Tejada, S. B. in *Proceedings of the 10th Annual Symposium on Analytical Chemistry of Pollutants*, Gordan and Breach Science Publishers, New York, 1980, pp. 193-244.

4. Schuetzle, D.; Lee, F. S. C.; Prater, T. J.; Tejada, S. B. *Int. J. Environ. Anal. Chem.* **1981,** *9*, 93.

5. Schuetzle, D.; Riley, T. L.; Prater, T. J.; Harvey, T. M.; Hunt, D. F. *Anal. Chem.* **1982,** *54*, 265.

6. Schuetzle, D.; Paputa, M.; Hampton, C. M.; Marano, R.; Riley, T.; Prater, T. J.; Skewes, L.; Salmeen, I. "The Identification and Potential Sources of Nitrated Polynuclear Aromatic Hydrocarbons (Nitro-PAH) in Diesel Particulate Extracts", pp.299-312 in *Mobile Source Emissions Including Polycyclic Organic Species*, D. Reidel Publishing Co., 1983.

7. Paputa-Peck, M. C.; Marano, R. S.; Schuetzle, D.; Riley, T. L.; Hampton, C. V.; Prater, T. J.; Skewes, L. M.; Jensen, T. E.; Ruehle, P. H.; Bosch, L. C.; Duncan, W. P. *Anal. Chem.* **1983,** *55*, 1946.

8. Williams, P. T.; Bartle, K. D.; Andrews, G. E. "Polycyclic Aromatic Compounds in Diesel Fuels and Particulates", pp. 1011-1027 in *Polynuclear Aromatic Hydrocarbons: Chemistry, Characterization and Carcinogenesis; Ninth International Symposium*, M. Cooke and A. J. Dennis, Eds., Battelle Press, Columbus, OH, 1986.

9. Xu, X. B.; Nachtman, J. P.; Jin, Z. L.; Wei, E. T.; Rappaport, S. M. *Anal. Chim. Acta* **1982,** *136,* 163.

10. Ramdahl, T.; Becher, G.; Björseth. A. *Environ. Sci.Technol.* **1982,** *16,* 861.

11. Nishioka, M. G.; Howard, C. C.; Lewtas, J. "Detection of Hydroxy-Nitro-PAHs and Nitro-PAHs in an Ambient Air Particulate Extract Using Bioassay Directed Fractionation", pp. 701-715 in *Polynuclear Aromatic Hydrocarbons: Chemistry, Characterization and Carcinogenesis; Ninth International Symposium,* M. Cooke and A. J. Dennis, Eds., Battelle Press, Columbus, OH, 1986.

12. Arey, J.; Harger, W. P.; Helmig, D.; Atkinson, R. *Mutat. Res.* **1992,** *281,* 67.

13. Chuang, C. C.; Mack, G. A.; Petersen, B. A.; Wilson, N. K. "Identification and Quantification of Nitropolynuclear Aromatic Hydrocarbons in Ambient and Indoor Air Particulate Samples" pp. 155-171 in *Polynuclear Aromatic Hydrocarbons: Chemistry, Characterization and Carcinogenesis; Ninth International Symposium,* M. Cooke and A. J. Dennis, Eds., Battelle Press, Columbus, OH, 1986.

14. Oehme, M.; Mano, S.; Stray, H. *HRC & CC* **1982,** *5,* 417.

15. Harris, W. R.; Chess. E K.; Okamoto, D.; Remsen, J. F.; Later, D. W. *Environ. Mutagen.* **1984,** *6,* 131.

16. McCoy, E. C.; Rosenkranz, H. S. *Cancer Lett.* **1982,** *15,* 9.

17. Schnieder, E.; Krenmayr, P.; Varmuza, K. *Monatshefte fur Chemie* **1990,** *121,* 393.

18. Ramdahl, T.; Urdal, K. *Anal. Chem.* **1982,** *54,* 2256.

19. Cronn, D. Ph. D. Dissertation, University of Washington, Seattle, 1975.

20. Jäger, J. *J. Chromatog.*, **1978,** *152,* 575.

21. Pitts, J. N., Jr.; Van Cauwenberghe, K. A.; Grosjean, D.; Schmidt, J. P.; Fitz, D. R.;

Belser, W. L.; Knudson, G. B.; Hynds, P. M. *Science*, **1978**, *202*, 515.

22. Ramdahl, T.; Sweetman, J. A.; Zielinska, B.; Harger, W. P.; Winer, A. M.; Atkinson, R.; "Determination of Nitrofluoranthenes and Nitropyrenes in Ambient Air and Their Contribution to Direct Mutagenicity", pp. 745-759 in *Polynuclear Aromatic Hydrocarbons: A Decade of Progress: Tenth International Symposium*, M. Cooke and A.J. Dennis, Eds., Battelle Press, Columbus, Ohio, 1988.

23. Nishioka, M. G.; Howard, C. C.; Contos, D. A.; Ball, L. M.; Lewtas, J. *Environ. Sci. Tech.* **1988**, *22*, 908.

24. Arey, J.; Zielinska, B.; Harger, W. P.; Atkinson, R.; Winer, A. M. *Mutat. Res.* **1988**, *207*, 45.

25. Helmig, D.; López-Cancio, J.; Arey, J.; Harger, W. P.; Atkinson, R. *Environ. Sci. Technol.* **1992**, *26*, 2207.

26. MacCrehan, W. A.; May, W. E. "Determination of Nitro-Polynuclear Aromatic Hydrocarbons in Diesel Soot by Liquid Chromatography with Fluorescence and Electrochemical Detection", pp. 857-869 in *Polynuclear Aromatic Hydrocarbons: Mechanisms, Methods and Metabolism: 8th International Symposium*, M. Cooke and A.J. Dennis, Eds., Battelle Press, Columbus, Ohio, 1985.

27. Campbell, R. M.; Lee, M. L. *Anal. Chem.* **1984**, *56*, 1026.

28. Morrison, R. J. S.; Rockney, B. H.; Grant, E. R. *J. Chem. Phys.* **1981**, *75*, 2643.

29. Morrison, R. J. S.;Grant, E. R. *J. Chem. Phys.* **1982**, *77*, 5994.

30. Moss, D. B.; Trentelman, K. A.; Houston, P. L. *J. Chem. Phys.* **1992**, *96*, 237.

31. Mcquaid, M. J.; Miziolek, A. W.; Sausa, R. C.; Merrow, C. N. *J. Phys. Chem.* **1991**, *95*, 2713.

32. Stewart, P. H.; Jeffries, J. B.; Zellweger, J. M.; McMillen, D. F.; Golden, D. M. *J. Phys. Chem.* **1989,** *93*, 3557.

33. Bowie, J. H.; Blumenthal, T.; Walsh, I. *Org. Mass Spectrom.* **1971,** *5*, 777.

34. Budzikiewicz, H.; Djerassi, C.; Williams, D. H. "Nitro and Related Compounds", pp. 512-519 in *Mass Spectrometry of Organic Compounds* , Holden-Day, Inc., San Francisco, 1967.

35. Ioki, Y. *J. C. S. Perkin II* **1977,** *10*, 1240.

36. Apel, E. C.; Nogar, N. S. *Int. J. Mass Spectrom. Ion Processes* **1986,** *70*, 243.

37. Zhu, J.; Lustig, D.; Sofer, I.; Lubman, D. M. *Anal. Chem.* **1990,** *62*, 2225.

38. Marshall, A.; Clark, A.; Jennings, R.; Ledingham, K. W. D.; Sander, J.; Singhal, R. P. *Int. J. Mass Spectrom. Ion Processes* **1992,** *112* , 273.

39. Marshall, A.; Clark, A.; Jennings, R.; Ledingham, K. W. D.; Sander, J.; Singhal, R. P. *Int. J. Mass Spectrom. Ion Processes* **1992,** *116* , 143.

40. Weissler, G. L.; Samson, J. A. R.; Ogawa, M.; Cook. G. R. *J. Opt. Soc. Am.* **1959,** *49*, 338.

41. Galloway, D. B.; Bartz, J. A.; Huey, L. G.; Crim, F. F. *J. Chem. Phys.* **1993,** *98*, 2107.

42. Mauney, T.; Adams, F.; Sine, M. K. *Sci. Tot. Environ.* **1984,** *36*, 215.

43.. Delmas, S.; Muller, J. F. *Analusis* **1992,** *20* , 165.

44. Pahl, D. A.; Zimmerman, D.; Ryan, R. "An Overview of Combustion Emissions in the United States," pp. 1-24 in *Emissions from Combustion Processes: Origin, Measurement, Control*, R. Clement and R. Kagel, Eds., Lewis Publishers, Inc., Boston, 1990.

# CHAPTER 2

## Laser Desorption-Laser Photoionization
## Time-of-Flight Mass Spectrometry

### 2.1 INTRODUCTION

The time-of-flight mass spectrometer operates on the principle that ions of different mass-to-charge ratios, accelerated to the same kinetic energy, have different flight times through a field-free region. The ability to produce a full mass spectrum for each laser pulse makes the TOF mass spectrometer ideally suited to a pulsed laser ionization source. Simplicity, low cost, ease of construction, high ion transmission, and a theoretically unlimited mass range are advantages with wide appeal to researchers performing pulsed ionization experiments. As time-of-flight mass spectrometry (TOFMS) has been the subject of several publications and reviews,[1-6] only a brief outline of TOFMS theory is given here. The remainder of this chapter discusses the sources of peak broadening and the technique of laser desorption as they pertain to our TOF mass spectrometer.

### 2.2 BASIC PRINCIPLES OF TOFMS

A linear TOF mass spectrometer consists of two regions as shown in Figure 2.1. The source region contains a series of charged grids used to accelerate the ions into the flight tube (field-free region) which houses the detector. All ions formed in the source region during each laser pulse are accelerated in the presence of an electric field ($E = V/d$) to a final kinetic energy ($zEd$). The final velocities of the ions differ in proportion to their various mass-to-charge ratios ($m/z$).

**Figure 2.1** Diagram and accompanying equations depicting the basic principles of time-of-flight mass spectrometry.

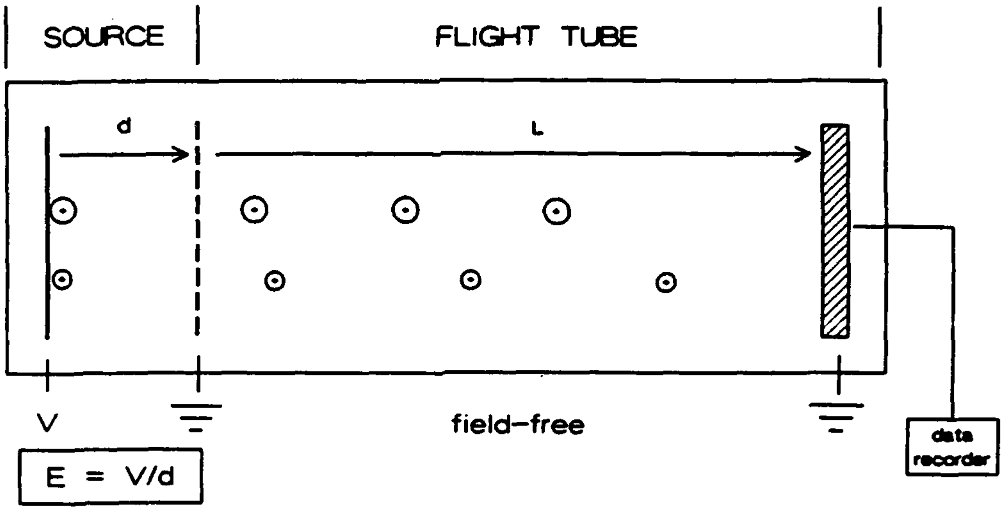
SOURCE
FLIGHT TUBE
d
L
V
field-free
E = V/d
data recorder

**Increase in Ion Kinetic Energy:**

$$K.E. = \tfrac{1}{2}mv^2 = zV = zEd$$

m = ion mass

z = ion charge

E = electric field

**Velocity of Ions after Acceleration:**

$$v = \sqrt{\frac{2zEd}{m}}$$

v = ion velocity

d = accel. distance

**Time of Flight through Field Free Region:**

$$t = (L)\sqrt{\frac{m}{2zEd}}$$

(time) = (dist) / (vel)

L = length of field free region

**Flight Time Proportional to Mass-to-Charge Ratio:**

$$t \propto \sqrt{\frac{m}{z}} \qquad \text{or} \qquad t^2 \propto \frac{m}{z}$$

Once an ion enters the field-free region, it drifts at its final velocity until impacting the detector. The flight time of each ion is directly proportional to the square root of its mass-to-charge ratio. Hence, ions with smaller m/z arrive at the detector earlier than those with larger m/z. The data acquisition system records the current generated as ions of all masses produced during each laser pulse strike the detector. Experimentally, signal intensity is recorded as a function of flight time. Data averaged over many pulses is converted to a plot of intensity versus m/z through a linear time extrapolation from low mass ions, providing a complete TOF mass spectrum.

## 2.3 FACTORS AFFECTING FLIGHT TIME

The primary factors that determine an ion's flight time are the instrument design and operating parameters. The distances between grids, applied voltages and drift region length are important considerations in design and operation of a TOF mass spectrometer. The two-step acceleration linear TOF mass spectrometer first described by Wiley and McLaren[7] in 1955 became the standard on which today's TOF mass spectrometers (including our own) are modelled. Figure 2.2 is a schematic of the Wiley and McLaren ion optics along with a few of the more complex, but pertinent, equations of ion motion.[1] Once the instrument is machined, the ion optics positioned, and the grid potentials chosen, the principal factors that determine ion flight time are built-in.

Ideally a TOF experiment would have all ions formed at a single position, at the same time, and accelerated to the same kinetic energy. Then ion flight time would be a function only of m/z and the TOF mass spectrometer would have infinite resolution (provided the data acquisition system could keep pace). Unfortunately, ideal does not equate to experimental. There are several other factors which decrease mass resolution

**Figure 2.2** Diagram illustrating the ion optics of a two-step acceleration time-of-flight mass spectrometer based on the 1955 design of Wiley and McLaren, and the corresponding equations of ion motion.

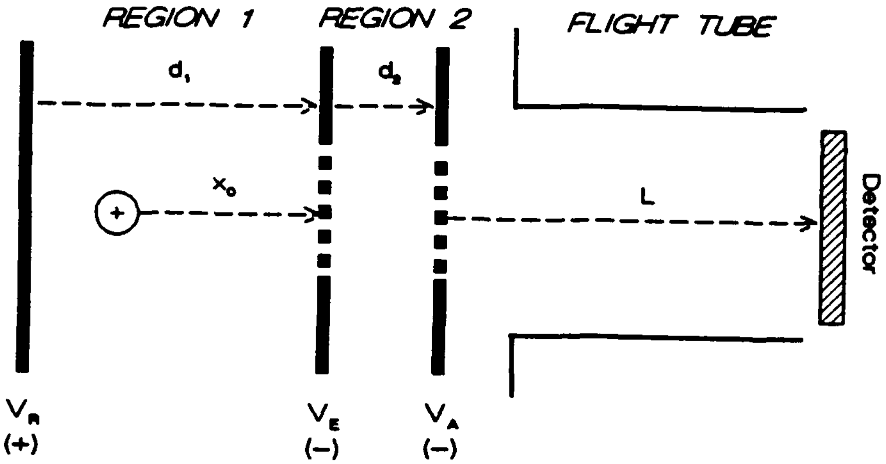

Electric Field Gradients:

$$E_1 = (V_R - V_E)/d_1 \quad \text{and} \quad E_2 = (V_E - V_A)/d_2$$

Acceleration of Ions:

$$a_1 = \frac{zE_1}{m} \quad \text{and} \quad a_2 = \frac{zE_2}{m}$$

m = ion mass

z = ion charge

Ion Velocity by Region:

$$v_1 = \left(v_0^2 + 2a_1x_0\right)^{1/2} \quad \text{and} \quad v_2 = \left(v_0^2 + 2a_1x_0 + 2a_2d_2\right)^{1/2}$$

$v_0$ = initial ion velocity

Flight Times by Region:

$$t_1 = \frac{(v_1 - v_0)}{a_1} \qquad t_2 = \frac{(v_2 - v_1)}{a_2} \qquad t_3 = \frac{L}{v_2}$$

L = length of field-free region

Total Ion Flight Time = $T = (t_1 + t_2 + t_3)$ and is now dependent on initial position and initial velocity of ion at time of formation!

by increasing the time width of the ion packet (group of same m/z ions) that reaches the detector. Contributions from some of these factors, as described by Opsal,[1] can be minimized by straightforward methods. The remaining factors, temporal, spatial, velocity and energy spreads at the initial ion formation, are the dominant causes for variation in flight times within an ion packet. These sources of peak broadening require closer inspection.

## 2.4 SOURCES OF BROADENING

Temporal broadening results from a spread in the initial formation time of the ions. The ions formed during the finite laser pulse are not all formed at the same moment. The effect of this initial time spread on the ion packet can be thought of qualitatively. For two equal m/z ions with the same initial position and velocity but formed at different times, the difference in their flight time is exactly the difference in their formation time. These two ions have the same kinetic energy on arrival at the detector, and the time width of the ion packet is independent of the length of the field-free region.[3]

There are two straightforward solutions to temporal broadening. The first solution is to increase the length of the field-free region which improves mass resolution by allowing greater separation between ion packets of constant width. The second solution is to shorten the pulse width of the laser ionization source. Picosecond laser sources virtually eliminate temporal broadening as a significant contribution to peak width by narrowing the temporal width during initial formation of the ion packet.[1,4]

Our TOF mass spectrometer uses a Nd:YAG pulsed laser for ionization with a pulse width of 8 to 10 nsec at 266 nm. Ionization is assumed to occur within a few nanoseconds. The current grid spacings, accelerating potentials and drift region length generate ion flight times on the order of microseconds. At m/z 200, peak widths are typically ~ 200 nsec. The theoretical contribution to peak width from temporal broadening due to laser pulse width is approximately 4% in our TOF instrument.

Spatial broadening is caused by variations in the initial position of the ions upon formation in the source region. Since a laser beam cannot be focussed to a point, ionization occurs over a finite spatial volume within the waist of the laser beam. Referring to Figure 2.2, the velocity achieved by an ion and consequently, its final kinetic energy, depend on the distance from the grid ($x_0$) at which the ion formed. Two equal m/z ions formed at the same time with the same initial velocity but in different locations, will be accelerated to different final kinetic energies. The magnitude of the resulting spread in ion flight times depends on the size of the laser beam focal spot.[3,4]

One solution to the problem of spatial broadening is to ionize by direct desorption from an equipotential surface. Desorption from a surface limits ion production to a very well-defined spatial region.[3,4] In our TOFMS, samples are desorbed from a flat surface positioned perpendicular to the flight tube, and the theoretical contribution to peak width from spatial broadening is < 1%. Spatial broadening was also addressed by Wiley and McLaren.[7] Their two-step acceleration scheme was designed to operate under space-focussed conditions. The low-voltage extraction ($V_E$) provided additional energy to ions at the rear of the source to help them catch up with ions near the source exit, thereby narrowing the initial ion packet. Then the larger acceleration potential ($V_A$) accelerated all the ions to their final energy. The space-focussing condition made flight time independent of initial position to the first order.[1,4]

Velocity broadening derives from the fact that ions form in the source with initial velocities that reflect those of their neutral precursors. For ions of equal m/z, the gas-phase velocity distribution is normally Maxwellian, as described by Opsal.[1,2,4] Obviously, equal m/z ions formed with different initial kinetic energies will have different flight times. An interesting case is that of two equal m/z ions formed at the same time and position with the same kinetic energy, but with their velocities in different directions. Both ions will be accelerated to the same final energy and velocity. However, the ion moving against the field must decelerate, stop, and turn around prior to acceleration. This turn-around time increases the time width of the ion packet and degrades mass resolution.[3]

Several methods have been introduced over the years to compensate for velocity broadening. The use of time-dependent drawout and acceleration fields has been shown to decrease velocity broadening by reducing the effect of turn-around time.[7,9] Ions travelling with initial velocities opposite the flight direction are accelerated over a longer distance upon application of the electric field pulse. The higher final energy of the "turn-around" ion allows it to catch up to its ion packet at the detector, minimizing peak broadening. The technique of direct ionization from surfaces can essentially eliminate the contribution from turn-around time since initial ion velocities cannot be negative.[3,4] Another option, increasing the grid potentials, compensates for velocity broadening by making the initial energy distributions small compared to the final kinetic energies.[3] With the current TOFMS operating potentials and sample desorption geometry, the theoretical contribution to peak width from initial velocity and kinetic energy distributions is ~ 2%.

The reflectron device developed by Mamyrin et al.,[10] corrects for resolution degradation caused by both initial spatial and velocity distributions. Two ions of equal m/z enter the electrostatic reflector with different velocities. The ion with greater velocity penetrates farther into the reflector region and must travel a longer distance than the slower moving ion. The faster ion spends more time in the reflector region, allowing the slower ion to catch up, thus narrowing the time width of the ion packet and improving resolution.[1,3,4,8] The reflectron does not correct for initial kinetic energy spread. The ion kinetic energy is the same upon exiting the reflectron as it was upon entering. The different path lengths travelled by the ions within the reflectron fields causes the narrowing of the ion packet which improves mass resolution.

The reflectron is a second-order space-focussing ion source, i.e. its space focus coincides with the position of the second detector. There are several considerations involved in the design and installation of a reflectron device. Factors to consider in reflectron design and installation include, but are certainly not limited to: dimensions of the TOFMS, length of the reflectron, grid spacings within the reflectron, potentials applied to the grids, distance from the start of the drift region to the reflectron entrance, and conversely, distance from the reflectron exit to the second detector. An excellent discussion of the reflectron device and associated mathematics is given by Boesl and Schlag.[11]

An alternative to compensating for the initial velocity spread is to reduce or eliminate the distribution by use of a supersonic molecular beam source.[12,13] In an ideal molecular beam, all the molecules are travelling in the same direction with the same velocity prior to ionization. The attainable reduction in velocity spread can increase the resolution of a standard linear TOF instrument to 1000 or higher.[8] Use of a pulsed valve also permits direct injection from 1 atm into vacuum,[14] which has great potential for real environmental applications.

Resolution in our TOF instrument is degraded primarily by the effects of spatial and velocity broadening. The finite laser beam volume and unusual desorption geometry make identification of a well-defined spatial region of ionization difficult (see Section 4.3: Single-Step LDLP Experiments). Since desorption from a surface perpendicular to the flight path is accomplished in our source, ions do not have negative velocities. However, the initial velocity distribution in the desorbed plume, which is otherwise uncorrected, is enough to make a significant contribution to peak broadening. Desorption from the Gelman fiber filters, used in air sampling, degrades resolution through temporal effects as well as spatial and velocity effects which are discussed in the next section. Mass resolution in our TOF instrument ($m/\Delta m$) is ~ 100. Improvement could definitely be achieved by addition of a supersonic molecular beam, a reflectron device, or both.

## 2.5 LASER DESORPTION

Laser-induced thermal desorption is a technique employed to vaporize neutral or ionic species from the condensed state by the rapid input of thermal energy into the condensed state. Generally, a rapid increase in surface temperature in the range of $10^8$ to $10^{11}$ K/sec occurs within the nanosecond pulse of the desorption laser.[15] The extent of fragmentation induced by laser desorption can be controlled by appropriate choice of power density.[16] Adjustments to the laser power density are made to maximize desorption yield while minimizing sample fragmentation and undesirable decomposition reactions. Therefore, the principal advantage of pulsed laser desorption is that the very short laser pulse width permits desorption of intact molecules before competing side reactions can occur .[17]

Two-step and single-step laser desorption experiments were performed in the current study. The two-step laser desorption-laser photoionization (LDLP) experiments utilized the focussed IR beam from a pulsed $CO_2$ laser to induce thermal desorption of samples adsorbed on Gelman glass fiber filters (a porous air-sampling-type filter). A short time after the desorption event, a focussed UV beam was directed into the plume of desorbed neutrals to effect multiphoton ionization. Separation of the desorption and ionization steps allowed better control over each process. The single-step LDLP experiments utilized the focussed UV beam of a pulsed Nd:YAG laser to effect desorption and postionization of solid samples deposited on an aluminum probe. The extent of fragmentation was controlled by varying the area of interaction between the laser beam and the sample surface, thus varying the power density at the surface. Due to the UV beam geometry through the source region (see Chapter 4: Figure 4.4), laser power density was not as finely adjustable in the single-step experiments.

The spectra obtained in the two-step experiments were significantly different from those obtained in the single-step experiments. The difference in the spectra is largely attributable to desorption of the sample from the porous Gelman glass fiber filters (in the two-step experiments) as opposed to desorption of the solid sample deposited on the bare aluminum probe surface (in the single-step experiments). When the IR laser beam impacts the filter surface, significant heating of the filter fibers occurs. Initially, molecules closest to the top of the filter surface are desorbed. The desorbed surface molecules have less thermal energy than the filter matrix because there has been a loss of energy to the desorption process ($\Delta H_{desorb}$). Over many pulses, the surface molecules are depleted and the molecules from deeper in the filter matrix make up a larger fraction of the desorbed species. Molecules desorbed from deeper within the matrix suffer collisions with the thermally energized filter fibers and can thermally equilibrate with the filter. Hence, when molecules farther from the surface exit the filter matrix, they possess more thermal energy than their surface counterparts in the desorption plume. Thus, desorption of samples adsorbed on the filters introduces broadening in our spectra by creating larger initial velocity and energy distributions.[18]

Molecules desorbed directly from the sample deposited onto the bare aluminum probe surface also lose energy to the desorption process. However, desorption and postionization both occur within the UV laser pulse. Molecules desorbed directly from the probe surface will have a narrower velocity and energy distribution than those desorbed from the filter matrix. Reduced velocity and energy profiles within the initial ion packet decrease peak broadening and increase mass resolution. Therefore, the spectra of compounds desorbed directly from the probe surface are generally better resolved than the spectra of compounds desorbed from the Gelman filters.[18]

The precise physical nature and mechanisms for ionization in laser desorption are uncertain at this time.[16,17] However, the presence of dimers (and even trimers) in our single-step spectra indicates that bimolecular reactions are occurring within the high-density plume of desorbed material. Ionization in this high-density plume could occur by several mechanisms including collision-induced, proton-transfer and multiphoton absorption-ionization processes. Chapter 3 discusses the latter, multiphoton ionization, in depth.

## 2.6 REFERENCES

1. Opsal, R. B. *Gas Chromatography Laser Ionization Mass Spectrometry*, Dissertation, Nov. 1985 (Indiana University).

2. Opsal, R. B.; Owens, K. G.; Reilly, J. P. *Anal. Chem.* **1985**, *57*, 1884.

3. Cotter, R. J. *Biomed. Environ. Mass Spectrom.* **1989**, *18*, 513.

4. Opsal, R. B.; Colby, S. M.; Wilkerson, C. W. Jr.; Reilly, J. P. "Resolution and Sensitivity in Laser Ionization Mass Spectrometry" pp. 490-509 in *Lasers and Mass Spectrometry*, D. M. Lubman, Ed., Oxford University Press, New York, 1990.

5. Price, D. *Time of Flight Mass Spectrometry*, D. Price and J. E. Williams, Eds., Pergamon Press, Oxford, New York, 1969.

6. Lubman, D. M.; Jordan, R. M. *Rev. Sci. Instrum.* **1985**, *56*, 373.

7. Wiley, W. C.; McLaren, I. H. *Rev. Sci. Instrum.* **1955**, *26*, 1150.

8. Lubman, D. M. *Mass Spectrom. Rev.* **1988**, *7*, 535.

9. Marable, N. L.; Sanzone, G. *Int. J. Mass Spectrom. Ion Phys.* **1974**, *13*, 185.

10. Mamyrin, B. A.; Kararaev, V. I.; Shmikk, D. V.; Zagulin, V. A. *Sov. Phys.-JETP* (Engl. Trans.) **1973**, *37*, 45.

11. Boesl, U.; Weinkauf, R.; Schlag, E. W. *Int. J. Mass Spectrom. Ion Process.* **1992**, *112*, 121.

12. Lubman, D. M. *Laser Focus / Electro-Optics* ***1984***, *20*, 110.

13. Owens, K. G.; Reilly, J. P. *J. Opt. Soc. Am. B.* **1985**, *2*, 1589.

14. Tembreull, R.; Lubman, D. M. *Anal. Chem.* **1984**, *56*, 1962.

15. Zenobi, R.;Hahn, J. H.; Zare, R. N. *Chem. Phys. Lett.* **1988**, *150*, 361.

16. Houk, R. S. "Laser Ionization Techniques for Analytical Mass Spectrometry" pp.

587-625 in *Analytical Applications of Lasers*, John Wiley & Sons, Inc., New York, 1986.

17. Land, D. P.; Wang, D. T. S.; Tai, T.; Sherman, M. G.; Hemminger, J. C.; McIver, R. T. Jr. "Postionization of Laser-Desorbed Neutrals for the Analysis of Molecular Adsorbates on Surfaces" pp. 157-177 in *Lasers in Mass Spectrometry*, D. M. Lubman, Ed., Oxford University Press, New York, 1990.

18. Per. Comm. with Dr. Donald P. Land, Asst. Prof., Dept. of Chemistry, University of California, Davis, March 1993.

# CHAPTER 3

## Theory of Multiphoton Ionization

### 3.1 INTRODUCTION

Photoionization can occur if the photon energy absorbed by a molecule is greater than its ionization potential (IP). Early direct photoionization used vacuum ultraviolet (VUV) radiation near 100 nm. The VUV lamps were low intensity, noncoherent sources which led to poor ion yields and low sensitivity. Absorption cross-sections for photo-ionization of an average molecule at the intensity of a conventional light source are:[1]

| | |
|---|---|
| One-photon | ~ $10^{-17}$ $cm^2$ |
| Two-photon | ~ $10^{-51}$ $cm^4s$ |
| Three-photon | ~ $10^{-82}$ $cm^6s^2$ |

The possibility of simultaneous two-photon absorption or emission in molecules was first postulated by Marie Goeppart-Mayer in 1931 by applying Dirac's dispersion theory.[2] Multiphoton ionization (MPI) depends on the concerted absorption of two or more photons by a molecule upon irradiation with an intense UV or visible light source. The cross-sections above indicate that the probability of MPI occurring at conventional light source intensity is extremely low. Not until the 1960s with the advent of high-peak power, tunable visible and UV laser sources did experimental observation of MPI processes become feasible.

### 3.2 APPLICATION TO MASS SPECTROMETRY

Employment of mass spectrometers to identify the ionization products of multiphoton processes began with Boesl *et.al.*, in 1978.[3] Multiphoton ionization combined with mass spectrometry allows identification of a molecule by its absorption-excitation spectrum related to a resonant intermediate state, as well as by its mass. The ionization cross-section of the detected ions reflects the optical spectrum of the intermediate state. When the laser frequency is resonant with a real intermediate electronic state, the ionization cross-section is significantly enhanced. Important information on the dynamic behavior involving energy relaxations and fragmentation reactions occurring in the excited states of neutral and ionic molecules is obtained by resonance enhanced multiphoton ionization (REMPI).[1]

The MPI method applied extensively in analytical chemistry is resonant two-photon ionization (R2PI). Absorption of two photons drives the molecular system through an excited electronic state to a final, photoionized condition. The two photons can have either the same or different frequencies but, the sum of their energies must exceed the ionization potential of the molecule for R2PI to occur. Most organic compounds of interest have IPs between 7 and 13 eV, allowing use of convenient near-UV pulsed laser sources (such as Nd:YAG and excimer-pumped dye lasers) to achieve R2PI.[4]

## 3.3 QUANTUM THEORY OF MPI

### 3.3.1 Time-Dependent Perturbation Theory

The derivation of multiphoton ionization transition probability from time-dependent perturbation theory[1,5-7] demonstrates the importance of resonance with an intermediate electronic state. To calculate the time evolution of a system caused by a perturbation, solve the Time-Dependent Schrödinger Equation:

$$\hat{H}\Psi = i\hbar\frac{\partial\Psi}{\partial t} \tag{3.1}$$

Consider a system in which the Hamiltonian is separable into its time-independent and time-dependent parts

$$\hat{H} = \hat{H}^0 + \lambda V(t) \tag{3.2}$$

where $V(t)$ is the perturbation and $\lambda$, the perturbation parameter, is small. The unperturbed eigenfunctions $\Psi^0$ are solutions of the equation

$$\hat{H}^0 \Psi_k^0 = i\hbar \frac{\partial \Psi_k^0}{\partial t} \tag{3.3}$$

and have the form

$$\Psi_k^0 = \psi_k \; e^{-iE_k t/\hbar} \tag{3.4}$$

where

$$\hat{H}^0 \psi_k = E_k \psi_k \tag{3.5}$$

Assume the eigenfunctions $\psi_k$ and the eigenvalues $E_k$ are known and that the eigenfunctions form a complete orthonormal set. Expanding the wavefunction $\Psi$ in terms of the unperturbed basis set $\Psi^0$ yields

$$\Psi = \sum_k a_k(t) \psi_k \; e^{-iE_k t/\hbar} \tag{3.6}$$

By normalization

$$\int_{\bullet} \Psi^{*} \Psi \, d\tau = \int_{\bullet} a_k^{*} a_k = 1$$

Therefore, the probability that the system is in state $k$ at time $t$ (i.e. the transition probability) is

$$P_k = |a_k(t)|^2 \tag{3.7}$$

### 3.3.2 Time-Dependent Coefficients

To determine the time-dependent coefficients,[1] substitute equations (3.2) and (3.6) into the time-dependent Schrödinger equation (3.1)

$$i\hbar \frac{\partial}{\partial t}\left( \sum_k a_k(t)\, \psi_k \, e^{-iE_k t/\hbar} \right) = \left( H^0 + \lambda V(t) \right) \sum_k a_k(t)\, \psi_k \, e^{-iE_k t/\hbar} \tag{3.8}$$

Equation (3.8) reduces to

$$i\hbar \sum_k \frac{\partial a_k(t)}{\partial t} \psi_k \, e^{-iE_k t/\hbar} = \lambda \sum_k a_k(t) V(t)\, \psi_k \, e^{-iE_k t/\hbar} \tag{3.9}$$

Multiply through by the complex conjugate and integrate over all space to obtain

$$i\hbar \sum_k \frac{\partial a_k(t)}{\partial t} \langle \psi_m | \psi_k \rangle e^{-i(E_m - E_k)t/\hbar} = \lambda \sum_k a_k(t) \langle \psi_m | V(t) | \psi_k \rangle e^{-i(E_m - E_k)t/\hbar} \tag{3.10}$$

Notice that the left-hand side of equation (3.9) contains a delta function which is nonzero only when $k = m$. Defining $(E_m - E_k) \equiv \omega_{mk}$ and $V_{mk} \equiv \langle \psi_m | V(t) | \psi_k \rangle$, equation (3.10) becomes

$$i\hbar\frac{\partial a_m(t)}{\partial t} = \lambda\sum_k a_k(t)\,V_{mk}e^{i\omega_{mk}t} \tag{3.11}$$

The resulting differential equations for the coefficients are solved by successive approximation

$$a_m(t) = \sum_{i=0}^{\infty}\lambda^i a_m^{(i)} = a_m^{(0)} + \lambda a_m^{(1)} + \lambda^2 a_m^{(2)} + \cdots \tag{3.12}$$

Substitute equation (3.12) into (3.11) and equate terms with coefficients of $\lambda^n$ to yield expressions for the time-dependent coefficients

$$i\hbar\frac{da_m^{(0)}}{dt} = 0 \qquad \therefore a_m^{(0)} \equiv \text{constant} \tag{3.13}$$

$$i\hbar\frac{da_m^{(1)}(t)}{dt} = \sum_k a_k^{(0)}\langle \psi_m | V(t) | \psi_k \rangle e^{i\omega_{mk}t} \qquad (1^{st}\ \text{order}) \tag{3.14}$$

$$i\hbar\frac{da_m^{(2)}(t)}{dt} = \sum_k a_k^{(1)}\langle \psi_m | V(t) | \psi_k \rangle e^{i\omega_{mk}t} \qquad (2^{nd}\ \text{order}) \tag{3.15}$$

### 3.3.3 Probability of a Two-Photon Process

Calculating the probability of a two-photon process requires knowledge of the interaction *V*(*t*) between the molecule and the electromagnetic field. The semiclassical approach assumes classical radiation interacting with a quantum-mechanical system. The semiclassical Hamiltonian is constructed by replacing the momentum in the classical Hamiltonian with its quantum-mechanical operator.[1,6,7] Collect terms, choose the Coulomb gauge (in which $\varphi = 0$ and $\nabla \circ \mathbf{A} = 0$ ) and express the results in vector notation to obtain the system Hamiltonian

$$\hat{H} = \frac{-\hbar^2}{2m}\nabla^2 + V(x,y,z) + \frac{i\hbar e}{mc}\mathbf{A}\cdot\nabla + \frac{e^2}{2mc^2}A^2 \tag{3.16}$$

The first two terms of equation (3.16) comprise $H^0$, the time-independent portion of the system Hamiltonian. The time-dependent perturbation is given by the last two terms

$$V(t) = \frac{i\hbar e}{mc}\mathbf{A}\cdot\nabla + \frac{e^2}{2mc}A^2 \tag{3.17}$$

Regard the vector potential **A** as a function of position and time. For plane-polarized light propagating along the **z** direction with its polarization in the **x** direction

$$\mathbf{A}(t) = \mathbf{A}_0 e^{\pm i(\mathbf{k}\cdot\mathbf{z} - \omega t)} \tag{3.18}$$

The propagation vector **k** is inversely proportional to wavelength ($\mathbf{k} = 2\pi/\lambda$). Wavelengths in the UV-visible region range from 1000 to 8000 Å , whereas molecular diameters are on the order of $10^1$ Å. The proportion $\left[(\mathbf{k}\cdot\mathbf{z}) \propto (\mathbf{z}/\lambda)\right]$ leads to the dipole approximation.[1,5] The electric dipole approximation assumes that **k·z** is small («1), allowing the terms exp(±*i***k·z**) in **A**(*t*) to be approximated by the first term of the expansion

$$e^{\pm i\mathbf{k}\cdot\mathbf{z}} = 1 \pm i\mathbf{k}\cdot\mathbf{z} \pm \tfrac{1}{2}(i\mathbf{k}\cdot\mathbf{z})^2 \pm \cdots \tag{3.19}$$

In this approximation, the $A^2$ term in the expression for $V(t)$ does not contribute to the inelastic process of multiphoton absorption due to the orthogonality within the set of zeroth-order molecular eigenstates.[1] The perturbation caused by the interaction of the molecule with the radiation field can therefore be written

$$V(t) = \frac{i\hbar e}{mc}(\mathbf{A}_0 \cdot \nabla)\left(e^{i\omega t} + e^{-i\omega t}\right) \tag{3.20}$$

For ease in following the next series of equations, $V(t)$ is redefined as

$$V(t) = \hat{H}'\left(e^{i\omega t} + e^{-i\omega t}\right) \qquad \text{where} \quad \hat{H}' = \frac{i\hbar e}{mc}(\mathbf{A}\cdot\nabla) \tag{3.21}$$

Consider a three level system in which $E_n < E_m < E_l$ and $\omega_{mn} \approx \omega_{lm}$. Assume that the system is initially in state *n*, and the zeroth-order coefficient of equation (3.13) is equal to one. The first-order coefficient is then given by

$$\frac{da_m^{(1)}(t)}{dt} = \frac{-i}{\hbar}\langle \psi_m | V(t) | \psi_n \rangle e^{i\omega_{mn} t} \tag{3.22}$$

Substitution of equation (3.21) into (3.22) leads to

$$\frac{da_m^{(1)}(t)}{dt} = \frac{-i}{\hbar}\langle m|\hat{H}'|n\rangle e^{i\omega_{mn}t}\left(e^{i\omega t} + e^{-i\omega t}\right) \tag{3.23}$$

Integration of both sides yields an expression that allows separation of the exponential terms into a term that is important for emission $(\omega_{mn} + \omega)$, and a term that is important for absorption $(\omega_{mn} - \omega)$.

$$a_m^{(1)}(t) = \frac{-i}{\hbar}\langle m|\hat{H}'|n\rangle \int_0^t e^{i(\omega_{mn}+\omega)t} + e^{i(\omega_{mn}-\omega)t}dt \tag{3.24}$$

Ignore the emission term and use only the absorption term to write the first-order coefficient for a single photon absorption

$$a_m^{(1)}(t) = \frac{-i}{\hbar}\frac{\langle m|\hat{H}'|n\rangle\left(e^{i(\omega_{mn}-\omega)t} - 1\right)}{i(\omega_{mn} - \omega)} \tag{3.25}$$

Now the second-order process is treated by substitution of equation (3.25) into the expression for the 2nd order time-dependent coefficient (3.15)

$$\frac{da_l^{(2)}(t)}{dt} = \frac{i}{\hbar}\sum_m \frac{\langle l|\hat{H}'|m\rangle\langle m|\hat{H}'|n\rangle\left(e^{i(\omega_{mn}-\omega)t} - 1\right)\left(e^{i\omega_{lm}t}\right)\left(e^{i\omega t} + e^{-i\omega t}\right)}{\hbar(\omega_{mn} - \omega)} \tag{3.26}$$

Multiplication of the exponentials in (3.26) once again leads to separate emission and absorption terms

$$\frac{da_l^{(2)}(t)}{dt} = \frac{i}{\hbar^2}\sum_m \frac{\langle l|\hat{H}'|m\rangle\langle m|\hat{H}'|n\rangle}{(\omega_{mn}-\omega)}\left(e^{i(\omega_{mn}-\omega)t}-1\right)\left(e^{i(\omega_{lm}+\omega)t}+e^{i(\omega_{lm}-\omega)t}\right) \tag{3.27}$$

To solve for the second-order coefficient, keep only the absorption terms and integrate with respect to time

$$a_l^{(2)}(t) = \frac{i}{\hbar^2}\sum_m \frac{\langle l|\hat{H}'|m\rangle\langle m|\hat{H}'|n\rangle}{(\omega_{mn}-\omega)}\int_0^t e^{i(\omega_{mn}+\omega_{lm}-2\omega)t} - e^{i(\omega_{lm}-\omega)t}dt \tag{3.28}$$

Completing the integration leads to a very interesting result.

$$a_l^{(2)}(t) = \frac{i}{\hbar^2}\sum_m \frac{\langle l|\hat{H}'|m\rangle\langle m|\hat{H}'|n\rangle}{(\omega_{mn}-\omega)}\left[\frac{(e^{i(\omega_{ln}-2\omega)t}-1)}{(\omega_{ln}-2\omega)}-\frac{(e^{i(\omega_{lm}-\omega)t}-1)}{(\omega_{lm}-\omega)}\right] \tag{3.29}$$

The important point to note is that a resonance now appears at $\omega_{ln} = 2\omega$ , corresponding to a resonant two-photon absorption.[6] The probability of this two-photon process is found by application of equation (3.7)

$$\mathrm{P}_{l\leftarrow n} = a_l^* a_l = \frac{1}{\hbar^4}\frac{\left|\langle l|\hat{H}'|m\rangle\langle m|\hat{H}'|n\rangle\right|^2}{(\omega_{mn}-\omega)^2}\left[\frac{4\sin^2\frac{(\omega_{ln}-2\omega)t}{2}}{(\omega_{ln}-2\omega)^2}\right] \tag{3.30}$$

Remember

$$\lim_{x \to 0} \frac{\sin^2 x}{x^2} = 1$$

Therefore, as the photon frequency ($\omega$) approaches the energy spacing for resonant absorption ($\omega_{mn}$), the probability for the two-photon process $\Rightarrow \infty$ ! The importance of resonance with a real intermediate electronic state for the multiphoton ionization process follows directly from this derivation. The special case of two equal energy photon absorption treated here may be modified for two-color MPI or n-photon MPI.

### 3.4 MPI FRAGMENTATION MECHANISM

Multiphoton ionization can induce fragmentation in a molecule during the ionization process. Figure 3.1 represents a resonant two-photon ionization and its competing processes.[8-10] Ground state molecule ABC absorbs a photon and transitions to an excited electronic state designated ABC*. From the excited state, several processes can occur:

1. Fluorescence or intramolecular relaxation which deplete the excited state population and reduce ion yield;
2. Photoisomerization to form molecule ACB* which can undergo subsequent absorption, ionization and dissociation;
3. Absorption of a second photon to reach the ionization continuum followed by photodissociation into ions and neutral (or radical) fragments which can subsequently absorb, ionize and dissociate.

**Figure 3.1** Schematic depicting the process of resonance-enhanced two-photon ionization (R2PI) and competing processes such as nonradiative decay, fluorescence, and photoisomerization which reduce the efficiency of R2PI.

# R2PI AND COMPETING PROCESSES

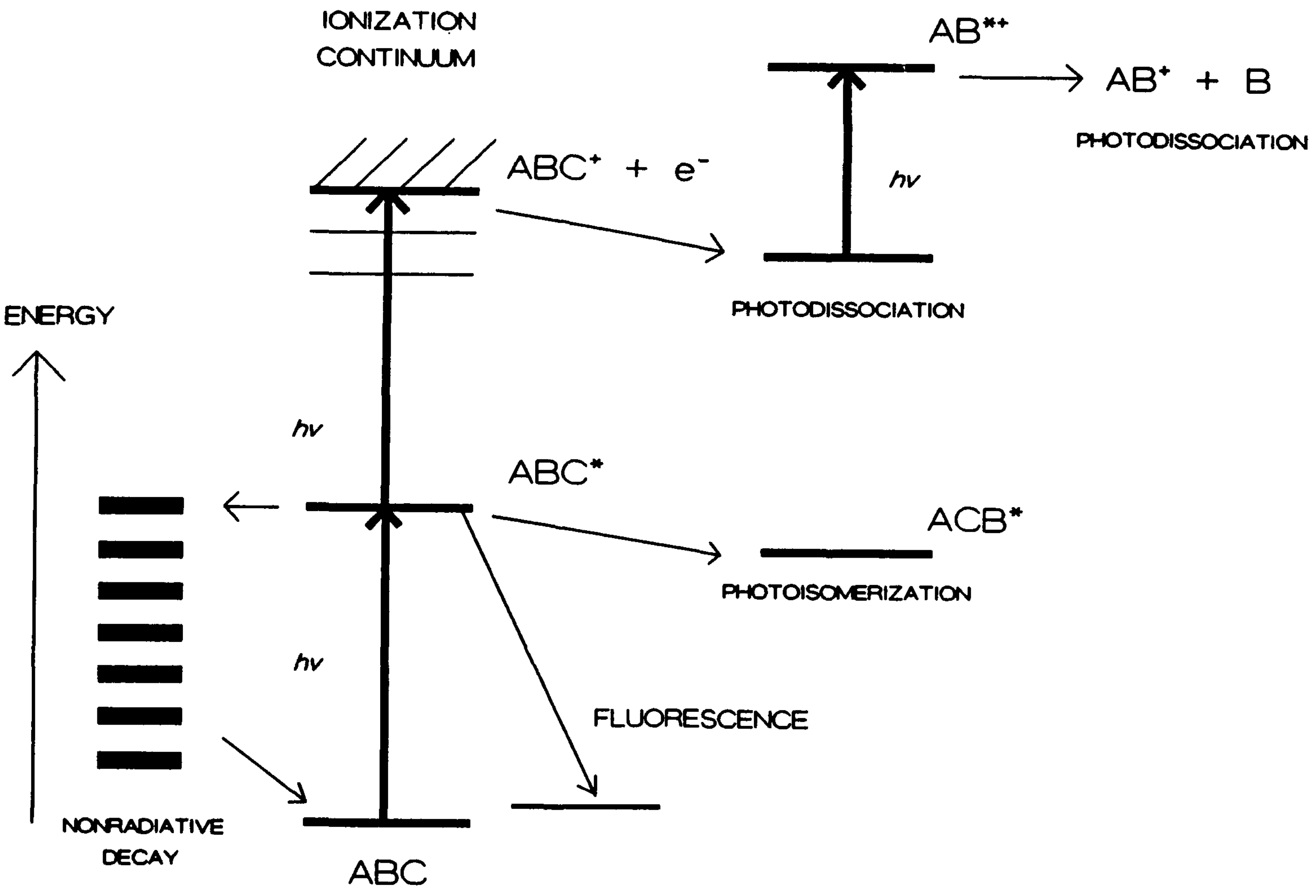
IONIZATION CONTINUUM
ABC⁺ + e⁻
AB*⁺
AB⁺ + B
PHOTODISSOCIATION
hν
PHOTODISSOCIATION
ENERGY
hν
ABC*
ACB*
PHOTOISOMERIZATION
hν
FLUORESCENCE
NONRADIATIVE DECAY
ABC

The absorption/ionization/photodissociation sequence is known as the "ladder switching" mechanism for UV laser induced multiphoton ionization.[10] MPI fragmentation occurs by multiple absorption/fragmentation steps along a ladder of consecutive and parallel reactions. The extent of fragmentation is controlled by laser intensity and wavelength selection.[5,10] The ability to control fragmentation is an important feature which allows the possibility to distinguish isomers or to selectively ionize components in a mixture. By careful choice of power and wavelength, compounds could be identified by their characteristic fragmentation patterns.

A second mechanism used to explain laser multiphoton ionization-dissociation (MPID) is the ladder mechanism, as discussed by El-Sayed et al.[11] In the ladder mechanism, only the parent species absorb photons and all fragment ions originate directly from excited states of the parent ions. In contrast, the ladder-switching mechanism permits larger fragment ions to absorb photons and directly produce smaller fragment ions, whereas all of the ladder mechanism fragment ions originate directly from the parent species. Fragmentation of the parent ion must occur within the laser pulse width to allow absorption of photons by the fragments and hence, ladder-switching, to occur. If dissociation occurs on a time scale longer than the pulse width, ladder-switching cannot occur. Thus, the ladder mechanism should be the dominant MPID process at extremely short (picosecond or less) pulse widths.[11]

## 3.5 ATTRIBUTES OF R2PI

Resonance with a real intermediate electronic state dramatically increases the probability of a two-photon transition, as demonstrated by quantum theory. Employment of R2PI techniques transform diffuse, nearly featureless one-photon ionization spectra into sharp, species distinctive spectra which display the intermediate state fine structure. Tunable near UV and visible wavelengths for MPI are efficiently, conveniently generated at high peak powers by readily available laser sources. Additionally, because ions and electrons are very efficiently detected, MPI is much more sensitive than direct absorption or even laser-induced fluorescence (LIF) in many cases.[6]

The potential for isomer-specific analysis and selective ionization of one component in a mixture makes R2PI of widespread interest to analytical chemists and environmental organizations. R2PI has several important attributes for mass spectrometry:[4]

1. Extent of fragmentation is controlled by laser power:
    a) "Soft" ionization produces primarily the molecular ion with little or no fragmentation (low to moderate laser power).
    b) "Hard" ionization produces increasing fragmentation as the power density increases (fragments as small as $C^+$ at very high powers).
2. Possible to generate optical absorption spectra of nonfluorescent compounds:
    a) Laser must provide sufficient up-pumping rate to ionize molecule prior to relaxation from excited state.
    b) Efficient ionization possible for nonfluorescing molecules with very short-lived (ps) excited states.
3. Ionization efficiencies are typically several percent within the laser beam volume while laser is on. Efficiency is limited by:
    a) Duty cycle of the laser
    b) Absorption cross-section of the molecule

### c) Radiationless transition rate of molecule

Advances in technology continue to improve the capabilities of R2PI. The introduction of shorter pulse width lasers has allowed researchers to compete with excited state relaxation and photodissociation processes. The lifetime of the intermediate electronic state that is initially excited in R2PI will significantly influence laser-induced ion yield. If the species has a subnanosecond radiative lifetime, which is very short compared to the widely used multinanosecond lasers, the molecule may relax after excitation and not be ionized, thus avoiding detection. By using light pulses of such short duration that relaxation or dissociation do not take place during the pulse itself, relaxation or dissociation can no longer affect the ionization process.

El-Sayed et al.[11] observed that the mechanism of laser MPID in benzaldehyde changed by shortening the excitation laser pulse width from 8 ns to 25 ps. The ion yield of the parent-like $C_7H_5O^+$ ion increased dramatically using the picosecond laser pulse width, implying a dominant ladder mechanism. More recently, Wilkerson and Reilly[12] employed a picosecond laser to effectively ionize monohalogenated benzenes (Cl, Br, and I), which are known to have subnanosecond lifetimes. Nanosecond laser pulses were unable to ionize the three halobenzenes under conditions of their experiments. Further advances in laser technology will continue to expand the range of accessible and observable molecular states.

The future of R2PI is bright. Laser technology is providing shorter pulse width lasers which can increase ionization efficiency and outrace radiationless transitions. Resolution continues to improve in mass spectrometers with the addition of pulsed nozzles and reflectrons in time-of-flight instruments. The use of a pulsed valve permits direct injection from 1 atm into vacuum, which has great potential for real environmental analysis. In addition, interfaces between multi-sector or FTMS instruments and laser ionization sources are coupling the selectivity of laser photoionization with a high resolution capability. Interfaces between laser ionization sources and capillary gas chromatography columns has expanded the variety of molecules which may be examined by R2PI methods. R2PI coupled with mass spectrometry has the potential to be a powerful tool for the detection and identification of trace pollutants in the complicated matrix of an environmental sample.

## 3.6 REFERENCES

1. Lin, S. H.; Fujimura, Y.; Neusser, H. J.; Schlag, E. W. *Multiphoton Spectroscopy of Molecules*, Academic Press, Inc., Orlando, Florida, 1984, Ch 1-2.

2. Goeppert-Mayer, M. *Ann. Phys. (Liepzieg)* **1931**, *9*, 273.

3. Boesl, U.; Neusser, H. J.; Schlag, E. W. *Z. Naturforsch. Teil A* **1978**, *33*, 1546.

4. Lubman, D. M. *Anal. Chem.* **1987**, *59*, 31A.

5. Flygare, W. H. *Molecular Structure and Dynamics*, Prentice-Hall, Engelwood Cliffs, New Jersey, 1978, Ch 1-3.

6. Steinfeld, J. I. *Molecules and Radiation: An Introduction to Modern Molecular Spectroscopy, Second Ed.*, The MIT Press, Cambridge, Mass., 1986, Ch 13.

7. McQuarrie, D. A. *Statistical Mechanics*, Harper & Row, New York, 1976, App F.

8. Andrews, D. L. *Lasers in Chemistry*, Springer-Verlag Berlin - Heidelberg, GDR, 1986, Ch 5.

9. Rebentrost, F. *Multiphoton Ionization and Fragmentation of Polyatomic Molecules*, pp. 161-169 in Laser Applications in Chemistry, K. L. Kompa and J. Wanner, Eds., Plenum Press, New York, 1984.

10. Kompa, K. L.; Wanner J. *Introduction*, pp. 1-11 in Laser Applications in Chemistry, K. L. Kompa and J. Wanner, Eds., Plenum Press, New York, 1984.

11. Yang, J.J.; Gobeli, D. A.; El-Sayed, M. A. *J. Phys. Chem.* **1985**, *89*, 3426.

12. Wilkerson, C. W.; Reilly, J. P. *Anal. Chem.* **1990**, *62*, 1804.

# CHAPTER 4

## Experimental Apparatus

### 4.1 INTRODUCTION

This chapter provides an overall description of the experimental apparatus used in the laser desorption-laser photoionization mass spectrometry (LDLPMS) studies of nitro-PAH compounds. Discussion includes a description of the experimental hardware and general experimental conditions of the LDLPMS system.[1] Supporting mass spectrometry studies of the nitro-PAH standards were performed on various instruments located at the Facility for Advanced Instrumentation (FAI) in cooperation with Dr. A. D. Jones. The final two sections are devoted to descriptions of the GC/MS, FAB, and EI MS/MS instrumentation and experiments.

### 4.2 LDLPMS INSTRUMENTATION

The block diagram shown in Figure 4.1 depicts the major components of the experimental apparatus used for the present study. At the core of the LDLPMS instrumentation is a custom-built TOF mass spectrometer operating in the linear mode.[2,3] A more detailed side view of the spectrometer is presented in Figure 4.2. The sample probe is inserted through a custom-designed fast load-lock assembly which eliminates the need to break vacuum while changing samples. The probe tip is situated between the repeller and extractor plates of the ion optics housed in the source region, and is in electrical contact with the repeller plate via an extension tab. The source region is fitted with S1-UV quartz and ZnSe (or $BaF_2$) optical windows for transmission of the UV and

**Figure 4.1** Block diagram depicting the major components of the laser desorption-laser photoionization time-of-flight mass spectrometry (LDLPMS) apparatus.

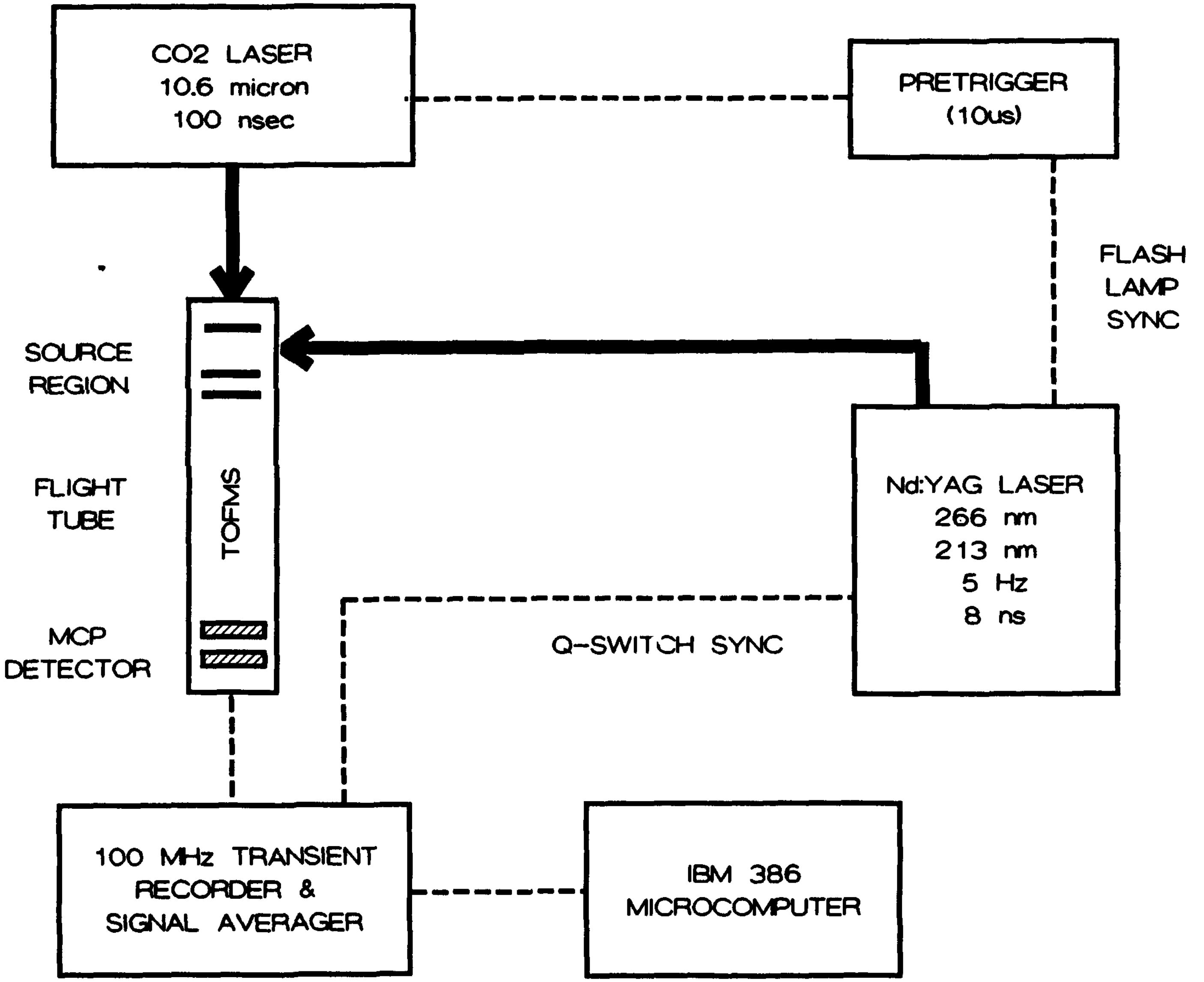

CO2 LASER
10.6 micron
100 nsec
PRETRIGGER
(10us)
FLASH
LAMP
SYNC
SOURCE
REGION
FLIGHT
TUBE
TOFMS
MCP
DETECTOR
Nd:YAG LASER
266 nm
213 nm
5 Hz
8 ns
Q-SWITCH SYNC
100 MHz TRANSIENT
RECORDER &
SIGNAL AVERAGER
IBM 386
MICROCOMPUTER

**Figure 4.2** Detailed side-view of the custom-built time-of-flight mass spectrometer used for the current study.

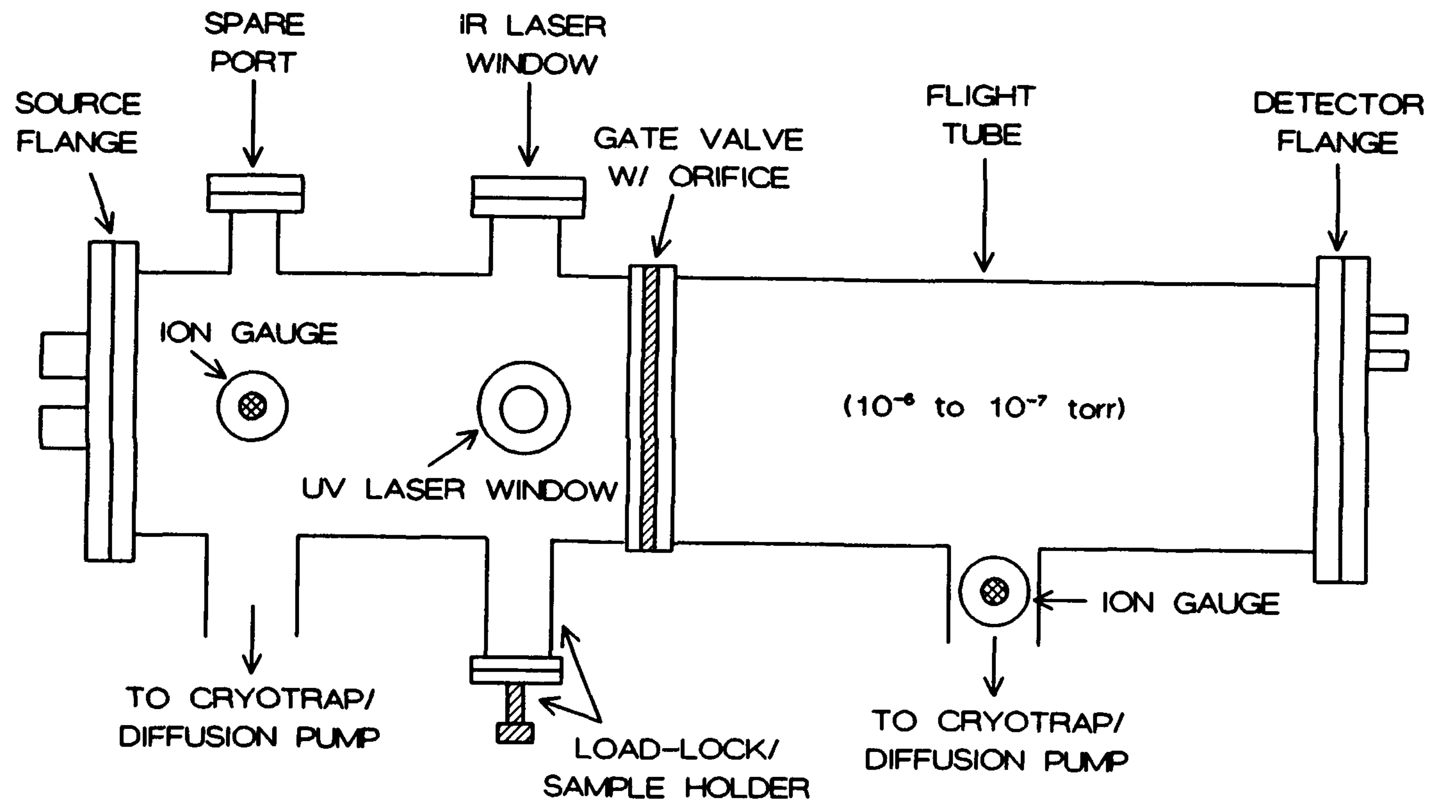
SPARE PORT
IR LASER WINDOW
SOURCE FLANGE
GATE VALVE W/ ORIFICE
FLIGHT TUBE
DETECTOR FLANGE
ION GAUGE
UV LASER WINDOW
(10$^{-6}$ to 10$^{-7}$ torr)
ION GAUGE
TO CRYOTRAP/ DIFFUSION PUMP
LOAD-LOCK/ SAMPLE HOLDER
TO CRYOTRAP/ DIFFUSION PUMP

IR laser beams, respectively. Two 4-inch oil diffusion pumps equipped with cryotraps (liquid $N_2$ cooled) separately pump down the source and flight tube regions to an operating vacuum of ~$10^{-6}$ torr.

Pulsed IR radiation at 10.6 microns is generated by a Lumonics Model 934 TEA $CO_2$ laser. The IR pulse duration is 100 nsec (FWHM) with a lower energy 2 μsec tail. The beam is attenuated to approximately 10 mJ/pulse and focussed through a 200 mm focal length ZnSe lens into the source region. Beam diameter at the sample is 2 $mm^2$, yielding power density of approximately $5 \times 10^6$ $W/cm^2$ when operating at a pulse rate of 5 Hz. Power measurements of the IR beam are made just prior to focussing using a Scientech Inc. Model 37-4002 power meter.

Pulsed UV radiation is produced by a Q-switched Quanta Ray DCR-3 Nd:YAG laser with an 8 nsec pulse width. The 1064 nm Nd:YAG fundamental is frequency quadrupled in KD*P to obtain 266 nm radiation. Sum mixing of the 1064 nm fundamental and the 266 nm fourth harmonic in BBO provides UV radiation at 213 nm.[4] The UV laser beam is narrowed through an iris to a diameter of 2 mm to reduce beam spread. Just prior to focussing through a 250 mm focal length S1-UV quartz lens, the beam diameter is 4 mm. At the focal point, the beam diameter is on the order of 10 microns, delivering power density in the range $10^8$ - $10^9$ $W/cm^2$ when the laser is operated at 5 Hz (See appendix A). UV beam power is measured prior to the spectrometer entrance window using a Molectron Model J9LP Pyroelectric Joulemeter interfaced to a PcJ meter (Q&A Instruments). Beam paths of both lasers in the source region are discussed in the next sections.

Positive ions formed by the LDLP process are accelerated through the ion optics into the flight tube and continue at constant velocity until impinging on the dual microchannel plate (MCP) detector. The detector, Comstock Model CP-602, is mounted in an off-axis geometry requiring that a deflection potential be applied to the ions as they exit the source region. The off-axis geometry reduces background noise by minimizing the transmission of neutral molecules to the detector, as only ions are directed toward the detector by the deflection potential.

The current generated at the MCP detector is 50-ohm terminated into a 100 MHz DSP Model 2001AS Transient Recorder and digitized with 8-bit precision. In a time window of 40 μsec, 32 KWord scans with a sampling interval of 10 nsec are collected. In a typical experiment, data is collected and signal averaged by a DSP Model 4101 Averaging Memory over 100 to 500 laser pulses, then transferred by a CAMAC interface to an Everex 386 microcomputer. Data acquisition and subsequent analysis are controlled by software developed in-house.[2] Raw data is collected as signal intensity versus flight time. The collected data is converted and stored as intensity versus flight time squared because mass-to-charge ratio is directly proportional to the square of flight time (see Chapter 2).

Figure 4.3 is a detailed timing diagram of the signals required for event synchronization in the LDLPMS experiment. Time t = 0 corresponds to the firing of the flashlamps in the Nd:YAG laser. The flashlamp sync is delayed by a custom-built timing circuit which adjusts the pretrigger for the $CO_2$ laser. At t = 200 μsec, the Nd:YAG laser Q-switch fires, simultaneously allowing the laser to fire. The relative arrival times of the IR and UV laser beams at the source can be observed with a photodiode detector and adjusted to obtain the optimum 10 μsec delay using the pretrigger circuit. The Q-switch

**Figure 4.3** Schematic showing the synchronization of events in an LDLPMS experiment, with time t = 0 corresponding to the firing of the flashlamps in the Nd:YAG laser.

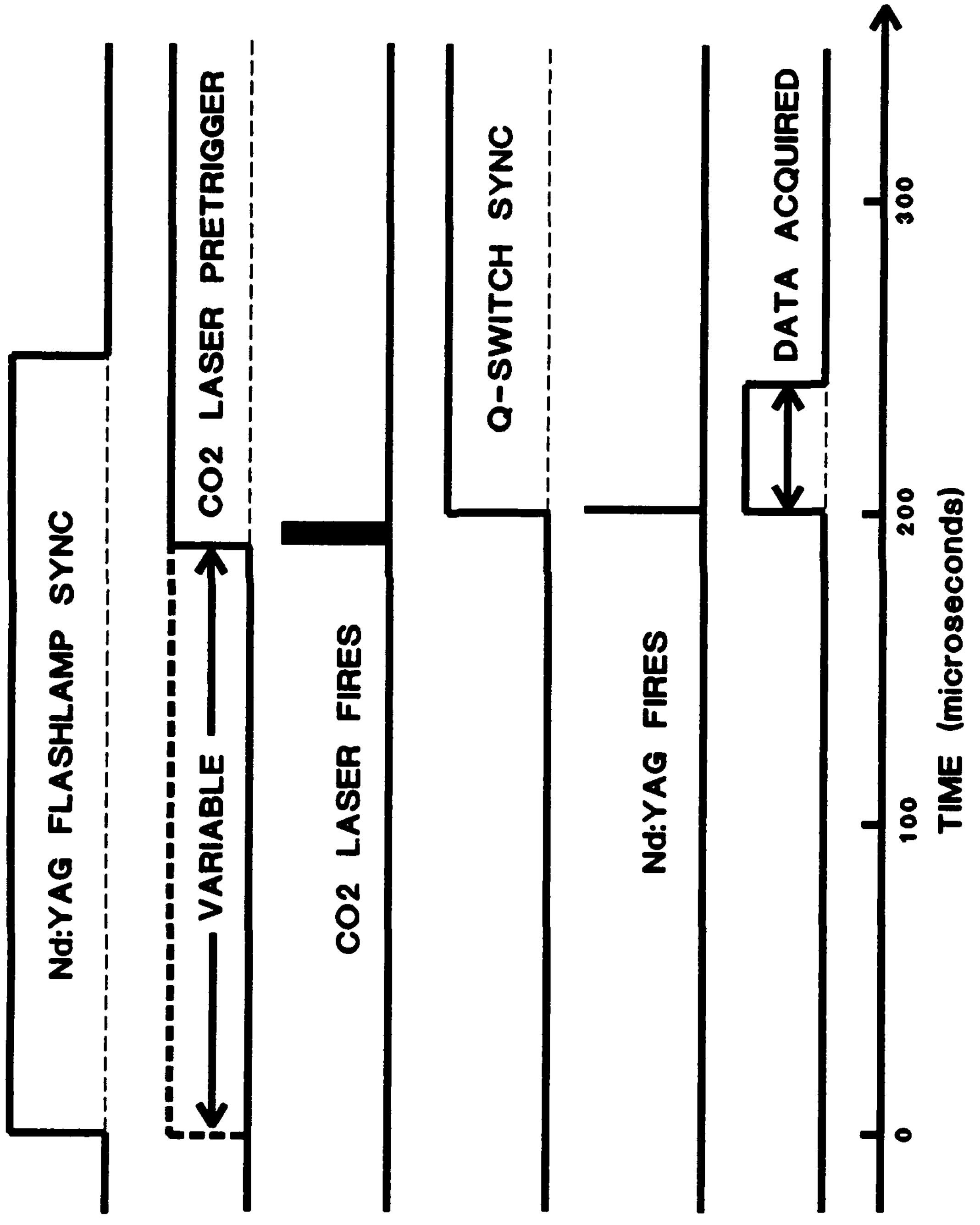
Nd:YAG FLASHLAMP SYNC
VARIABLE
CO2 LASER PRETRIGGER
CO2 LASER FIRES
Q-SWITCH SYNC
Nd:YAG FIRES
DATA ACQUIRED
0
100
200
300
TIME (microseconds)

sync is used to trigger the data acquisition electronics and lets the time origin in the TOF spectra correspond to the arrival time of the UV laser beam at the source.

## 4.3 SINGLE-STEP LDLP EXPERIMENTS

The probe position and beam path geometry within the source region for a single-step LDLP experiment are illustrated in Figure 4.4. This figure also details the repeller, extractor, accelerator, and deflector potentials used under normal experimental conditions. The aluminum probe tip has a flattened face which is positioned perpendicular to the flight tube axis. The probe can be raised or lowered externally to allow analysis at different locations on the same sample. The electrical contact between the probe tip and the repeller plate ensures that the electric field gradient remains uniform.

A typical sample is prepared by depositing a 20-30 μl aliquot of a standard solution via syringe, directly onto the flattened aluminum probe face. The sample is allowed to air dry, forming a thin (< 1 mm) solid layer, and is then inserted into the source region. The nitro-PAH and nitrobenzocoumarin standards, listed in Table 4.1 along with their purities, were obtained from Aldrich Chemical Co. and used as received. Sample solutions are prepared at concentrations of 5-10 mg/ml in $CH_2Cl_2$. The relatively high concentration allows the solid layer to be thick enough to minimize interference caused by unintentionally desorbed aluminum ions.

Pulsed UV radiation at 213 nm or 266 nm is focussed into the source region perpendicular to the flight tube axis, reducing the initial spatial spread at ion formation. The UV beam path is directed such that the laser beam grazes the surface of the sample. It is possible that a laser-induced thermal desorption (LITD) occurs at the fringe of the beam waist. The LITD process imparts enough energy to the desorbed molecules to move

**Figure 4.4** Diagram of the source region in the TOFMS illustrating the desorption geometry for a single-step laser photoionization experiment.

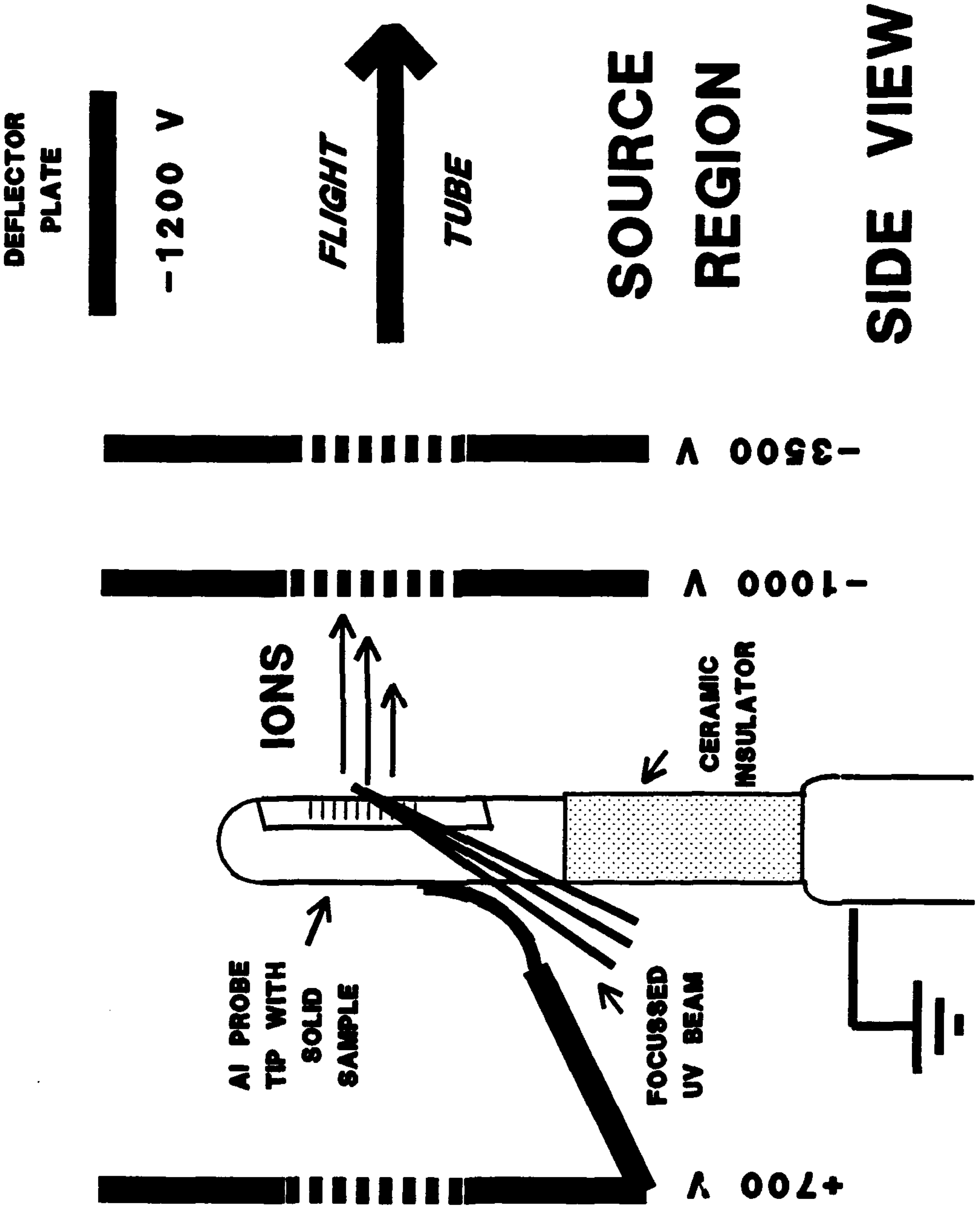
SOURCE REGION
SIDE VIEW
DEFLECTOR PLATE
-1200 V
FLIGHT TUBE
-3500 V
-1000 V
IONS
CERAMIC INSULATOR
Al PROBE TIP WITH SOLID SAMPLE
FOCUSSED UV BEAM
+700 V

**Table 4.1** Properties of nitro-PAH and nitrated heterocyclic compounds showing purity, molecular weight, formula and structure of each nitro-PAH and nitrobenzocoumarin standard used in the current study.

**Table 4.1** Properties of Nitro-PAH and Nitrated Heterocyclic Compounds

| COMPOUND (PURITY) | MOLECULAR FORMULA | MOLECULAR WEIGHT | MOLECULAR STRUCTURE |
|---|---|---|---|
| 9-NITRO-ANTHRACENE (97%) | $C_{14}H_9NO_2$ | 223 | 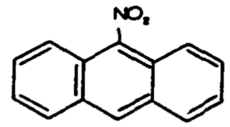 |
| 6-NITRO-3,4-BENZOCOUMARIN (98%) | $C_{13}H_7NO_4$ | 241 | 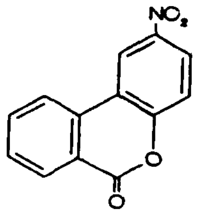 |
| 7-NITRO-3,4-BENZOCOUMARIN (98%) | $C_{13}H_7NO_4$ | 241 | 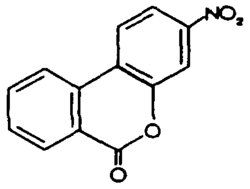 |
| 2-NITRO-FLUORENE (98%) | $C_{13}H_9NO_2$ | 211 | 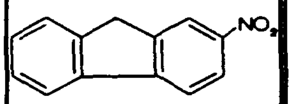 |
| 2-NITRO-9-FLUORENONE (99%) | $C_{13}H_7NO_3$ | 225 | 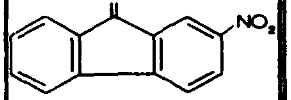 |
| 1-NITROPYRENE (97%) | $C_{16}H_9NO_2$ | 247 | 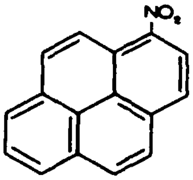 |

them a few microns from the surface and into a region of higher power density. Positive ions then form just above the surface in the high-density plume by multiphoton ionization (MPI), chemical ionization, and/or collision processes.[5] Laser energy generally ranges from 5-20 μJ/pulse, yielding maximum laser power densities on the order of $10^8$ - $10^9$ W/cm$^2$ at the focus. Positive ions formed during each laser pulse are accelerated into the field-free flight tube and drift until impacting the (MCP) detector.

## 4.4 TWO-STEP LDLP EXPERIMENTS

A two-step LDLP experiment separates the desorption and ionization steps by using the IR laser to induce thermal desorption and the UV laser to effect MPI in the gas phase molecules. Figure 4.5 depicts the IR and UV beam path geometry within the source region and lists the grid potentials used under normal experimental conditions. The aluminum probe tip has a flattened face which is positioned perpendicular to the flight tube axis. The probe can be raised or lowered externally to allow analysis at different locations on the same sample. The electrical contact between the repeller plate and the probe tip ensures that the electric field gradient remains uniform.

Glass fiber air-sampling filters (Gelman type A/E) are often used as the sample substrate in these two-step experiments. Sample preparation involves dropping approximately 50 μl of sample solution by syringe onto a ~1 cm$^2$ piece of Gelman filter and allowing the filter to air dry. The filter is then attached to the flattened probe face with double-sided sticky tape and inserted into the source region. The nitro-PAH standards, listed in Table 4.1 along with their purities, were obtained from Aldrich Chemical Co. and used as received. Standard sample solutions are prepared at concentrations of 5-10 mg/ml in $CH_2Cl_2$. Samples of NIST SRM 1650 diesel particulate

**Figure 4.5** Side view of the source region in the TOFMS depicting the IR and UV beam path geometry in a two-step laser desorption-laser photoionization experiment.

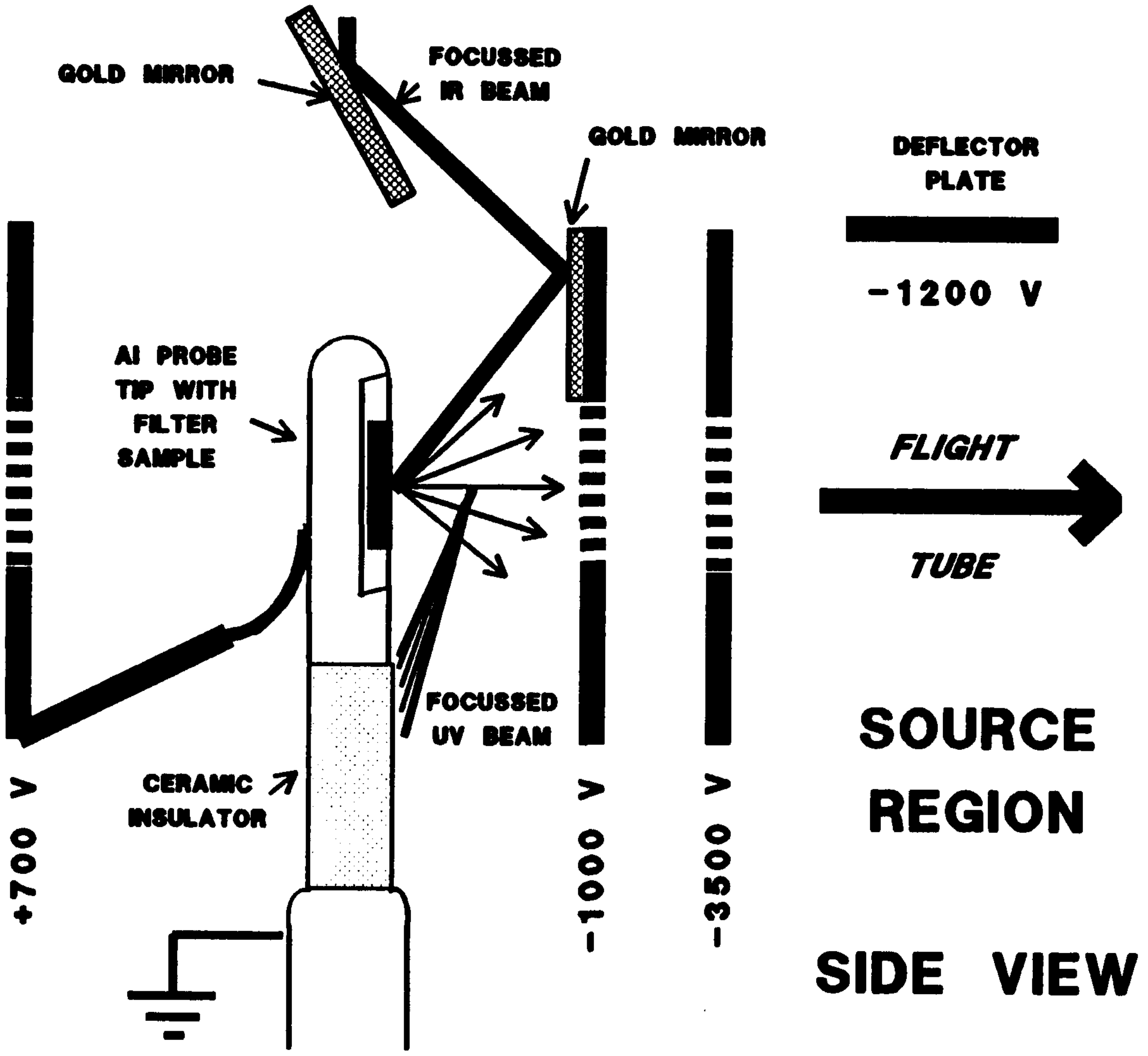
GOLD MIRROR
FOCUSSED IR BEAM
GOLD MIRROR
DEFLECTOR PLATE
-1200 V
AI PROBE TIP WITH FILTER SAMPLE
FLIGHT
TUBE
FOCUSSED UV BEAM
CERAMIC INSULATOR
+700 V
-1000 V
-3500 V
SOURCE REGION
SIDE VIEW

matter are prepared in two ways. A few milligrams of the particulate is smeared directly onto a Gelman filter, or the concentrated extract collected from a Soxhlet extraction is dropped by syringe onto a Gelman filter.

The IR beam from the $CO_2$ laser is focussed into the source region from above and is directed onto the sample surface by two intra-cavity gold-plated mirrors. These mirrors are positioned such that the IR beam impinges on the surface at an approximate 30° angle. The IR laser power density is on the order of $10^6$ W/cm$^2$. The IR laser pulse generates a thermally desorbed plume of primarily neutral molecules which have their primary velocity component along the flight tube axis. Approximately 10μsec after arrival of the IR beam, the focussed UV beam is pulsed into the plume of desorbed neutrals to effect MPI. The UV beam path is perpendicular to the flight tube axis and approximately 1 mm from the filter surface. The vertical and horizontal positions of the two beams are adjusted externally to optimize the ion yield.[1] Positive ions formed in the source region are accelerated into the flight tube and drift until impacting the MCP detector.

## 4.5 MASS CALIBRATION OF LDLPMS SPECTRA

The raw data of an LDLPMS experiment is collected as signal intensity versus flight time. Because mass-to-charge ratio (m/z) is directly proportional to the square of the flight time, the data files are converted and stored as intensity and flight time squared data-pairs. Software developed in-house allows mass calibration of each spectra by fitting the flight time squared values for the lower m/z ion fragments to a second order polynomial and extrapolating to the higher m/z ions. A sample calibration using a typical single-step spectrum of pyrene is demonstrated in Appendix B, and the significance of the fitting constants is explained.

## 4.6 GC/MS EXPERIMENTS

Analysis of the standard reference compounds in Table 4.1 by gas chromatography/ mass spectrometry (GC/MS) was performed at the Facility for Advanced Instrumentation (FAI) at the University of California, Davis, in cooperation with Dr. A. Daniel Jones. Electron ionization (EI) spectra were obtained for all compounds and negative ion chemical ionization ($CI^-$) spectra were obtained for 9-nitroanthracene and 6-nitro-3,4-benzocoumarin (2-nitro-6H-dibenzo[b,d]pyran-6-one). Appendix C contains the total ion chromatogram (TIC) and the selected ion integrations (SII) used for comparison with our laser photoionization mass spectra.

All spectra were acquired on a Hewlett-Packard 5890 GC equipped with a 15 meter, 0.25 mm i.d. DB-5 fused silica capillary column and interfaced to a VG Trio 2 mass spectrometer. The injector temperature was 275°C and the transfer line temperature was 285°C. Approximately 2µl of sample solution, concentration ≈100µg/ml in $CH_2Cl_2$, were injected on column. The column was held at 40°C for one minute prior to ramping at 10°C/ min to a final temperature of 285°C where it held for 5 minutes. Helium was the carrier gas at a linear velocity of 35 cm/sec.

The same temperature program (NITRO) was used for both EI and $CI^-$ experiments. However in EI, positive ions were produced by a 70eV beam of electrons via the reaction

$$M + e^- \rightarrow M^+ + 2e^-$$

EI produced generally strong molecular ion and ($M-NO_2$) ion peaks for all nitro-PAH along with extensive middle and lower mass fragments which help determine fragmentation pathways.

In $CI^-$, methane was used as the bath gas at a source pressure of ~$10^{-3}$ torr, measured at the source manifold. Negative molecular ions were formed by the resonant electron-capture reaction:

$$M + e^- \rightarrow M^-$$

Nitro-PAH have high electron-affinity and the two spectra acquired showed intense molecular anion peaks accompanied by intense $NO_2^-$ anion peaks. However, these spectra contained little structural information.

## 4.7 FAB AND EI MS/MS EXPERIMENTS

Fast atom bombardment (FAB) and electron ionization MS/MS experiments were performed at the FAI by Dr. A. Daniel Jones. Appendix D contains all the FAB spectra and Appendix E contains all the EI MS/MS spectra acquired through these experiments. All mass spectrometric measurements were performed in a VG ZAB-HS-2F mass spectrometer with BE geometry. Sample concentrations were 1 mg/ml in $CH_2Cl_2$.

An Ion Tech FAB gun operating at 8 keV with Xe gas produced the secondary neutral beam for the FAB experiments. A 3μl aliquot of the solution was deposited onto a stainless steel probe and evacuated in the foreline. After pressure stabilization, the probe was inserted into position and bombarded with the neutral Xe beam. The source pressure was maintained at approximately $10^{-5}$ mbar during the experiments. FAB spectra were obtained for all six standards deposited onto the bare probe and for selected compounds using a 3-nitrobenzylalcohol (NBA) or glycerol matrix.

EI MS/MS experiments used the same instrument to perform daughter ion, parent ion, and neutral loss analysis of selected standards.[6] A 2μl aliquot of sample solution was injected into a quartz crucible and introduced into the source via the solids probe. The ions formed by 70eV electron ionization were accelerated by 8 keV toward the magnetic sector. Fragmentation occurring in the first field-free region of the instrument was studied by performing scans of constant B/E (daughter scans), constant $B^2/E$ (parent scans), and constant $(B/E^1)^2/(1-E^1)$ for neutral loss scans. Nitrogen was introduced into the first field-free region at a pressure of $1 \times 10^{-5}$ mbar. The parent ion, daughter ion, and constant neutral loss experiments were particularly helpful in determining the fragmentation pathway of the nitrobenzocoumarin compounds.

## 4.8 REFERENCES

1. Smith, C. H.; Jones, A. D.; Kelly, P. B. California Air Resources Board Report # A9-32-099, Apr. 1992.

2. Young, M. K. G. *Characterization of Polycyclic Aromatic Hydrocarbons and Chlorinated Polycyclic Aromatic Hydrocarbons in Soots by Laser Desorption-Laser Photoionization Mass Spectrometry*, Dissertation, (University of California, Davis), Dec., 1991.

3. Young, M. K. G.; Jones, A. D.; Kelly, P. B. Proceedings of the 39th ASMS Conference on Mass Spectrometry and Allied Topics, Nashville, TN., May 19-24, 1991, p. 342.

4. Hudson, B.; Kelly, P.B.; Ziegler, L. D.; Desiderio, R. A.; Gerrity, D. P.; Hess, W.; Bates, R. "Far Ultraviolet Laser Resonance Raman Studies of Electronic Excitations," pp. 1-32 in *Advances in Laser Spectroscopy: Volume 3*, B. A. Garetz and J. R. Lombardi, Eds., John Wiley & Sons Ltd., Chichester, Great Britain, 1986.

5. Land, D.P.; Wang, D. T.; Tai, T.; Sherman, M. G.; Hemminger, J. C.; McIver, R. T. Jr. "Postionization of Laser-Desrobed Neutrals for the Analysis of Molecular Adsorbates on Surfaces" pp. 157-177 in *Lasers in Mass Spectrometry*, D. M. Lubman, Ed., Oxford University Press, New York, 1990.

6. Jennings, K. R.; Mason, R. S. "Tandem Mass Spectrometry Utilizing Linked Scanning of Double-Focusing[sic] Instruments" pp. 197-222 in *Tandem Mass Spectrometry*, F. W. McLafferty, Ed., John Wiley & Sons, Inc., New York, 1983.

# CHAPTER 5

## Laser Photoionization Time-of-Flight Mass Spectrometry of Nitrated Polycyclic Aromatic Hydrocarbons

### 5.1 ABSTRACT

The mass spectra of several nitrated polycyclic aromatic hydrocarbons (nitro-PAH) have been investigated by single-step laser photoionization time-of-flight mass spectrometry. Pulsed UV radiation at 266 nm or 213 nm was used for the desorption and ionization of the solid sample deposited on an aluminum probe. Four nitro-PAH standards have been examined: 9-nitroanthracene, 1-nitropyrene, 2-nitro-9-fluorenone, and 2-nitrofluorene. Positive molecular ion was observed for each nitro-PAH, generally with the stronger signal appearing in the 213 nm photoionization spectra. A very strong $[M\text{-}NO]^+$ ion peak was observed in all spectra which was often the base peak. An intense $NO^+$ ion peak accompanies the $[M\text{-}NO]^+$ signal at 213 nm, but is only weakly present at 266 nm. The laser mass spectra of 2-nitro-9-fluorenone show an interesting extension of the general nitro-PAH fragmentation pathway observed in the current study. Comparison of the various spectra suggests that nitro-PAH undergo an excited state nitro-nitrite photorearrangement prior to releasing NO, which is subsequently ionized by a multiphoton ionization process. Photorearrangement of nitro-PAH may play a significant role in their atmospheric transformation reactions.

### 5.2 INTRODUCTION

The analytical chemistry of nitrated polycyclic aromatic hydrocarbons (nitro-PAH) is of widespread interest due to the highly mutagenic properties of this chemical class.

Nitro-PAH are derivatives of PAH, which are abundant in fossil fuels and are the incomplete combustion products of organic materials. Direct emission into the atmosphere from combustion sources distributes PAH between the gas and particle phases.[1] Nitro-PAH present in direct emissions are primarily the electrophilic nitration products resulting from adsorbed phase reactions of PAH with $NO_x$ and $HNO_3$. Nitro-PAH found in the atmosphere are often the result of an atmospheric transformation of the parent PAH by the gas-phase reaction with OH radical in the presence of $NO_x$ pollutants.[2] Once formed, atmospheric nitro-PAH can readily condense on respirable particulate matter.

Nitro-PAH have been determined in a variety of environmental samples including diesel exhaust,[3-9] urban and indoor air particulate,[10-13] aluminum smelter effluent,[14] coal fly ash,[15] and wood and cigarette smoke condensates.[16,17] Determinations of nitro-PAH in particulate matter have generally involved organic solvent extraction, HPLC fractionation, and identification by various low and high resolution GC/MS techniques: methods which tend to be time-consuming, labor-intensive and expensive. The concentration of nitro-PAH in environmental samples is typically one to two orders of magnitude less than that of the unsubstituted PAH present. Low concentrations coupled with their ubiquitous presence and potent direct-acting mutagenicity underscore the importance of developing highly sensitive and selective methods for determination of nitro-PAH in environmental samples. Laser photoionization mass spectrometry (LPMS) offers the potential for such sensitive, selective determinations.

The study of laser-induced dissociation, ionization, and fragmentation in nitroaromatic molecules has generally been limited to nitrobenzene and its derivatives. In experiments performed by Apel and Nogar[18] and Marshall et al.,[19,20] the intense $NO^+$

ion peak observed in the laser photoionization mass spectra of nitrobenzene was attributed to predissociation of the parent to lose $NO_2$ , then predissociation of $NO_2$ and subsequent two-photon ionization of the NO fragment. Molecular ion was not observed and the base peak was either $[M-NO_2]^+$ or $NO^+$, depending on experimental conditions. Lubman et al.[21] were able to observe molecular ion for a number of substituted nitrobenzenes using laser ionization at 213 nm or 266 nm under atmospheric pressure conditions. Photoionization of nitro-containing compounds is a challenge owing to their fragility and propensity to predissociate upon irradiation with UV light. Lubman attributes the successful "soft" ionization (i.e. little fragmentation of the parent ion) of the fragile nitroaromatics to the moderating effect of He background gas, which has a low collisional effectiveness. A very recent study on the photodissociation of nitrobenzene by Huey et al.[22] identified three primary photodissociation pathways for the molecule. An observed competition between the production of NO and $NO_2$ (for $\lambda \geq 280$ nm) allowed the possibility of a nitro-nitrite rearrangement mechanism, as both products could be formed through a common nitrite transition state.

In order to examine the application of laser photoionization time-of-flight mass spectrometry (LPMS) to characterization and analysis of nitro-PAH, mass spectra have been obtained at 266 nm and 213 nm for four nitro-PAH standards: 9-nitroanthracene, 1-nitropyrene, 2-nitro-9-fluorenone and 2-nitrofluorene. Molecular ion was observed for each nitro-PAH, along with a very strong $[M-NO]^+$ ion peak which was often the base peak. An intense $NO^+$ ion peak appears in the spectra at 213 nm, but is only weakly present at 266 nm. Similarities in the spectra of these four nitro-PAH indicate competing photofragmentation pathways which could be characteristic of other highly-conjugated nitro-containing compounds. Acquisition of representative spectra and identification of characteristic photofragments are prerequisites for application of the LPMS method to determination of nitro-PAH in environmental samples.

## 5.3 EXPERIMENTAL

Nitro-PAH standards were purchased from Aldrich Chemical Co., and were used without further purification. The compounds studied were (molecular weight in parenthesis) 9-nitroanthracene (223), 1-nitropyrene (247), 2-nitro-9-fluorenone (225) and 2-nitrofluorene(211). Molecular structure and stated purity are given in Table 5.1.

Laser photoionization mass spectra are obtained using a custom-built time-of-flight mass spectrometer operating in the linear mode.[23,24] The sample probe is inserted into the source region through a custom-designed fast load-lock assembly which positions the aluminum probe tip between the extractor and repeller plates of the Wiley-McLaren[25] based two-stage ion optics. The aluminum probe tip has a flattened face which is positioned perpendicular to the flight tube axis. The probe can be raised and lowered externally to allow analysis at different locations on the same sample. The source region is fitted with S1-UV quartz windows to allow transmission of the UV laser beam. Two oil diffusion pumps equipped with cryotraps separately pump down the source and flight tube regions to an operating vacuum of ~ $10^{-6}$ torr.

Sample solutions of the nitro-PAH standards are prepared at concentrations of 5-10 mg/ml in $CH_2Cl_2$. A typical sample is prepared by depositing a 20-30 μl aliquot of a standard solution, via syringe, directly onto the flattened probe face and allowing it to air dry. The relatively high concentration of the standard solution yields a residual solid layer thick enough to minimize interference from aluminum ion formation during

**Table 5.1** Properties of nitro-PAH showing purity, molecular weight, formula and structure of each nitro-PAH compound used in the current study.

Table 5.1 Properties of Nitro-PAH Standards

| COMPOUND (PURITY) | MOLECULAR FORMULA | MOLECULAR WEIGHT | MOLECULAR STRUCTURE |
|---|---|---|---|
| 9-NITRO-ANTHRACENE (97%) | $C_{14}H_9NO_2$ | 223 | 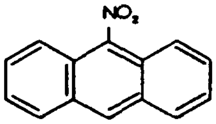 |
| 1-NITROPYRENE (97%) | $C_{16}H_9NO_2$ | 247 | 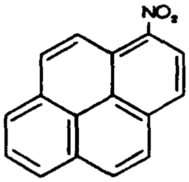 |
| 2-NITRO-9-FLUORENONE (99%) | $C_{13}H_7NO_3$ | 225 | 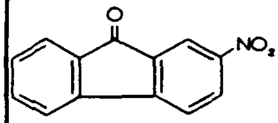 |
| 2-NITRO-FLUORENE (98%) | $C_{13}H_9NO_2$ | 211 | 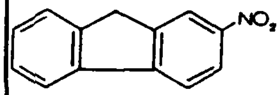 |

ionization of the sample.

Pulsed UV radiation at 266 nm is produced using the fourth harmonic of a Q-switched Quanta Ray DCR-3 Nd:YAG laser with an 8 ns pulse width. Sum mixing of the Nd:YAG laser's 1064 nm fundamental and the 266 nm fourth harmonic in BBO (β - barium borate crystal) generates the 213 nm photons.[26] The UV laser beam is focussed into the source region through a 250 mm S1-UV quartz lens, which is also used to direct the UV beam path such that the laser beam grazes the surface of the sample. Laser energy is measured just prior to the spectrometer entrance window by a Molectron Model J9LP Joulemeter interfaced to a PcJ meter (Q&A Instruments).

The laser-induced thermal desorption induced at the fringe of the beam waist imparts enough energy to the desorbed molecules to move them a few microns from the surface, and into a region of higher power density. Positive ions form just above the surface in the high-density plume by multiphoton ionization, chemical ionization, and/or collision processes. Laser energy typically ranges from 5-20 μJ/pulse while operating at 5 Hz, yielding maximum power densities on the order of $10^8$ - $10^9$ W/cm$^2$ at the focus.

Positive ions formed during each laser pulse are accelerated into the flight tube and drift until impinging on the dual microchannel plate (MCP) detector. Current generated at the MCP detector is 50-ohm terminated into a 100 MHz DSP Model 2001AS Transient Recorder and digitized with 8-bit precision. In a typical experiment, data is collected and signal averaged by a DSP Model 4101 Averaging Memory over 100-200 laser pulses, then transferred by a CAMAC interface to an Everex 386 microcomputer. Data acquisition and subsequent analysis are controlled by software developed in-house.[23,27] The Q-switch sync is used to trigger the data acuqisition electronics, allowing the time origin in the mass spectra correspond to arrival of the UV beam at the source.

## 5.4 RESULTS AND DISCUSSION

### 5.4.1 Laser Photoionization of 9-nitroanthracene and 1-nitropyrene

The molecular structures, formulas and weights of all four nitro-PAH examined are collected in Table 5.1 for convenient reference. The laser photoionization mass spectra of 9-nitroanthracene and 1-nitropyrene possess many similar features (as might be expected), and easily lend to side-by-side interpretation. Figure 5.1 presents the photoionization mass spectra of 9-nitroanthracene at 213 nm and 266 nm. Molecular ion is observed in both spectra, although slightly attenuated under 266 nm irradiation. The base peak in each spectra corresponds to the $[M\text{-}NO]^+$ fragment ion. Other significant high mass fragments are $[M\text{-}NO_2]^+$ and $[M\text{-}NO\text{-}CO]^+$ ions. The $NO^+$ ion is a prominent fragment in the 213 nm spectrum of 9-nitroanthracene, but was not observed in the 266 nm spectrum.

The "dimers" labelled in the spectra are dimers of nitroanthracene fragments and bimolecular photoproducts produced on the surface during the desorption process. The most probable identities of the three most prominent "dimer" peaks are $C_{28}H_{18}$ (m/z 354: dimer anthracene), $C_{28}H_{18}O$ (m/z 370) and $C_{28}H_{16}O_2$ (m/z 384). Observation of dimers and photoproducts in the mass spectra indicates the possibility of condensed-phase chemistry occurring on the surface as well as bimolecular interactions occurring in the high-density desorption plume.

The photoionization mass spectra of 1-nitropyrene obtained at 213 nm and 266 nm are shown in Figure 5.2. Molecular ion is observed in both spectra and is a strong peak in the 213 nm spectrum. As in the 9-nitroanthracene spectra, the base peak in the spectra

**Figure 5.1** Single-step laser photoionization mass spectra of 9-nitroanthracene obtained at 213 nm and 266 nm.

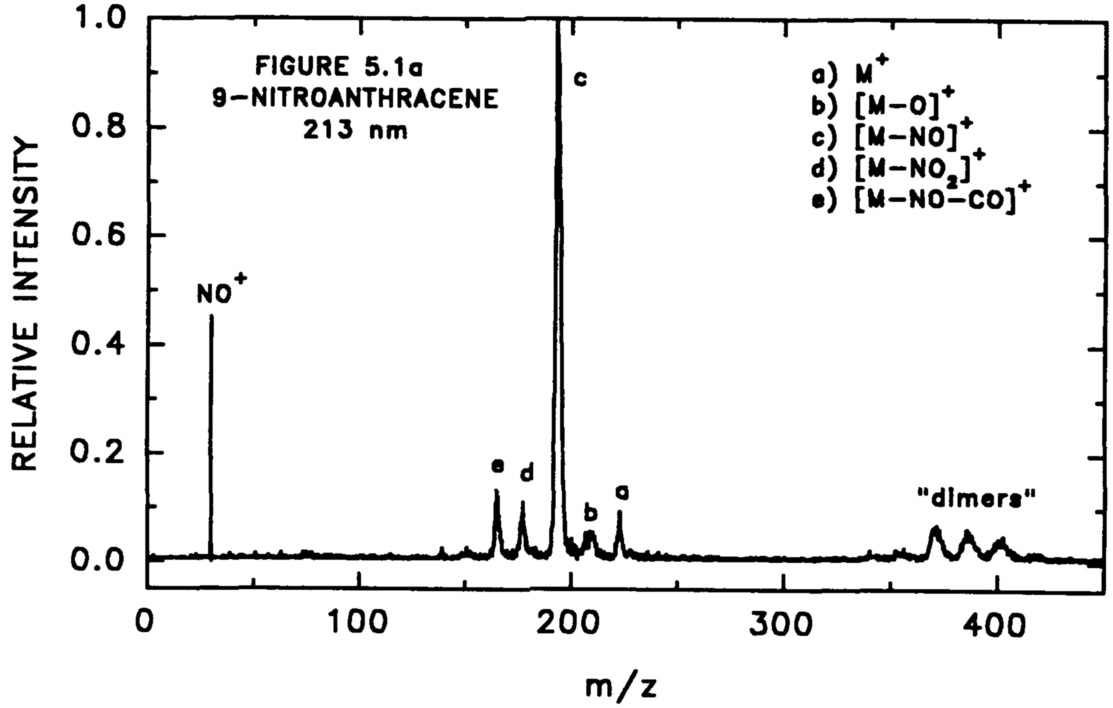
FIGURE 5.1a
9-NITROANTHRACENE
213 nm
a) M$^+$
b) [M-O]$^+$
c) [M-NO]$^+$
d) [M-NO$_2$]$^+$
e) [M-NO-CO]$^+$
NO$^+$
c
e
d
b
a
"dimers"
RELATIVE INTENSITY
1.0
0.8
0.6
0.4
0.2
0.0
0
100
200
300
400
m/z

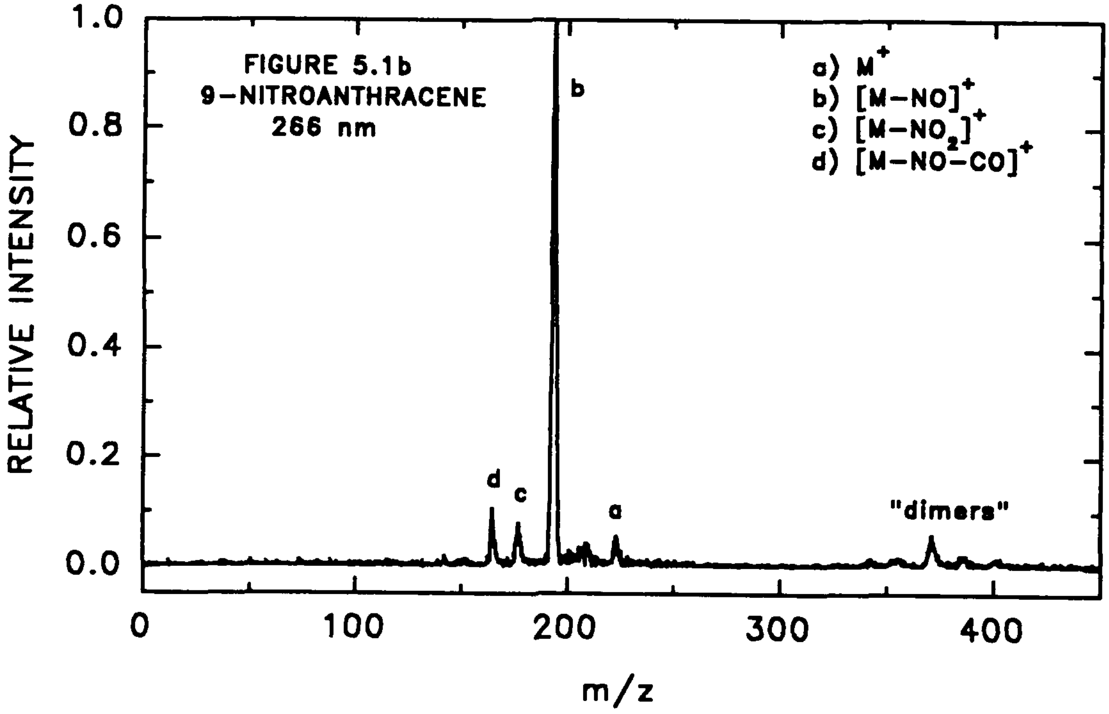
FIGURE 5.1b
9-NITROANTHRACENE
266 nm
a) M$^+$
b) [M-NO]$^+$
c) [M-NO$_2$]$^+$
d) [M-NO-CO]$^+$
b
d
c
a
"dimers"
RELATIVE INTENSITY
1.0
0.8
0.6
0.4
0.2
0.0
0
100
200
300
400
m/z

**Figure 5.2** Single-step laser photoionization mass spectra of 1-nitropyrene obtained at 213 nm and 266 nm.

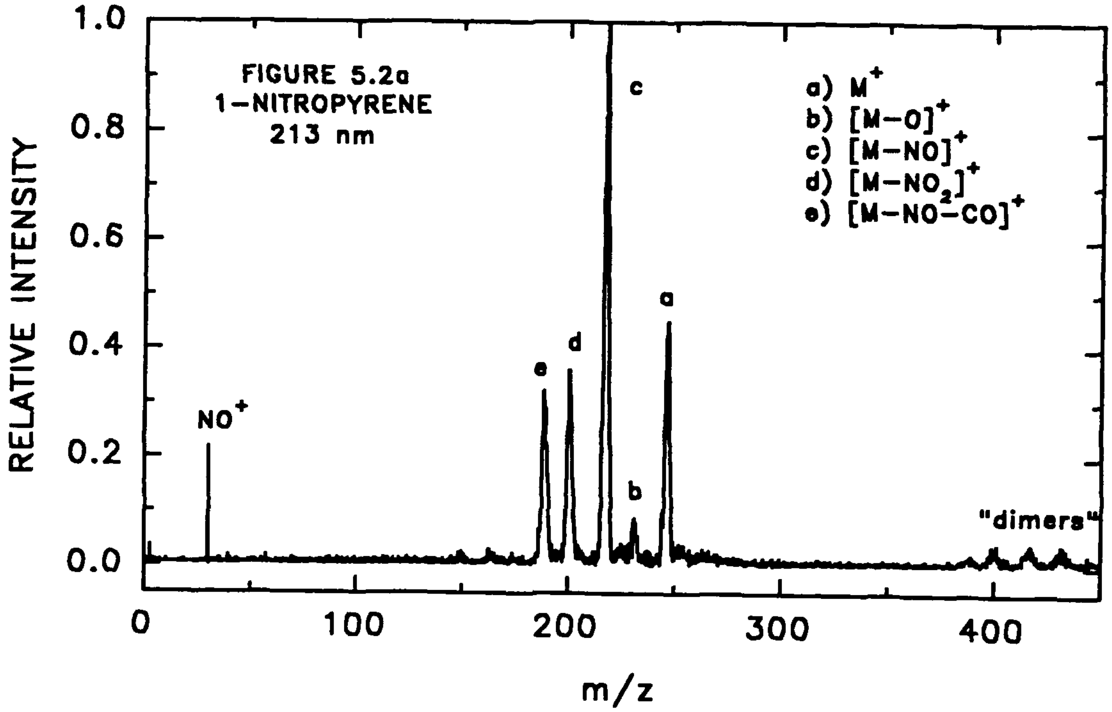
FIGURE 5.2a
1-NITROPYRENE
213 nm
a) $M^+$
b) $[M-O]^+$
c) $[M-NO]^+$
d) $[M-NO_2]^+$
e) $[M-NO-CO]^+$
$NO^+$
e
d
c
b
a
"dimers"
RELATIVE INTENSITY
1.0
0.8
0.6
0.4
0.2
0.0
0
100
200
300
400
m/z

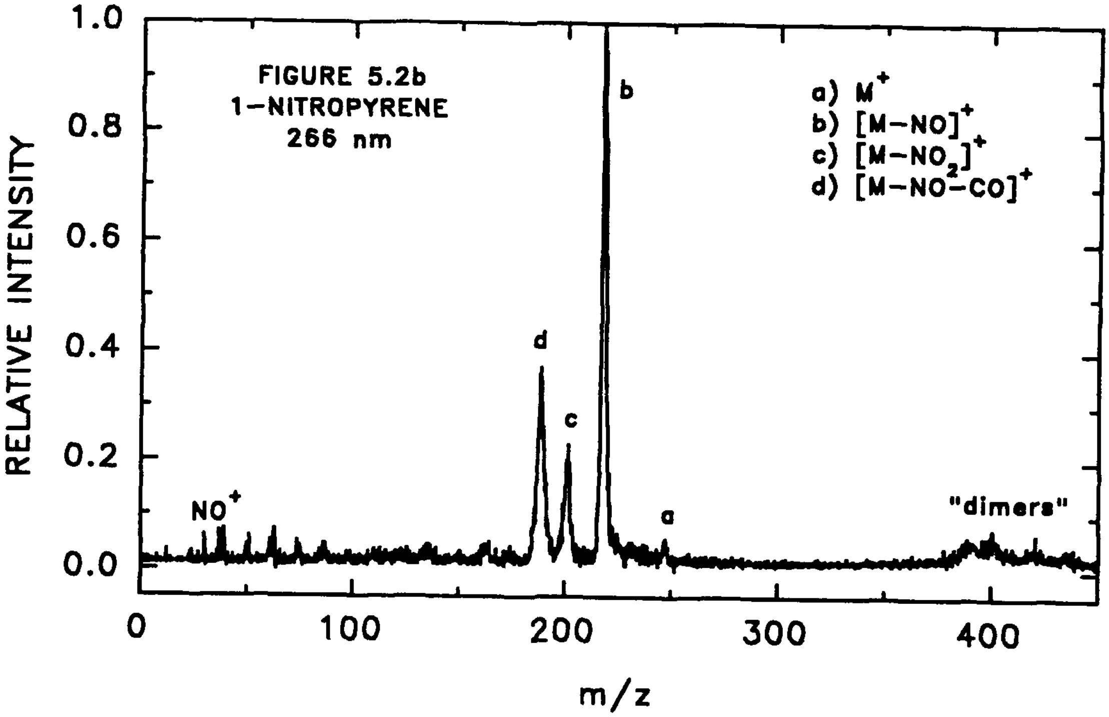
FIGURE 5.2b
1-NITROPYRENE
266 nm
a) $M^+$
b) $[M-NO]^+$
c) $[M-NO_2]^+$
d) $[M-NO-CO]^+$
$NO^+$
d
c
b
a
"dimers"
RELATIVE INTENSITY
1.0
0.8
0.6
0.4
0.2
0.0
0
100
200
300
400
m/z

of 1-nitropyrene is the $[M\text{-}NO]^+$ fragment ion, with the accompanying significant peaks belonging to the $[M\text{-}NO_2]^+$ and $[M\text{-}NO\text{-}CO]^+$ ions. The $[M\text{-}O]^+$ ion peak is fairly weak, but better defined in the 213 nm spectrum of 1-nitropyrene than in either of the 9-nitroanthracene spectra. Once again dimers and photoproducts are observed, most likely identified as $C_{32}H_{18}$ (m/z 402: dimer pyrene), $C_{32}H_{18}O$ (m/z 418), and $C_{32}H_{16}O_2$ (m/z 432). The $NO^+$ ion peak is still a prominent fragment at 213 nm, however a weak m/z 30 peak also appears at 266 nm among the low mass carbon fragments.

The major peaks observed in the photoionization spectra of 9-nitroanthracene and 1-nitropyrene suggest competing fragmentation pathways in the nitro-PAH. Two mechanisms for the formation of the $NO^+$ ion in nitrobenzene proposed by Marshall et al.,[20] parallel the apparent nitro-PAH fragmentation pathways. The primary fragmentation route produces the stable $[M\text{-}NO]^+$ ion and the $NO^+$ ion through predissociation of the parent molecule to lose NO, and subsequent two-photon ionization of the resulting fragments:[20]

$$M + h\nu \rightarrow (M\text{-}NO) + NO$$

$$(M\text{-}NO) + 2h\nu \rightarrow (M\text{-}NO)^+ + e^-$$

$$NO + 2h\nu \rightarrow NO^+ + e^-$$

The competing fragmentation pathway which yields the $[M\text{-}NO_2]^+$ ion (parent-PAH ion) can also lead to the production of $NO^+$. The decomposition route involves predissociation of the parent molecule to release $NO_2$, followed by predissociation of the $NO_2$ fragment and subsequent two-photon ionization of NO (IP 9.25 eV):[20,28]

$$M + h\nu \rightarrow (M\text{-}NO_2) + NO_2$$

$$NO_2 + h\nu \rightarrow NO + O$$

$$NO + 2h\nu \rightarrow NO^+ + e^-$$

Predissociation of the parent to lose $NO_2$ is identified by Marshall et al.[20] as the major route to formation of $NO^+$ in nitrobenzene, based on their experimental results. Their principal objection to $NO^+$ formation via predissociation of the parent to lose NO was the absence of the $[M\text{-}NO]^+$ ion in photoionization mass spectra of nitrobenzene and o-nitrotoluene, while the $[M\text{-}NO_2]^+$ ion was present in the nitrobenzene spectrum. However, the spectra observed for nitro-PAH in the current study imply that parent predissociation to yield (M-NO) and NO fragments is a major mechanism for nitro-PAH decomposition. Photorearrangement within nitro-PAH to lose NO as a major decomposition pathway may have a significant effect on atmospheric photochemistry of the nitro-PAH species.

The loss of NO from nitro-containing molecules has been postulated to proceed through a nitro-nitrite rearrangement mechanism.[29-31] The nitro-nitrite rearrangement involves isomerization from $-NO_2$ to -ONO at the carbon atom to which the nitro group was originally attached. Ioki[32] reported the e.s.r. detection of several aryloxyl radicals formed by nitro-compounds upon UV illumination. Specifically, the e.s.r. spectrum of 6-nitrobenzo[a]pyrene after UV illumination, showed hyperfine structure identical to the e.s.r. spectrum of benzo[a]pyren-6-oxyl radical produced by proton abstraction from benzo[a]pyren-6-ol. Ioki concludes that formation of aryloxyl radicals is a consequence of photorearrangement of the nitro group, noting that highly conjugated aromatic compounds form more stable free radicals by delocalizing the unpaired electron.

Nitro-PAH are, by definition, highly conjugated aromatic compounds. The laser photoionization mass spectra presented for 9-nitroanthracene and 1-nitropyrene show formation of a stable $[M-NO]^+$ ion, which is the base peak in their typical soft ionization spectra. Figure 5.3 illustrates the competing photofragmentation pathways for 1-nitropyrene which are generally applicable to other nitro-PAH in the current study. The loss of 58 amu, corresponding to the $[M-NO-CO]^+$ ion peak, could occur through either stepwise (M-NO-CO) or concerted ($M-CNO_2$) mechanisms, as both are energetically feasible at the wavelengths used for ionization. After loss of $NO_2$ or (NO-CO), fragmentation follows the characteristic PAH pattern by sequential loss of acetylene ($C_2H_2$), and other $C_nH_x$ fragments.

Figure 5.4 presents hard ionization spectra of 9-nitroanthracene obtained at 213 nm and 266 nm which are representative of other hard ionization spectra acquired for nitro-PAH currently under study. The spectra tend to be noisier due to background interference from the higher density of desorbed material in the plume. Notice that the $[M-NO]^+$ ion peak has decreased in magnitude as compared to the other significant high mass fragments, and that the molecular ion is almost nonexistent in both spectra. The $NO^+$ ion peak now dominates the 213 nm mass spectrum and has also made a modest appearance among the low mass carbon fragments in the 266 nm spectrum.

Opsal and Reilly[33] performed laser ionization GC/MS on several nitro- and nitroso-containing compounds using a 193-nm ArF laser and a 248-nm KrF laser for ionization sources. Significant $NO^+$ yield was obtained for a variety of nitro- and nitroso-molecules by ArF laser-induced ionization. However, even with more energetic KrF pulses, only modest m/z 30 yield was obtained from nitro-containing compounds. Opsal and Reilly recounted that NO absorption begins at 226 nm ($A^2\Sigma^+ \leftarrow X^2\Pi$) and is particularly strong in the 190 to 200 nm region due to the $C^2\Pi \leftarrow X^2\Pi$ and $D^2\Sigma \leftarrow X^2\Pi$

**Figure 5.3** Schematic depicting the proposed photofragmentation pathways for 1-nitropyrene, which may be generally applicable to other nitro-PAH compounds.

COMPETING FRAGMENTATION PATHWAYS IN NITRO-PAH

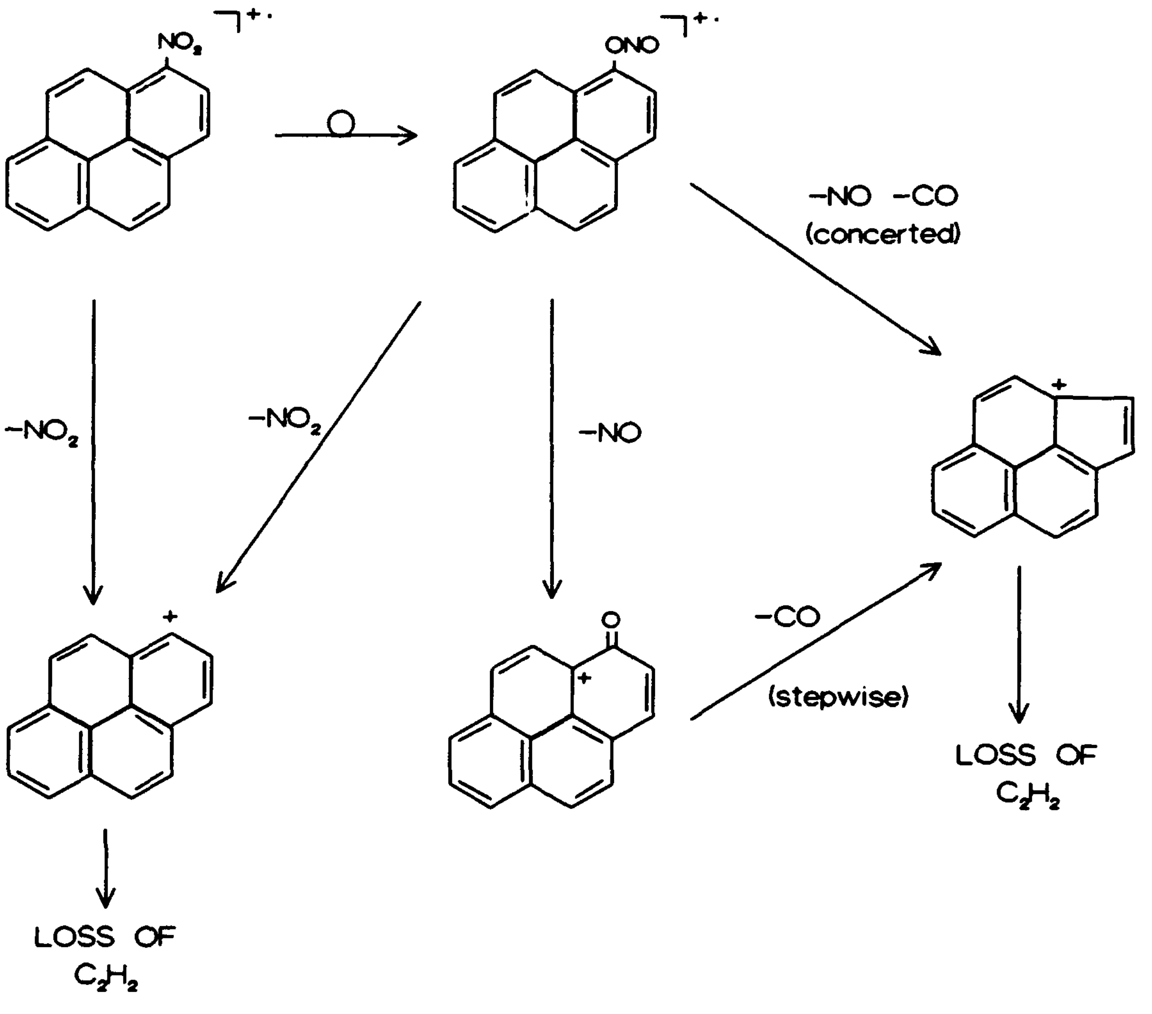
$NO_2$
+·
ONO
+·
O
–NO –CO
(concerted)
$-NO_2$
$-NO_2$
–NO
+
O
+
–CO
(stepwise)
+
LOSS OF $C_2H_2$
LOSS OF $C_2H_2$

**Figure 5.4** Single-step laser photoionization mass spectra of 9-nitroanthracene showing the effect of hard ionization at both 213 nm and 266 nm.

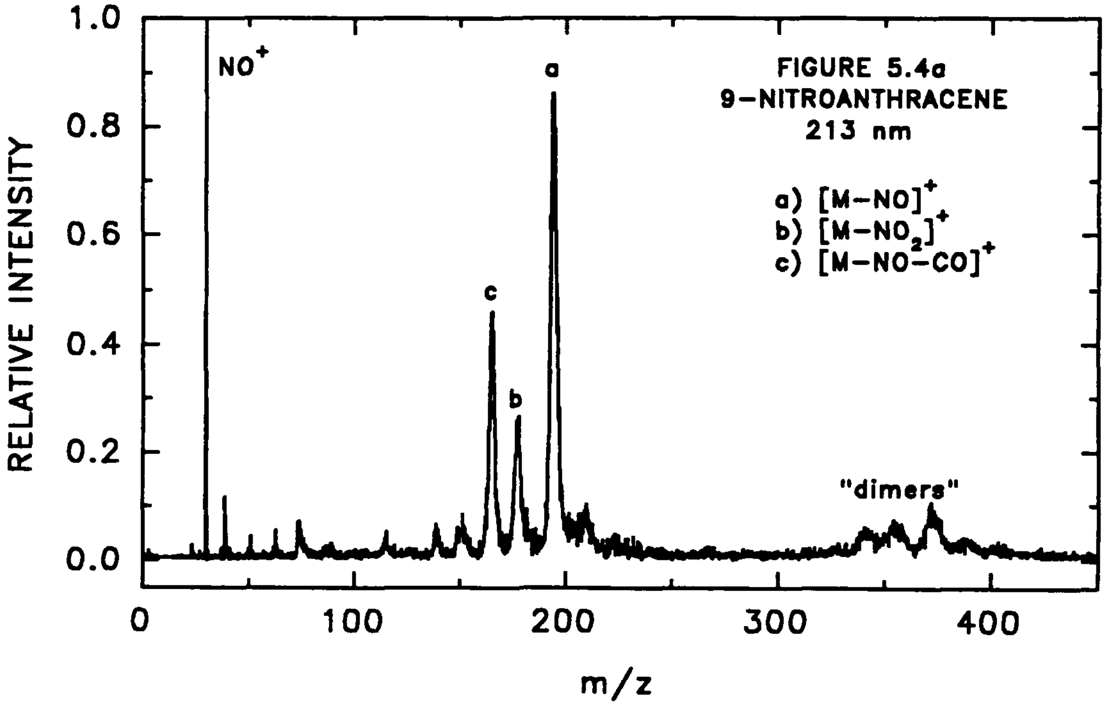

FIGURE 5.4a
9-NITROANTHRACENE
213 nm

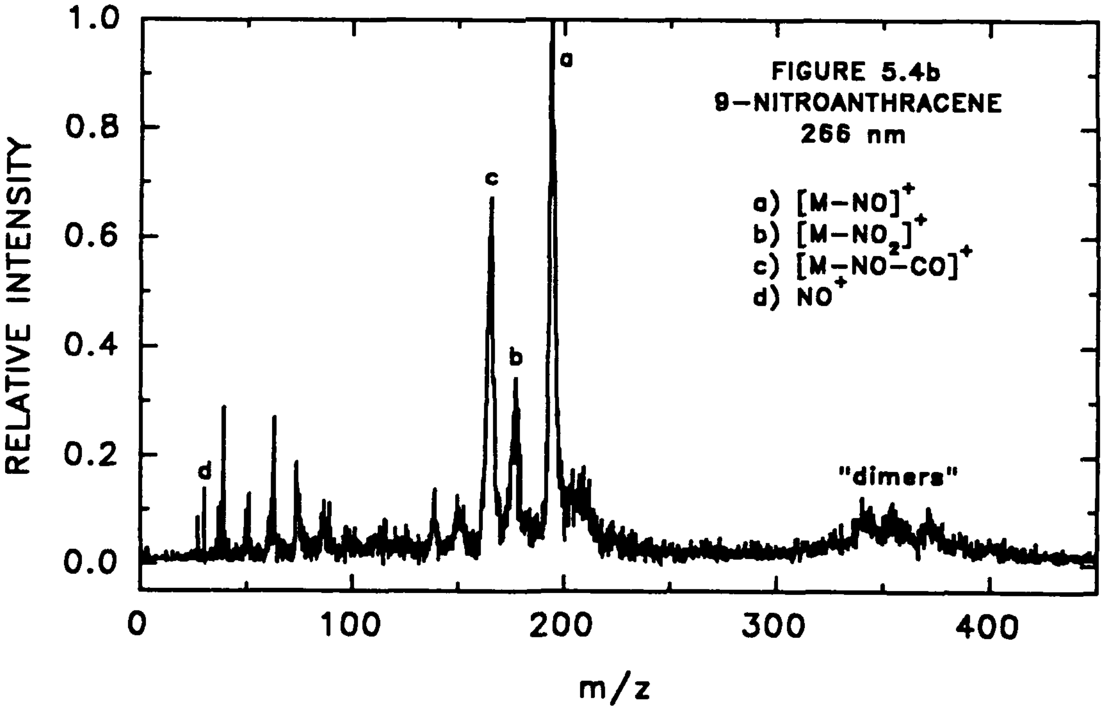

FIGURE 5.4b
9-NITROANTHRACENE
266 nm

bands. Additionally, Morrison et al.[34,35] concluded from their photodissociation study of $NO_2$ that the high energy predissociation pathway, $NO_2 \rightarrow NO(X^2\pi) + O(^1D)$, became important soon after the $B^2B_2$ state of $NO_2$ became energetically accessible (< 475 nm: two-photon).

Therefore, at 213 nm the predissociation pathway of $NO_2$ is accessible with one photon to generate NO, in addition to the NO produced from the photoisomerization-predissociation of the parent molecule. Additional NO production coupled with the resonant absorption routes available for NO below 226 nm explains the predominance of $NO^+$ ion in the 213-nm spectra as compared to the 266-nm spectra. The modest presence of an m/z 30 ion in the hard ionization mass spectra at 266 nm is probably due more to nonresonant MPI processes, or collisional and charge transfer ionization of NO in the plume, than to a resonant two-photon process.

### 5.4.2 Laser Photoionization of 2-nitrofluorene and 2-nitro-9-fluorenone

As shown by the structures given in Table 5.1, 2-nitrofluorene and 2-nitro-9-fluorenone each contain a cyclopenta-fused ring. The photofragmentation pathways of 2-nitrofluorene closely parallel those of 9-nitroanthracene and 1-nitropyrene already presented. However, the carbonyl group in 2-nitro-9-fluorenone causes some interesting variations in its fragmentation patterns that are apparent by comparison to the spectra of 2-nitrofluorene. Figure 5.5 shows the laser mass spectra of 2-nitrofluorene and Figure 5.6 presents the laser mass spectra of 2-nitro-9 fluorenone obtained by 213 nm and 266 nm photoionization. The 213-nm spectra are examples of soft ionization, while the mass spectra shown for 266 nm illustrate hard ionization of these two cyclopenta-fused ring nitro-PAH.

**Figure 5.5** Single-step laser photoionization mass spectra of 2-nitrofluorene showing soft ionization at 213 nm and hard ionization at 266 nm.

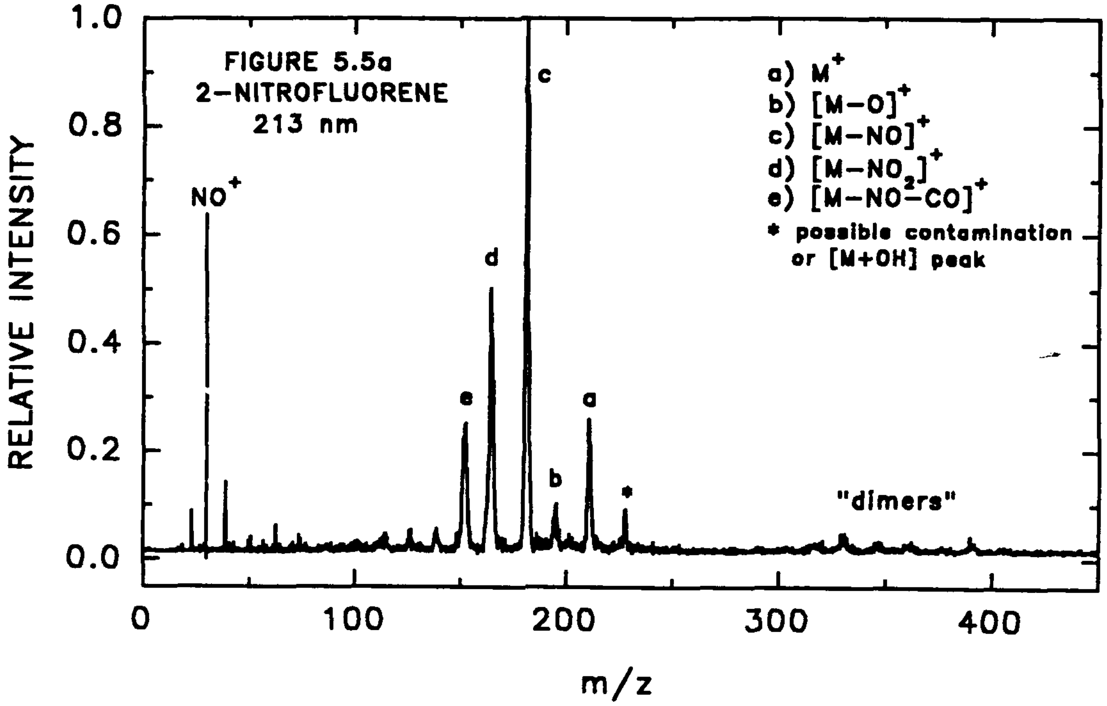

FIGURE 5.5a
2-NITROFLUORENE
213 nm

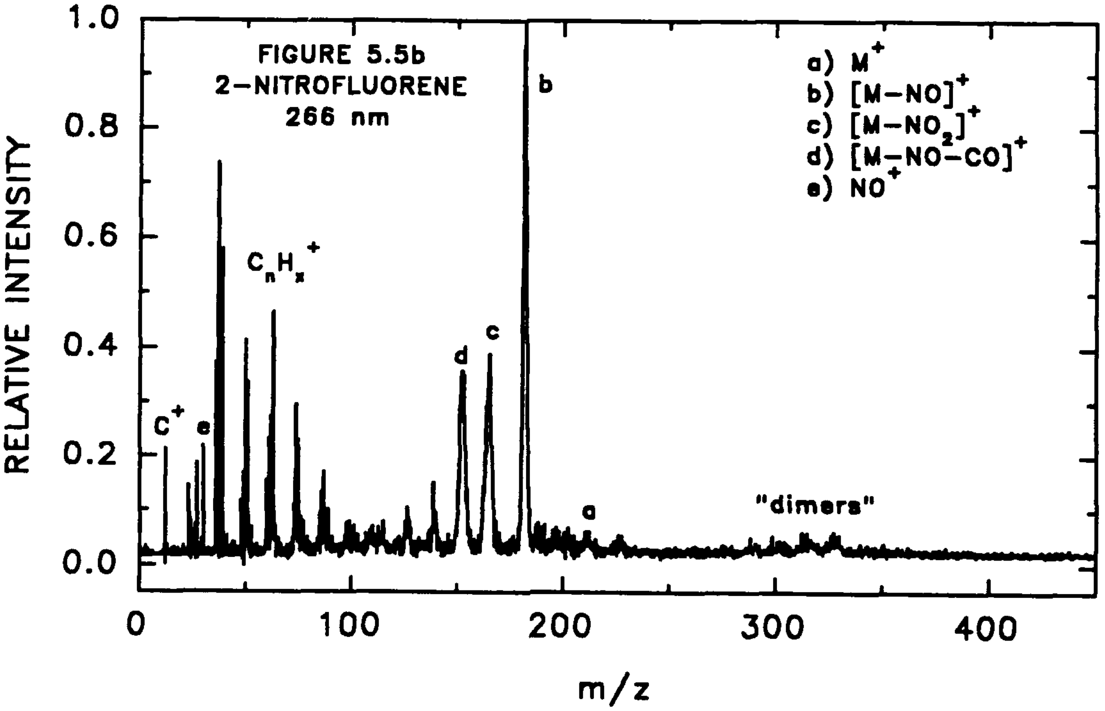

FIGURE 5.5b
2-NITROFLUORENE
266 nm

**Figure 5.6** Single-step laser photoionization mass spectra of 2-nitro-9-fluorenone showing soft ionization at 213 nm and hard ionization at 266 nm.

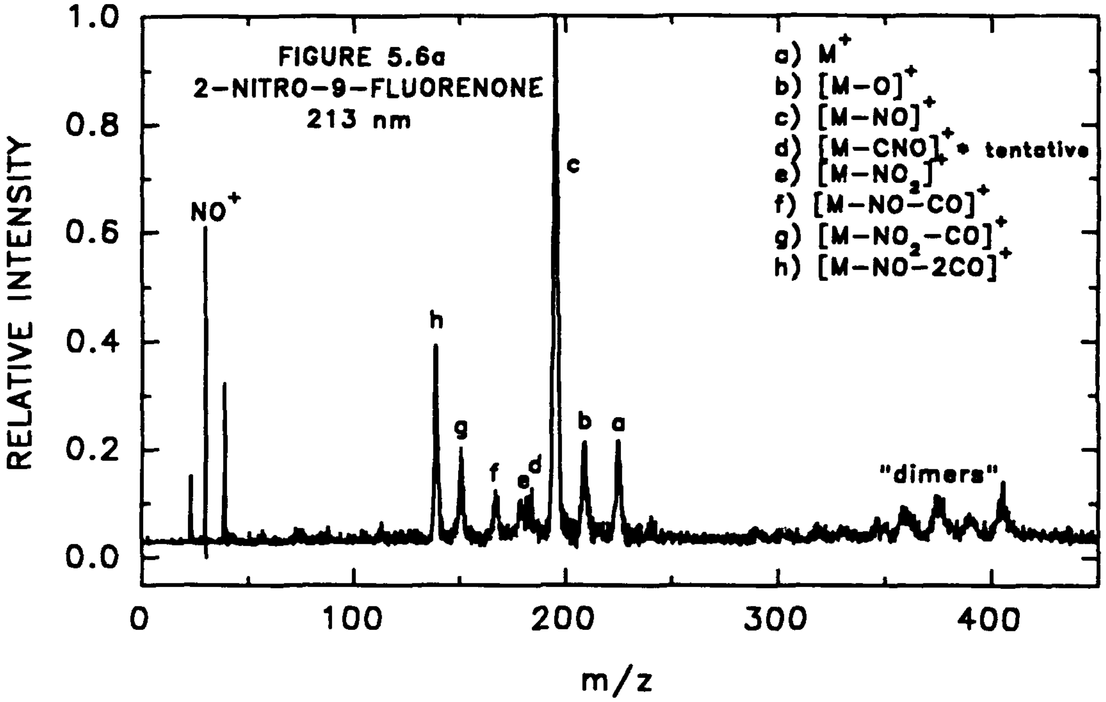
FIGURE 5.6a
2-NITRO-9-FLUORENONE
213 nm
a) $M^+$
b) $[M-O]^+$
c) $[M-NO]^+$
d) $[M-CNO]^+$* tentative
e) $[M-NO_2]^+$
f) $[M-NO-CO]^+$
g) $[M-NO_2-CO]^+$
h) $[M-NO-2CO]^+$
$NO^+$
h
g
f
e
d
c
b
a
"dimers"
RELATIVE INTENSITY
0.0
0.2
0.4
0.6
0.8
1.0
0
100
200
300
400
m/z

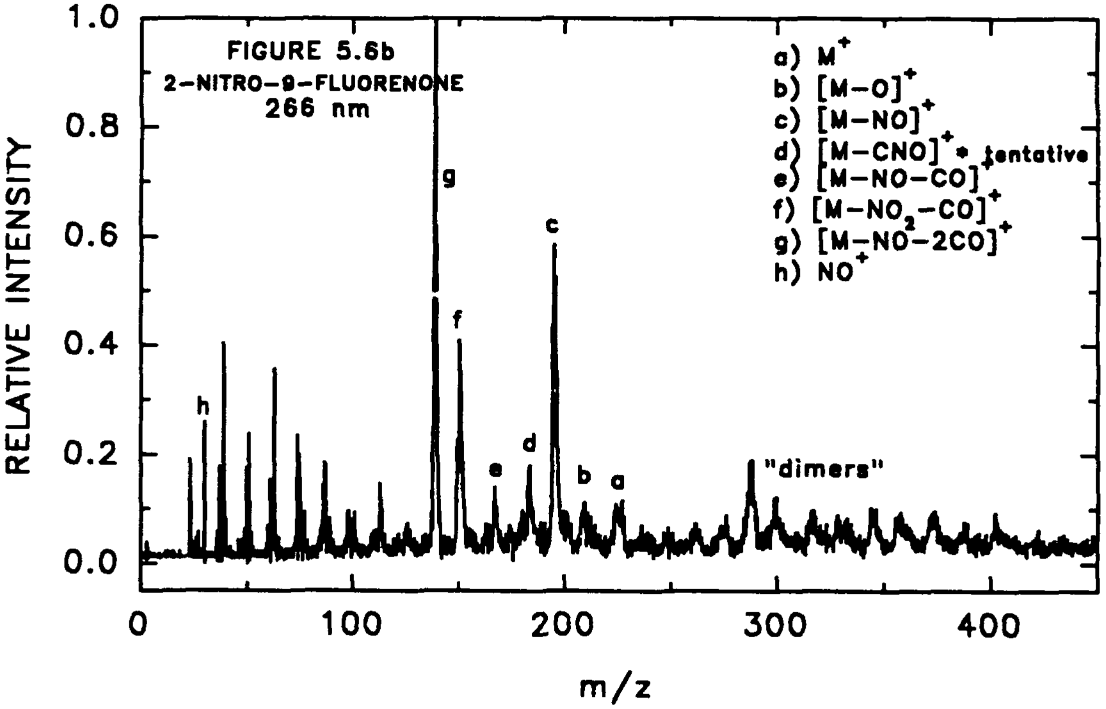
FIGURE 5.6b
2-NITRO-9-FLUORENONE
266 nm
a) $M^+$
b) $[M-O]^+$
c) $[M-NO]^+$
d) $[M-CNO]^+$* tentative
e) $[M-NO-CO]^+$
f) $[M-NO_2-CO]^+$
g) $[M-NO-2CO]^+$
h) $NO^+$
g
c
f
h
d
e
b
a
"dimers"
RELATIVE INTENSITY
0.0
0.2
0.4
0.6
0.8
1.0
0
100
200
300
400
m/z

The laser mass spectra of 2-nitrofluorene in Figure 5.5 contain the major fragment ions $[M-NO]^+$, $[M-NO_2]^+$, and $[M-NO-CO]^+$, as did the previously presented nitro-PAH spectra. The molecular ion is observed at both wavelengths, though obviously attenuated at 266 nm due to the hard ionization condition. The molecular ion was typically stronger in 213 nm spectra, and the $[M-O]^+$ ion peak was also more discernible at 213 nm. Dimers and photoproducts appear in the spectra due to surface chemistry and bimolecular interactions within the desorption plume. The $NO^+$ ion is the predominant low mass fragment in the 213-nm spectrum, but is also modestly present among the low mass carbon fragments in the 266 nm spectrum. The wavelength dependence of the $NO^+$ ion signal is also apparent in Figure 5.4, and was accounted for in the discussion of the hard ionization of 9-nitroanthracene.

Photoionization mass spectra of 2-nitro-9-fluorenone in Figure 5.6 show many of the major high mass fragments common to all the other nitro-PAH spectra presented thus far. Molecular ion is observed at both wavelengths as is the $[M-O]^+$ ion. The $NO^+$ ion is the dominant fragment in the 213-nm spectrum, and is a moderately strong peak in the 266-nm hard ionization spectrum. The $[M-NO]^+$ ion is the base peak at 213 nm and a strong peak in the 266-nm spectrum. However, the $[M-NO-CO]^+$ fragment makes only a modest appearance at either wavelength, and the $[M-NO_2]^+$ ion is weakly present and is overshadowed by a peak of m/z 183 (possibly $[M-CNO]^+$ ).

The two most interesting major fragment ions of 2-nitro-9-fluorenone appear in the mid-mass range at m/z 151 and m/z 139. The peak corresponding to m/z 151 is attributable to a diphenylene ion, $[M-NO_2-CO]^+$, formed from the loss of the nitro group and the carbonyl group that bridged the two benzene rings in the fluorenone structure.

**Figure 5.7** Proposed photofragmentation pathways and structures for the m/z 151 and m/z 139 fragment ions of 2-nitro-9-fluorenone.

PATHWAYS TO MID-MASS FRAGMENTS: 2-$NO_2$-9-FLUORENONE

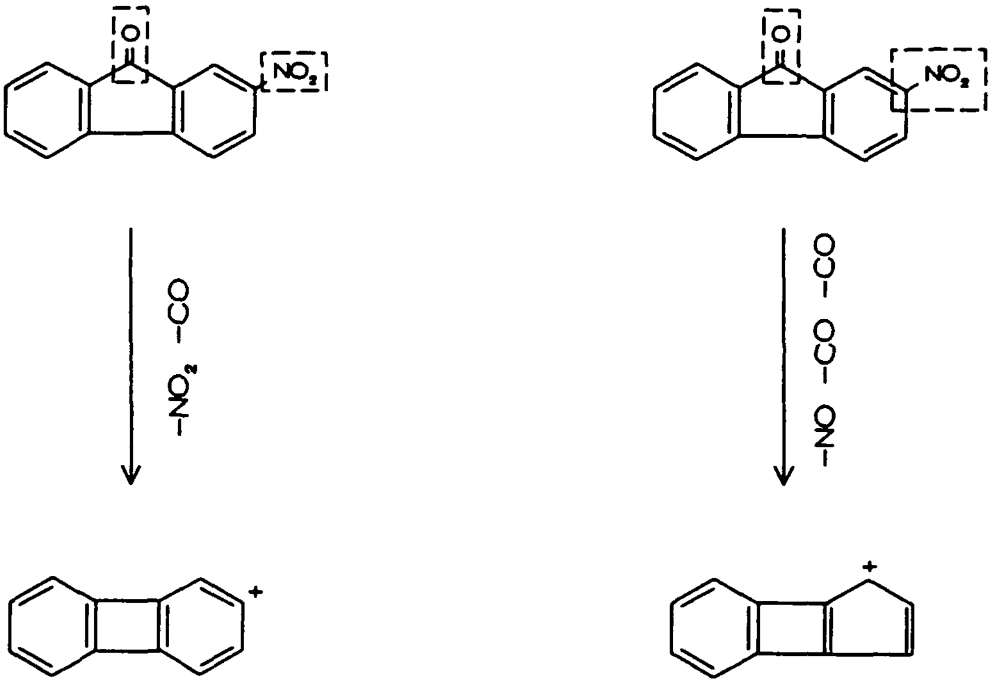
O
$NO_2$
O
$NO_2$
$-NO_2$ $-CO$
$-NO$ $-CO$ $-CO$
+
+

$C_{12}H_7^+$
m/z 151

$C_{11}H_7^+$
m/z 139

The m/z 139 peak is assignable to $C_{11}H_7^+$, formed by the loss of the carbonyl group from the [M-NO-CO] fragment. The routes to the [M-$NO_2$-CO] and $C_{11}H_7$ fragments and their possible structures are depicted in Figure 5.7. The opening of the carbonyl bridge is facilitated by the $n \rightarrow \pi^*$ transition excited within the carbonyl group of the fluorenone. The absence of a carbonyl bridge in 2-nitrofluorene causes it to fragment by the common PAH pattern, loss of acetylene, after $NO_2$ or (NO-CO) fragments have departed from the parent molecule.

## 5.5 CONCLUSIONS

Comparison of the laser photoionization mass spectra obtained for the four nitro-PAH standards, 9-nitroanthracene, 1-nitropyrene, 2-nitrofluorene and 2-nitro-9-fluorenone, leads to the conclusion that there are competing photofragmentation pathways in nitro-PAH which can result in the production of $NO^+$. The primary fragmentation route appears to proceed through a nitro-nitrite photoisomerization, allowing predissociation of the parent molecule to release NO, with subsequent two-photon ionization of the NO fragment. Photorearrangement within the nitro-PAH to lose NO may have a significant effect on their atmospheric transformation reactions. The competing pathway involves predissociation of the parent to lose $NO_2$ , followed by predissociation of the $NO_2$ fragment to produce the NO fragment, which is then ionized. Predissociation of $NO_2$ to (NO + O) has been shown to dominate the two-photon photodissociation at wavelengths shorter than 475 nm.[34]

Photoionization using 266 nm and 213 nm radiation produced characteristic high- and mid-mass fragmentation patterns for the nitro-PAH studied which could be generalized for other nitro-PAH compounds. The abundant $NO^+$ ion, observed even for relatively soft ionizations of the nitro-PAH standards, could dominate the spectrum under hard ionization conditions. Despite the dominant $NO^+$ ion, the higher mass characteristic fragments remained as strong, identifiable peaks in the spectrum. Future work includes application of LPMS to identify nitro-PAH in mixtures and ultimately, in environmental samples, possibly using $NO^+$ ion detection to determine their presence.

## 5.6 REFERENCES

1. Helmig, D.; Arey, J.; Atkinson, R.; Harger, W. P.; McElroy, P. A. *Atmos. Environ.* **1992**, *26A*, 1735.

2. Arey, J.; Zielinska, B.; Atkinson, R.; Aschmann, S. M. *Int. J. Chem. Kinet.* **1989**, *21*, 775.

3. Schuetzle,D.; Lee, F. S. C.; Prater, T. J.; Tejada, S. B. in *Proceedings of the 10th Annual Symposium on Analytical Chemistry of Pollutants*, Gordan and Breach Science Publishers, New York, 1980, pp. 193-244.

4. Schuetzle, D.; Lee, F. S. C.; Prater, T. J.; Tejada, S. B. *Int. J. Environ. Anal. Chem.* **1981**, *9*, 93.

5. Schuetzle, D.; Riley, T. L.; Prater, T. J.; Harvey, T. M.; Hunt, D. F. *Anal. Chem.* **1982**, *54*, 265.

6. Schuetzle, D.; Paputa, M.; Hampton, C. M.; Marano, R.; Riley, T.; Prater, T. J.; Skewes, L.; Salmeen, I. "The Identification and Potential Sources of Nitrated Polynuclear Aromatic Hydrocarbons (Nitro-PAH) in Diesel Particulate Extracts", pp.299-312 in *Mobile Source Emissions Including Polycyclic Organic Species*, D. Reidel Publishing Co., 1983.

7. Paputa-Peck, M. C.; Marano, R. S.; Schuetzle, D.; Riley, T. L.; Hampton, C. V.; Prater, T. J.; Skewes, L. M.; Jensen, T. E.; Ruehle, P. H.; Bosch, L. C.; Duncan, W. P. *Anal. Chem.* **1983**, *55*, 1946.

8. Williams, P. T.; Bartle, K. D.; Andrews, G. E. "Polycyclic Aromatic Compounds in Diesel Fuels and Particulates", pp. 1011-1027 in *Polynuclear Aromatic Hydrocarbons: Chemistry, Characterization and Carcinogenesis; Ninth International Symposium*, M. Cooke and A. J. Dennis, Eds., Battelle Press, Columbus, OH, 1986.

9. Xu, X. B.; Nachtman, J. P.; Jin, Z. L.; Wei, E. T.; Rappaport, S. M. *Anal. Chim. Acta* **1982**, *136*, 163.

10. Ramdahl, T.; Becher, G.; Björseth. A. *Environ. Sci.Technol.* **1982**, *16*, 861.

11. Nishioka, M. G.; Howard, C. C.; Lewtas, J. "Detection of Hydroxy-Nitro-PAHs and Nitro-PAHs in an Ambient Air Particulate Extract Using Bioassay Directed Fractionation", pp. 701-715 in *Polynuclear Aromatic Hydrocarbons: Chemistry, Characterization and Carcinogenesis; Ninth International Symposium*, M. Cooke and A. J. Dennis, Eds., Battelle Press, Columbus, OH, 1986.

12. Arey, J.; Harger, W. P.; Helmig, D.; Atkinson, R. *Mutation Res.* **1992**, *281*, 67.

13. Chuang, C. C.; Mack, G. A.; Petersen, B. A.; Wilson, N. K. "Identification and Quantification of Nitropolynuclear Aromatic Hydrocarbons in Ambient and Indoor Air Particulate Samples" pp. 155-171 in *Polynuclear Aromatic Hydrocarbons: Chemistry, Characterization and Carcinogenesis; Ninth International Symposium*, M. Cooke and A. J. Dennis, Eds., Battelle Press, Columbus, OH, 1986.

14. Oehme, M.; Mano, S.; Stray, H. *HRC & CC* **1982**, *5*, 417.

15. Harris, W. R.; Chess, E. K.; Okamoto, D.; Remsen, J. F.; Later, D. W. *Environ. Mutagen.* **1984**, *6*, 131.

16. McCoy, E. C.; Rosenkranz, H. S. *Cancer Lett.* **1982**, *15*, 9.

17. Schnieder, E.; Krenmayr, P.; Varmuza, K. *Monatshefte fur Chemie* **1990**, *121*, 393.

18. Apel, E. C.; Nogar, N. S. *Int. J. Mass Spectrom. Ion Processes* **1986**, *70*, 243.

19. Marshall, A.; Clark, A.; Jennings, R.; Ledingham, K. W. D.; Sander, J.; Singhal, R. P. *Int. J. Mass Spectrom. Ion Processes* **1992**, *112* , 273.

20. Marshall, A.; Clark, A.; Jennings, R.; Ledingham, K. W. D.; Sander, J.; Singhal, R.

P. *Int. J. Mass Spectrom. Ion Processes* **1992,** *116* , 143.

21. Zhu, J.; Lustig, D.; Sofer, I.; Lubman, D. M. *Anal. Chem.* **1990,** *62,* 2225.

22. Galloway, D. B.; Bartz, J. A.; Huey, L. G.; Crim, F. F. *J. Chem. Phys.* **1993,** *98,* 2107.

23. Young, M. K. G. *Characterization of Polycyclic Aromatic Hydrocarbons and Chlorinated Polycyclic Aromatic Hydrocarbons in Soots by Laser Desorption-Laser Photoionization Mass Spectrometry,* Dissertation, (University of California, Davis), Dec., 1991.

24. Young, M. K. G.; Jones, A. D.; Kelly, P. B. Proceedings of the 39th ASMS Conference on Mass Spectrometry and Allied Topics, Nashville, TN., May 19-24, 1991, p. 342.

25. Wiley, W. C.; McLaren, I. H. *Rev. Sci. Instrum.* **1955,** *26,* 1150.

26. Hudson, B.; Kelly, P.B.; Ziegler, L. D.; Desiderio, R. A.; Gerrity, D. P.; Hess, W.; Bates, R. "Far Ultraviolet Laser Resonance Raman Studies of Electronic Excitations," pp. 1-32 in *Advances in Laser Spectroscopy: Volume 3,* B. A. Garetz and J. R. Lombardi, Eds., John Wiley & Sons Ltd., Chichester, Great Britain, 1986.

27. Smith, C. H. Dissertation, University of California, Davis, Fall 1993, in preparation.

28. Weissler, G. L.; Samson, J. A. R.; Ogawa, M.; Cook. G. R. *J. Opt. Soc. Am.* **1959,** *49,* 338.

29. Stewart, P. H.; Jeffries, J. B.; Zellweger, J. M.; McMillen, D. F.; Golden, D. M. *J. Phys. Chem.* **1989,** *93,* 3557.

30. Bowie, J. H.; Blumenthal, T.; Walsh, I. *Org. Mass Spectrom.* **1971,** *5,* 777.

31. Budzikiewicz, H.; Djerassi, C.; Williams, D. H. "Nitro and Related Compounds", pp.

512-519 in *Mass Spectrometry of Organic Compounds* , Holden-Day, Inc., San Francisco, 1967.

32. Ioki, Y. *J. C. S. Perkin II* **1977**, *10*, 1240.
33. Opsal, R. B.; Reilly, J. P. *Anal. Chem.* **1986**, *58*, 2919.
34. Morrison, R. J. S.; Rockney, B. H.; Grant, E. R. *J. Chem. Phys.* **1981**, *75*, 2643.
35. Morrison, R. J. S.;Grant, E. R. *J. Chem. Phys.* **1982**, *77*, 5994.

# CHAPTER 6

## Laser Photoionization Time-of-Flight Mass Spectrometry of Nitrobenzocoumarins and Coumarin Derivative Compounds

### 6.1 ABSTRACT

The mass spectra of several nitrobenzocoumarin and coumarin derivative compounds have been investigated by single-step laser photoionization time-of-flight mass spectrometry. Pulsed UV radiation at 213 nm was used for desorption and ionization of the solid sample deposited on an aluminum probe. Two nitrobenzocoumarin isomers have been examined: 6-nitro-3,4-benzocoumarin and 7-nitro-3,4-benzocoumarin. The polar nitrobenzocoumarins proved fragile under UV irradiation and readily fragmented to produce intense m/z 139 and m/z 30 ($NO^+$) ions. The considerably weaker high mass fragments of the nitrobenzocoumarins included the molecular ion and characteristic $[M\text{-}NO]^+$, $[M\text{-}NO\text{-}CO]^+$, $[M\text{-}NO_2\ \text{-}CO]^+$, and $[M\text{-}NO\text{-}2CO]^+$ ions. Complementary EI MS/MS experiments have been performed on a VG ZAB-HS-2F mass spectrometer with BE geometry to aide interpretation of the nitrobenzocoumarin laser mass spectra.

Three coumarin derivative compounds have been studied: 7-hydroxycoumarin, 7-hydroxy-4-methylcoumarin and 2-nitro-6(5H)-phenanthridinone. The mass spectra of the two hydroxy-containing derivatives yielded information on the fragmentation of the coumarin backbone. The nitrophenanthridinone compound produced a series of significant high and mid-mass fragment ions including $M^+$, $[M\text{-}NO]^+$, $[M\text{-}NO_2]^+$, and $[M\text{-}NO\text{-}CO]^+$, which are characteristic of nitro-PAH fragmentation patterns. Comparison of the spectra acquired for the nitrobenzocoumarin isomers and the coumarin derivatives provides insight

into the photofragmentation patterns of oxygenated nitro-PAH derivatives and possibly, their atmospheric transformation reactions.

## 6.2 INTRODUCTION

The analytical chemistry of nitrated polycyclic aromatic hydrocarbons (nitro-PAH) is of widespread interest due to the highly mutagenic properties of this chemical class. Nitro-PAH are derivatives of PAH, which are abundant in fossil fuels and are the incomplete combustion products of organic materials. Nitro-PAH have been determined in a variety of environmental samples including diesel exhaust particulate,[1-7] ambient air particulate,[8-11] coal fly ash[12] and wood smoke condensates.[13] Nitro-PAH present in direct emissions are primarily electrophilic nitration products resulting from adsorbed-phase reactions of PAH with $NO_x$ and $HNO_3$.[14] Nitro-PAH found in the atmosphere often result from the atmospheric transformation of the parent PAH by gas-phase reaction with OH radical in the presence of $NO_x$ pollutants.[14] The gas-phase reaction products rapidly become particle-associated due to their low volatility. The majority of nitro-PAH found in ambient air particulate matter are believed to be formed in the atmosphere.[15-17]

Nitrofluoranthenes and nitropyrenes are generally the nitro-PAH found in the highest concentrations in ambient air particulate extracts.[18-21] However, Arey et al.[22] have shown that nitro-PAH, primarily nitrofluoranthenes and nitropyrenes, account for only about 10% of the overall mutagenicity of ambient air particulate extract. Previous reports by Nishioka et al.,[23,24] Schuetzle and Lewtas,[25] and Lewtas et al.[26] used bioassay-directed fractionation to demonstrate that most of the ambient air particulate mutagenicity is attributable to organic compounds which are more polar than nitro-PAH. Specifically, Nishioka et al.[24] reported the first mass spectrometric evidence for hydroxylated nitro-

PAH and hydroxylated nitro-polycyclic aromatic ketones (nitro-PAK) in mutagenic polar fractions of ambient air particulate extract.

The 6-nitro-3,4-benzocoumarin compound investigated in the current study was initially identified (as 2-nitro-6H-dibenzo[b,d]pyran-6-one) by Arey et al.,[27] in environmental chamber experiments, as a product of the gas-phase reaction of phenanthrene with the OH radical in the presence of $NO_x$. Two isomers, the 2- and 4-nitro-6H-dibenzo[b,d]pyran-6-one, have been subsequently quantified by Helmig et al.[28] in southern California ambient air samples and NIST SRM 1649 urban dust. Both isomers were identified in the most mutagenic fractions of the particulate extracts. The contribution of 4-nitrodibenzopyranone to the mutagenic activity was negligible however, ~45% of the total activity in the particle-phase extracts was attributed to the 2-nitro isomer. In addition, methyl derivatives of the nitrodibenzopyranones and nitrophenanthropyranone compounds have been tentatively identified in mutagenic polar subfractions of southern California ambient air particulate.[29] The potent direct-acting mutagenicity of nitrodibenzopyranones (nitrobenzocoumarins) and their derivatives, coupled with their generally low concentrations in environmental samples, underscores the importance of developing sensitive, selective methods for their detection and identification.

In order to examine the application of laser photoionization time-of-flight mass spectrometry (LPMS) to characterization and analysis of nitrobenzocoumarin and coumarin derivatives, mass spectra have been obtained for five compounds: 6-nitro-3,4-benzocoumarin, 7-nitro-3,4-benzocoumarin, 7-hydroxycoumarin, 7-hydroxy-4-methylcoumarin and 2-nitro-6(5H)-phenanthridinone. The hydroxy-containing coumarin compounds provide information on the fragmentation of the coumarin backbone, while the nitrophenanthridinone yield information related to the higher mass fragmentation patterns of the nitrobenzocoumarins.

The two polar nitrobenzocoumarin isomers are labile and readily fragment under UV irradiation. The laser mass spectra of the labile nitrobenzocoumarins show weak intensity in the mid- to high-mass region, but an intense peak is observed at m/z 139, along with the characteristic $NO^+$ ion peak. A series of interrelated EI MS/MS experiments, including daughter ion and constant neutral loss, have been performed on 7-nitro-3,4-benzocoumarin to complement the laser photoionization study. The EI MS/MS spectra obtained in the current study are contained in Appendix E. Acquisition of representative laser mass spectra and identification of characteristic photofragments may contribute to the understanding of the atmospheric transformations of nitrobenzocoumarins, and are prerequisites to the application of the LPMS method for their determination in environmental samples.

## 6.3 EXPERIMENTAL

Nitrobenzocoumarin and coumarin derivative standards were purchased from Aldrich Chemical Co., and were used without further purification. The compounds studied were (molecular weight in parenthesis) 6-nitro-3,4-benzocoumarin (241), 7-nitro-3,4-benzocoumarin (241), 7-hydroxycoumarin (162), 7-hydroxy-4-methylcoumarin (176) and 2-nitro-6(5H)-phenanthridinone. Molecular structure and purity are given in Table 6.1.

Laser photoionization mass spectra are obtained using a custom-built time-of-flight mass spectrometer operating in the linear mode.[30,31] The sample probe is inserted into the source region through a custom-designed fast load-lock assembly which positions the

**Table 6.1** Properties of nitrobenzocoumarins and coumarin derivatives showing purity, molecular weight, formula and structure of each coumarin compound used in the current study.

**Table 6.1** Properties of Nitrobenzocoumarins and Coumarin Derivatives

| COMPOUND (PURITY) | MOLECULAR FORMULA | MOLECULAR WEIGHT | MOLECULAR STRUCTURE |
|---|---|---|---|
| 6-NITRO-3,4-BENZOCOUMARIN (98%) | $C_{13}H_7NO_4$ | 241 | 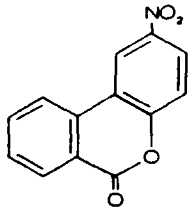 |
| 7-NITRO-3,4-BENZOCOUMARIN (98%) | $C_{13}H_7NO_4$ | 241 | 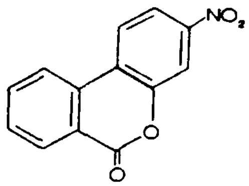 |
| 7-HYDROXY-COUMARIN (99%) | $C_9H_6O_3$ | 162 | 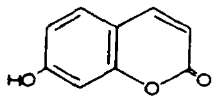 |
| 7-HYDROXY-4-METHYL-COUMARIN (97%) | $C_{10}H_8O_3$ | 176 | 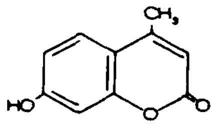 |
| 2-NITRO-6(5H)-PHENANTHRIDINONE (90%) | $C_{13}H_8N_2O_3$ | 240 | 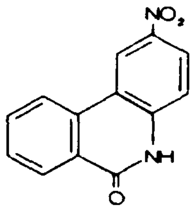 |

aluminum probe tip between the extractor and repeller plates of the Wiley-McLaren[32] based two-stage ion optics. The aluminum probe tip has a flattened face which is positioned perpendicular to the flight tube axis. The probe can be raised and lowered externally to allow analysis at different locations on the same sample. The source region is fitted with S1-UV quartz windows to allow transmission of the UV laser beam. Two oil diffusion pumps, equipped with liquid nitrogen cooled cryotraps, separately pump down the source and flight tube regions to an operating vacuum of ~ $10^{-6}$ torr.

Sample solutions of the nitrobenzocoumarin and hydroxy-coumarin standards are prepared at concentrations of 5-10 mg/ml in $CH_2Cl_2$. A typical sample is prepared by depositing a 20-30 µl aliquot of a standard solution, via syringe, directly onto the flattened probe face and allowing it to air dry. The relatively high concentration of the standard solution yields a residual solid layer thick enough to minimize interference from aluminum ion formation during ionization of the sample. The nitrophenanthridinone sample is prepared by directly attaching its crystals to the probe face using double-sided sticky tape, as the solid is fairly insoluble in $CH_2Cl_2$ (and several other solvents).

Pulsed UV radiation at 266 nm is produced using the fourth harmonic of a Q-switched Quanta Ray DCR-3 Nd:YAG laser with an 8 ns pulse width. Sum mixing of the Nd:YAG laser's 1064 nm fundamental and the 266 nm fourth harmonic in BBO (β - barium borate crystal) generates the 213 nm photons.[33] The UV laser beam is focussed into the source region through a 250 mm S1-UV quartz lens, which is also used to direct the UV beam path such that the laser beam grazes the surface of the sample. Laser energy is measured just prior to the spectrometer entrance window by a Molectron Model J9LP Joulemeter interfaced to a PcJ meter (Q&A Instruments).

The laser-induced thermal desorption induced at the fringe of the beam waist imparts enough energy to the desorbed molecules to move them a few microns from the surface, and into a region of higher power density. Positive ions form just above the surface in the high-density plume by multiphoton ionization and/or collision processes. Laser energy typically ranges from 5-20 μJ/pulse while operating at 5 Hz, yielding maximum power densities on the order of $10^8$ - $10^9$ W/cm$^2$ at the focus.

Positive ions formed during each laser pulse are accelerated into the flight tube and drift until impinging on the dual microchannel plate (MCP) detector. Current generated at the MCP detector is 50-ohm terminated into a 100 MHz DSP Model 2001AS Transient Recorder and digitized with 8-bit precision. In a typical experiment, data is collected and signal averaged by a DSP Model 4101 Averaging Memory over 100-200 laser pulses, then transferred by a CAMAC interface to an Everex 386 microcomputer. Data acquisition and subsequent analysis are controlled by software developed in-house.[30,34] The Q-switch sync is used to trigger the data acquisition electronics, allowing the time origin in the mass spectra correspond to arrival of the UV beam at the source.

Electron ionization MS/MS experiments on 7-nitro-3,4-benzocoumarin are performed at the Facility for Advanced Instrumentation (FAI) by Dr. A. Daniel Jones. Daughter ion, parent ion and constant neutral loss spectra are obtained using a VG ZAB-HS-2F mass spectrometer with BE geometry. A 2.0 μl aliquot of sample solution (~ 1.0 mg/ml) is injected into a quartz crucible and introduced into the source via the solids probe. The ions formed by 70 eV electron ionization are accelerated by 8 keV toward the magnetic sector. Nitrogen at a pressure of $10^{-5}$ mbar is introduced into the first field-free region. Fragmentation occurring in the first field-free region is studied by performing scans of constant B/E (daughter scans), constant $B^2/E$ (parent scans) and constant $(B/E^1)^2/(1-E^1)$ for neutral loss scans.

## 6.4 RESULTS AND DISCUSSION

### 6.4.1 Laser Photoionization and EI MS/MS of Nitrobenzocoumarins

The molecular structures, formulas and weights of all the nitrobenzocoumarin and coumarin derivatives examined in the current study are collected in Table 6.1 for convenient reference. The fragmentation patterns observed in the laser mass spectra of the two nitrobenzocoumarin isomers are very similar (as might be expected) and easily allow side-by-side interpretation. Figure 6.1 presents the photoionization mass spectrum of 7-nitro-3,4-benzocoumarin at 213 nm. The spectrum shown in Figure 6.2 illustrates a slightly harder photoionization of 6-nitro-3,4-benzocoumarin at 213 nm. Laser power density is increased by increasing the interaction area between the laser beam and the solid sample. As demonstrated in Chapter 5 for the nitro-PAH, under hard ionization conditions the $NO^+$ ion dominates the spectrum, with a corresponding decrease in intensity of the higher mass peaks.

The laser mass spectrum of 7-nitro-3,4-benzocoumarin displayed in Figure 6.1 clearly shows the higher mass fragment peaks, although their intensity is much less than the m/z 139 ion peak. The peak assignments and m/z values are collected in Table 6.2. The general high mass fragmentation pattern of the 7-nitrobenzocoumarin is also discernable in the spectrum of the 6-nitro isomer, shown in Figure 6.2. Accompanying peak designations are give in Table 6.3. The molecular ion is observed in each spectrum and the major mid- to high-mass peaks arise from a loss of NO or $NO_2$ , followed by successive loss of CO fragments. Similar to the nitro-PAH spectra presented in Chapter

**Figure 6.1** Single-step laser photoionization mass spectrum of 7-nitro-3,4-benzocoumarin showing the prominent m/z 139 ion peak.

**Table 6.2** Peak assignments for the single-step laser photoionization mass spectrum of 7-nitro-3,4-benzocoumarin obtained at 213 nm.

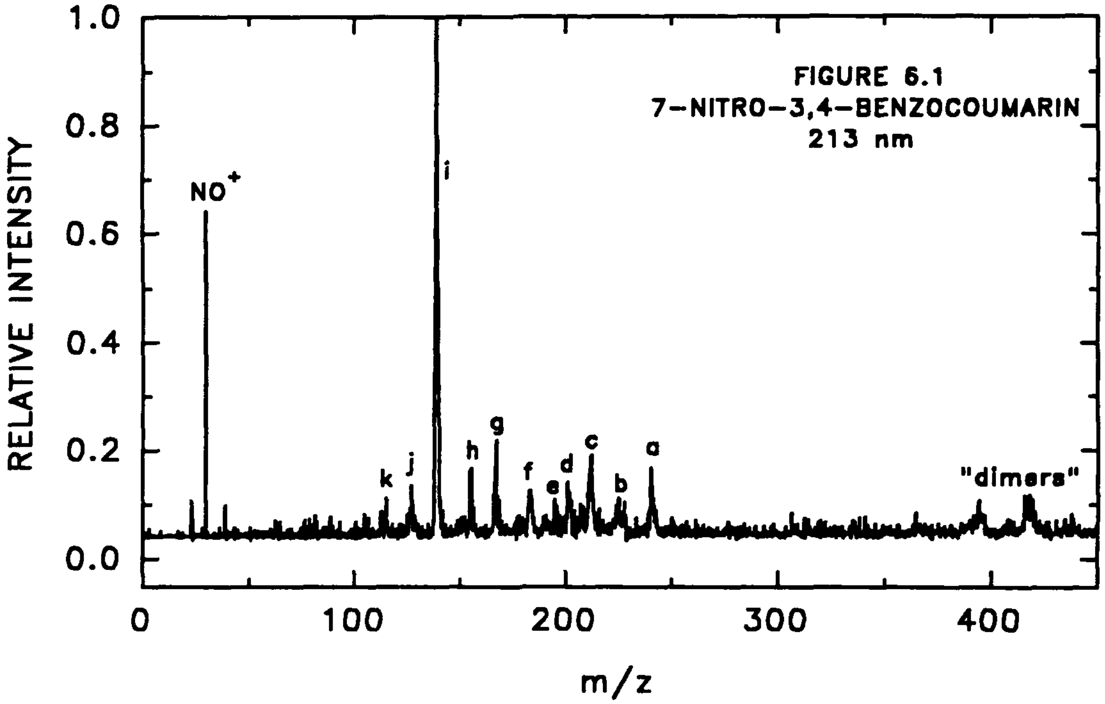

Table 6.2 Peak Assignments for 7-nitro-3,4-benzocoumarin

| Peak | Assignment | m/z |
|---|---|---|
| a | $M^+$ | 241 |
| b | $(M\text{-}O)^+$ | 225 |
| c | $(M\text{-}NO)^+$ | 211 |
| d | $(M\text{-}CCO)^+$ | 201 |
| e | $(M\text{-}NO_2)^+$ | 195 |
| f | $(M\text{-}NO\text{-}CO)^+$ | 183 |
| g | $(M\text{-}NO_2\text{-}CO)^+$ | 167 |
| h | $(M\text{-}NO\text{-}CO\text{-}CO)^+$ | 155 |
| i | $(M\text{-}NO_2\text{-}CO\text{-}CO)^+$ | 139 |
| j | $(M\text{-}NO\text{-}CO\text{-}CO\text{-}CO)^+$ | 127 |
| k | $(M\text{-}NO_2\text{-}CO\text{-}CO\text{-}C_2H_2)^+$ | 113 |

**Figure 6.2** Single-step laser photoionization mass spectrum of 6-nitro-3,4-benzocoumarin displaying a dominant $NO^+$ ion peak.

**Table 6.3** Peak assignments for the single-step laser photoionization mass spectrum of 6-nitro-3,4-benzocoumarin obtained at 213 nm.

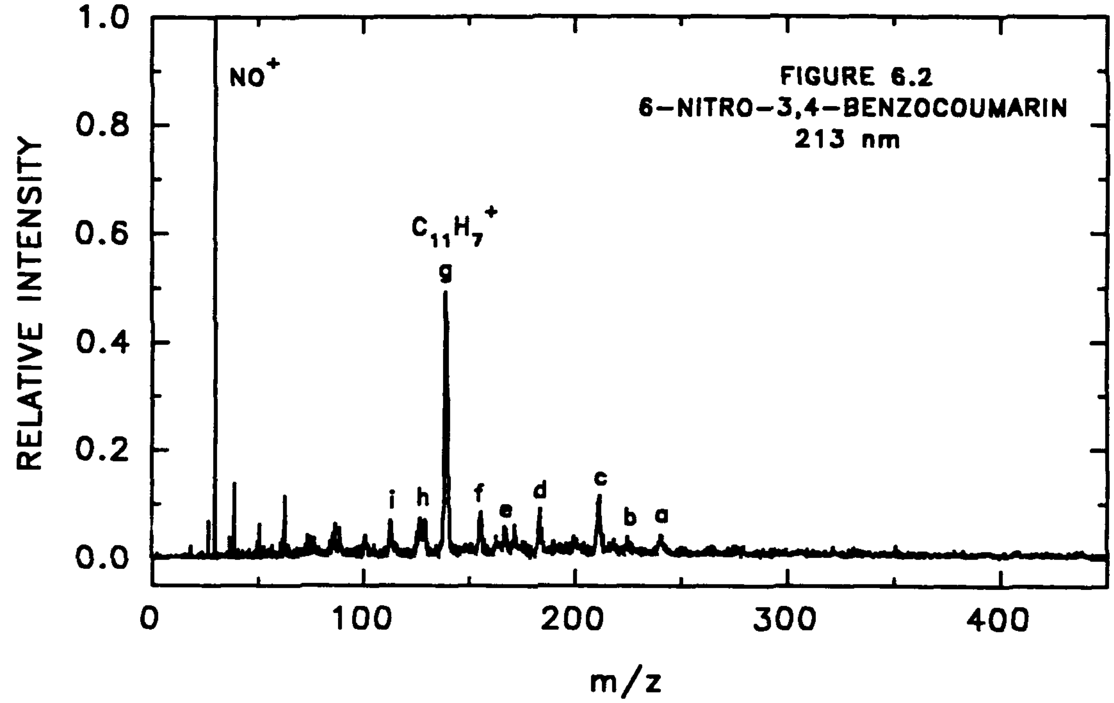

FIGURE 6.2
6-NITRO-3,4-BENZOCOUMARIN
213 nm

**Table 6.3** Peak Assignments for 6-nitro-3,4-benzocoumarin

| Peak | Assignment | m/z |
|---|---|---|
| a | $M^+$ | 241 |
| b | $(M\text{-}O)^+$ | 225 |
| c | $(M\text{-}NO)^+$ | 211 |
| d | $(M\text{-}NO\text{-}CO)^+$ | 183 |
| e | $(M\text{-}NO_2\ \text{-}CO)^+$ | 167 |
| f | $(M\text{-}NO\text{-}CO\text{-}CO)^+$ | 155 |
| g | $(M\text{-}NO_2\text{-}CO\text{-}CO)^+$ | 139 |
| h | $(M\text{-}NO\text{-}CO\text{-}CO\text{-}CO)^+$ | 127 |
| i | $(M\text{-}NO_2\text{-}CO\text{-}CO\text{-}C_2H_2)^+$ | 113 |

5, the $NO^+$ ion is the prominent low mass fragment in the 7-nitrobenzocoumarin spectrum, and is the base peak in the spectrum of the 6-nitro isomer. By far, the most intense fragment in the mid- to high-mass region is the m/z 139 ion peak, and the question of its identity led to the performance of EI MS/MS experiments.

Two main possibilities existed for the identity of the m/z 139 ion, p-nitrophenol or a carbon-hydrogen fragment with a diphenylene-type structure. The first EI MS/MS experiment performed on 7-nitro-3,4-benzocoumarin identified ion fragments that showed a constant neutral loss (CNL) of 30. The CNL experiment is designed to identify nitro-containing fragments of the parent ion, as a neutral loss of 30 would correspond to a loss of the NO fragment. The m/z 139 fragment does not appear in the CNL spectrum shown in Appendix E.

Subsequent EI MS/MS experiments were performed to determine the parent and the daughter ions of the m/z 139 fragment. The parent ion spectrum revealed that m/z 139 arose primarily from the m/z 167 fragment ion. The daughter ion spectrum determined that m/z 113 was the only daughter ion arising from the m/z 139 fragment, corresponding to a loss of acetylene ($C_2H_2$: m/z 26). No peaks corresponding to a loss of NO (m/z 30), $NO_2$ (m/z 46), OH (m/z 17), or $H_2O$ (m/z 18) were observed. Comparison of the CNL, parent and daughter ion spectra (all presented in Appendix E), clearly points to identification of the m/z 139 peak as $C_{11}H_7^+$, with the same possible structure as shown in Figure 5.7 for the m/z 139 fragment of 2-nitro-9-fluorenone.

An unexpected result of the EI MS/MS daughter ion experiments was the appearance of a strong peak at m/z 201 in the daughter ion spectrum of the 7-nitro-3,4-benzocoumarin molecular ion (m/z 241). A small m/z 200 peak is observed in the CNL spectrum. A subsequent daughter ion spectrum of m/z 200 showed a major peak at m/z 170, corresponding to a loss of NO (m/z 30). The daughter spectra for m/z 241 and m/z 200 are also contained in Appendix E. In the laser mass spectrum of 7-nitro-3,4-benzocoumarin (Figure 6.1), a peak is observed at m/z 201. Based on the EI MS/MS experiments, the m/z 201 peak in the laser mass spectrum is tentatively assigned as the $[M\text{-}CCO]^+$ ion. The CCO fragment is presumed to arise from fragmentation of the coumarin lactone structure.

Comparison of the various spectra obtained for the two nitrobenzocoumarin isomers indicates competing fragmentation pathways for nitrobenzocoumarins similar to the pathways deduced for nitro-PAH photofragmentation in Chapter 5. The appearance of the $[M\text{-}NO]^+$ ion as one of the stronger high mass peaks allows the possibility of a nitro-nitrite rearrangement occurring during the desorption-photoionization process. However, the intense $C_{11}H_7^+$ ion peak (m/z 139), arising from the pathway $[M\text{-}NO_2\text{-}CO\text{-}CO]$, implies that loss of $NO_2$ is the major fragmentation pathway for the nitrobenzocoumarin compounds under UV irradiation. The $[M\text{-}NO_2]^+$ ion (m/z 195) is particularly weak in the spectrum of 7-nitro-3,4-benzocoumarin, and apparently absent in the spectrum of the 6-nitro isomer. The weak appearance of the $[M\text{-}NO_2]^+$ ion is attributable to the instability of the phenanthrene lactone fragment ion, formed by loss of $NO_2$ from the parent, and its propensity to rapidly release carbon monoxide to form the highly stable m/z 139 ion.

### 6.4.2 Laser Photoionization of Coumarin Derivative Compounds

The laser mass spectra of 7-hydroxycoumarin and 7-hydroxy-4-methylcoumarin have been obtained at 213 nm in order to study fragmentation of the coumarin backbone structure contained in the nitrobenzocoumarins. The third derivative examined, 2-nitro-6(5H)-phenanthridinone, possesses a structure very similar to the nitrobenzocoumarins, with the substitution of an amino (NH) group into the phenanthrene lactone structure. The laser mass spectra of nitrophenanthridinone have been acquired for comparison with the photoionization spectra of the nitrobenzocoumarin compounds. Molecular structures of the three coumarin derivatives are displayed in Table 6.1 for reference.

The 213 nm photoionization spectra and peak assignments for 7-hydroxycoumarin and 7-hydroxy-4-methylcoumarin are presented in Figure 6.3. A strong, apparently protonated molecular ion peak is observed for each hydroxylated coumarin. Protonation could easily occur by intermolecular interactions in the high density desorption plume. Both spectra show major fragments 'c', attributable to the loss of COH (m/z 29) from the protonated molecular ion. The COH fragment most likely departs from the hydroxylated aromatic ring portion of the molecules. The spectrum of 7-hydroxycoumarin also contains a major fragment at m/z 107 and an accompanying m/z 105 peak. The m/z 107 peak is tentatively attributed to loss of two carbon monoxide molecules from the protonated molecular ion. The m/z 105 fragment, which is also observed for 7-hydroxy-4-methylcoumarin, is assigned as successive loss of two COH fragments from the hydroxycoumarin and loss of (COH-$CH_3$-CO) from the methylcoumarin protonated molecular ions. Apparently, the coumarin backbone fragments by successive loss of carbon monoxide, rather than concerted loss of the entire carbon dioxide molecule.

Figure 6.4 displays the laser mass spectra of 2-nitro-6(5H)-phenanthridinone obtained at 213 nm. The peak assignment information is given in Table 6.4. The mid- to high-mass peaks in the spectrum are of moderate to strong intensity and are readily

**Figure 6.3** Single-step laser photoionization mass spectra of 7-hydroxycoumarin and 7-hydroxy-4-methylcoumarin obtained at 213 nm.

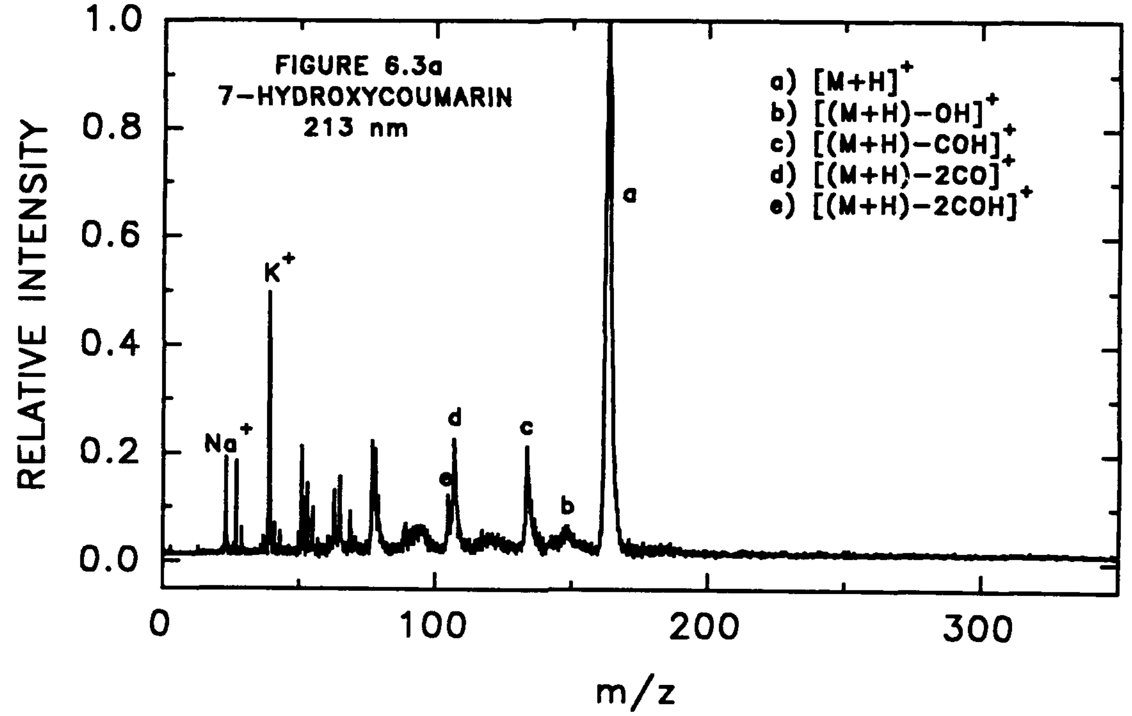
FIGURE 6.3a
7-HYDROXYCOUMARIN
213 nm
a) $[M+H]^+$
b) $[(M+H)-OH]^+$
c) $[(M+H)-COH]^+$
d) $[(M+H)-2CO]^+$
e) $[(M+H)-2COH]^+$
$Na^+$
$K^+$
a
b
c
d
e
RELATIVE INTENSITY
1.0
0.8
0.6
0.4
0.2
0.0
0
100
200
300
m/z

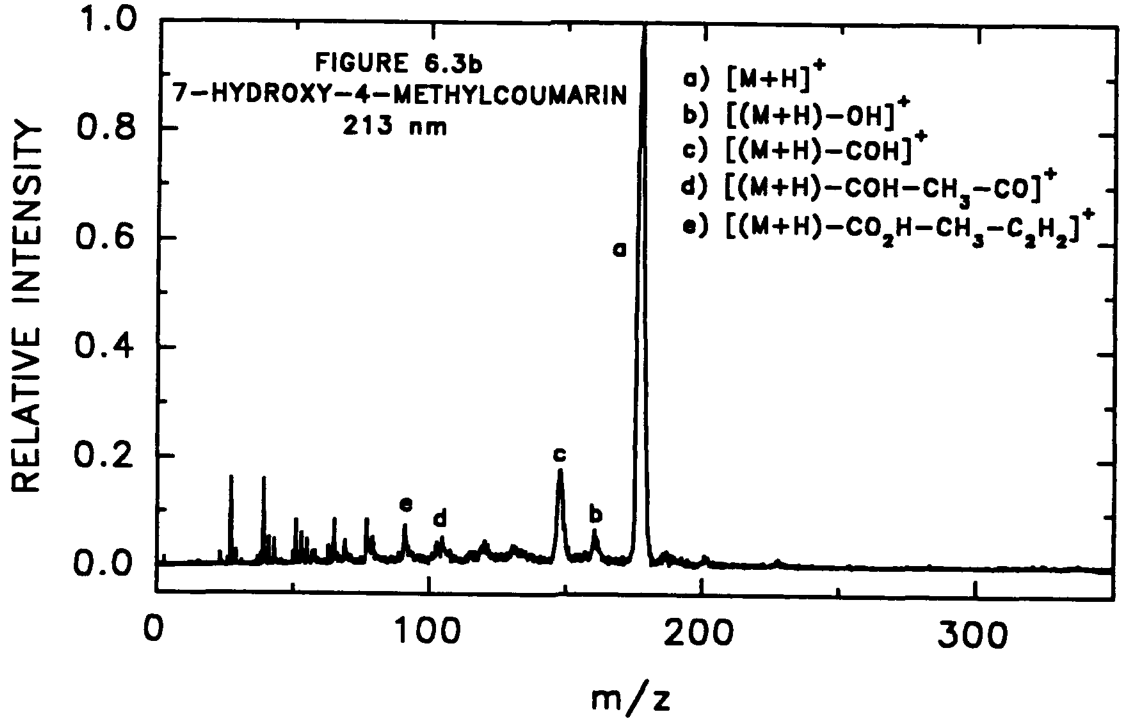
FIGURE 6.3b
7-HYDROXY-4-METHYLCOUMARIN
213 nm
a) $[M+H]^+$
b) $[(M+H)-OH]^+$
c) $[(M+H)-COH]^+$
d) $[(M+H)-COH-CH_3-CO]^+$
e) $[(M+H)-CO_2H-CH_3-C_2H_2]^+$
a
b
c
d
e
RELATIVE INTENSITY
1.0
0.8
0.6
0.4
0.2
0.0
0
100
200
300
m/z

**Figure 6.4** Single-step laser photoionization mass spectrum of 2-nitro-6(5H)-phenanthridinone, displaying more intensity in the mid- and high-mass regions than the nitrobenzocoumarin spectra.

**Table 6.4** Peak assignments for the single-step laser photoionization mass spectrum of 2-nitro-6(5H)-phenanthridinone obtained at 213 nm.

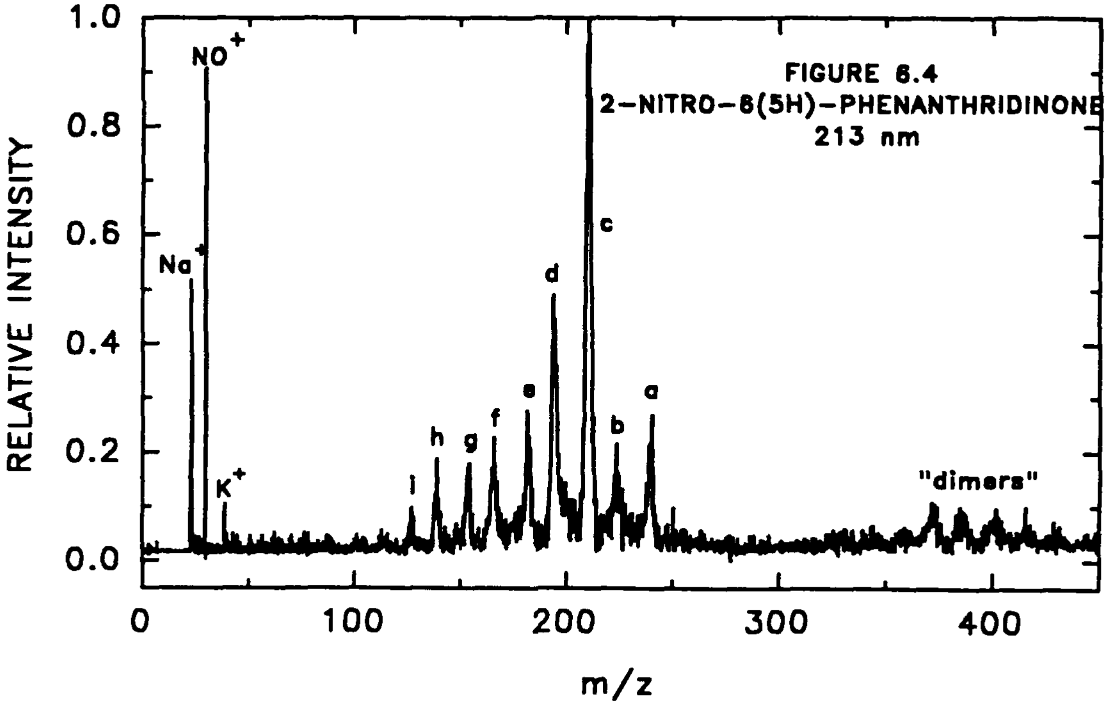

Table 6.4 Peak Assignments for 2-nitro-6(5H)-phenanthridinone

| Peak | Assignment | m/z |
|---|---|---|
| a | $M^+$ | 240 |
| b | $(M\text{-}O)^+$ | 224 |
| c | $(M\text{-}NO)^+$ | 210 |
| d | $(M\text{-}NO_2)^+$ | 194 |
| e | $(M\text{-}NO\text{-}CO)^+$ | 182 |
| f | $(M\text{-}NO_2\text{-}CO)^+$ | 166 |
| g | $(M\text{-}NO\text{-}CO\text{-}CO)^+$ | 154 |
| h | $(M\text{-}NO_2\text{-}CO\text{-}CNH)^+$ | 139 |
| i | $(M\text{-}NO\text{-}CO\text{-}CO\text{-}CNH)^+$ | 127 |

calibrated. The phenanthridinone structure appears better able to stabilize the $[M\text{-}NO]^+$ ion, possibly formed by a nitro-nitrite photorearrangement. In addition, the $[M\text{-}NO_2]^+$, $[M\text{-}NO\text{-}CO]^+$, and $[M\text{-}NO_2\text{-}CO]^+$ fragment ions are easily identified in the spectrum. As is characteristic of nitroaromatics, the $NO^+$ ion is prominent in the low mass region (the m/z 23 peak is attributed to a Na impurity). Overall, the observed fragmentation pattern of 2-nitro-6(5H)-phenanthridinone initially follows the nitro-PAH fragmentation pattern, then continues to fragment by successive loss of CO, along the lines of the coumarin compounds. The nitrophenanthridinone mid- and high-mass fragments showed much more intensity than those of the nitrobenzocoumarins and provided confirmation of the proposed fragmentation of the nitrobenzocoumarin compounds.

## 6.5 CONCLUSIONS

The 213-nm photofragmentation pathways of two nitrobenzocoumarin isomers have been tentatively determined through a series of single-step laser photoionization time-of-flight mass spectrometry experiments on 6- and 7-nitro-3,4-benzocoumarin and three coumarin derivative compounds. Complementary EI MS/MS experiments performed on 7-nitro-3,4-benzocoumarin proved valuable in identifying the primary mid-mass photofragment of the nitrobenzocoumarin compounds. The major mid-mass fragment, observed at m/z 139, has been assigned to the $C_{11}H_7^+$ ion, with the possible structure equivalent to that proposed for the m/z 139 fragment of 2-nitro-9-fluorenone in Figure 5.7. The laser mass spectra obtained for two hydroxylated coumarin compounds and a nitrophenanthridinone confirmed the proposed fragmentation pathways for the nitrobenzocoumarins currently under study.

The nitrobenzocoumarin isomers are proposed to fragment by initially following the characteristic nitro-PAH fragmentation pathway. Fragmentation then continues by successive loss of carbon monoxide, along the lines of the coumarin backbone fragmentation pattern. The very intense m/z 139 peak, arising from the pathway [M-$NO_2$-CO-CO], coupled with observation of the prominent, often dominant, $NO^+$ ion in the nitrobenzocoumarin spectra, suggests that loss of $NO_2$ may be the primary fragmentation pathway for nitrobenzocoumarins. However, presence of significant fragments arising from loss of NO, followed by consecutive loss of CO, indicates a competing fragmentation pathway exists for nitrobenzocoumarin molecules.

Nitrobenzocoumarins have been identified as products in the gas-phase reactions of phenanthrene with OH radical in the presence of $NO_x$,[27] a common urban air pollutant. The 6-nitrobenzocoumarin isomer was identified and quantified in southern California urban air particulate samples and in NIST SRM 1649 urban dust.[28] Up to ~45% of the overall direct-acting mutagenicity of the urban air particulate extracts was attributed to the presence of 6-nitro-3,4-benzocoumarin. It is hoped that the current study of nitrobenzocoumarin photofragmentation patterns will contribute to a better understanding of the atmospheric transformation reactions of this potent mutagenic class. Future work includes application of negative ion laser time-of-flight mass spectrometry to the nitrobenzocoumarin compounds, and ultimately, application of LPMS to determine the presence of highly mutagenic nitrobenzocoumarins in environmental samples.

## 6.6 REFERENCES

1. Schuetzle,D.; Lee, F. S. C.; Prater, T. J.; Tejada, S. B. in *Proceedings of the 10th Annual Symposium on Analytical Chemistry of Pollutants*, Gordan and Breach Science Publishers, New York, 1980, pp. 193-244.

2. Schuetzle, D.; Lee, F. S. C.; Prater, T. J.; Tejada, S. B. *Int. J. Environ. Anal. Chem.* **1981**, *9*, 93.

3. Schuetzle, D.; Riley, T. L.; Prater, T. J.; Harvey, T. M.; Hunt, D. F. *Anal. Chem.* **1982**, *54*, 265.

4. Schuetzle, D.; Paputa, M.; Hampton, C. M.; Marano, R.; Riley, T.; Prater, T. J.; Skewes, L.; Salmeen, I. "The Identification and Potential Sources of Nitrated Polynuclear Aromatic Hydrocarbons (Nitro-PAH) in Diesel Particulate Extracts", pp.299-312 in *Mobile Source Emissions Including Polycyclic Organic Species*, D. Reidel Publishing Co., 1983.

5. Paputa-Peck, M. C.; Marano, R. S.; Schuetzle, D.; Riley, T. L.; Hampton, C. V.; Prater, T. J.; Skewes, L. M.; Jensen, T. E.; Ruehle, P. H.; Bosch, L. C.; Duncan, W. P. *Anal. Chem.* **1983**, *55*, 1946.

6. Williams, P. T.; Bartle, K. D.; Andrews, G. E. "Polycyclic Aromatic Compounds in Diesel Fuels and Particulates", pp. 1011-1027 in *Polynuclear Aromatic Hydrocarbons: Chemistry, Characterization and Carcinogenesis; Ninth International Symposium*, M. Cooke and A. J. Dennis, Eds., Battelle Press, Columbus, OH, 1986.

7. Xu, X. B.; Nachtman, J. P.; Jin, Z. L.; Wei, E. T.; Rappaport, S. M. *Anal. Chim. Acta* **1982**, *136*, 163.

8. Ramdahl, T.; Becher, G.; Björseth. A. *Environ. Sci.Technol.* **1982**, *16*, 861.

9. Nishioka, M. G.; Howard, C. C.; Lewtas, J. "Detection of Hydroxy-Nitro-PAHs and

Nitro-PAHs in an Ambient Air Particulate Extract Using Bioassay Directed Fractionation", pp. 701-715 in *Polynuclear Aromatic Hydrocarbons: Chemistry, Characteri_ation and Carcinogenesis; Ninth International Symposium*, M. Cooke and A. J. Dennis, Eds., Battelle Press, Columbus, OH, 1986.

10. Arey, J.; Harger, W. P.; Helmig, D.; Atkinson, R. *Mutat. Res.* **1992**, *281*, 67.

11. Chuang, C. C.; Mack, G. A.; Petersen, B. A.; Wilson, N. K. "Identification and Quantification of Nitropolynuclear Aromatic Hydrocarbons in Ambient and Indoor Air Particulate Samples" pp. 155-171 in *Polynuclear Aromatic Hydrocarbons: Chemistry, Characterization and Carcinogenesis; Ninth International Symposium*, M. Cooke and A. J. Dennis, Eds., Battelle Press, Columbus, OH, 1986.

12. Harris, W. R.; Chess, E. K.; Okamoto, D.; Remsen, J. F.; Later, D. W. *Environ. Mutagen.* **1984**, *6*, 131.

13. Schnieder, E.; Krenmayr, P.; Varmuza, K. *Monatshefte fur Chemie* **1990**, *121*, 393.

14. Arey, J.; Zielinska, B.; Atkinson, R.; Aschmann, S. M. *Int. J. Chem. Kinet.* **1989**, *21*, 775.

15. Arey, J.; Zielinska, B.; Atkinson, R.; Winer, A. M.; Ramdahl, T.; Pitts, J. N. Jr. *Atmos. Environ.* **1986**, *20*, 2339.

16. Arey, J.; Zielinska, B.; Atkinson, R.; Winer, A. M. *Atmos. Environ.* **1987**, *21*, 1437.

17. Zielinska, B.; Arey, J.; Atkinson, R.; Winer, A. M. *Atmos. Environ.* **1989**, *23*, 223.

18. Arey, J.; Atkinson, R.; Zielinska, B.; McElroy, P. A. *Environ. Sci. Technol.* **1989**, *23*, 321.

19. Ramdahl, T.; Zielinska, B.; Arey, J.; Atkinson, R.; Winer, A. M.; Pitts, J. N. Jr. *Nature*, **1986**, *321*, 425.

20. Nielsen, T.; Ramdahl, T. *Atmos. Environ.* **1986**, *20*, 1507.

21. Atkinson, R.; Aschmann, S. M. *Int. J. Chem. Kinet.*, **1988**, *20*, 513.

22. Arey, J.; Zielinska, B.; Harger, W. P.; Atkinson, R.; Winer, A. M. *Mutat. Res.* **1988**, *207*, 45.

23. Nishioka, M. G.; Howard, C. C.; Lewtas, J. "Detection of Hydroxy-Nitro-PAHs and Nitro-PAHs in an Ambient Air Particulate Extract Using Bioassay Directed Fractionation", pp. 701-715 in *Polynuclear Aromatic Hydrocarbons: Chemistry, Characterization and Carcinogenesis; Ninth International Symposium*, M. Cooke and A. J. Dennis, Eds., Battelle Press, Columbus, OH, 1986.

24. Nishioka, M. G.; Howard, C. C.; Contos, D. A.; Ball, L. M.; Lewtas, J. *Environ. Sci. Tech.* **1988**, *22*, 908.

25. Schuetzle, D.; Lewtas, J. *Anal. Chem.* **1986**, *58*, 1060A.

26. Lewtas, J.; Chuang, J.; Nishioka, M.; Petersen, B. *Int. J. Environ. Anal. Chem.* **1990**, *39*, 245.

27. Arey, J.; Harger, W. P.; Helmig, D.; Atkinson, R. *Mutation Res.* **1992**, *281*, 67.

28. Helmig, D.; López-Cancio, J.; Arey, J.; Harger, W. P.; Atkinson, R. *Environ. Sci. Technol.* **1992**, *26*, 2207.

29. Helmig, D.; Arey, J.; Harger, W. P.; Atkinson, R.; López-Cancio, J. *Environ. Sci. Technol.* **1992**, *26* , 622.

30. Young, M. K. G. *Characterization of Polycyclic Aromatic Hydrocarbons and Chlorinated Polycyclic Aromatic Hydrocarbons in Soots by Laser Desorption-Laser Photoionization Mass Spectrometry*, Dissertation, (University of California, Davis), Dec., 1991.

31. Young, M. K. G.; Jones, A. D.; Kelly, P. B. Proceedings of the 39th ASMS Conference on Mass Spectrometry and Allied Topics, Nashville, TN., May 19-24, 1991, p. 342.

32. Wiley, W. C.; McLaren, I. H. *Rev. Sci. Instrum.* **1955**, *26*, 1150.

33. Hudson, B.; Kelly, P.B.; Ziegler, L. D.; Desiderio, R. A.; Gerrity, D. P.; Hess, W.; Bates, R. "Far Ultraviolet Laser Resonance Raman Studies of Electronic Excitations," pp. 1-32 in *Advances in Laser Spectroscopy: Volume 3*, B. A. Garetz and J. R. Lombardi, Eds., John Wiley & Sons Ltd., Chichester, Great Britain, 1986.

34. Smith, C. H. Dissertation, University of California, Davis, Fall 1993, in preparation.

# CHAPTER 7

## Laser Photoionization Time-of-Flight Mass Spectrometry of Mixtures Containing Nitrated Polycyclic Aromatic Hydrocarbons

### 7.1 ABSTRACT

The mass spectra of several two-component mixtures of nitrated polycyclic aromatic hydrocarbons (nitro-PAH ) have been investigated by single-step laser photoionization time-of-flight mass spectrometry. Additionally, laser mass spectra of a six-component mixture containing two nitro-PAH and four PAH standards have been examined. Pulsed UV radiation at 213 nm was used for the desorption and ionization of the solid sample deposited on an aluminum probe. Four nitro-PAH standards were studied: 9-nitroanthracene, 1-nitropyrene, 2-nitrofluorene, and 2-nitro-9-fluorenone. The two-component mixtures contained two of the four standard nitro-PAH in equivalent mass amounts. The composition of the PAH/nitro-PAH mixture was modelled after the composition of NIST SRM 1650 diesel particulate matter.

Strong $NO^+$ ion peaks are visible in all the two-component nitro-PAH mass spectra. In two-component mixtures containing 1-nitropyrene, the high mass peaks in the spectra are predominantly fragments of 1-nitropyrene. The $[M-NO]^+$ ion peak is the strongest high mass fragment peak observed for both 9-nitroanthracene and 2-nitrofluorene in mixtures with 1-nitropyrene. The laser mass spectra of the six-component PAH/nitro-PAH mixture were dominated by PAH molecular ions and fragment ions. Significant intensity in the $NO^+$ ion peak was only observed under very hard ionization conditions. Comparison of the various spectra suggest that identification of a singular nitro-PAH

component in a mixture of nitro-PAH could be accomplished by laser photoionization methods.

The photofragmentation patterns determined for the nitro-PAH standards in Chapter 5 show characteristic $[M\text{-}NO]^+$, $[M\text{-}NO_2]^+$ and $[M\text{-}NO\text{-}CO]^+$ ions as well as the molecular ion and a strong $NO^+$ ion peak. The $NO^+$ ion peak is also a strong fragment ion in nitrobenzene laser mass spectra however, the $[M\text{-}NO]^+$ ion, characteristic of highly conjugated nitro-PAH, is typically not observed in laser ionization spectra of lesser conjugated nitro-aromatics such as nitrobenzene.[1] The characteristic high mass fragments, combined with observation of the strong $NO^+$ ion peak, may be useful in the determination of nitro-PAH in PAH-dominated mixtures.

## 7.2 INTRODUCTION

The analytical chemistry of nitrated polycyclic aromatic hydrocarbons (nitro-PAH) is of widespread interest due to the highly mutagenic properties of this chemical class. Nitro-PAH are derivatives of PAH, which are abundant in fossil fuels and are the incomplete combustion products of organic materials. Direct emission into the atmosphere from combustion sources distributes PAH between the gas and particle phases.[2] Nitro-PAH present in direct emissions are primarily the electrophilic nitration products resulting from adsorbed-phase reactions of PAH with $NO_x$ and $HNO_3$.[3] Nitro-PAH found in the atmosphere are often the result of an atmospheric transformation of the parent PAH by the gas-phase reaction with OH radical in the presence of $NO_x$ pollutants.[3] Once formed, atmospheric nitro-PAH can readily condense on respirable particulate matter.

Nitro-PAH have been determined in a variety of environmental samples including diesel exhaust,[4-10] urban and indoor air particulate,[11-14] aluminum smelter effluent,[15] coal fly ash,[16] and wood and cigarette smoke condensates.[17,18] The concentration of nitro-PAH in environmental samples is typically one to two orders of magnitude less than that of the unsubstituted PAH present. Low concentrations coupled with their ubiquitous presence and potent direct-acting mutagenicity underscore the importance of developing highly sensitive and selective methods for determination of nitro-PAH in environmental samples. Laser photoionization mass spectrometry (LPMS) offers the potential for accomplishing such sensitive,selective determinations.

As demonstrated by several studies on diesel particulate matter[4-9] and urban air particulate,[10-14] an environmental sample is an extremely complex mixture containing PAH, nitro-PAH, hydroxylated and oxygenated PAH-derivatives, as well as numerous aliphatic and inorganic compounds. Determinations of nitro-PAH in environmental samples have generally involved organic solvent extraction, HPLC fractionation, and identification by various low and high resolution GC/MS methods. Particulate extracts are typically fractionated into non-polar (PAH), moderately polar (nitro-PAH), and highly polar (oxy- and hydroxy-PAH) subfractions for chemical and bioassay analysis. Schuetzle et al.[7] found approximately 200 nitro-PAH species present in the moderately polar fractions of diesel exhaust extract. The definitive analysis of individual nitro-PAH in environmental samples is complicated by the complexity of the samples and the generally low concentration of nitro-PAH relative to unsubstituted PAH.

In order to examine the application of laser photoionization time-of-flight mass spectrometry (LPMS) to characterization and analysis of nitro-PAH in mixtures, mass spectra have been obtained at 213 nm for two-component mixtures of four nitro-PAH standards: 9-nitroanthracene, 1-nitropyrene, 2-nitrofluorene, and 2-nitro-9-fluorenone. In addition, a six component mixture containing four PAH and two nitro-PAH standards was investigated to evaluate the potential of LPMS for determination of nitro-PAH in a mixture with unsubstituted PAH. The composition of the six component mixture was modelled on the composition of NIST SRM 1650 diesel particulate matter. The high mass regions in all the laser mass spectra of two-component mixtures containing 1-nitropyrene were dominated by 1-nitropyrene fragment ions. However, it was usually possible to identify characteristic peaks of each nitro-PAH component in the two-component mixture spectra. The presence of nitro-PAH in the six-component mixture was more difficult to detect as the characteristic $NO^+$ ion was abundant only under hard ionization conditions, which significantly decreased the resolution of high mass peaks in our spectra. The representative spectra acquired in the current study are prerequisites for application of the LPMS method to the determination of nitro-PAH in more complex mixtures.

## 7.3 EXPERIMENTAL

PAH and nitro-PAH standards were purchased from Aldrich Chemical Co., and were used without further purification. The PAH standards used were (molecular weight and stated purity in parenthesis): phenanthrene (178, 98%), pyrene (202, 99%), chrysene (228, 98%), and benzo[e]pyrene (252, 99%). The nitro-PAH compounds studied were 9-nitroanthracene (223, 97%), 1-nitropyrene (247, 97%), 2-nitrofluorene(211, 98%), and 2-nitro-9-fluorenone (225, 99%).

Laser photoionization mass spectra are obtained using a custom-built time-of-flight mass spectrometer operating in the linear mode.[19,20] The sample probe is inserted into the source region through a fast load-lock assembly which positions the aluminum probe tip between the extractor and repeller plates of the Wiley-McLaren[21] based two-stage ion optics. The aluminum probe tip has a flattened face which is positioned perpendicular to the flight tube axis. The probe can be raised and lowered externally to allow analysis at different locations on the same sample. The source region is fitted with S1-UV quartz windows to allow transmission of the UV laser beam. Two oil diffusion pumps equipped with cryotraps separately pump down the source and flight tube regions to an operating vacuum of ~ $10^{-6}$ torr.

Sample solutions of the two-component mixtures of nitro-PAH standards contain an equal amount (~ 1 mg) of each component, prepared at concentrations of 5-10 mg/ml in $CH_2Cl_2$. The six-component PAH/nitro-PAH mixture consists of phenanthrene (7.1 ± 0.1mg), pyrene (4.9 ± 0.1mg), chrysene (2.9 ± 0.1mg), benzo[e]pyrene (1.0 ± 0.1mg), 1-nitropyrene (2.0 ± 0.1mg), and 2-nitrofluorene (0.15 ± 0.05mg), prepared to 15-20 mg/ml in $CH_2Cl_2$. A typical sample is prepared by depositing a 20-30 μl aliquot of a standard solution, via syringe, directly onto the flattened probe face and allowing it to air dry, forming a thin solid layer. The relatively high concentration of the standard solution yields a residual solid layer thick enough to minimize interference from aluminum ion formation during ionization of the sample.

Pulsed UV radiation at 266 nm is produced using the fourth harmonic of a Q-switched Quanta Ray DCR-3 Nd:YAG laser with an 8 ns pulse width. Sum mixing of the Nd:YAG 1064 nm fundamental and the 266 nm fourth harmonic in BBO (β -barium borate crystal) generates the 213 nm photons.[22] The UV laser beam is focussed into the source region through a 250 mm S1-UV quartz lens, which is also used to direct the UV beam path such that the laser beam grazes the surface of the sample. Laser energy is measured just prior to the spectrometer entrance window by a Molectron Model J9LP Joulemeter interfaced to a PcJ meter (Q&A Instruments).

The laser-induced thermal desorption induced at the fringe of the beam waist imparts enough energy to the desorbed molecules to move them a few microns from the surface, and into a region of higher power density. Positive ions form just above the surface in the high-density plume by multiphoton ionization and/or collision processes. Laser energy typically ranges from 5-20 μJ/pulse while operating at 5 Hz, yielding maximum power densities on the order of $10^8$ - $10^9$ W/cm$^2$ at the focus.

Positive ions formed during each laser pulse are accelerated into the flight tube and drift until impinging on the dual microchannel plate (MCP) detector. Current generated at the MCP detector is 50-ohm terminated into a 100 MHz DSP Model 2001AS Transient Recorder and digitized with 8-bit precision. In a typical experiment, data is collected and signal averaged by a DSP Model 4101 Averaging Memory over 100-500 laser pulses, then transferred by a CAMAC interface to an Everex 386 microcomputer. Data acquisition and subsequent analysis are controlled by software developed in-house.[20,23] The Q-switch sync is used to trigger the data acquisition electronics, allowing the time origin in the mass spectra to correspond to arrival of the UV beam at the source.

## 7.4 RESULTS AND DISCUSSION

### 7.4.1 Two-Component Mixtures of Nitro-PAH

The molecular structures, formulas and weights of all four nitro-PAH standards used to make up the two-component mixtures are collected in table 5.1 for convenient reference. The laser photoionization mass spectra of 9-nitroanthracene, 1-nitropyrene, 2-nitrofluorene, and 2-nitro-9-fluorenone presented in Chapter 5 show fragmentation patterns characteristic of nitro-PAH. Using 213 nm photoionization, molecular ion is observed in the nitro-PAH spectra and the base peak is often the $[M-NO]^+$ fragment ion. Other characteristic high mass fragments of nitro-PAH are the $[M-NO_2]^+$ and $[M-NO-CO]^+$ ions. Dimers and photoproducts observed in the high mass region are attributable to condensed-phase surface chemistry and bimolecular interactions occurring during the desorption process. The $NO^+$ ion is the prominent low mass fragment in the 213 nm spectra of all the nitro-PAH standards in the current study.

Laser photoionization mass spectra obtained at 213 nm, are presented for five two-component mixtures of the nitro-PAH standards. The nitro-PAH two-component mixtures (and molecular weights of the components) investigated in the current study are:

Sample 1: 1-nitropyrene (247) and 9-nitroanthracene (223)
Sample 2: 1-nitropyrene (247) and 2-nitrofluorene (211)
Sample 3. 1-nitropyrene (247) and 2-nitro-9-fluorenone (225)
Sample 4: 9-nitroanthracene (223) and 2-nitrofluorene(211)
Sample 5: 2-nitrofluorene (211) and 2-nitro-9-fluorenone (225)

Equal mass amounts of each nitro-PAH were used to make up the two-component mixtures. The sixth combination, 9-nitroanthracene (223) and 2-nitro-9-fluorenone (225), is not examined because the high mass fragments are not separable at current instrument mass resolution capability.

The photoionization mass spectrum of sample 1, 1-nitropyrene and 9-nitroanthracene, is shown in Figure 7.1, and peak assignments are given in Table 7.1. The molecular ion, along with the $[M-NO]^+$, $[M-NO_2]^+$, and $[M-NO-CO]^+$ major fragment ions of each component in sample 1 are observable in the spectrum. The fragment ions belong-

**Figure 7.1** Single-step laser photoionization mass spectrum of an equal mass mixture of 1-nitropyrene and 9-nitroanthracene, obtained at 213 nm.

**Table 7.1** Peak assignments for the single-step laser photoionization mass spectrum of a two-component mixture containing 1-nitropyrene and 9-nitroanthracene.

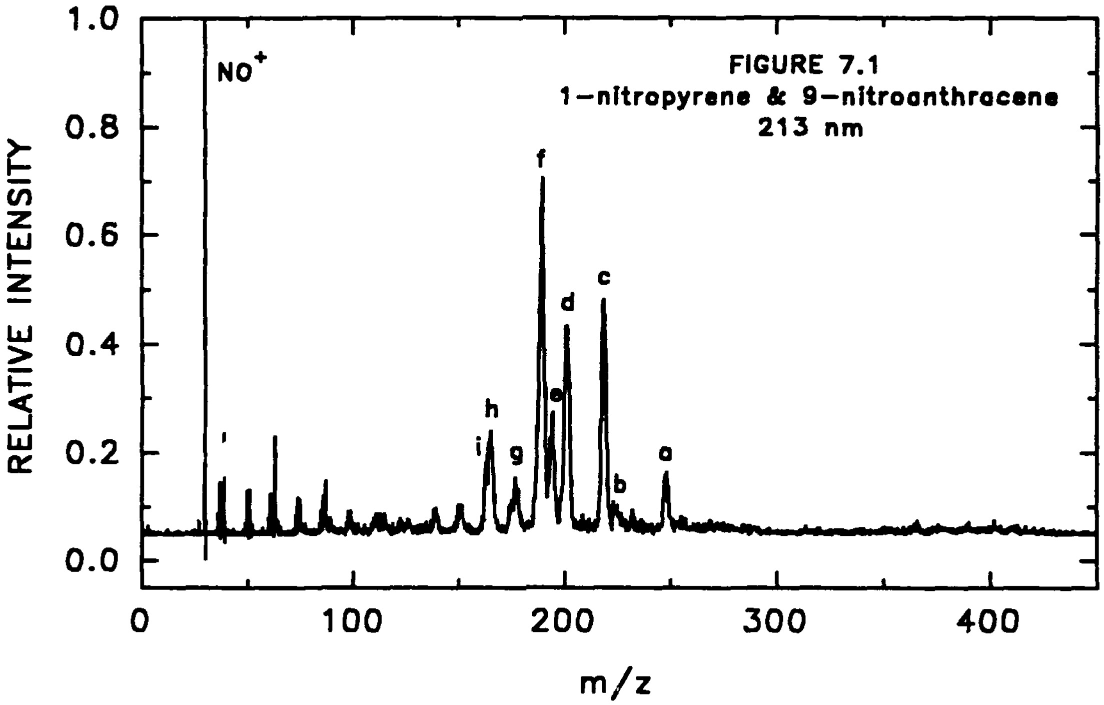

Table 7.1 Peak Assignments: 1-nitropyrene [1NP] & 9-nitroanthracene [9NA]

| Peak | Assignment | m/z |
|---|---|---|
| a | $M^+$ [1NP] | 247 |
| b | $M^+$ [9NA] | 223 |
| c | $(M\text{-}NO)^+$ [1NP] | 217 |
| d | $(M\text{-}NO_2)^+$ [1NP] | 201 |
| e | $(M\text{-}NO)^+$ [9NA] | 193 |
| f | $(M\text{-}NO\text{-}CO)^+$ [1NP] | 189 |
| g | $(M\text{-}NO_2)^+$ [9NA] | 177 |
| h | $(M\text{-}NO\text{-}CO)^+$ [9NA] | 165 |
| i | $(M\text{-}NO\text{-}CO\text{-}C_2H_2)^+$ [1NP] | 163 |

ing to 1-nitropyrene are considerably more intense than the corresponding fragments ions of 9-nitroanthracene, with the most intense high mass fragment being the $[M\text{-}NO\text{-}CO]^+$ ion of 1-nitropyrene. Characteristic $C_nH_x^+$ ions are observed in the low mass region, but the dominant peak in the spectrum corresponds to the $NO^+$ ion.

Figure 7.2 presents the laser mass spectrum of sample 2, 1-nitropyrene and 2-nitrofluorene, with the corresponding peak assignments given in Table 7.2. The spectrum of sample 2 is dominated by the fragment ions of 1-nitropyrene. The only peak which can be definitely assigned to 2-nitrofluorene is the peak at m/z 181, corresponding to its $[M\text{-}NO]^+$ ion. However, peaks 'g' and 'h' are broader and more intense than is usual for 1-nitropyrene alone. The broadening and enhancement of peaks 'g' and 'h' could be due to overlap between the generally strong $[M\text{-}NO_2]^+$ and $[M\text{-}NO\text{-}CO]^+$ ions of 2-nitrofluorene and the weaker mid-mass ions of 1-nitropyrene, which arise from the loss of acetylene in the major 1-nitropyrene fragments. As expected, the $NO^+$ ion is the prominent low mass peak in the spectrum.

The laser mass spectrum of sample 3, 1-nitropyrene and 2-nitro-9-fluorenone, is displayed in Figure 7.3, and accompanying peak assignments are given in Table 7.3. The only peak in the spectrum which is directly attributable to 2-nitro-9-fluorenone is the weak signal at m/z 225, corresponding to its molecular ion. The photoionization spectra of 2-nitro-9-fluorenone presented in Chapter 5 showed strong mid-mass fragments at m/z 139 and m/z 151, resulting from fragmentation of the fluorenone backbone structure. The slight enhancement in the mid-mass fragment region of the spectrum of sample 3 could be due to contributions from 2-nitro-9-fluorenone. Overall the spectrum is dominated by the fragment ions of 1-nitropyrene. The common low mass carbon fragment pattern is

**Figure 7.2** Single-step laser photoionization mass spectrum of an equal mass mixture of 1-nitropyrene and 2-nitrofluorene, obtained at 213 nm.

**Table 7.2** Peak assignments for the single-step laser photoionization mass spectrum of a two-component mixture containing 1-nitropyrene and 2-nitrofluorene.

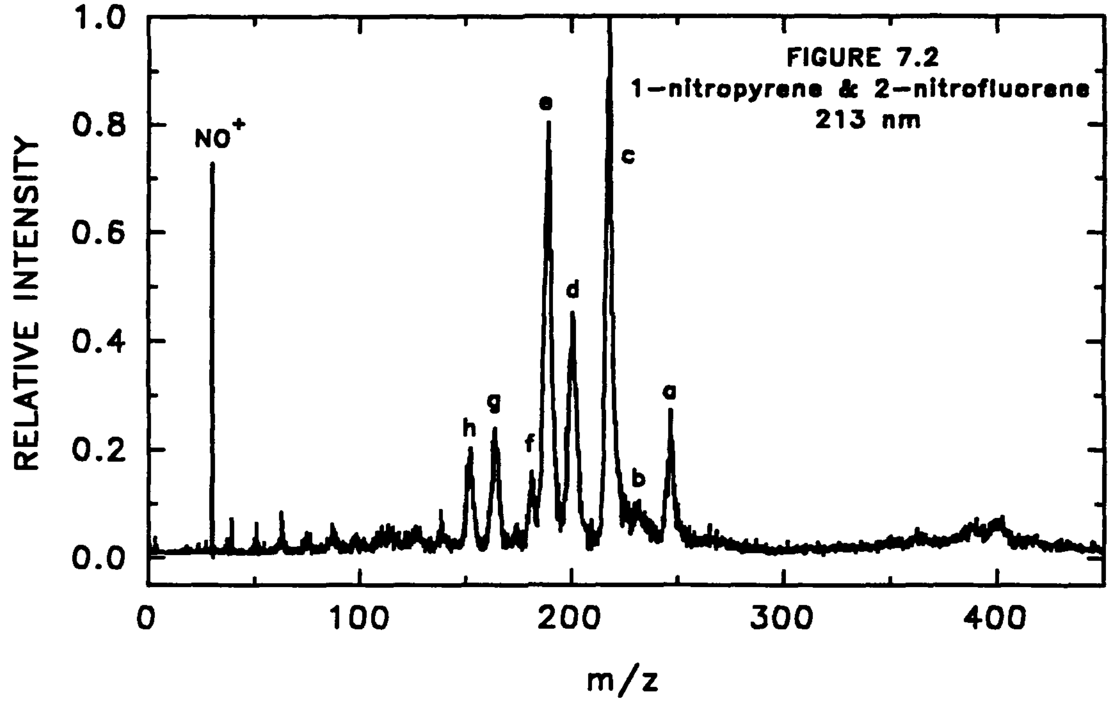

Table 7.2 Peak Assignments: 1-nitropyrene [1NP] & 2-nitrofluorene [2NF]

| Peak | Assignment | m/z |
|---|---|---|
| a | $M^+$ [1NP] | 247 |
| b | $(M\text{-}O)^+$ [1NP] | 231 |
| c | $(M\text{-}NO)^+$ [1NP] | 217 |
| d | $(M\text{-}NO_2)^+$ [1NP] | 201 |
| e | $(M\text{-}NO\text{-}CO)^+$ [1NP] | 189 |
| f | $(M\text{-}NO)^+$ [2NF] | 181 |
| g | $(M\text{-}NO_2)^+$[2NF]+$(M\text{-}NO\text{-}CO\text{-}C_2H_2)^+$[1NP] | 165 + 163 |
| h | $(M\text{-}NO\text{-}CO)^+$[2NF]+$(M\text{-}NO_2\text{-}2C_2H_2)^+$[1NP] | 153 + 149 |

**Figure 7.3** Single-step laser photoionization mass spectrum of an equal mass mixture of 1-nitropyrene and 2-nitro-9-fluorenone, obtained at 213 nm.

**Table 7.3** Peak assignments for the single-step laser photoionization mass spectrum of a two-component mixture containing 1-nitropyrene and 2-nitro-9-fluorenone.

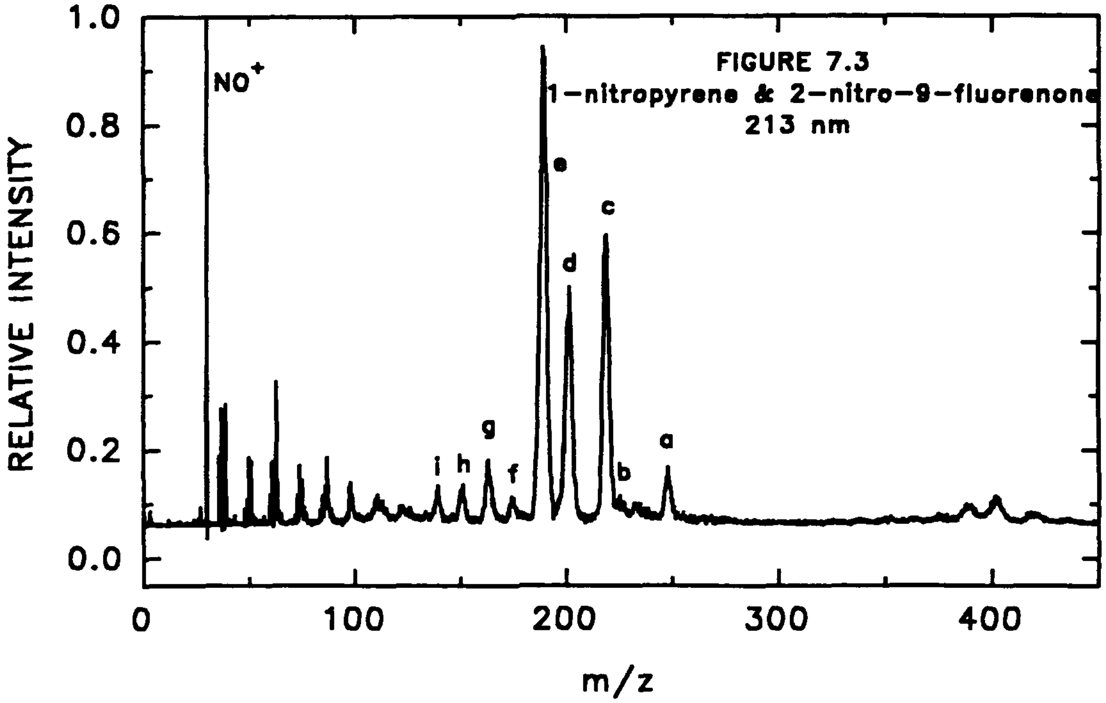

**Table 7.3** Peak Assignments: 1-nitropyrene [1NP] & 2-nitro-9-fluorenone [N9F]

| Peak | Assignment | m/z |
|---|---|---|
| a | $M^+$ [1NP] | 247 |
| b | $M^+$ [N9F] | 225 |
| c | $(M\text{-}NO)^+$ [1NP] | 217 |
| d | $(M\text{-}NO_2)^+$ [1NP] | 201 |
| e | $(M\text{-}NO\text{-}CO)^+$ [1NP] | 189 |
| f | $(M\text{-}NO_2\text{-}C_2H_2)^+$ [1NP] | 175 |
| g | $(M\text{-}NO\text{-}CO\text{-}C_2H_2)^+$ [1NP] | 163 |
| h | $(M\text{-}NO_2\text{-}2C_2H_2)^+$[1NP]+$(M\text{-}NO_2\text{-}CO)^+$[N9F] | 149 + 151 |
| i | $(M\text{-}NO\text{-}2CO)^+$[N9F]+(Peak g-$C_2H_2)^+$[1NP] | 139 + 137 |

apparent in the spectrum however, $NO^+$ is the predominant low mass peak once again.

Comparison of the spectra of two-component mixtures containing 1-nitropyrene demonstrates that 1-nitropyrene has a larger cross-section of absorbance at 213 nm than 9-nitroanthracene, 2-nitrofluorene, and particularly, 2-nitro-9-fluorenone. All of the spectra are dominated by the fragment ions of 1-nitropyrene, which is the most highly conjugated of the four nitro-PAH compounds studied. However, the spectra also show that 9-nitroanthracene, 2-nitrofluorene and 1-nitropyrene continue to follow their characteristic fragmentation pathways, yielding $[M\text{-}NO]^+$, $[M\text{-}NO_2]^+$, and $[M\text{-}NO\text{-}CO]^+$ high mass fragments, in two-component mixtures with another nitro-PAH. The major high mass fragments of 9-nitroanthracene and 2-nitrofluorene can be identified in the laser mass spectra of their equal mass mixtures with 1-nitropyrene.

The 213-nm photoionization spectrum of sample 4, 9-nitroanthracene and 2-nitrofluorene, is shown in Figure 7.4, and labelled peaks are identified in Table 7.4. The molecular ion of each component is observed, and the $[M\text{-}NO]^+$ ions are distinguishable in the spectrum. The enhanced intensity in peak 'f ' is probably due to contributions from two primary fragments; the $[M\text{-}NO_2]^+$ ion of 2-nitrofluorene and the $[M\text{-}NO\text{-}CO]^+$ ion of 9-nitroanthracene which have the coincident m/z of 165. Similarly, the enhancement in peak 'h' (m/z 139) is due to loss of acetylene from the corresponding m/z 165 ions. The broadness in peak 'g' is attributable to overlap of the $[M\text{-}NO\text{-}CO]^+$ ion (m/.z 153) of 2-nitrofluorene and the $[M\text{-}NO_2\text{-}C_2H_2]^+$ ion (m/z 151) of 9-nitroanthracene. Overall the fragment ions of 9-nitroanthracene appear to dominate the spectrum. The intense $NO^+$ fragment ion (m/z 30) is the base peak in the spectrum.

Figure 7.5 displays the spectrum of the final two-component mixture, sample 5,

**Figure 7.4** Single-step laser photoionization mass spectrum of an equal mass mixture of 9-nitroanthracene and 2-nitrofluorene, obtained at 213 nm.

**Table 7.4** Peak assignments for the single-step laser photoionization mass spectrum of a two-component mixture containing 9-nitroanthracene and 2-nitrofluorene.

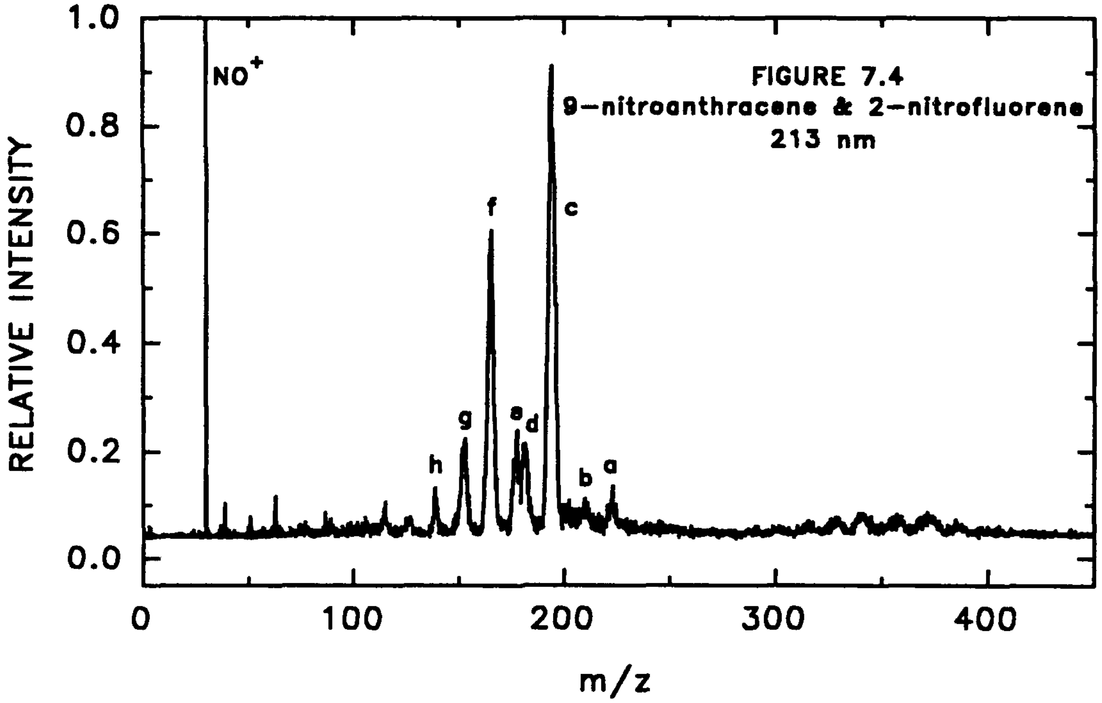

FIGURE 7.4
9–nitroanthracene & 2–nitrofluorene
213 nm

**Table 7.4** Peak Assignments: 9-nitroanthracene [9NA] & 2-nitrofluorene [2NF]

| **Peak** | **Assignment** | **m/z** |
|---|---|---|
| a | $M^+$ [9NA] | 223 |
| b | $M^+$ [2NF] | 211 |
| c | $(M\text{-}NO)^+$ [9NA] | 193 |
| d | $(M\text{-}NO)^+$ [2NF] | 181 |
| e | $(M\text{-}NO_2)^+$ [9NA] | 177 |
| f | $(M\text{-}NO\text{-}CO)^+$ [9NA]+$(M\text{-}NO_2)^+$ [2NF] | 165 |
| g | $(M\text{-}NO_2\text{-}C_2H_2)^+$[9NA]+$(M\text{-}NO\text{-}CO)^+$[2NF] | 151 + 153 |
| h | $(M\text{-}NO_2\text{-}C_2H_2)^+$[2NF]+(Peak f-$C_2H_2)^+$[9NA] | 139 |

**Figure 7.5** Single-step laser photoionization mass spectrum of an equal mass mixture of 2-nitrofluorene and 2-nitro-9-fluorenone, obtained at 213 nm.

**Table 7.5** Peak assignments for the single-step laser photoionization mass spectrum of a two-component mixture containing 2-nitrofluorene and 2-nitro-9-fluorenone.

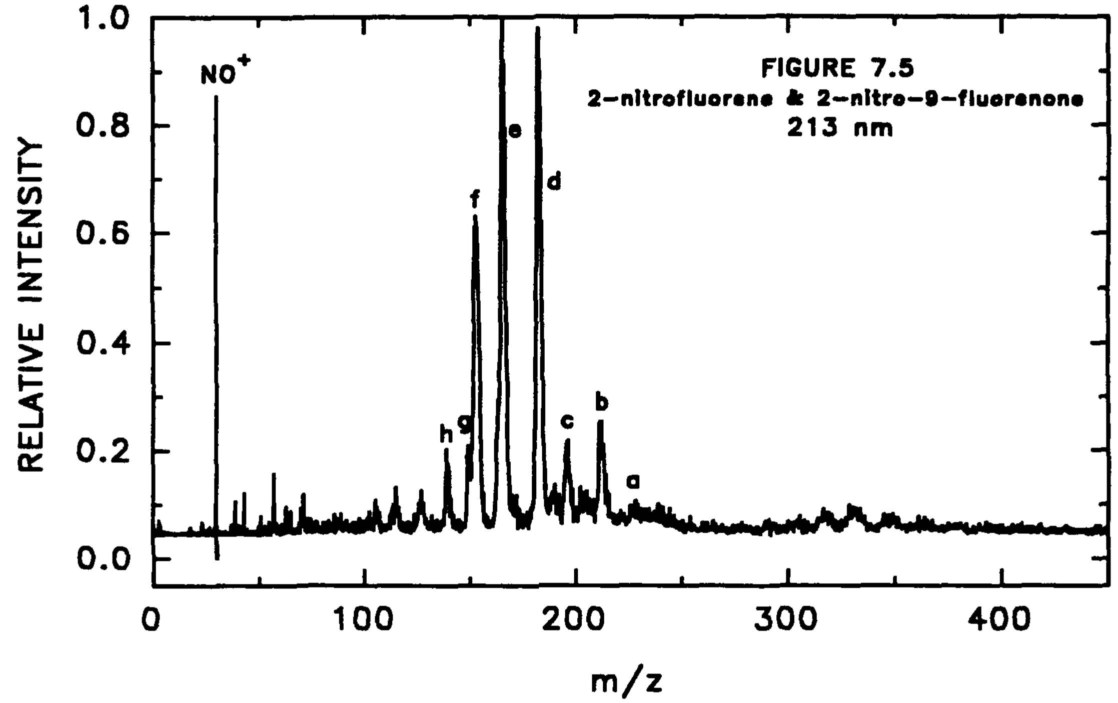

Table 7.5 Peak Assignments: 2-nitrofluorene [2NF] & 2-nitro-9-fluorenone [N9F]

| Peak | Assignment | m/z |
|---|---|---|
| a | $M^+$ [N9F] | 225 |
| b | $M^+$ [2NF] | 211 |
| c | $(M\text{-}NO)^+$ [N9F] | 195 |
| d | $(M\text{-}NO)^+$ [2NF] | 181 |
| e | $(M\text{-}NO_2)^+$ [2NF] + $(M\text{-}NO\text{-}CO)^+$ [N9F] | 165 + 167 |
| f | $(M\text{-}NO\text{-}CO)^+$ [2NF] | 153 |
| g | $(M\text{-}NO_2\text{-}CO)^+$ [N9F] | 151 |
| h | $(M\text{-}NO\text{-}2CO)^+$[N9F]+$(M\text{-}NO_2\text{-}C_2H_2)^+$[2NF] | 139 |

along with tabulated peak information in Table 7.5. In this mixture of 2-nitrofluorene and 2-nitro-9-fluorenone, major high mass peaks of each component are distinguishable with the peaks of 2-nitrofluorene exceeding the 2-nitro-9-fluorenone peaks in intensity. The molecular ion of 2-nitro-9-fluorenone is weakly present, but its $[M\text{-}NO]^+$ ion makes a stronger appearance. The $[M\text{-}NO\text{-}CO]^+$ ion (m/z 167) of 2-nitro-9-fluorenone has probably contributed to the enhanced $[M\text{-}NO_2]^+$ ion peak (m/z 165, peak 'e') of 2-nitrofluorene. Peak 'g' at m/z 151 corresponds to the diphenylene fragment ion of 2-nitro-9-fluorenone and the increased intensity of the m/z 139 ion indicates contribution from its $C_{11}H_7^+$ ion. Proposed structures of both the diphenylene and $C_{11}H_7^+$ ion fragments are illustrated in Figure 5.7. All the expected high mass fragment ions of 2-nitrofluorene are clearly observed and the characteristic $NO^+$ ion is prominent in the low mass region of the spectrum.

Comparing the spectra of sample 4 and sample 5, it appears that 9-nitroanthracene with its more extensive pi system, has a larger cross section for absorbance or photoionization at 213 nm than either 2-nitrofluorene or 2-nitro-9-fluorenone, with their cyclopenta-fused ring structures. The additional electron withdrawing carbonyl group of 2-nitro-9-fluorenone appears to decrease its absorbance cross section relative to 2-nitrofluorene, and the results could be generalized to include 9-nitroanthracene as well. It is possible to distinguish the major high mass peaks of 9-nitroanthracene, 2-nitrofluorene and 2-nitro-9-fluorenone in two-component mixtures with each other, and the nitro-PAH still exhibit the characteristic fragments, $[M\text{-}NO]^+$, $[M\text{-}NO_2]^+$ and $[M\text{-}NO\text{-}CO]^+$, for each component. The $NO^+$ ion is as prominent in the two-component mixture spectra as it was in the single component spectra, allowing the possibility that the $NO^+$

ion could be a useful marker for nitro-PAH in heterogenous mixtures with unsubstituted PAH compounds.

### 7.4.2 Six Component PAH/nitro-PAH Mixture

The laser photoionization mass spectra of a six component PAH/nitro-PAH mixture have been obtained using 213 nm radiation. Three spectra are presented in Figures 7.6, 7.7a and 7.7b, with accompanying major peak assignments given in Tables 7.6 and Figures 7.7a and 7.7b. The composition of the six-component mixture is based on the concentrations (ppm) of the selected PAH and nitro-PAH determined for NIST SRM 1650 diesel particulate matter and is listed in section 7.3 above. The three mass spectra displayed show the effect of increasing laser power density by increasing the area of laser interaction with the solid sample. Figure 7.6 illustrates a relatively soft ionization, while Figure 7.7b represents a hard ionization of the same sample.

The soft ionization laser mass spectrum of the six component mixture presented in Figure 7.6 shows a molecular ion peak for each of the four PAH components, as identified in Table 7.6. The appearance of PAH molecular ions is not unexpected as the highly conjugated PAH molecules are good chromophores in the near-UV region. The other notably intense high mass peak occurs at m/z 217, corresponding to the $[M\text{-}NO]^+$ ion peak of 1-nitropyrene. No distinct peaks are observed in the spectrum that are directly attributable to 2-nitrofluorene. The broad, moderately intense mid-mass fragment at ~m/z 108 is attributable to a common PAH carbon cluster fragment, $C_9H_x^+$. The characteristic nitro-PAH fragment ion, $NO^+$, is not observed in the spectrum, partly due to the soft ionization condition and the relatively low nitro-PAH concentration as compared to the unsubstituted PAH concentration. The visible low mass carbon fragments

**Figure 7.6** Single-step laser photoionization mass spectrum of a six-component PAH/nitro-PAH mixture, based on the composition determined for NIST SRM 1650 diesel particulate matter, obtained at 213 nm under soft ionization conditions.

**Table 7.6** Peak assignments for the single-step laser photoionization mass spectrum of a six-component PAH/nitro-PAH mixture containing phenanthrene[PH], pyrene[PY], chrysene[CR], benzo[e]pyrene[BeP], 1-nitropyrene[1NP], and 2-nitrofluorene[2NF].

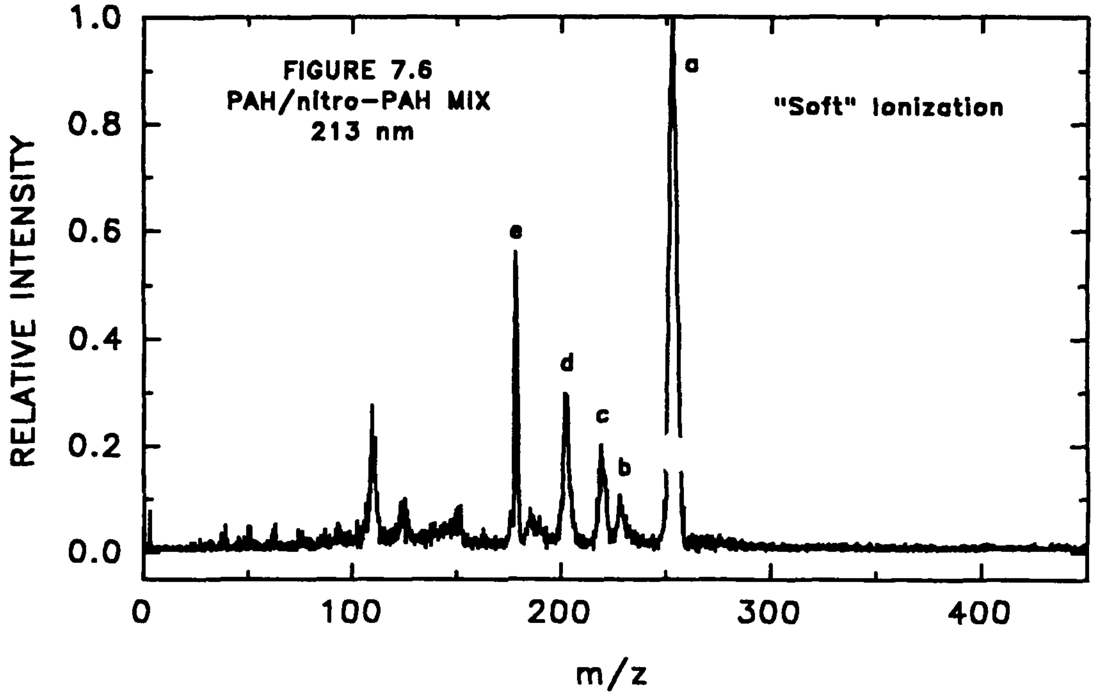

Table 7.6 Peak Assignments: Soft Ionization of PAH/nitro-PAH Mixture

| Peak | Assignment | m/z |
|---|---|---|
| a | $M^+$ [BeP] | 252 |
| b | $M^+$ [CR] | 228 |
| c | $(M\text{-}NO)^+$ [1NP] | 217 |
| d | $M^+$ [PY] | 202 |
| e | $M^+$ [PH] | 178 |

**Figure 7.7** Single-step laser photoionization mass spectra illustrating a moderate (7.7a) and a hard (7.7b) ionization of the six-component PAH/nitro-PAH mixture, obtained at 213 nm.

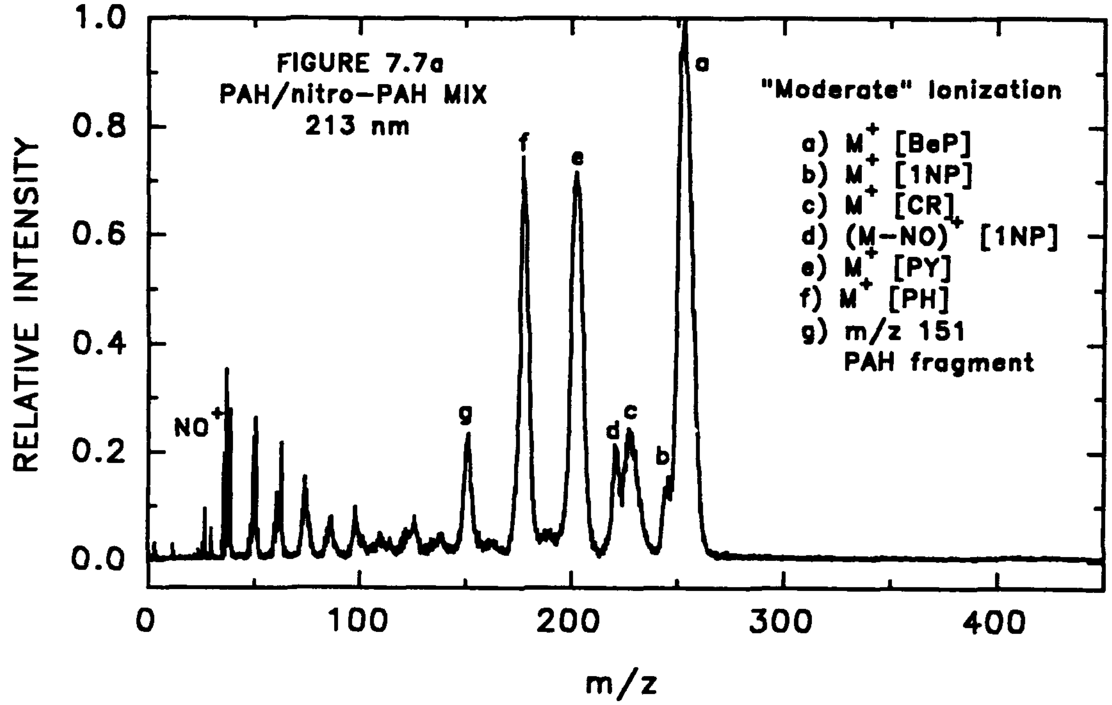

FIGURE 7.7a
PAH/nitro-PAH MIX
213 nm

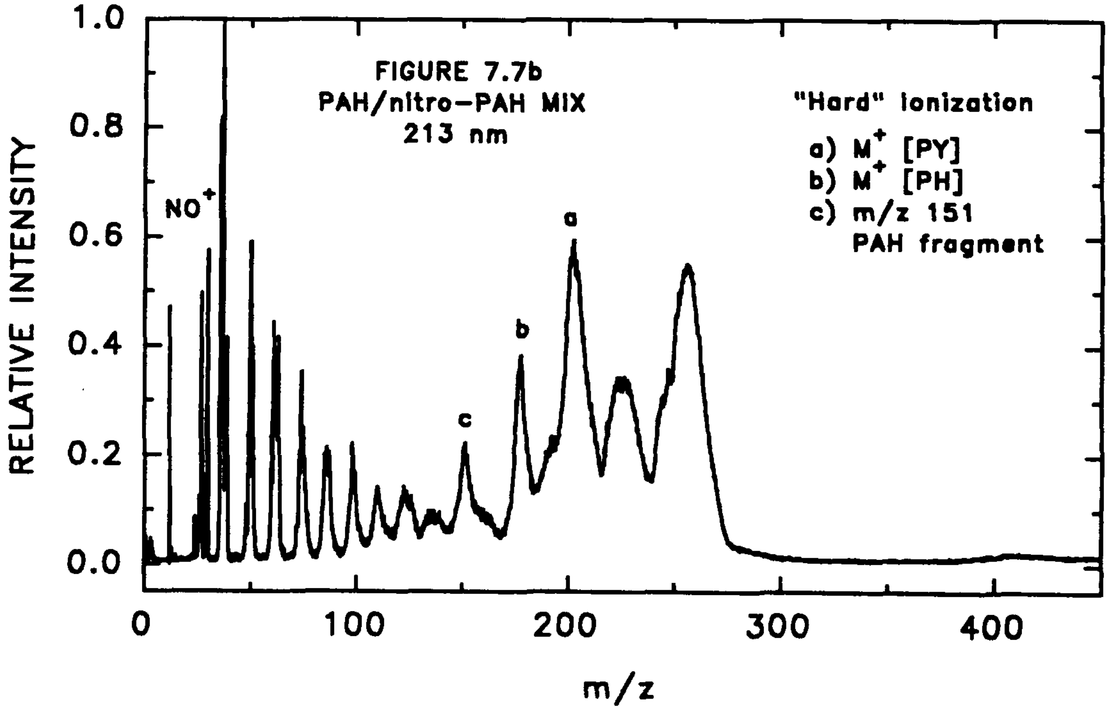

FIGURE 7.7b
PAH/nitro-PAH MIX
213 nm

are of low intensity, as is expected for a soft ionization condition.

The mass spectrum shown in Figure 7.7a illustrates a moderately hard ionization resulting from an increased area of interaction between the laser beam and the solid sample. The molecular ion peaks of the four PAH standards are intense peaks in the spectrum, but are considerably broadened. The $[M-NO]^+$ ion of 1-nitropyrene is also observed and significantly broadened. The fairly weak fragment observed on the leading edge of the benzo[e]pyrene molecular ion peak is tentatively attributed to the molecular ion of 1-nitropyrene, although the mass resolution must be improved before a definite assignment is possible. The most interesting peak in the spectrum occurs at m/z 30. The $NO^+$ ion has made a weak, but distinct appearance among the much more abundant low mass carbon fragments.

Figure 7.7b represents a hard ionization mass spectrum of the same six-component sample obtained by further increasing the area of interaction between the laser beam and the solid sample. The high mass peaks in the spectrum are broadened almost beyond the point of recognition, and the mass resolution among the low mass carbon peaks is also significantly decreased compared to the previous two spectra. However, the $NO^+$ ion is now a strong, recognizable peak with intensity comparable to that of the surrounding low mass carbon fragments. The significantly enhanced appearance of the distinctive m/z 30 ion peak in the hard ionization spectrum is convincing evidence for the presence of a nitro-containing compound in the sample. Combined with the other two six-component spectra, the presence of 1-nitropyrene in the mixture could be tentatively established, demonstrating the utility of the technique for the screening of more complex samples for the presence of 1-nitropyrene.

Comparing the three photoionization spectra of the six-component mixture shows the growth of the characteristic $NO^+$ fragment belonging to the nitro-PAH as laser-sample interaction volume (and thus laser power density) is increased. The unsubstituted PAH generally require higher power density than their more fragile nitro-PAH counterparts to induce significant fragmentation. The increased power density fragments the nitro-PAH to a greater extent than the PAH present, producing NO fragments by predissociation mechanisms which are subsequently ionized by a two-photon absorption. The m/z 30 peak "grows" into the low mass region as increasing power density generates more of the $NO^+$ ion relative to the production of low mass carbon fragments.

The increased intensity of the $NO^+$ signal is obtained at the expense of mass resolution, particularly in the high mass range. The considerable broadening observed at higher power densities could be caused by a significant increase in the initial kinetic energy spread of the ions. The much higher density of ions in the desorption plume at higher power densities also increases the potential for collisional interactions, charge transfer, repulsive "space-charge" affects,[24] and other intermolecular processes which could contribute to peak broadening by creating large initial velocity, temporal and spatial distributions. The observed broadening should be improved by the installation of a new source region and ion optics to the time-of-flight (TOF) mass spectrometer, allowing consistent desorption geometry, sample positioning and power density application.

## 7.5 CONCLUSIONS

The laser photoionization mass spectra obtained at 213 nm for the five two-component nitro-PAH mixtures demonstrate that the nitro-PAH continue to exhibit characteristic fragmentation patterns when in the presence of another nitro-PAH. The major fragments of more highly conjugated nitro-PAH dominate the mass spectra in two-component mixtures with lesser conjugated counterparts. 1-nitropyrene and 9-nitroanthracene have larger absorbance cross sections at 213 nm and are better able to stabilize their major high mass fragment ions than 2-nitrofluorene and 2-nitro-9-fluorenone. It is possible to distinguish between 9-nitroanthracene or 2-nitrofluorene in a two-component mixture with 1-nitropyrene by laser photoionization mass spectrometry. Additionally, 9-nitroanthracene, 2-nitrofluorene and 2-nitro-9-fluorenone can be separately identified in laser mass spectra of two-component mixtures amongst themselves.

The $NO^+$ ion is the predominant low mass ion generated by photoionization of nitro-PAH, and under hard ionization conditions becomes the dominant peak in the spectra of nitro-PAH compounds. Competing fragmentation pathways leading to the production of $NO^+$ were described in Chapter 5. The great intensity of the m/z 30 ion is attributable to a resonant two-photon ionization of the NO fragment, which absorbs strongly as 213 nm. All the 213 nm laser mass spectra of the two-component mixtures contain intense $NO^+$ ion peaks, which could be useful for detecting the presence of nitro-PAH in more complex mixtures with other organic compounds.

Comparison of three laser mass spectra of the six-component PAH/nitro-PAH mixture illustrates the effect of increased laser power density on the observed relative intensity of the $NO^+$ ion peak. The characteristic m/z 30 fragment ion grows into the spectrum, dramatically increasing its intensity relative to the other low mass carbon fragments, as laser power density is increased to produce hard ionization. The $[M-NO]^+$ ion of 1-nitropyrene observed in the spectra under softer ionization, coupled with the appearance of the $NO^+$ ion in the harder ionization spectra, allows tentative identification of 1-nitropyrene in the PAH/nitro-PAH mixture. Results demonstrate the utility of the LDLPMS technique for the screening of more complex samples for the presence of 1-nitropyrene.

The present study shows some potential for application of LPMS to detect the presence of other nitro-PAH in mixtures with unsubstituted PAH, by observation of characteristic high mass nitro-PAH fragments coupled with the presence of the $NO^+$ ion. Using wavelength matching of the NO absorption may significantly improve the sensitivity for detection of $NO^+$, thereby improving the sensitivity of the screening for nitro-PAH in real-world samples. Work to improve the mass resolution of the TOF mass spectrometer by installation of a new source region and ion optics is currently underway. Application of the LPMS method to more complex mixtures, and ultimately, to detection of nitro-PAH in environmental samples, is the subject of future research.

## 7.6 REFERENCES

1. Marshall, A.; Clark, A.; Jennings, R.; Ledingham, K. W. D.; Sander, J.; Singhal, R. P. *Int. J. Mass Spectrom. Ion Processes* **1992,** *116* , 143.

2. Helmig, D.; Arey, J.; Atkinson, R.; Harger, W. P.; McElroy, P. A. *Atmos. Environ.* **1992,** *26A*, 1735.

3. Arey, J.; Zielinska, B.; Atkinson, R.; Aschmann, S. M. *Int. J. Chem. Kinet.* **1989,** *21*, 775.

4. Schuetzle, D.; Lee, F. S. C.; Prater, T. J.; Tejada, S. B. in *Proceedings of the 10th Annual Symposium on Analytical Chemistry of Pollutants*, Gordan and Breach Science Publishers, New York, 1980, pp. 193-244.

5. Schuetzle, D.; Lee, F. S. C.; Prater, T. J.; Tejada, S. B. *Int. J. Environ. Anal. Chem.* **1981,** *9*, 93.

6. Schuetzle, D.; Riley, T. L.; Prater, T. J.; Harvey, T. M.; Hunt, D. F. *Anal. Chem.* **1982,** *54*, 265.

7. Schuetzle, D.; Paputa, M.; Hampton, C. M.; Marano, R.; Riley, T.; Prater, T. J.; Skewes, L.; Salmeen, I. "The Identification and Potential Sources of Nitrated Polynuclear Aromatic Hydrocarbons (Nitro-PAH) in Diesel Particulate Extracts", pp.299-312 in *Mobile Source Emissions Including Polycyclic Organic Species*, D. Reidel Publishing Co., 1983.

8. Paputa-Peck, M. C.; Marano, R. S.; Schuetzle, D.; Riley, T. L.; Hampton, C. V.; Prater, T. J.; Skewes, L. M.; Jensen, T. E.; Ruehle, P. H.; Bosch, L. C.; Duncan, W. P. *Anal. Chem.* **1983,** *55*, 1946.

9. Williams, P. T.; Bartle, K. D.; Andrews, G. E. "Polycyclic Aromatic Compounds in Diesel Fuels and Particulates", pp. 1011-1027 in *Polynuclear Aromatic Hydrocarbons:*

*Chemistry, Characterization and Carcinogenesis; Ninth International Symposium*, M. Cooke and A. J. Dennis, Eds., Battelle Press, Columbus, OH, 1986.

10. Xu, X. B.; Nachtman, J. P.; Jin, Z. L.; Wei, E. T.; Rappaport, S. M. *Anal. Chim. Acta* **1982**, *136*, 163.

11. Ramdahl, T.; Becher, G.; Björseth. A. *Environ. Sci.Technol.* **1982**, *16*, 861.

12. Nishioka, M. G.; Howard, C. C.; Lewtas, J. "Detection of Hydroxy-Nitro-PAHs and Nitro-PAHs in an Ambient Air Particulate Extract Using Bioassay Directed Fractionation", pp. 701-715 in *Polynuclear Aromatic Hydrocarbons: Chemistry, Characterization and Carcinogenesis; Ninth International Symposium*, M. Cooke and A. J. Dennis, Eds., Battelle Press, Columbus, OH, 1986.

13. Arey, J.; Harger, W. P.; Helmig, D.; Atkinson, R. *Mutation Res.* **1992**, *281*, 67.

14. Chuang, C. C.; Mack, G. A.; Petersen, B. A.; Wilson, N. K. "Identification and Quantification of Nitropolynuclear Aromatic Hydrocarbons in Ambient and Indoor Air Particulate Samples" pp. 155-171 in *Polynuclear Aromatic Hydrocarbons: Chemistry, Characterization and Carcinogenesis; Ninth International Symposium*, M. Cooke and A. J. Dennis, Eds., Battelle Press, Columbus, OH, 1986.

15. Oehme, M.; Mano, S.; Stray, H. *HRC & CC* **1982**, *5*, 417.

16. Harris, W. R.; Chess, E. K.; Okamoto, D.; Remsen, J. F.; Later, D. W. *Environ. Mutagen.* **1984**, *6*, 131.

17. McCoy, E. C.; Rosenkranz, H. S. *Cancer Lett.* **1982**, *15*, 9.

18. Schnieder, E.; Krenmayr, P.; Varmuza, K. *Monatshefte fur Chemie* **1990**, *121*, 393.

19. Young, M. K. G. *Characterization of Polycyclic Aromatic Hydrocarbons and Chlorinated Polycyclic Aromatic Hydrocarbons in Soots by Laser Desorption-Laser*

*Photoionization Mass Spectrometry*, Dissertation, (University of California, Davis), Dec., 1991.

20. Young, M. K. G.; Jones, A. D.; Kelly, P. B. Proceedings of the 39th ASMS Conference on Mass Spectrometry and Allied Topics, Nashville, TN., May 19-24, 1991, p. 342.

21. Wiley, W. C.; McLaren, I. H. *Rev. Sci. Instrum.* **1955**, *26*, 1150.

22. Hudson, B.; Kelly, P.B.; Ziegler, L. D.; Desiderio, R. A.; Gerrity, D. P.; Hess, W.; Bates, R. "Far Ultraviolet Laser Resonance Raman Studies of Electronic Excitations," pp. 1-32 in *Advances in Laser Spectroscopy: Volume 3*, B. A. Garetz and J. R. Lombardi, Eds., John Wiley & Sons Ltd., Chichester, Great Britain, 1986.

23. Smith, C. H. Dissertation, University of California, Davis, Fall 1993, in preparation.

24. Opsal, R. B. *Gas Chromatography Laser Ionization Mass Spectrometry*, Dissertation, Nov. 1985 (Indiana University).

# CHAPTER 8

## Laser Desorption-Laser Photoionization Time-of-Flight Mass Spectrometry Applied to Nitro-PAH and Diesel Particulate Matter

### 8.1 ABSTRACT

The mass spectra of several PAH and nitro-PAH compounds have been investigated using two-step laser desorption-laser photoionization time-of-flight mass spectrometry (LDLPMS). In addition, LDLPMS has been applied to the analysis of NIST SRM 1650 diesel particulate matter. A pulsed $CO_2$ laser, wavelength 10.6 µm, was used for desorption of the samples from a glass fiber filter substrate (filters often used for air sampling). The desorbed neutral molecules were subsequently photoionized by either 266-nm or 213-nm radiation. Two nitro-PAH, 1-nitropyrene and 2-nitrofluorene, were examined individually and in a six-component mixture with four PAH standards. The composition of the six-component mixture was based on the composition of NIST SRM 1650 diesel particulate matter, in order to evaluate the application of LDLPMS for detection of nitro-PAH in multi-component mixtures.

The NIST SRM 1650 diesel particulate matter was analyzed as received by LDLPMS. A dichloromethane extract of the diesel particulate matter was also analyzed by two-step and single-step LDLPMS. The characteristic $NO^+$ (m/z 30) peak was the base peak in the laser mass spectra of the nitro-PAH standards. However, the m/z 30 peak was broad and weakly observed in two-step mass spectra of the six-component mixture and the diesel particulate matter. The single-step mass spectra of the diesel extract showed a stronger m/z 30 ion peak among the abundant carbon fragments. Broad

high mass peaks combined with the overall complexity of the diesel particulate sample allowed only tentative assignment of the high mass peaks in the diesel particulate spectra. Preliminary results indicate that modification of the mass spectrometer and sample preparation methods are warranted if LDLPMS is to be successfully applied to the characterization of environmental samples.

## 8.2 INTRODUCTION

The analytical chemistry of nitrated polycyclic aromatic hydrocarbons (nitro-PAH) is of widespread interest due to the highly mutagenic properties of this chemical class. Nitro-PAH are derivatives of PAH, which are abundant in fossil fuels and are the incomplete combustion products of organic materials. Direct emission into the atmosphere from combustion sources distributes PAH between the gas and particle phases.[1] Nitro-PAH present in direct emissions are primarily the electrophilic nitration products resulting from adsorbed-phase reactions of PAH with $NO_x$ and $HNO_3$.[2] In addition, nitro-PAH formed in the gas-phase can readily condense on carbonaceous material.

Nitro-PAH have been determined in a variety of environmental samples including diesel exhaust,[3-9] urban and indoor air particulate,[10-13] aluminum smelter effluent,[14] coal fly ash,[15] and wood and cigarette smoke condensates.[16,17] The concentration of nitro-PAH in environmental samples is typically one to two orders of magnitude less than that of the unsubstituted PAH present. Low concentrations coupled with their ubiquitous presence and potent direct-acting mutagenicity underscore the importance of developing highly sensitive and selective methods for determination of nitro-PAH in environmental samples.

The first positive identification of a nitro-PAH in an environmental sample was reported by Schuetzle et al.[3,4] in 1980. Positive identification of 1-nitropyrene in the moderately polar (transition) fraction of diesel exhaust particulate extract was made using a combination of direct-probe HRMS and HR GC/MS. Subsequent research by Schuetzle et al.[5,6] and Paputa-Peck et al.[7] indicated the presence of 20 nitro-PAH isomer groups containing approximately 200 nitro-PAH species in the transition fractions of diesel particulate extracts. Later analysis of diesel particulate extract by MacCrehan et al.[18] used HPLC reduction methods to convert nonfluorescent nitro-PAH to highly fluorescent amino derivatives for fluorescence and electro-chemical detection. Lee et al.[19] employed HPLC-reduction to form pentafluoropropyl (PFP) amides from the nitro-components of diesel exhaust particulate. Over 120 nitro-PAH were tentatively identified as PFP amides using nitrogen-selective thermionic and flame ionization detection. Both HPLC-reduction studies confirmed the extremely complex nature of diesel exhaust extracts.

The *in situ* characterization of PAH in diesel particulate matter was investigated by Di Lorenzo[20] and Klempier et al.[21] using direct-probe mass spectrometry. Each study compared the EI mass spectra of diesel soot taken before and after extraction. Results showed that extraction of PAH from the particulate was incomplete, and that higher mass PAH remained adsorbed in the sample matrix after extraction, thus avoiding chemical and biological characterization by conventional analytical methods. Ross et al.[22] evaluated the application of secondary ion mass spectrometry (SIMS) to the *in situ* characterization PAH compounds adsorbed on activated charcoal. The SIMS method achieved a detection limit of ~2 ng for phenanthrene adsorbed on carbon.

The application of laser photoionization mass spectrometry to the *in situ* characterization of PAH and nitro-PAH on particulate has been limited. An investigation by Sine et al.[23] employed a LAMMA-500 laser microprobe mass analyzer to characterize soot from an experimental oil shale retort. A wide variety of organic and inorganic compounds were identified, including twenty-five unsubstituted PAH from m/z 252 to m/z 620. A recent study by Delmas and Muller[24] examined FTMS laser microprobe for the *in situ* determination of nitro-PAH adsorbed on two carriers, activated charcoal and silica gel. The PAH-doped particles were analyzed before and after exposure to a gaseous $NO_2/HNO_3$ mixture, and fragments corresponding to the $[M-NO]^-$ anion of three nitro-PAH were identified in the resulting mass spectra.

In order to investigate the application of laser desorption-laser-photoionization time-of-flight mass spectrometry (LDLPMS) to characterization of nitro-PAH in environmental samples, mass spectra have been obtained for two nitro-PAH standards, and for a six-component PAH/nitro-PAH mixture. In addition, LDLP mass spectra have been acquired for NIST SRM 1650 diesel particulate matter. The diesel particulate was examined as received, and a dichloromethane extract of the particulate matter was also analyzed. The characteristic $NO^+$ ion, which is predominant in the LDLP mass spectra of the nitro-PAH standards, is only weakly present in the mass spectra of the PAH/nitro-PAH mixture, or in the diesel particulate spectra. Broad high mass peaks, coupled with the overall complexity of the diesel particulate sample, allowed only tentative assignment of the diesel particulate spectra. Preliminary results indicate that modification of the mass spectrometer and sample preparation methods are warranted if LDLPMS is to be successfully applied to the characterization of environmental samples in the future.

## 8.3 EXPERIMENTAL

PAH and nitro-PAH standards were purchased from Aldrich Chemical Co., and were used without further purification. The PAH standards used were (molecular weight and stated purity in parenthesis): phenanthrene (178, 98%), pyrene (202, 99%), chrysene (228, 98%), and benzo[e]pyrene (252, 99%). The nitro-PAH compounds studied were: 1-nitropyrene (247, 97%) and 2-nitrofluorene (211, 98%). Dichloromethane, used for extraction and sample preparation, was also purchased from Aldrich Chemical Co. NIST SRM 1650 diesel particulate matter was obtained from the National Institute of Standards & Technology and is representative of heavy-duty diesel engine particulate emissions.

Laser photoionization mass spectra are obtained using a custom-built time-of-flight mass spectrometer operating in the linear mode.[25,26] The sample probe is inserted into the source region through a custom-designed fast load-lock assembly which positions the aluminum probe tip between the extractor and repeller plates of the Wiley-McLaren[27] based two-stage ion optics. The aluminum probe tip has a flattened face which is positioned perpendicular to the flight tube axis. The probe can be raised and lowered externally to allow analysis at different locations on the same sample. The source region is fitted with S1-UV quartz windows to allow transmission of the UV laser beam and a ZnSe (or $BaF_2$) window to allow IR beam transmission. Two oil diffusion pumps, equipped with liquid nitrogen cooled cryotraps, separately pump down the source and flight tube regions to an operating vacuum of $\sim 10^{-6}$ torr.

Sample solutions of the two nitro-PAH standards are prepared at 5-10 mg/ml in $CH_2Cl_2$. The six-component PAH/nitro-PAH mixture consists of phenanthrene (7.1 ± 0.1mg), pyrene (4.9 ± 0.1mg), chrysene (2.9 ± 0.1mg), benzo[e]pyrene (1.0 ± 0.1mg), 1-nitropyrene (2.0 ± 0.1mg), and 2-nitrofluorene (0.15 ± 0.05mg), prepared to 15-20 mg/ml in $CH_2Cl_2$. Sample preparation involves dropping approximately 50 μl of sample solution via syringe onto a ~ 1 $cm^2$ piece of Gelman type A/E glass fiber filter and allowing the filter to air dry. The filter is then attached to the flattened probe face with double-sided sticky tape. The diesel particulate matter is analyzed directly by smearing the soot onto a ~ 1 $cm^2$ piece of sticky tape, which is already attached to the probe face, then tapping to remove loose particulate.

A 24-hour Soxhlet extraction of 200 mg of diesel particulate matter was performed using 200 ml of dichloromethane. The extract was evaporated to ~5 ml, then centrifuged for 30 min to help remove residual soot particles. The extract was transferred by syringe into a darkened glass vial and concentrated, under nitrogen flow, to ~ 1 ml. Samples of the diesel extract are prepared by dropping ~ 50 μl of the extract by syringe onto a ~ 1 $cm^2$ piece of Gelman filter and allowing the filter to air dry. The filter is attached to the probe face with sticky tape and inserted into the source region. Diesel extract samples used in the single-step LDLP experiments are prepared by depositing ~ 20-30 μl of extract directly onto the flattened aluminum probe face and allowing it to air dry.

Pulsed IR radiation at 10.6 microns if generated by a Lumonics Model 934 TEA $CO_2$ laser. The IR pulse width is 100 ns (FWHM) with a lower energy 2 μs tail. The beam is attenuated to approximately 10 mJ/pulse and focussed into the source region through a ZnSe lens. Beam diameter at the sample is ~ 2 $mm^2$ yielding a power density of $5 \times 10^6$ $W/cm^2$ when operating at a pulse rate of 5 Hz. Power measurements of the IR beam are made just prior to focussing using a Scientech Inc. Model 37-4002 power meter.

Pulsed UV radiation at 266 nm is produced using the fourth harmonic of a Q-switched Quanta Ray DCR-3 Nd:YAG laser with an 8 ns pulse width. Sum mixing of the Nd:YAG 1064 nm fundamental and the 266 nm fourth harmonic in BBO (β -barium borate crystal) generates the 213 nm photons.[28] The UV laser beam is focussed into the source region through a 250 mm S1-UV quartz lens, which is also used to direct the UV beam path. For two-step LDLP experiments, the laser beam is focussed such that ionization occurs ~ 1 mm from the filter surface. In single-step experiments, the laser beam is positioned to graze the surface of the sample. Laser energy is measured prior to the entrance window by a Molectron Model J9LP Joulemeter interfaced to a PcJ meter (Q&A Instruments). Laser energy typically ranges from 5-20 μJ/pulse while operating at 5 Hz, yielding maximum power densities on the order of $10^8$ - $10^9$ W/cm$^2$ at the focus.

Event synchronization in the LDLPMS experiment is controlled through a custom-built timing circuit which adjusts the pretrigger for the CO$_2$ laser. Time $t = 0$ corresponds to the firing of the Nd:YAG flashlamps. At $t = 200$ μsec, the Nd:YAG laser Q-switch fires, simultaneously allowing the laser to fire. The relative arrival times of the IR and UV laser beams at the source region are observed with a photodiode detector and adjusted to obtain the optimum 10 μs delay using the pretrigger circuit.

Positive ions formed during each laser pulse are accelerated into the flight tube and drift until impinging on the dual microchannel plate (MCP) detector. Current generated at the MCP detector is 50-ohm terminated into a 100 MHz DSP Model 2001AS Transient Recorder and digitized with 8-bit precision. In a typical experiment, data is collected and signal averaged by a DSP Model 4101 Averaging Memory over 100-500 laser pulses, then transferred by a CAMAC interface to an Everex 386 microcomputer. Data acquisition and subsequent analysis are controlled by software developed in-house.[26,29] The Q-switch sync is used to trigger the data acquisition electronics, allowing the time origin in the mass spectra to correspond to arrival of the UV beam at the source.

## 8.4 RESULTS AND DISCUSSION

### 8.4.1 LDLPMS of 1-nitropyrene and 2-nitrofluorene

The two-step laser desorption-laser photoionization mass spectra of 1-nitropyrene and 2-nitrofluorene, obtained using 213 nm ionizing radiation, are shown in Figure 8.1. In each of the spectra, the $[M\text{-}NO_2]^+$ and $[M\text{-}NO\text{-}CO]^+$ ions are the strongest high mass peaks. The molecular ion and $[M\text{-}NO]^+$ ion peaks are either too broad to be assigned or not observed at all. The mid-mass fragments of 1-nitropyrene, $[M\text{-}NO_2\text{-}C_2H_2]^+$, $[M\text{-}NO\text{-}CO\text{-}C_2H_2]^+$, and $[M\text{-}NO_2\text{-}2C_2H_2]^+$, appear in the spectrum, though considerably broadened. The characteristic $NO^+$ fragment ion is the base peak for both spectra.

The peaks in the two-step LDLP spectra of 1-nitropyrene and 2-nitrofluorene are significantly broader than the peaks shown for the single-step experiments in Chapters 5 - 7. The difference in the spectra is largely attributable to desorption of the sample from the porous Gelman glass fiber filters (in the two-step experiments) as opposed to desorption of the solid sample deposited on the bare aluminum probe surface (in the single-step experiments). When the IR laser beam impacts the filter surface, significant heating of the filter fibers occurs. Initially, molecules closest to the top of the filter surface are desorbed. The desorbed surface molecules have less thermal energy than the filter matrix because there has been a loss of energy to the desorption process ($\Delta H_{desorb}$). Over many pulses, the surface molecules are depleted and the molecules from deeper in the filter matrix make up a larger fraction of the desorbed species. Molecules desorbed from deeper within the matrix suffer collisions with the thermally energized filter fibers

**Figure 8.1** Two-step laser desorption-laser photoionization mass spectra of 1-nitropyrene and 2-nitrofluorene, obtained at 213 nm.

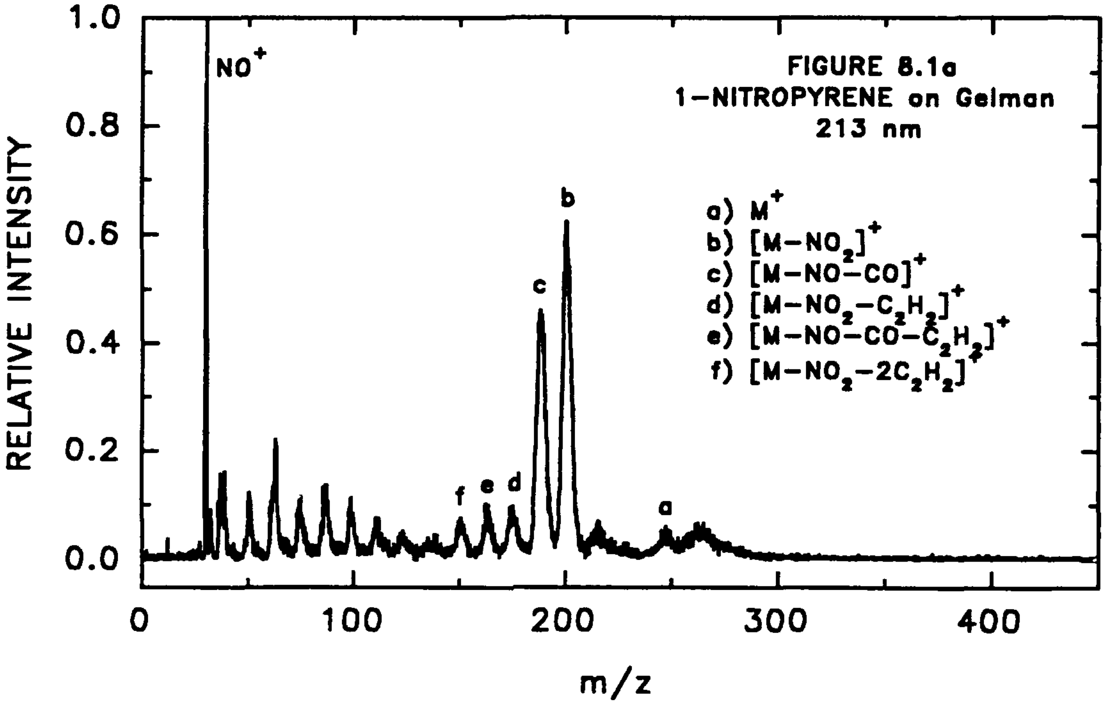

FIGURE 8.1a
1-NITROPYRENE on Gelman
213 nm

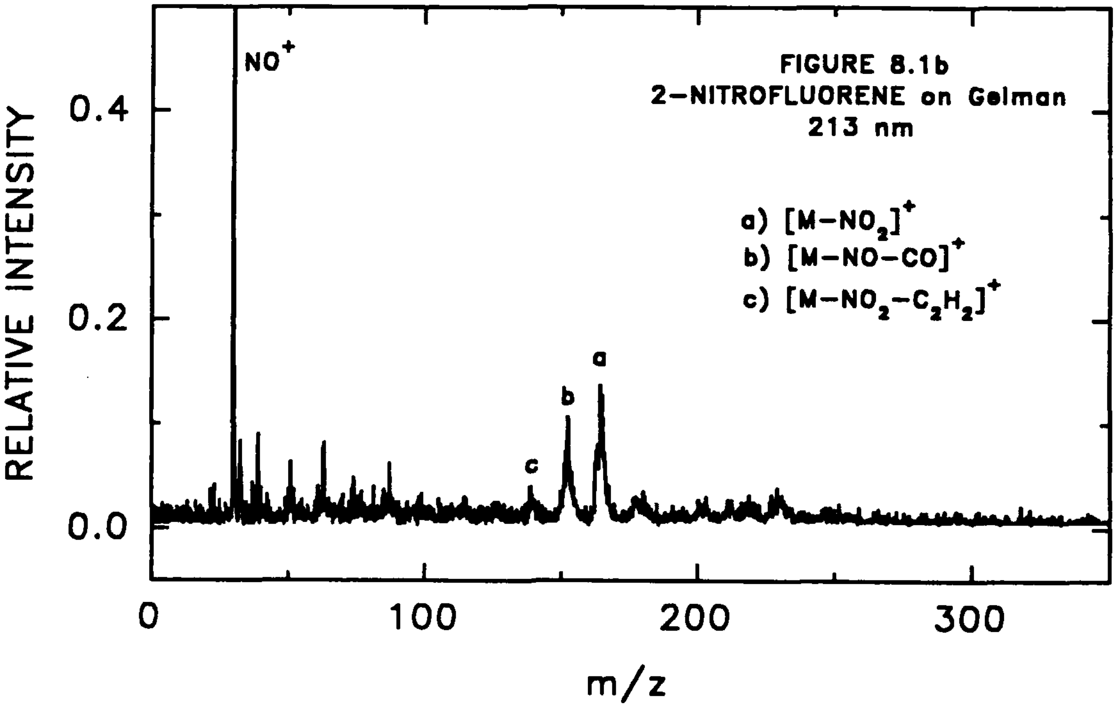

FIGURE 8.1b
2-NITROFLUORENE on Gelman
213 nm

and can thermally equilibrate with the filter. Hence, when molecules farther from the surface exit the filter matrix, they possess more thermal energy than their surface counterparts in the desorption plume. Thus, desorption of samples adsorbed on the filters introduces broadening in our spectra by creating larger initial velocity and energy distributions.[30]

Molecules desorbed directly from the sample deposited onto the bare aluminum probe surface also lose energy to the desorption process. However, desorption and postionization both occur within the UV laser pulse. Molecules desorbed directly from the probe surface will have a narrower velocity and energy distribution than those desorbed from the filter matrix. Reduced velocity and energy profiles within the initial ion packet decrease peak broadening and increase mass resolution. Therefore, the spectra of compounds desorbed directly from the probe surface are generally better resolved than the spectra of compounds desorbed from the Gelman filters.[30]

The difference in observed fragmentation patterns for the two nitro-PAH may also be a function of desorption from the Gelman filters. The molecules desorbed from filters in the two-step experiments are thermally hotter than the molecules desorbed and ionized directly from the bare aluminum probe surface in the single-step experiments. The additional thermal energy may produce more extensive fragmentation in the fragile nitro-molecules prior to and during the ionization process. Thus, the molecular ion and $[M-NO]^+$ peaks of 1-nitropyrene and 2-nitrofluorene in the two-step LDLP spectra of Figure 8.1 are weak and broad, while the parent-PAH fragment and the $[M-NO-CO]^+$ fragments become the dominant high mass peaks. The precise physical nature and mechanisms for ionization in laser desorption are uncertain. However, ionization in the high-density plume produced by bare probe surface (single-step) laser desorption could occur several mechanisms. Possible collision-induced, proton-transfer and MPI absorption processes occurring in the desorption plume could help to stabilize the higher mass ions of the fragile nitro-compounds, which are typically strong peaks in single-step LDLP spectra.

### 8.4.2 LDLPMS of a Six-Component PAH/nitro-PAH Mixture

The composition of the six-component PAH /nitro-PAH mixture is based on the concentrations (ppm) of each of the six components that have been determined for NIST SRM 1650 diesel particulate matter. Figure 8.2 presents a soft ionization and a moderate ionization LDLP spectrum of the six-component mixture adsorbed on a Gelman filter. In the soft ionization spectrum, a peak corresponding to the molecular ion of each PAH compound is identifiable, though most are fairly broad peaks. Two other broad high mass peaks are observed in the spectrum which calibrate as m/z 246, possibly $M^+$ of 1-nitropyrene, and m/z 193, which is unassigned at this point. Mid-mass PAH fragments appear at m/z 151 and m/z 107, but the low mass carbon fragments and the $NO^+$ ion are absent, as is appropriate for a soft ionization process. No peaks appearing in the spectrum are directly attributable to the 2-nitrofluorene component, probably due in part to its much lower concentration.

The peak widths in the Gelman filter (two-step) moderate ionization spectrum are on par with the broadness of the peaks observed in the bare probe (single-step) moderate ionization spectrum (Figure 7.7b). Once again, a molecular ion peak is observed for each PAH component, and the molecular ion of 1-nitropyrene can be tentatively assigned. The broad m/z 193 peak remains unassigned however, a small peak appearing at m/z 218 can be tentatively assigned as the $[M\text{-}NO]^+$ ion of 1-nitropyrene. Low mass carbon

**Figure 8.2** Two-step laser desorption-laser photoionization mass spectra of a six-component PAH/nitro-PAH mixture containing phenanthrene [PH], pyrene [PY], chrysene [CR], benzo[e]pyrene [BeP], 1-nitropyrene [1NP], and 2-nitrofluorene [2NF], depicting soft and moderate ionization conditions at 213 nm.

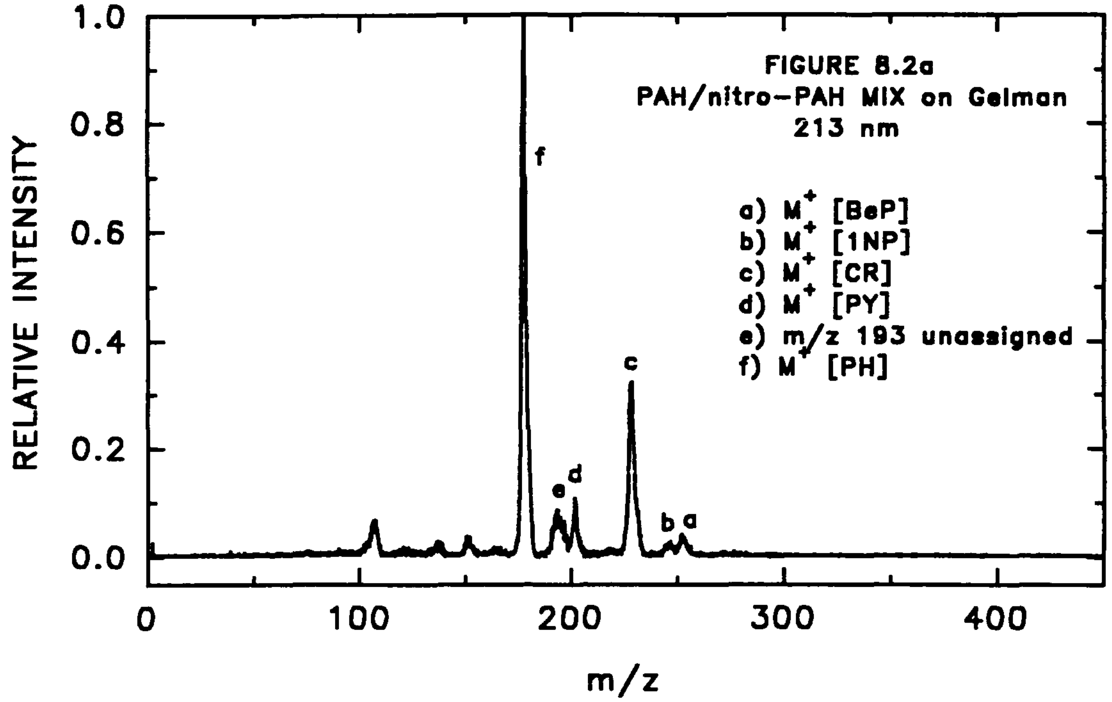
FIGURE 8.2a
PAH/nitro-PAH MIX on Gelman
213 nm
a) M$^+$ [BeP]
b) M$^+$ [1NP]
c) M$^+$ [CR]
d) M$^+$ [PY]
e) m/z 193 unassigned
f) M$^+$ [PH]
RELATIVE INTENSITY
1.0
0.8
0.6
0.4
0.2
0.0
0
100
200
300
400
m/z
f
c
e
d
b
a

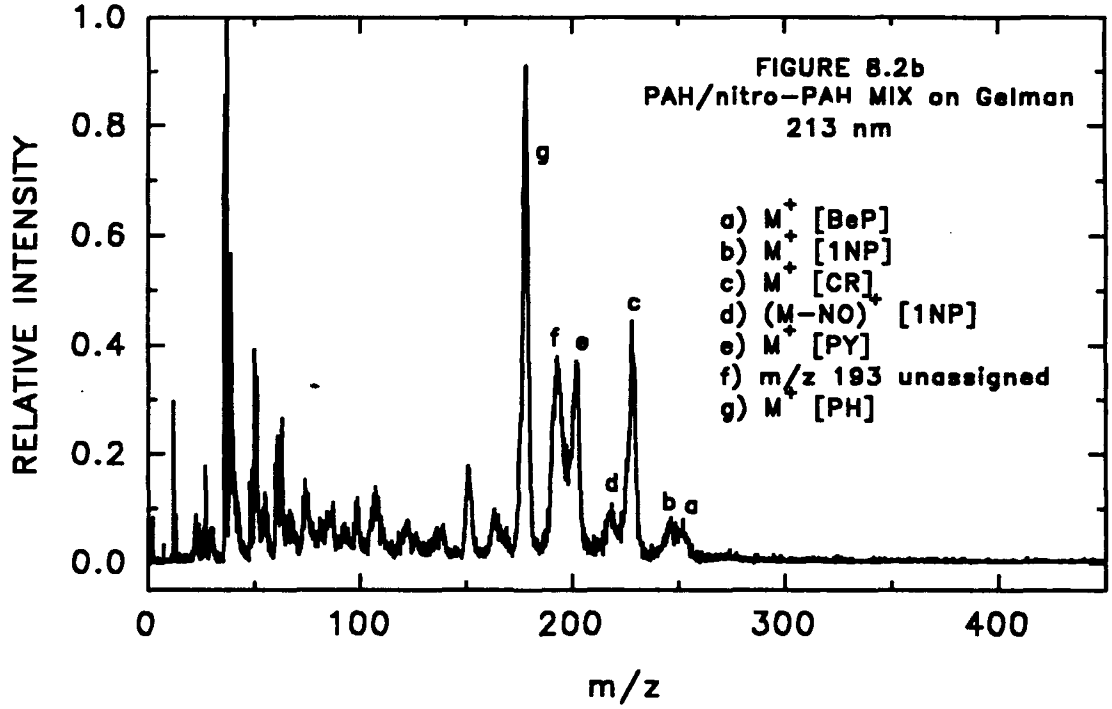
FIGURE 8.2b
PAH/nitro-PAH MIX on Gelman
213 nm
a) M$^+$ [BeP]
b) M$^+$ [1NP]
c) M$^+$ [CR]
d) (M−NO)$^+$ [1NP]
e) M$^+$ [PY]
f) m/z 193 unassigned
g) M$^+$ [PH]
RELATIVE INTENSITY
1.0
0.8
0.6
0.4
0.2
0.0
0
100
200
300
400
m/z
g
f
e
c
d
b
a

fragments are abundant in the spectrum, and a small peak at ~ m/z 30 can be observed. Due to peak broadening, the m/z ~ 30 peak cannot be definitively assigned to the $NO^+$ ion. Similar to the other spectra of the six-component mixture, no peaks unique to 2-nitrofluorene are observed in the spectrum. The much lower concentration of 2-nitrofluorene in the mixture (as in an actual environmental sample) could easily account for the absence of its ion peaks in the spectra.

### 8.4.3 LDLPMS Applied to Diesel Particulate Matter

The two-step LDLP mass spectra of diesel particulate matter are presented in Figure 8.3. Spectrum 8.3a was obtained by applying the two-step LDLP process to a sample of the as received particulate matter attached to the flattened probe face with double-sided sticky tape. For spectrum 8.3a, 266 nm radiation was used for ionization of the desorbed molecules. Spectrum 8.3b was acquired by two-step LDLP of the diesel particulate extract dropped onto a Gelman glass fiber filter, using 213 nm ionizing radiation. Due to the extensive broadening of the peaks and the large departure of the baseline from zero, especially in the mid-to high mass range, the m/z values of the higher mass peaks could only be tentatively assigned for either spectra. Expansion of the low mass regions of the spectra revealed no m/z 30 peak in the 266-nm spectrum (as expected) however, a weak m/z 30 peak is observed in the 213-nm spectrum.

Figure 8.4 displays two hard ionization spectra of diesel particulate extract, both obtained at 213 nm. Spectrum 8.4a was obtained using two-step LDLP to desorb the extract from a Gelman filter, while spectrum 8.4b was acquired by desorbing the extract deposited on the bare probe surface. The baseline of each spectrum improved considerably over the softer ionization spectra of Figure 8.3 as the higher mass

**Figure 8.3** Two-step laser desorption-laser photoionization mass spectra of diesel particulate on sticky tape at 266 nm, and diesel particulate extract on a Gelman filter at 213 nm, containing tentative mass-to-charge assignments.

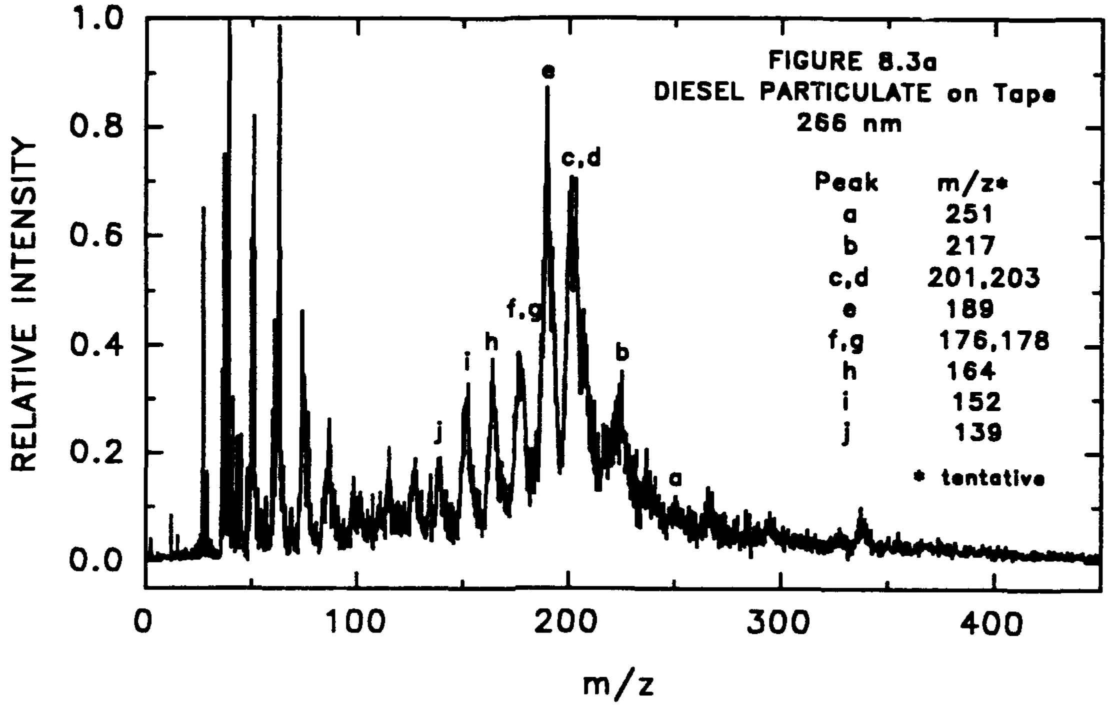

FIGURE 8.3a
DIESEL PARTICULATE on Tape
266 nm

| Peak | m/z* |
|---|---|
| a | 251 |
| b | 217 |
| c,d | 201,203 |
| e | 189 |
| f,g | 176,178 |
| h | 164 |
| i | 152 |
| j | 139 |

* tentative

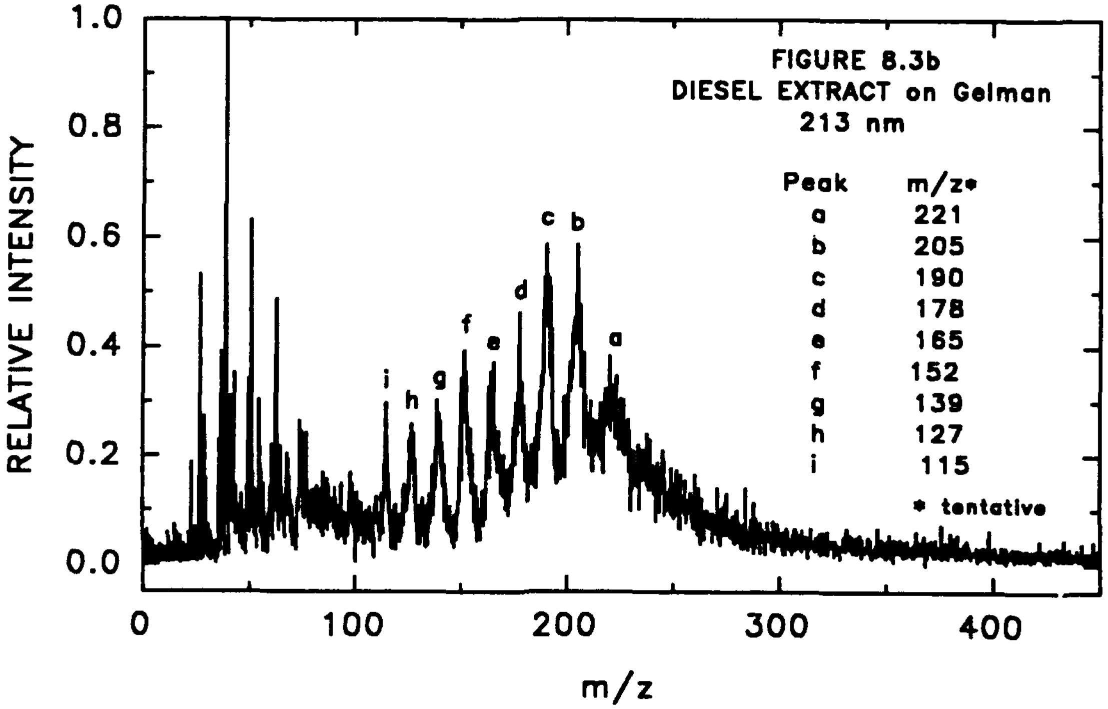

FIGURE 8.3b
DIESEL EXTRACT on Gelman
213 nm

| Peak | m/z* |
|---|---|
| a | 221 |
| b | 205 |
| c | 190 |
| d | 178 |
| e | 165 |
| f | 152 |
| g | 139 |
| h | 127 |
| i | 115 |

* tentative

**Figure 8.4** Two-step and single-step laser desorption-laser photoionization mass spectra of diesel particulate extract, obtained at 213 nm, displaying expansions of the mid- to high-mass regions and tentative mass-to-charge assignments.

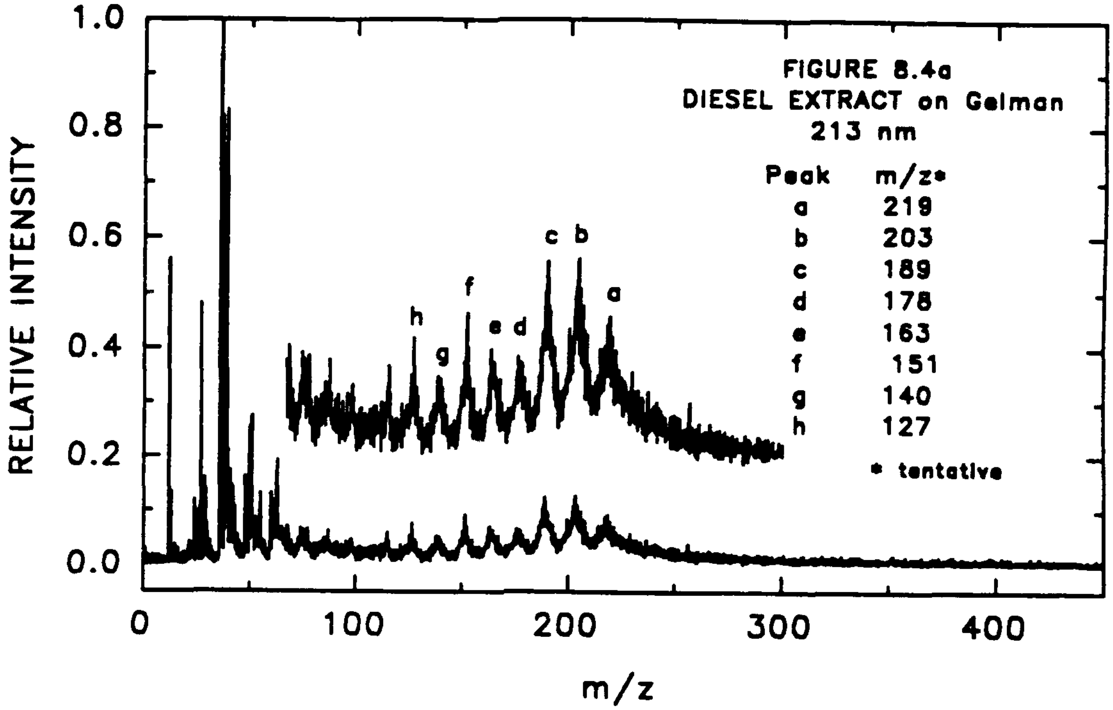

FIGURE 8.4a
DIESEL EXTRACT on Gelman
213 nm

| Peak | m/z* |
|---|---|
| a | 219 |
| b | 203 |
| c | 189 |
| d | 178 |
| e | 163 |
| f | 151 |
| g | 140 |
| h | 127 |

* tentative

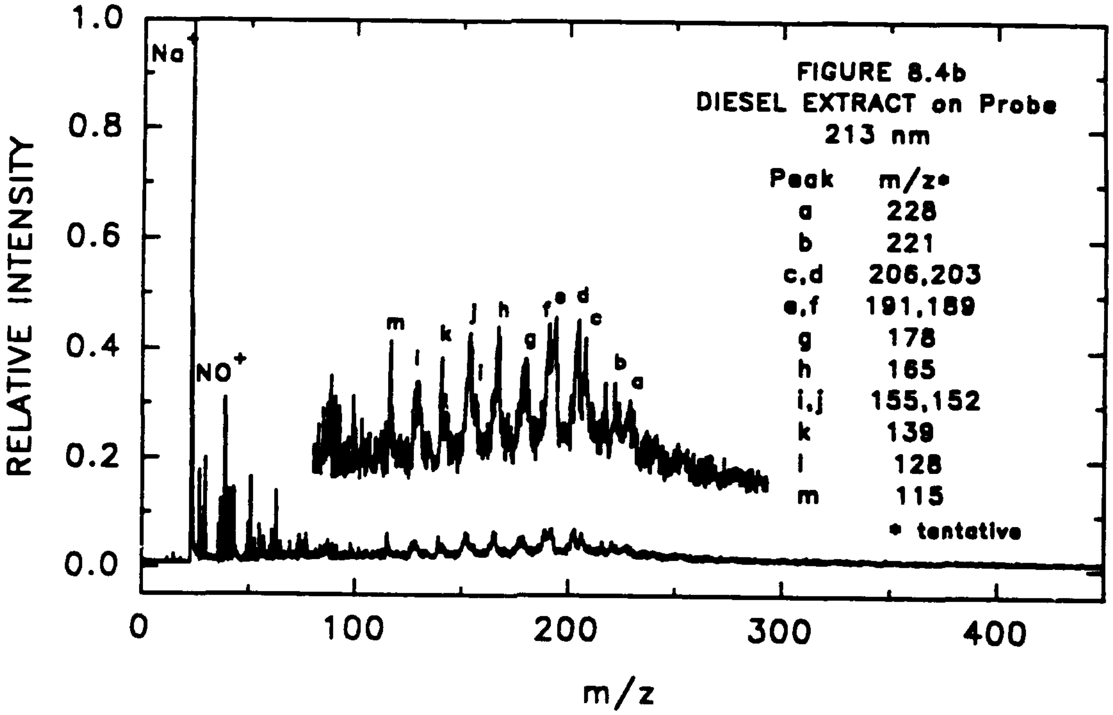

FIGURE 8.4b
DIESEL EXTRACT on Probe
213 nm

| Peak | m/z* |
|---|---|
| a | 228 |
| b | 221 |
| c,d | 206,203 |
| e,f | 191,189 |
| g | 178 |
| h | 165 |
| i,j | 155,152 |
| k | 139 |
| l | 128 |
| m | 115 |

* tentative

compounds fragmented to produce more low mass carbon fragments. The high mass peaks are still very broad, though noticeably sharper in 8.4b than in 8.4a. The m/z 30 ion makes a very weak appearance in the Gelman filter desorption spectrum (8.4a). In the probe surface desorption spectrum(8.4b), the apparently stronger m/z 30 ion peak is dwarfed by an intense sodium peak, as sodium is prevalent in environmental soot samples. The m/z values of the high mass peaks could only be tentatively assigned, although some tentative m/z values did correspond to known PAH components and fragments. The absolute identification of particular PAH or nitro-PAH compounds was not possible due to the overall complexity of the spectra. However, the work to date demonstrates the feasiblity of tentative identification of PAH in environmental samples. The LDLPMS method may be used to screen samples for the presence of PAH for subsequent analysis by EPA procedures.

The congested appearance of the spectra obtained from the diesel particulate matter is attributable to a number of factors, not the least of which is the sheer complexity of the sample itself. Schuetzle et al.[4] identified thirteen PAH species in diesel particulate extracts between m/z 202 and m/z 208 alone. In a subsequent report, thirteen nitro-PAH with the molecular weight of 247 amu were identified in the transition fractions of diesel particulate extract, along with over 100 other nitro-PAH isomers![5] The time-of-flight mass spectrometer used in the current study has unit mass resolution of ~ 100 amu. Thus, the current instrument is unable to separate the many closely-spaced higher mass peaks which appear in the spectra of the diesel particulate matter. Even with improved mass resolution, extraction and fractionation of a particulate sample may be necessary to reduce the complexity of the sample prior to analysis, and allow more certain identification of individual components by LDLPMS.

## 8.5 CONCLUSIONS

Two-step laser desorption-laser photoionization mass spectrometry was applied to two nitro-PAH standards, a six-component PAH/nitro-PAH mixture, and NIST SRM 1650 diesel particulate matter, with mixed results. The spectra obtained for the two-nitro-PAH standards showed an intense $NO^+$ ion peak, and the prominent high mass fragments were attributed to the parent-PAH fragment ion and the $[M\text{-}NO\text{-}CO]^+$ ion, all of which are characteristic nitro-PAH fragments. The PAH molecular ion peaks could be easily identified in the spectra of the six-component mixture, and peaks from 1-nitropyrene could be tentatively identified however, no peaks were observed for 2-nitrofluorene, which was present in very low concentration. An m/z 30 ion peak made a weak appearance in the two-step spectra of the mixture, under hard ionization conditions, but could not be definitely assigned to the $NO^+$ ion. Peak broadening in the two-step LDLP spectra, especially in the higher mass region, was attributed largely to velocity and energy distributions induced by desorption of the samples from the Gelman filter matrix.

The LDLP spectra of diesel particulate matter, obtained at 266 nm and 213 nm using the as received particulate and a dichloromethane extract, showed very broad high mass peaks which were unassignable to particular PAH or nitro-PAH compounds. However, tentative mass assignments, some of which corresponded to known PAH components, could be made for the higher mass peaks in the diesel particulate extract spectra. The direct desorption of diesel particulate extract from the aluminum probe surface (single-step experiment), produced the only spectrum to show an appreciable m/z 30 ion peak, although the peak was dwarfed by an intense sodium peak.

The congested appearance of the spectra obtained from the diesel particulate matter is attributable to a number of factors, not the least of which is the sheer complexity of the sample itself. The mass resolution of the current instrument is unable to separate the many closely-spaced higher mass peaks which appear in the diesel particulate spectra. Even with improved mass resolution, extraction and fractionation of a particulate sample may be necessary to reduce the complexity of the sample being analyzed, and allow more certain identification of individual components by LDLPMS. Modification of sample preparation procedures by use of HPLC, or introduction of the particulate extract through a heated capillary GC interface could considerably improve the detection of nitro-PAH in environmental samples.

## 8.6 REFERENCES

1. Helmig, D.; Arey, J.; Atkinson, R.; Harger, W. P.; McElroy, P. A. *Atmos. Environ.* **1992**, *26A*, 1735.

2.. Arey, J.; Zielinska, B.; Atkinson, R.; Aschmann, S. M. *Int. J. Chem. Kinet.* **1989**, *21*, 775.

3. Schuetzle,D.; Lee, F. S. C.; Prater, T. J.; Tejada, S. B. in *Proceedings of the 10th Annual Symposium on Analytical Chemistry of Pollutants*, Gordan and Breach Science Publishers, New York, 1980, pp. 193-244.

4. Schuetzle, D.; Lee, F. S. C.; Prater, T. J.; Tejada, S. B. *Int. J. Environ. Anal. Chem.* **1981**, *9*, 93.

5. Schuetzle, D.; Riley, T. L.; Prater, T. J.; Harvey, T. M.; Hunt, D. F. *Anal. Chem.* **1982**, *54*, 265.

6. Schuetzle, D.; Paputa, M.; Hampton, C. M.; Marano, R.; Riley, T.; Prater, T. J.; Skewes, L.; Salmeen, I. "The Identification and Potential Sources of Nitrated Polynuclear Aromatic Hydrocarbons (Nitro-PAH) in Diesel Particulate Extracts", pp.299-312 in *Mobile Source Emissions Including Polycyclic Organic Species*, D. Reidel Publishing Co., 1983.

7. Paputa-Peck, M. C.; Marano, R. S.; Schuetzle, D.; Riley, T. L.; Hampton, C. V.; Prater, T. J.; Skewes, L. M.; Jensen, T. E.; Ruehle, P. H.; Bosch, L. C.; Duncan, W. P. *Anal. Chem.* **1983**, *55*, 1946.

8. Williams, P. T.; Bartle, K. D.; Andrews, G. E. "Polycyclic Aromatic Compounds in Diesel Fuels and Particulates", pp. 1011-1027 in *Polynuclear Aromatic Hydrocarbons: Chemistry, Characterization and Carcinogenesis; Ninth International Symposium*, M. Cooke and A. J. Dennis, Eds., Battelle Press, Columbus, OH, 1986.

9. Xu, X. B.; Nachtman, J. P.; Jin, Z. L.; Wei, E. T.; Rappaport, S. M. *Anal. Chim. Acta* **1982**, *136*, 163.

10. Ramdahl, T.; Becher, G.; Björseth. A. *Environ. Sci.Technol.* **1982**, *16*, 861.

11. Nishioka, M. G.; Howard, C. C.; Lewtas, J. "Detection of Hydroxy-Nitro-PAHs and Nitro-PAHs in an Ambient Air Particulate Extract Using Bioassay Directed Fractionation", pp. 701-715 in *Polynuclear Aromatic Hydrocarbons: Chemistry, Characterization and Carcinogenesis; Ninth International Symposium*, M. Cooke and A. J. Dennis, Eds., Battelle Press, Columbus, OH, 1986.

12. Arey, J.; Harger, W. P.; Helmig, D.; Atkinson, R. *Mutation Res.* **1992**, *281*, 67.

13. Chuang, C. C.; Mack, G. A.; Petersen, B. A.; Wilson, N. K. "Identification and Quantification of Nitropolynuclear Aromatic Hydrocarbons in Ambient and Indoor Air Particulate Samples" pp. 155-171 in *Polynuclear Aromatic Hydrocarbons: Chemistry, Characterization and Carcinogenesis; Ninth International Symposium*, M. Cooke and A. J. Dennis, Eds., Battelle Press, Columbus, OH, 1986.

14. Oehme, M.; Mano, S.; Stray, H. *HRC & CC* **1982**, *5*, 417.

15. Harris, W. R.; Chess, E. K.; Okamoto, D.; Remsen, J. F.; Later, D. W. *Environ. Mutagen.* **1984**, *6*, 131.

16. McCoy, E. C.; Rosenkranz, H. S. *Cancer Lett.* **1982**, *15*, 9.

17. Schnieder, E.; Krenmayr, P.; Varmuza, K. *Monatshefte fur Chemie* **1990**, *121*, 393.

18. MacCrehan, W. A.; May, W. E. "Determination of Nitro-Polynuclear Aromatic Hydrocarbons in Diesel Soot by Liquid Chromatography with Fluorescence and Electrochemical Detection", pp. 857-869 in *Polynuclear Aromatic Hydrocarbons: Mechanisms, Methods and Metabolism: 8th International Symposium*, M. Cooke and A.J.

Dennis, Eds., Battelle Press, Columbus, Ohio, 1985.

19. Campbell, R. M.; Lee, M. L. *Anal. Chem.* **1984,** *56*, 1026.

20. Di Lorenzo, A. *Advan. Mass Spectrom.* **1980,** *8B*, 1377.

21. Klempier, N.; Binder, H. *Anal. Chem.* **1983,** *55*, 2104.

22. Ross, M. M.; Colton, R. J. *Anal. Chem.* **1983,** *55*, 150.

23. Mauney, T.; Adams, F.; Sine, M. K. *Sci. Tot. Environ.* **1984,** *36*, 215.

24. Delmas, S.; Muller, J. F. *Analusis* **1992,** *20* , 165.

25. Young, M. K. G. *Characterization of Polycyclic Aromatic Hydrocarbons and Chlorinated Polycyclic Aromatic Hydrocarbons in Soots by Laser Desorption-Laser Photoionization Mass Spectrometry*, Dissertation, (University of California, Davis), Dec., 1991.

26. Young, M. K. G.; Jones, A. D.; Kelly, P. B. Proceedings of the 39th ASMS Conference on Mass Spectrometry and Allied Topics, Nashville, TN., May 19-24, 1991, p. 342.

27. Wiley, W. C.; McLaren, I. H. *Rev. Sci. Instrum.* **1955,** *26*, 1150.

28. Hudson, B.; Kelly, P.B.; Ziegler, L. D.; Desiderio, R. A.; Gerrity, D. P.; Hess, W.; Bates, R. "Far Ultraviolet Laser Resonance Raman Studies of Electronic Excitations," pp. 1-32 in *Advances in Laser Spectroscopy: Volume 3*, B. A. Garetz and J. R. Lombardi, Eds., John Wiley & Sons Ltd., Chichester, Great Britain, 1986.

29. Smith, C. H. Dissertation, University of California, Davis, Fall 1993, in preparation.

30. Per. Comm. with Dr. Donald P. Land, Asst. Prof., Dept. of Chemistry, University of California, Davis, March 1993.

# CHAPTER 9

# Conclusions

## 9.1 SUMMARY

The primary objectives of the current research were to obtain representative laser photoionization mass spectra of standard nitro-PAH and nitrated heterocyclic compounds, identify their characteristic photofragmentation patterns, and assess the feasibility of application of LDLPMS for their detection in real environmental samples. Laser mass spectra were acquired at 213 nm and 266 nm for four nitro-PAH standards: 9-nitroanthracene, 1-nitropyrene, 2-nitrofluorene, and 2-nitro-9-fluorenone. All of the 213-nm nitro-PAH mass spectra contained a strong to intense m/z 30 ion peak, which was attributed to the $NO^+$ ion. The m/z 30 ion peak was weakly present in the 266-nm spectra, but only under hard ionization conditions. The strong intensity of the $NO^+$ ion peak in the 213-nm spectra was due to resonance-enhanced two-photon ionization of the neutral NO fragment. Absorption by the NO molecule begins at 226 nm ($A^2\Sigma^+ \leftarrow X^2\Pi$) and is particularly strong in the 190 to 200 nm region due to the $C^2\Pi \leftarrow X^2\Pi$ and the $D^2\Sigma \leftarrow X^2\Pi$ bands. Room temperature NO does not absorb wavelengths longer than 226 nm.[1] Thus, the presence of an m/z 30 peak in the 266-nm spectra was attributed to ionization of NO via nonresonant, collision and/or charge transfer ionization processes occurring in the high density desorption plume during hard ionization of the nitro-PAH.

Characteristic mid- and high-mass photofragments were identified for the four nitro-PAH standards including $M^+$, $[M\text{-}NO]^+$, $[M\text{-}NO_2]^+$, and $[M\text{-}NO\text{-}CO]^+$ fragment ions.

Generally, the $[M\text{-}NO]^+$ was the base peak in the nitro-PAH laser mass spectra, though the $NO^+$ ion peak could dominate at 213 nm under hard ionization conditions. Two competing fragmentation pathways were proposed for the production of $NO^+$ by the laser photoionization of nitro-PAH. The primary route to $NO^+$ formation was identified as predissociation of the parent molecule to lose NO, followed by a two-photon ionization of the neutral NO fragment. The competing pathway was identified as predissociation of the parent molecule to lose $NO_2$, subsequent predissociation of the $NO_2$ fragment to yield NO + O, then two-photon ionization of NO to form the $NO^+$ ion.

Both photodissociation pathways had been considered by Marshall et al.[2,3] to explain the observed intense $NO^+$ ion peak in the laser mass spectra of nitrobenzene in the wavelength range 232.5 nm to 260 nm. The second route, predissociation of the parent to lose $NO_2$, was identified by Marshall as the primary mechanism for production of $NO^+$ from nitrobenzene. The first pathway was discounted by Marshall, primarily due to the absence of an $[M\text{-}NO]^+$ ion peak in the laser mass spectra of nitrobenzene. In our work on the more conjugated nitro-PAH compounds, the $[M\text{-}NO]^+$ fragment ion was more intense than the $[M\text{-}NO_2]^+$ fragment ion in all of the soft ionization nitro-PAH spectra. Comparison of the nitro-PAH laser mass spectra lead to the conclusion that the first route, predissociation of the parent molecule to lose NO, is the primary photodissociation pathway in nitro-PAH leading to production of the $NO^+$ ion.

The mechanism proposed for the loss of the neutral NO fragment from the parent nitro-PAH molecule is the nitro-nitrite rearrangement, which involves isomerization from $\text{-}NO_2$ to -ONO at the carbon atom to which the nitro group was originally attached. Convincing evidence for the nitro-nitrite rearrangement was presented by Ioki[4] in his report of the e.s.r spectra of aryloxyl radicals formed by UV illumination of solutions of nitro-containing compounds (e.g. 6-nitrobenzo[a]pyrene in benzene). The e.s.r. experiments demonstrated that the more highly conjugated compounds formed more stable aryloxyl radicals upon UV illumination. The appearance of a strong $[M\text{-}NO]^+$ ion peak in all of the nitro-PAH mass spectra is consistent with a nitro-nitrite photoisomerization, probably occurring from an intermediate excited electronic state accessed by absorbance of the first photon during the R2PI process.

The 213-nm laser photoionization mass spectra of two nitrobenzocoumarin isomers and three coumarin derivative compounds were obtained to investigate the photofragmentation patterns of nitrated heterocyclic compounds. The mass spectra of 7-hydroxycoumarin and 7-hydroxy-4-methylcoumarin showed intense, apparently protonated molecular ion peaks. The coumarin backbone fragmented by successive loss of carbon monoxide. The 2-nitro-6-(5H)-phenanthridinone compound was less fragile under UV irradiation than the nitrobenzocoumarins and its laser mass spectrum showed much more intense high mass peaks. The photofragmentation pattern of the nitrophenanthridinone initially followed the characteristic nitro-PAH fragmentation pattern by loss of NO, $NO_2$ and (NO-CO) fragments. Subsequent fragmentation followed the coumarin pathway by sequential loss of carbon monoxide.

The laser mass spectrum of nitrophenanthridinone was useful in assigning the mass spectra of 6- and 7-nitrobenzocoumarin. In addition, complementary EI MS/MS experiments performed on 7-nitrobenzocoumarin were valuable in determining the fragmentation pathways, and in identifying the major mid-mass fragment ion at m/z 139. The m/z 139 ion peak was often the base peak in the nitrobenzocoumarin laser mass spectra, and based on the EI MS/MS experiments, the peak was identified as $C_{11}H_7^+$ with a diphenylene-type structure proposed for the fragment ion.

Several two-component mixtures of nitro-PAH and a six-component PAH/nitro-PAH mixture were also examined by 213-nm laser mass spectrometry. For laser photoionization of a two-component mixture, the peaks due to the more highly conjugated compound dominated the spectra. Generally, peaks attributable to the presence of each nitro-PAH component were observed in the mass spectrum. The nitro-PAH continued to exhibit their characteristic fragmentation patterns, displaying $[M\text{-}NO]^+$, $[M\text{-}NO_2]^+$, $[M\text{-}NO\text{-}CO]^+$ and an intense $NO^+$ ion peaks in their two-component mixture mass spectra. The PAH/nitro-PAH mixture contained four PAH and two nitro-PAH compounds in concentrations (ppm) comparable to those determined for NIST SRM 1650 diesel particulate matter. Molecular ion peaks of the PAH were easily observed in the spectra, and weak peaks corresponding to the molecular ion and the $[M\text{-}NO]^+$ peaks of 1-nitropyrene were also identified. No peaks directly attributable to 2-nitrofluorene were observed, undoubtedly partly due to its much lower concentration. The $NO^+$ ion signal rivaled the low mass carbon fragment intensities only under hard ionization conditions, which significantly broadened the mid- to high-mass peaks. The weak appearance of the $NO^+$ ion in the soft ionization spectra of the PAH/nitro-PAH mixture spectra indicated potential difficulties for the determination of nitro-PAH in environmental samples.

A two-step laser desorption-laser photoionization method was used to investigate the laser mass spectra of two nitro-PAH, the six-component mixture, NIST SRM 1650 diesel particulate matter, and a dichloromethane extract of the diesel particulate. The ultimate goal of the project under study is to directly analyze environmental samples, collected on air sampling filters, for the presence of nitro-PAH compounds. However, laser desorption from the Gelman filter matrix using a 10.6 micron $CO_2$ laser, produced mass spectra with much broader peaks than direct desorption of the solid nitro-PAH deposited on the bare aluminum probe. The broadening associated with the filter desorption process is probably due to matrix-induced velocity and energy distributions at initial ion formation.

The characteristic $NO^+$ ion peak was observed only in hard ionization spectra of the PAH/nitro-PAH mixture and the diesel particulate samples. The strongest $NO^+$ ion peak observed for a diesel particulate sample was in the single-step spectrum of the diesel particulate extract, directly desorbed from the probe surface. However, all of the peaks in the single-step spectrum were dwarfed by an intense sodium peak. Sodium and potassium are abundant in environmental samples and will interfere with attempts to directly analyze such samples by a direct desorption-ionization process. One advantage of the two-step desorption process is its insensitivity to sodium and potassium.

Due to the sheer complexity of the diesel particulate matter and the peak broadening in the high mass regions of the particulate and extract mass spectra, the peaks could only be assigned tentative mass-to-charge ratios. The definite identification of particular compounds in the diesel sample was not possible using the laser mass spectra obtained in the current investigation, although many of the tentative m/z correspond to known PAH compounds. The work to date demonstrates the feasibility of tentative identification of PAH in environmental samples. The LDLPMS method may be used to screen particulate samples for the presence of PAH for subsequent analysis by EPA procedures.

Dectection of nitro-PAH in environmental samples is complicated by their generally low concentrations. Diesel particulate contains a much higher concentration of unsubstituted PAH than nitro-PAH, and since PAH more readily form positive ions than their nitro counterparts, the positive ion spectra may exhibit primarily PAH molecular ions. The large number of positive ions formed in the photoionization of the diesel particulate samples produced very congested spectra. Nitro-PAH have a much higher electron affinity than unsubstituted PAH. Examination of the positive ion spectra suggests that one possible way to reduce the complexity of the diesel particulate laser mass spectra would be operation in the negative ion detection mode.

## 9.2 FUTURE DIRECTIONS

### 9.2.1 Supplemental LDLPMS Experiments

The LDLPMS experiments conducted thus far have identified characteristic fragmentation patterns for representative nitro-PAH and nitrated heterocyclic compounds in the positive ion mode. Since nitro-containing compounds have a great electron affinity, an interesting investigation would be the acquisition of the negative ion laser mass spectra of the nitro-PAH and nitrated heterocyclic compounds. The chemical ionization negative ion mass spectra of 9-nitroanthracene and 6-nitro-3,4-benzocoumarin were obtained using a Hewlett-Packard 5890 GC interfaced to a VG Trio 2 mass spectrometer, and are contained in Appendix C. The negative ion mass spectra are much less complex than their positive ion counterparts and show intense molecular ion peaks for both nitro-PAH examined. In addition, a strong m/z 46 peak is observed in the spectra, attributable to the $NO_2^-$ anion. Possibly the m/z 46 peak could be used as a marker for the presence of nitro-containing compounds in the negative ion mass spectra of complex environmental samples.

The successful extension of LDLPMS to the determination of nitro-PAH in environmental samples, for the near future, could involve some modification to sample preparation procedures. The spectra presented in Chapter 8 demonstrate the difficulties involved in direct LDLPMS analysis of particulate adsorbed on air-sampling filters. Extraction and probably fractionation of a particulate sample may be necessary to reduce the complexity of the sample prior to mass analysis. Possibly, introduction of the extract into the source through a capillary inlet and subsequent photoionization, coupled with selected ion monitoring of the $NO^+$ ion or the $NO_2^-$ anion signal, could significantly improve detection sensitivity for nitro-compounds in environmental samples.

A group of interesting follow-on experiments for the nitro-PAH compounds involves a matrix-assisted laser desorption. The molecular ion peaks observed for the nitro-PAH and nitrated heterocyclic compounds in the current study could very well be due to the protonated molecular ions. Given the molecular weights of the nitro-compounds studied and the present instrument resolution, the difference between the molecular ion and its protonated counterpart is not discernable in our mass spectra. The improved mass resolution expected with installation of the new source and ion optics should allow distinction between the protonated and nonprotonated molecular ions. If the protonated molecular ion is observed, desorption from a nitrobenzylalcohol or cinnapinic acid matrix should enhance the yield of the protonated molecular ion. Fragmentation patterns of the protonated molecular ion could be investigated, and the relationship between concentration of the nitro-compound within the matrix and ion yield could be determined.

### 9.2.2 Improvements to Instrumentation

The time-of-flight mass spectrometer (TOFMS) used for the current research is a custom-built instrument operating in the linear mode. The flight times of ions in the TOFMS are determined by several factors including the dimensions of the drift region, the distance between grids, and the applied grid potentials. Many of the causes of peak broadening, and hence degraded mass resolution, were discussed in depth in Chapter 2. A large part of the degraded resolution in our instrument is due to spatial, velocity, and energy spreads (enhanced by desorption from Gelman filters) within the initial ion packet. The present instrument has unit mass resolution to ~ 100 amu however, modifications can be made to the instrument to improve its resolving power.

The addition of a reflectron device could correct for resolution degradation caused by both initial spatial and velocity spreads. The reflectron acts as a second-order space-focussed ion source (i.e. the space focus of the reflectron is at the second detector). Factors to consider in the reflectron design and installation include, but are certainly not limited to: length of the reflectron, grid spacings within the reflectron, potentials applied to the grids, distance from the start of the drift region to the reflectron entrance, and conversely, distance from the reflectron exit to the second detector. Resolution ($m/\Delta m$) of over 10,000 have been achieved by coupling laser induced surface ionization with a reflectron device.[5] An excellent discussion of the reflectron device and the associated mathematics of its design and installation is given by Boesl and Schlag.[6]

An alternative to compensating for the initial velocity spread is to reduce or eliminate the distribution by use of a supersonic molecular beam source.[7] The sample can be desorbed from a surface and entrained in the molecular beam, seeded into the expansion gas, or leaked in via a capillary inlet, allowing examination of a variety of sample types. Use of a pulsed valve also permits direct injection from 1 atm into vacuum, which offers great potential for real environmental applications.[8] The reduction in velocity spread attainable with a molecular beam can increase the resolution of a linear TOF instrument to 1000 or higher.[9] The coupling of a molecular beam with a reflectron device can increase $m/\Delta m$ to 12,000 or more.[10]

Current plans include the installation of a new source region and ion optics for the TOFMS, and reconfiguration of the grid potentials and the microchannel plate detectors for operation in the negative ion mode. The installation of the new source and ion optics will improve mass resolution, especially in the high mass range where the nitro-PAH molecular ions and anions are observed. Distinction could then be made, in the positive ion mode, between the protonated and the nonprotonated molecular ion and the ratio of protonated to nonprotonated could be determined. Operation in negative ion mode will allow the acquisition of negative ion laser mass spectra for the nitro-PAH standards, which should prove much less complicated than their positive ion counterparts. Application of negative ion laser mass spectrometry has the potential to reduce the complexity of the spectra of environmental samples, and permit determination of nitro-PAH by their molecular anion and the characteristic $NO_2^-$ (m/z 46) anion peaks.

## 9.3 REFERENCES

1. Opsal, R. B.; Reilly, J. P. *Anal. Chem.* **1986**, *58*, 2919.

2. Marshall, A.; Clark, A.; Jennings, R.; Ledingham, K. W. D.; Sander, J.; Singhal, R. P. *Int. J. Mass Spectrom. Ion Processes* **1992**, *112* , 273.

3. Marshall, A.; Clark, A.; Jennings, R.; Ledingham, K. W. D.; Sander, J.; Singhal, R. P. *Int. J. Mass Spectrom. Ion Processes* **1992**, *116* , 143.

4. Ioki, Y. *J. C. S. Perkin II* **1977**, *10*, 1240.

5. Yang, M.; Reilly, J. P. *Int. J. Mass Spectrom. Ion Process.* **1987**, *75*, 209.

6. Boesl, U.; Weinkauf, R.; Schlag, E. W. *Int. J. Mass Spectrom. Ion Process.* **1992**, *112*, 121.

7. Lubman, D. M. *Laser Focus / Electro-Optics 1984*, *20*, 110.

8. Tembreull, R.; Lubman, D. M. *Anal. Chem.* **1984**, *56*, 1962.

9. Lubman, D. M. *Mass Spectrom. Rev.* **1988**, *7*, 535.

10. Opsal, R. B.; Colby, S. M.; Wilkerson, C. W. Jr.; Reilly, J. P. "Resolution and Sensitivity in Laser Ionization Mass Spectrometry" pp. 490-509 in *Lasers and Mass Spectrometry*, D. M. Lubman, Ed., Oxford University Press, New York, 1990.

# APPENDIX A

## Calculation of Laser Power Density

Laser beam divergence is due to diffraction effects. The consequence of divergence is an inability to focus the laser beam down to a point. The beam waist at the focus (non-TEM$_{00}$ beam) is given by

$$w_f \cong \frac{4\lambda f}{3\pi w}$$

$f$ = focal length of lens
$w$ = beam radius prior to focussing
$\lambda$ = wavelength of light

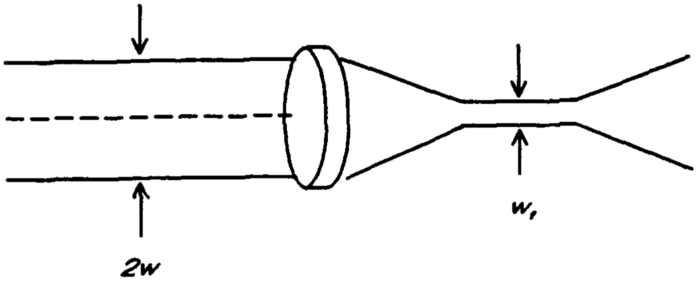

For $\lambda$ = 266 nm; $w$ = 2 mm; $f$ = 250 mm:

$w_f \cong$ 14.1 μm

Therefore, the spot size at focus ($s_{266}$) is

$$\frac{\pi d^2}{4} = \frac{\pi w_f^2}{4} \qquad \text{and} \qquad s_{266} \cong 1.6 \times 10^{-4}\ \text{mm}^2$$

For $\lambda$ = 213 nm; $w$ = 2 mm; $f$ = 250 mm;

$w_f \cong 11.3$ μm and $s_{213} \cong 1.0 \times 10^{-4}$ mm$^2$

Laser power density is dependent upon pulse width and repetition rate as well as spot size. Define a conversion factor, $F$, for the Nd:YAG laser with repetition rate of 5 Hz and FWHM pulse width of 8 ns to be

$$F = \left[ \frac{1\ \text{sec}}{5\ \text{pulses}} \times \frac{1}{8\ \text{ns}} \times \frac{10^9\ \text{ns}}{\text{sec}} \times \frac{\text{J}}{10^3\ \text{mJ}} \times \frac{10^2\ \text{mm}^2}{\text{cm}^2} \right]$$

$$F = 2.5 \times 10^6 \frac{\text{J} \cdot \text{mm}^2}{\text{mJ} \cdot \text{cm}^2}$$

Laser power density (LPD) is then defined by

$$\text{LPD}(\text{W/cm}^2) = \frac{F \cdot P}{s}$$

$P$ = laser power before focussing

$s$ = laser spot size at focus

For 266 nm with $P$ = 10 μJ/pulse

$$\text{LPD} = \frac{2.5 \times 10^6 \text{J} \cdot \text{mm}^2}{\text{mJ} \cdot \text{cm}^2} \times \frac{10\mu\text{J}}{\text{pulse}} \times \frac{5\ \text{pulses}}{1\ \text{sec}} \times \frac{\text{mJ}}{1000\mu\text{J}} \times \frac{1}{1.6 \times 10^{-4} \text{mm}^2}$$

$$\therefore\ \text{LPD} = 7.8 \times 10^8\ \text{W / cm}^2$$

For 213 nm at $P$ = 10 μJ/pulse, similar calculation yields

$$\text{LPD} = 1.3 \times 10^9\ \text{W/cm}^2$$

The confocal lens parameter determines the beam waist length. Essentially, this is the region in which there is plane parallel light. The confocal lens parameter is given by*

$$B = \frac{2\pi w_0^2}{\lambda} \quad \text{where} \quad w_0 = \frac{\lambda}{\pi\theta}$$

$B$ = confocal lens parameter

$$\therefore B = \frac{2\lambda}{\pi\theta^2}$$

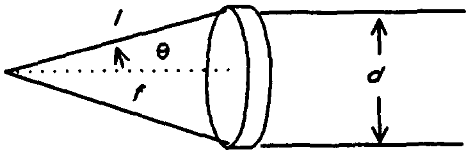

In the small angle approximation, *tan* θ ≈ θ , therefore

$$\theta \approx \tan\theta \approx \frac{d}{2f}$$

and the beam waist length is

$$2B \approx \frac{16\lambda f^2}{\pi d^2}$$ $d$ = laser beam diameter before focussing

The beam waist length at 266 nm with a 4 mm beam diameter is

$$2B \approx \frac{16\left(266\times10^{-9}\,\mathrm{m}\right)\left(.25\mathrm{m}\right)^2}{\pi\left(4.0\times10^{-3}\,\mathrm{m}\right)} \approx 5.3\mathrm{mm}$$

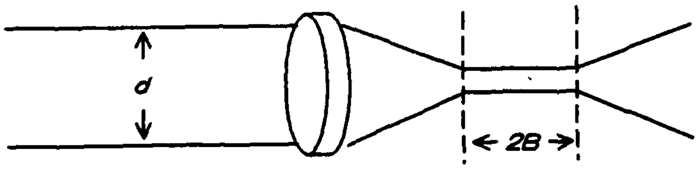

*CRC Handbook of Lasers, with Selected Data on Optical Technology, R. J. Pressley, Ed., Chemical Rubber Co., Cleveland, Ohio, 1971, p. 422.

# APPENDIX B

## Calibration of LDLPMS Spectra

Mass calibration of a LDLPMS spectrum is accomplished by fitting the flight time squared values of low mass fragments appearing in the spectrum to a second order polynomial, then extrapolating to fit the high mass peaks. The fitting equation is:

$$y = ax^2 + bx + c$$

where $y$ is the mass-to-charge ratio (m/z), and $x$ is the corresponding flight time squared ($t^2$). The 'b' constant contains the direct proportionality constants between m/z and $t^2$ (see Chapter 2). The 'a' constant corrects for nonlinearity in the electric field gradient used to accelerate the ions. The 'c' constant corrects for the time lag between arrival of the trigger to begin data acquisition and arrival of a theoretical m/z = 0 ion at the detector.

The top spectrum in Figure B.1 is a typical single-step spectrum of pyrene standard, taken at 213 nm. This is a calibrated spectrum, plotted as relative intensity versus m/z. The bottom spectrum in Figure B.1 is an expansion of the low mass fragments which were used to obtain the calibration. Normally, the expansion is a plot of raw signal intensity versus flight time squared with the expansion range determined by the intensity and resolution of the low mass fragments. The in-house program FASTPLT3.FOR allows the user to set x and y ranges and generates the expansion plot.

Another in-house program, MASS4.FOR, may be used to obtain a printout of the raw data to aid in assigning the low mass peaks. Figure B.2 is a raw data printout containing flight time squared, peak height, area, and width values for the example pyrene spectrum. Based on similar fragmentation patterns observed in other aromatic compounds, m/z assignments are made in groupings of $C_nH_x^+$ by comparing flight time squared values and corresponding intensities with the expansion plot of the low mass peaks. Within the low mass fragments, a flight time squared difference of ~ 2 $\mu sec^2$ corresponds to a m/z difference of approximately 1 amu.

MASS4.FOR also runs the calibration routine which fits the spectrum to the second order polynomial. Up to four sets of calibration constants may be stored within the program and any one of the four sets may be selected to give an initial estimate for the true calibration. The program uses the selected set of calibration constants to perform an initial fit, then gives the user an opportunity to save that calibration, or make individual m/z assignments to achieve a better fit. The "OLD CALIB" column in Figure B.3 contains values calculated using a stored set of calibration constants. The "TRUE MASS" column contains user-assigned m/z values (***** indicates that no m/z value was assigned for that particular flight time). The "A*X^2 + B*X + C" column contains the new m/z values for the spectrum based on the user-assigned m/z values and the fitting equation. Residuals are given in the "DIFF" column. New values for the fitting constants appear at the end of the printout. The new calibration may be saved and/or the fit may be refined by repeating the mass assignment procedure and including more (or different) m/z values.

The 'a' constant is typically on the order of $10^{-6}$ while the 'c' constant is on the order of $10^{-3}$ for calibration of both single-step and two-step spectra. However, the 'b' constant differs between the single-step and two-step experiments. For single-step LDLP, $b \approx (.57 \text{ to } .59)$, and for two-step LDLP, $b \approx (.47 \text{ to } .49)$. The variation is partly attributed to the different initial formation positions of the ions within the source region. The single-step ions form about 2 mm farther away from the accelerating grids than the two-step ions, and therefore gain greater kinetic energy prior to entering the drift region. Since the 'b' constant is directly related to the kinetic energy, ions with greater kinetic energy will have a larger value for 'b'.

Once a satisfactory calibration is obtained, the constants may be written into the storage lines of MASS4.FOR and applied to subsequent spectra. A reasonable fit of successive spectra can be obtained using previously calculated constants, provided the experimental conditions such as sample position, beam position and laser power have not changed appreciably. However, if experimental conditions have changed, or if a more refined fit is desired, the spectra must be calibrated individually using MASS4.FOR and the procedures outlined in this appendix. Efforts are currently underway to automate LDLPMS spectra calibration procedures in conjunction with the projected installation of a new source region and ion optics.

**Figure B.1** Single-step laser photoionization mass spectrum of pyrene obtained at 213 nm, and an expansion of the low mass region of the spectrum showing the carbon cluster fragments ($C_nH_x$) used to calibrate the mass spectrum.

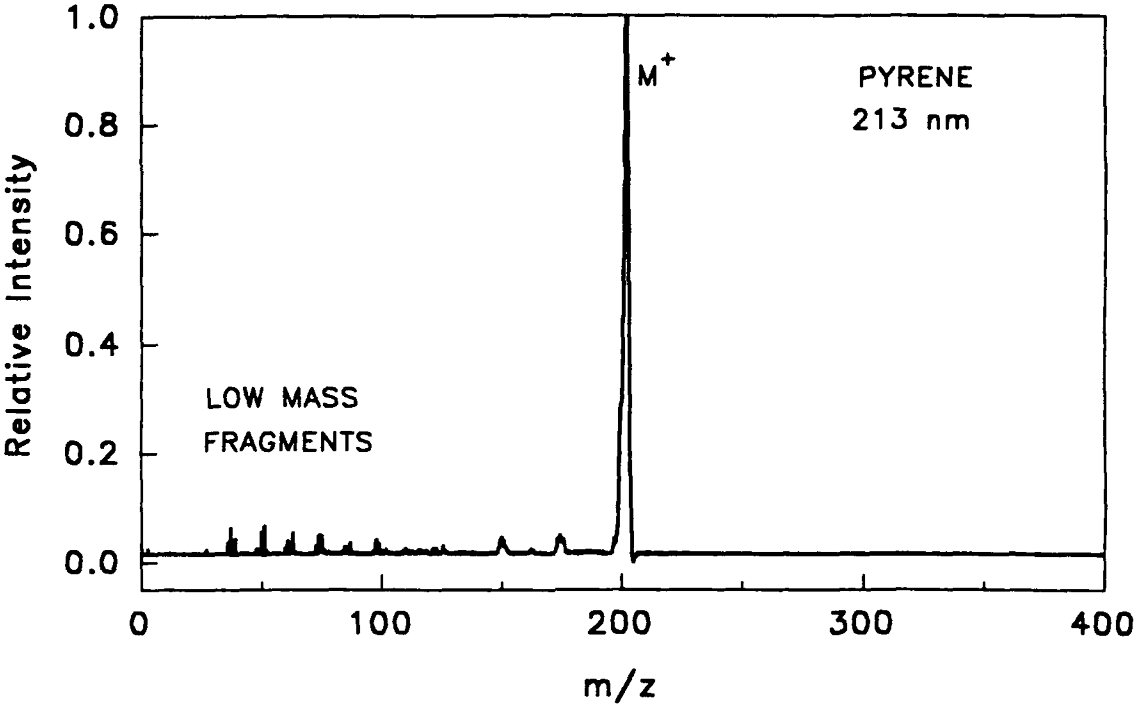
1.0
0.8
0.6
0.4
0.2
0.0
Relative Intensity
0
100
200
300
400
m/z
M+
PYRENE
213 nm
LOW MASS
FRAGMENTS

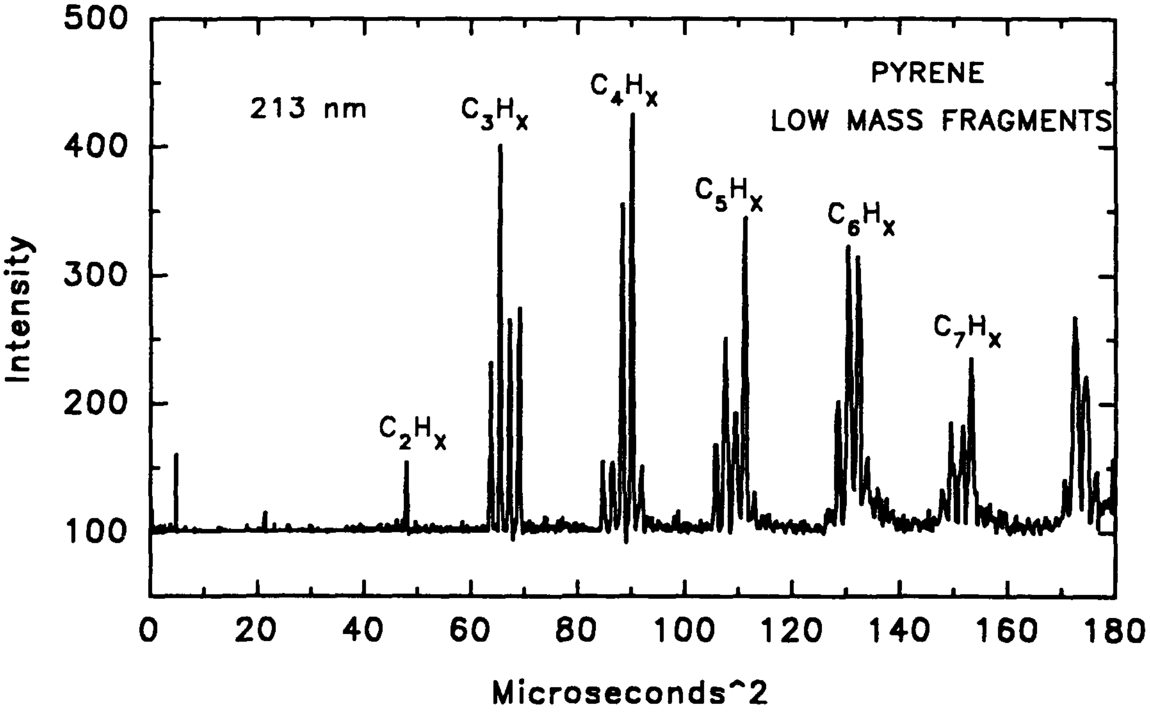
500
400
300
200
100
Intensity
0
20
40
60
80
100
120
140
160
180
Microseconds^2
213 nm
$C_2H_x$
$C_3H_x$
$C_4H_x$
$C_5H_x$
$C_6H_x$
$C_7H_x$
PYRENE
LOW MASS FRAGMENTS

**Figure B.2** Raw data printout listing flight time squared and intensity values for each peak (above a user-selected intensity limit) in the laser mass spectrum of pyrene.

```
FILE BEING ANALYZED IS C:\DATA\PY101209.DAT          TIME:10:38 DATE

intensity limit:     .00100       N POINTS FWHM: 3
PEAK  CHANNEL        TIME              HEIGHT              AREA          HWHM

 1       220.8          4.8             58.50             120.00          1.8
 2       463.6         21.4             14.50              42.00          1.3
 3       693.2         47.9             54.50             188.00          1.8
 4       799.0         63.7            130.00             313.00          2.0
 5       809.8         65.4            298.00             686.00          2.0
 6       821.0         67.2            167.00             456.00          1.3
 7       831.8         69.0            173.50             549.00          2.0
 8       879.2         77.1             11.00              70.00          3.5
 9       921.4         84.7             51.50             146.00          2.3
10       931.2         86.5             52.00             189.00          1.3
11       941.0         88.4            249.00             670.00          1.5
12       950.6         90.2            308.00             945.00          1.3
13       959.9         92.0             41.00             114.00          1.3
14      1029.5        105.8             65.00             205.00          1.5
15      1038.2        107.6            119.50             523.00          1.3
16      1047.2        109.4             61.50             334.00          1.0
17      1055.8        111.3            236.00             715.00          1.5
18      1134.9        128.6             77.50             459.00          3.3
19      1143.3        130.5            203.00             760.00          1.3
20      1151.4        132.4            176.50             643.00          1.0
21      1224.5        149.7             25.50             333.00          3.0
22      1232.8        151.7             42.00              88.00           .8
23      1314.3        172.5            157.00             747.00          3.0
24      1394.2        194.1             12.50             336.00          3.3
25      1468.7        215.4             53.00             537.00          4.3
26      1489.9        221.7             38.00             295.00          3.3
27      1540.9        237.1             -2.00             440.00         10.8
28      1626.9        264.4            179.00            2459.00         11.8
29      1693.1        286.3             54.50             433.00          4.3
30      1753.6        307.2            135.00            2856.00          9.8
31      1810.9        327.6             20.00             191.00          7.3
32      1887.0        355.7           6228.50           81347.00         11.0
33      1956.7        382.5              7.50              83.00          5.0
34      1976.6        390.3              6.50              59.00           .8
35      2003.1        400.8             10.50             112.00          5.0
```

**Figure B.3** Output from the calibration program, MASS4.FOR, showing old and new calibration values for the selected peaks in the pyrene mass spectrum, as well as fitting constants for the spectrum.

```
PEAK USEC ^2   WEIGHT   OLD CALIB   TRUE MASS      A*X^2+B*X+C   DIFF

  1     4.8      0.         2.79    *********        2.74     ******
  2    21.4      0.        12.33    *********       12.12     ******
  3    47.9      1.        27.59        27.00       27.12       -.12
  4    63.7      1.        36.67        36.00       36.06       -.06
  5    65.4      1.        37.67        37.00       37.04       -.04
  6    67.2      1.        38.72        38.00       38.07       -.07
  7    69.0      1.        39.75        39.00       39.09       -.09
  8    77.1      0.        44.41    *********       43.67     ******
  9    84.7      1.        48.78        48.00       47.97        .03
 10    86.5      1.        49.82        49.00       49.00        .00
 11    88.4      1.        50.88        50.00       50.04       -.04
 12    90.2      1.        51.92        51.00       51.06       -.06
 13    92.0      1.        52.95        52.00       52.08       -.08
 14   105.8      1.        60.90        60.00       59.91        .09
 15   107.6      1.        61.94        61.00       60.93        .07
 16   109.4      1.        63.02        62.00       62.00        .00
 17   111.3      1.        64.06        63.00       63.02       -.02
 18   128.6      1.        74.03        73.00       72.85        .15
 19   130.5      1.        75.13        74.00       73.93        .07
 20   132.4      1.        76.20        75.00       74.99        .01
 21   149.7      0.        86.19    *********       84.84     ******
 22   151.7      0.        87.36    *********       85.98     ******
 23   172.5      0.        99.30    *********       97.77     ******
 24   194.1      0.       111.74    *********      110.04     ******
 25   215.4      0.       124.00    *********      122.15     ******
 26   221.7      0.       127.61    *********      125.71     ******
 27   237.1      0.       136.50    *********      134.50     ******
 28   264.4      0.       152.17    *********      149.99     ******
 29   286.3      0.       164.81    *********      162.49     ******
 30   307.2      0.       176.79    *********      174.35     ******
 31   327.6      0.       188.53    *********      185.98     ******
 32   355.7      1.       204.73       202.00      202.02       -.02
 33   382.5      0.       220.12    *********      217.28     ******
 34   390.3      0.       224.62    *********      221.75     ******
 35   400.8      0.       230.68    *********      227.76     ******
 THE STARTING  MASS IS       .008
 THE ENDING MASS IS       920.659
THE FITTING CONSTANTS ARE
 A =       .00000625
 B =      .56569439
 C =       .00759003
```

# APPENDIX C

## GC/MS Spectra of Nitro-PAH and Nitrobenzocoumarin Standards

**Spectra Titles** **Page**

1. TIC of 9-nitroanthracene ........................................ 210
2. EI/MS of 9-nitroanthracene ........................................ 211
3. NICI of 9-nitroanthracene ........................................ 212
4. TIC of 1-nitropyrene ........................................ 213
5. EI/MS of 1-nitropyrene ........................................ 214
6. EI/MS of 2-nitrofluorene ........................................ 215
7. TIC of 2-nitro-9-fluorenone ........................................ 216
8. EI/MS of 2-nitro-9-fluorenone ........................................ 217
9. TIC of 6-nitro-3,4-benzocoumarin ........................................ 218
10. EI/MS of 6-nitro-3,4-benzocoumarin ........................................ 219
11. NICI of 6-nitro-3,4-benzocoumarin ........................................ 220
12. TIC of 7-nitro-3,4-benzocoumarin ........................................ 221
13. EI/MS of 7-nitro-3,4-benzocoumarin ........................................ 222
14. TIC of 1-nitronaphthalene ........................................ 223
15. EI/MS of 1-nitronaphthalene ........................................ 224

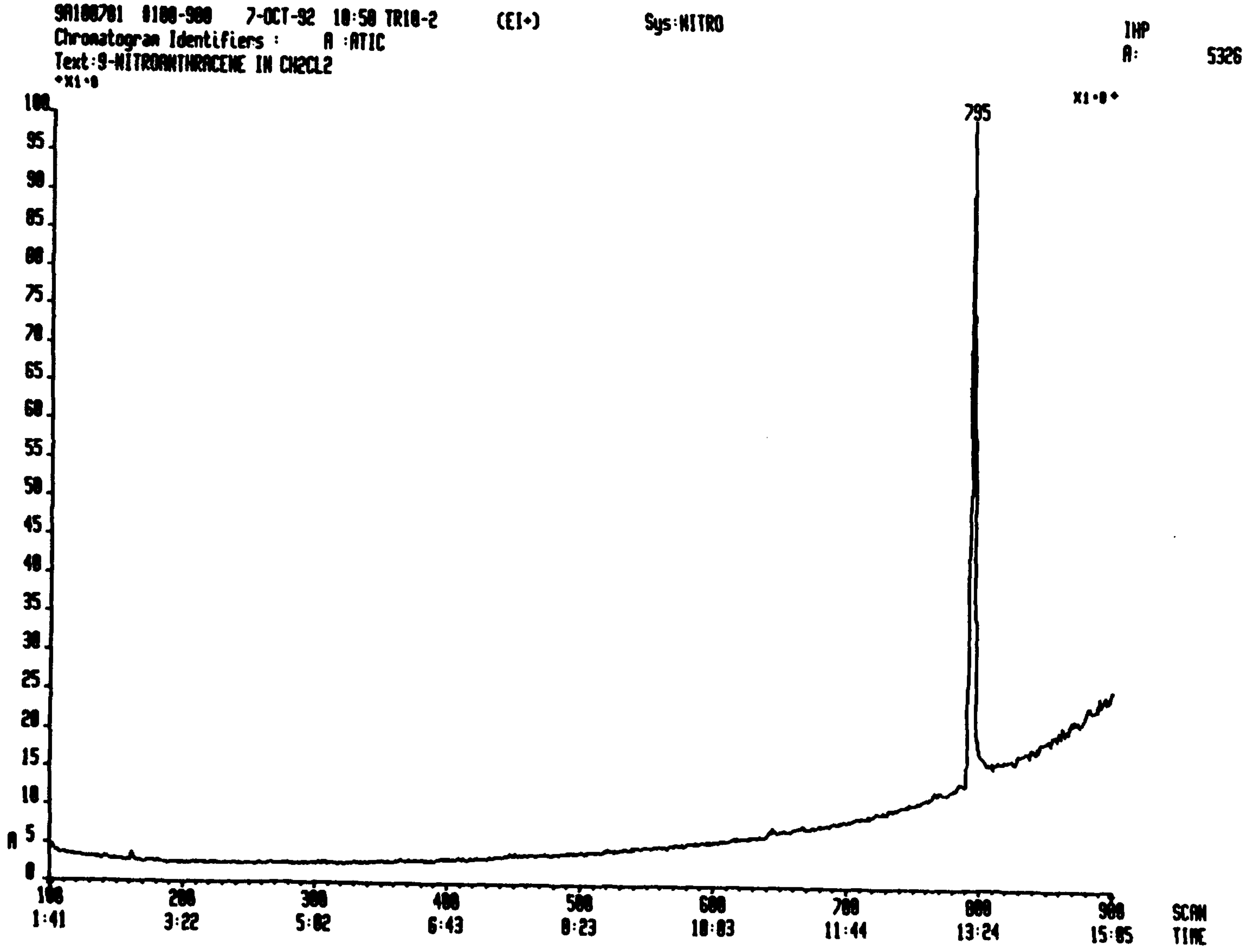

9A100701 #100-900 7-OCT-92 10:50 TR10-2 (EI+) Sys:NITRO
Chromatogram Identifiers : A :ATIC
Text:9-NITROANTHRACENE IN CH2CL2
*X1·0
IHP
A: 5326
X1·0*
795
100
95
90
85
80
75
70
65
60
55
50
45
40
35
30
25
20
15
10
5
0
A
100 1:41
200 3:22
300 5:02
400 6:43
500 8:23
600 10:03
700 11:44
800 13:24
900 15:05
SCAN
TIME

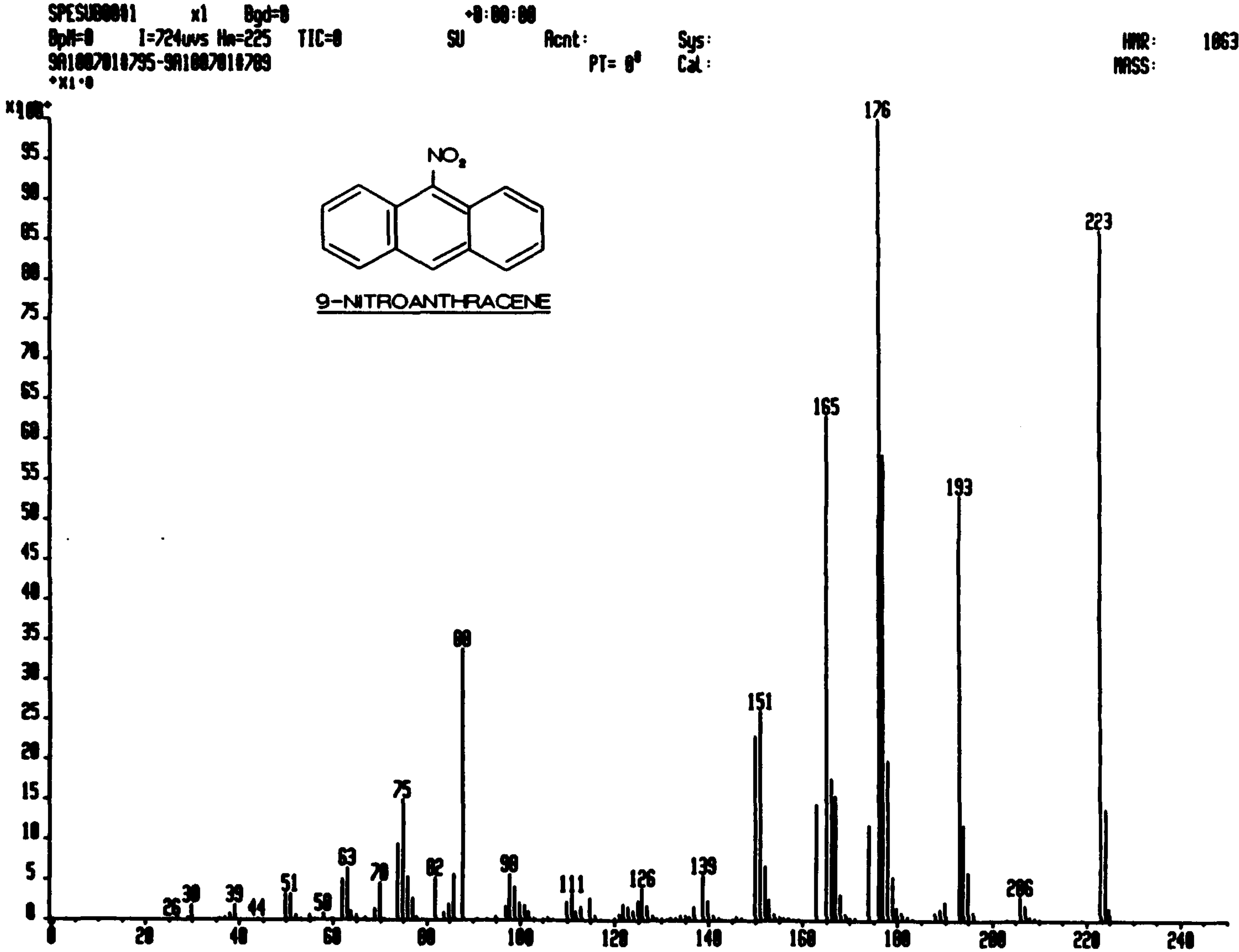
SPESUB0001 x1 Bgd=0
BpM=0 I=724uvs Hm=225 TIC=0
9A1007010795-9A1007010789
+X1.0
+0:00:00
SU
Rcnt:
PT= 0⁰
Sys:
Cal:
HMR: 10639000
MASS: 176
X100
95
90
85
80
75
70
65
60
55
50
45
40
35
30
25
20
15
10
5
0
NO2
9-NITROANTHRACENE
26
30
39
44
51
58
63
70
75
82
88
98
111
126
139
151
165
176
193
206
223
0
20
40
60
80
100
120
140
160
180
200
220
240

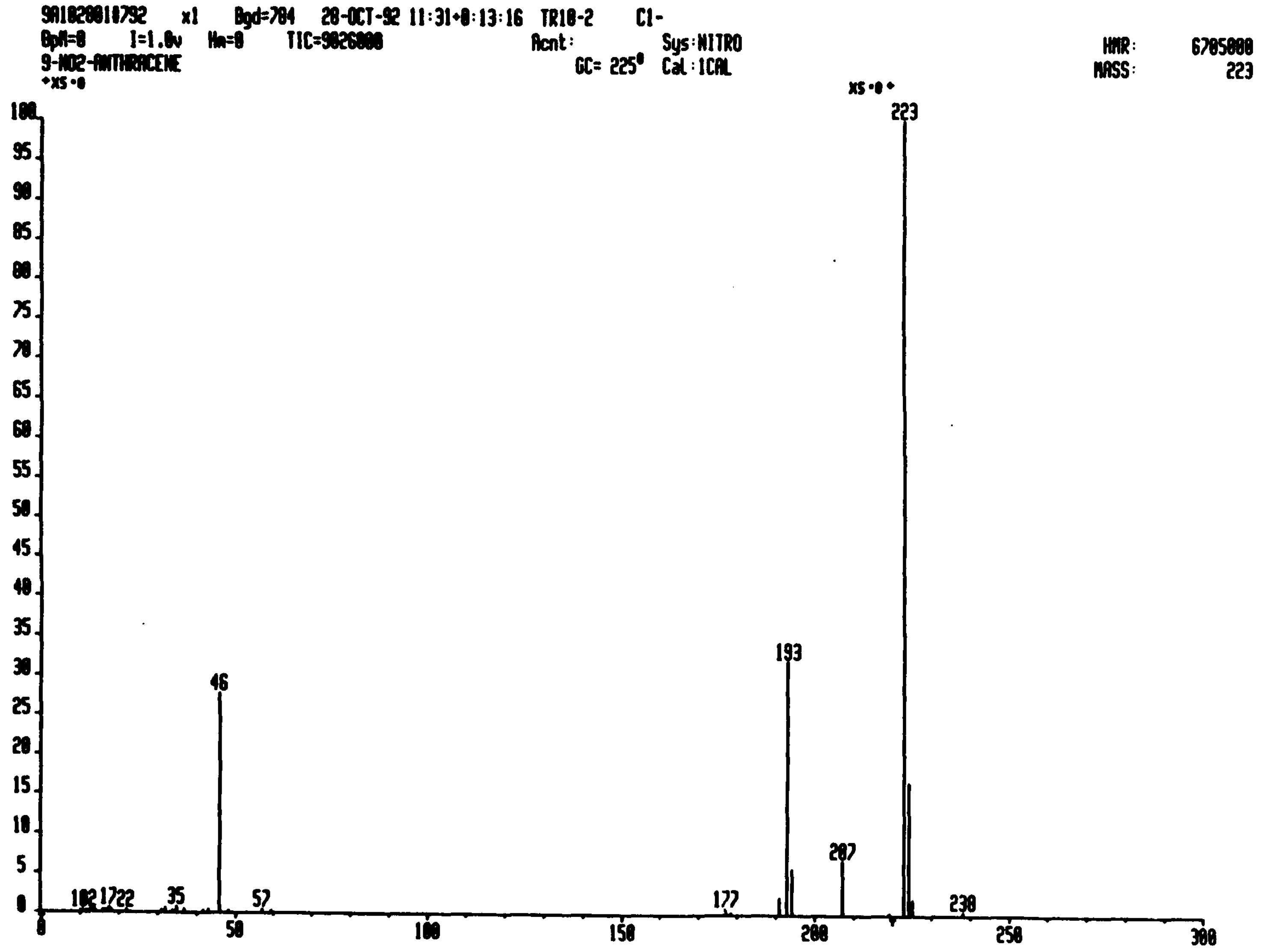
9A1020010792 x1 Bgd=704 20-OCT-92 11:31+0:13:16 TR10-2 CI-
BpM=0 I=1.0v Hm=0 TIC=9026000 Acnt: Sys:NITRO
9-NO2-ANTHRACENE GC= 225° Cal:ICAL
*xs·0
HMR: 6705000
MASS: 223
xs·0*
100
95
90
85
80
75
70
65
60
55
50
45
40
35
30
25
20
15
10
5
0
223
193
46
207
10
17
22
35
57
177
230
0
50
100
150
200
250
300

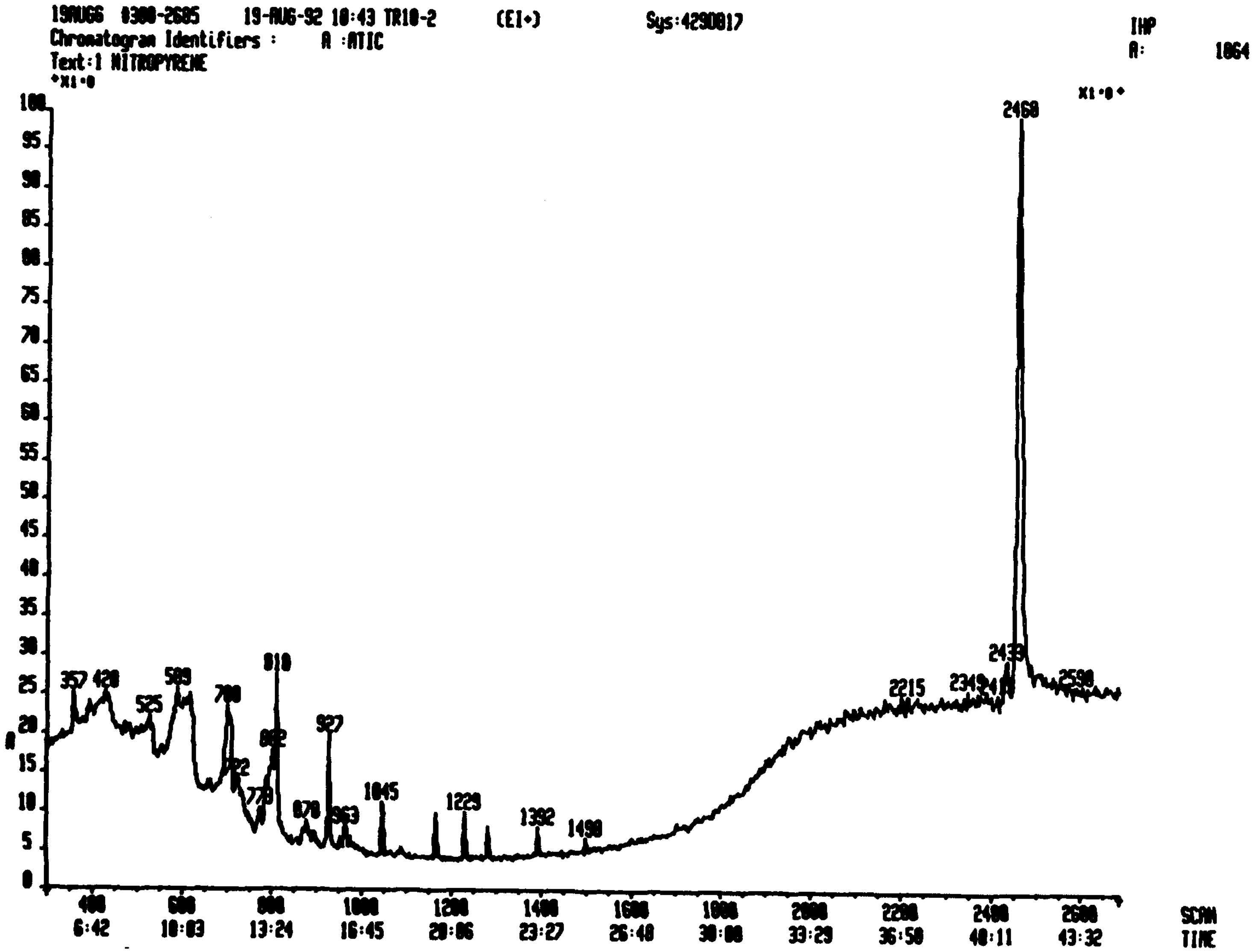
19AUG6 0300-2605
19-AUG-92 10:43 TR10-2
(EI+)
Sys:4290817
Chromatogram Identifiers : A :ATIC
Text:1 NITROPYRENE
*X1·0
IHP
A: 1064
X1·0*
100
95
90
85
80
75
70
65
60
55
50
45
40
35
30
25
20
15
10
5
0
A
357
420
525
589
700
722
778
810
882
870
927
963
1045
1229
1392
1490
2215
2349
2410
2433
2460
2590
400
6:42
600
10:03
800
13:24
1000
16:45
1200
20:06
1400
23:27
1600
26:48
1800
30:08
2000
33:29
2200
36:50
2400
40:11
2600
43:32
SCAN
TIME

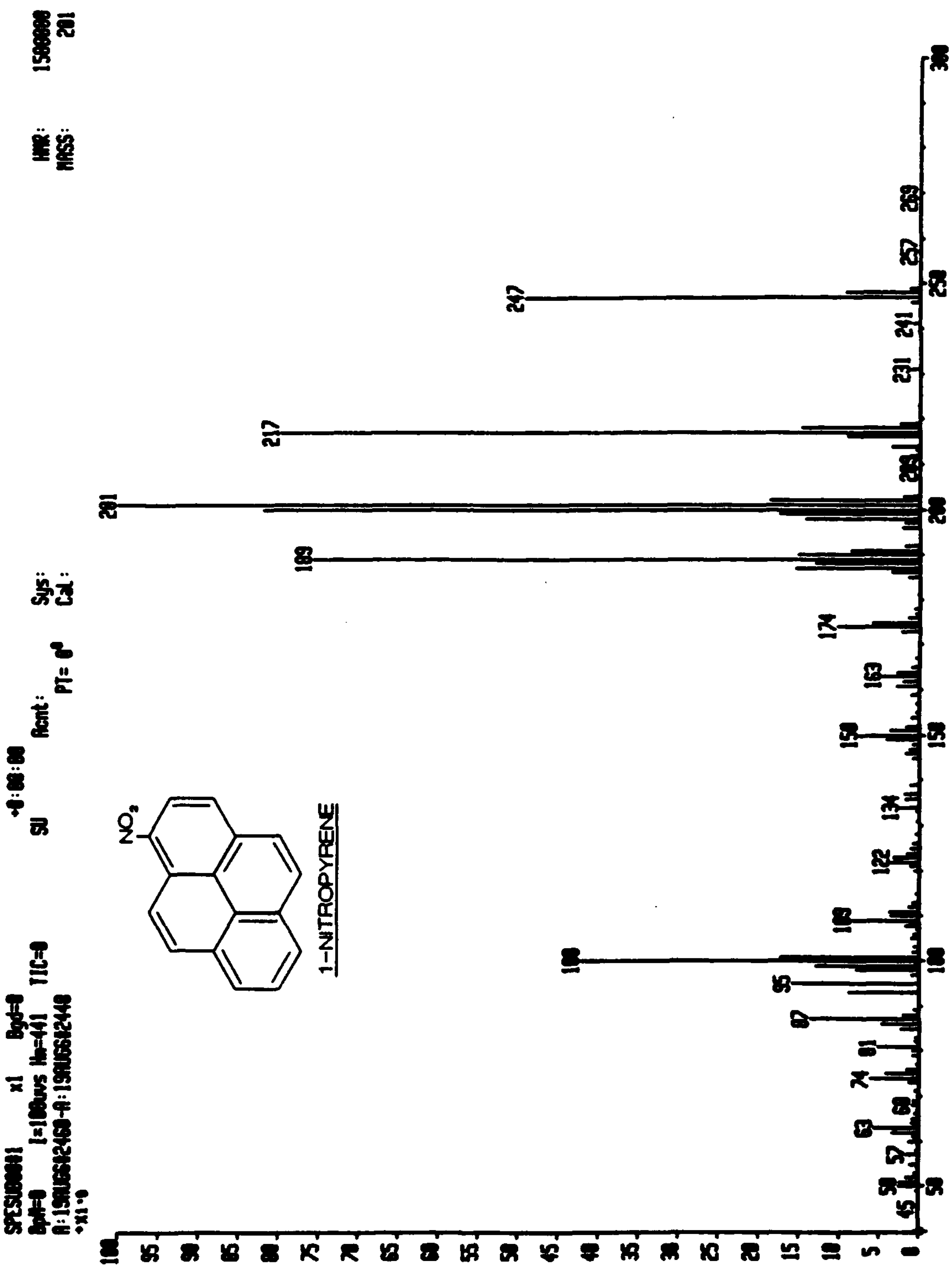

1-NITROPYRENE

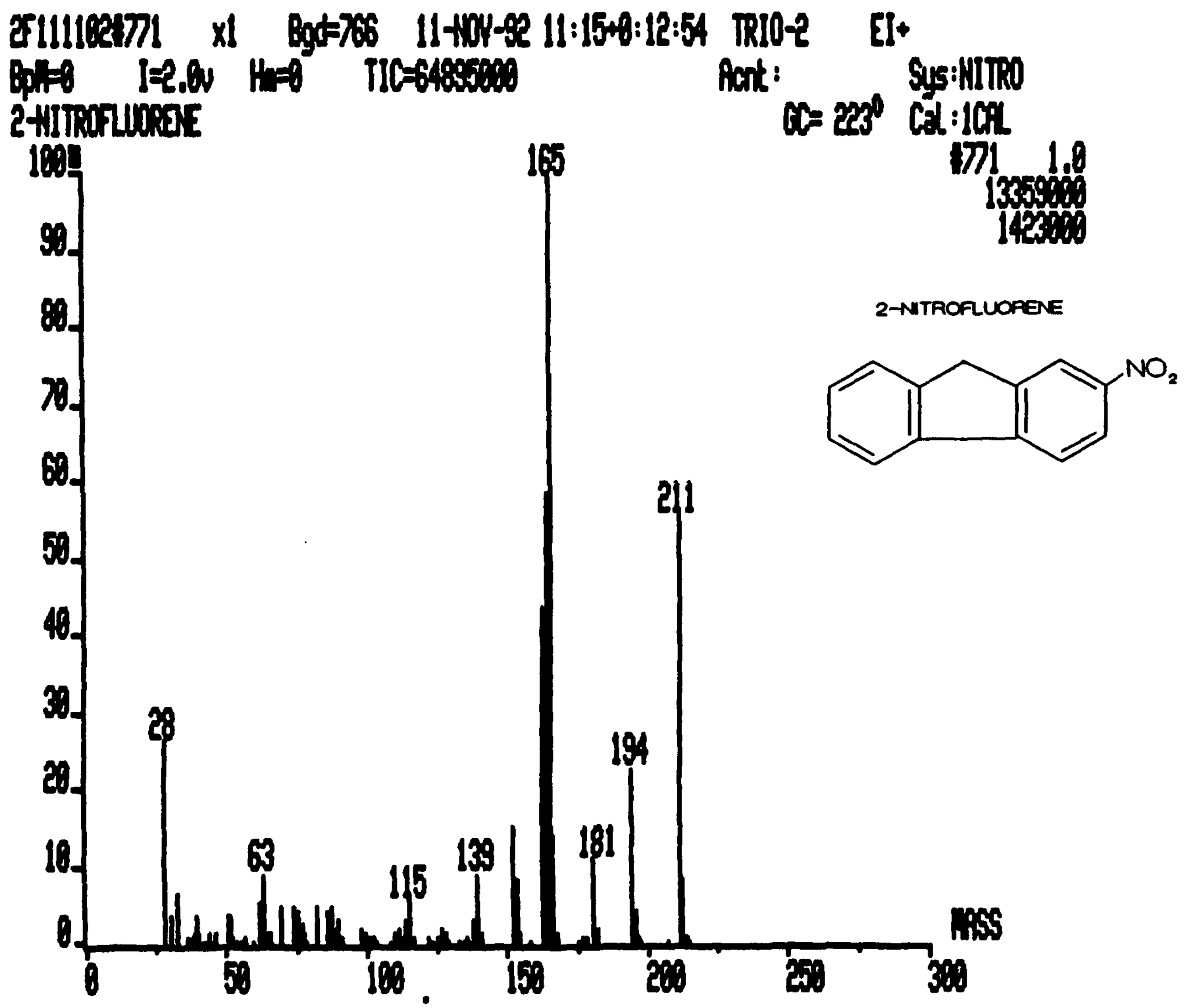
2F111102#771 x1 Bgd=766 11-NOV-92 11:15+0:12:54 TRIO-2 EI+
BpM=0 I=2.0v Hm=0 TIC=64895000 Acnt: Sys:NITRO
2-NITROFLUORENE GC= 223° Cal:1CAL
#771 1.0
13359000
1423000
100
90
80
70
60
50
40
30
20
10
0
28
63
115
139
165
181
194
211
0
50
100
150
200
250
300
MASS
2-NITROFLUORENE
NO2

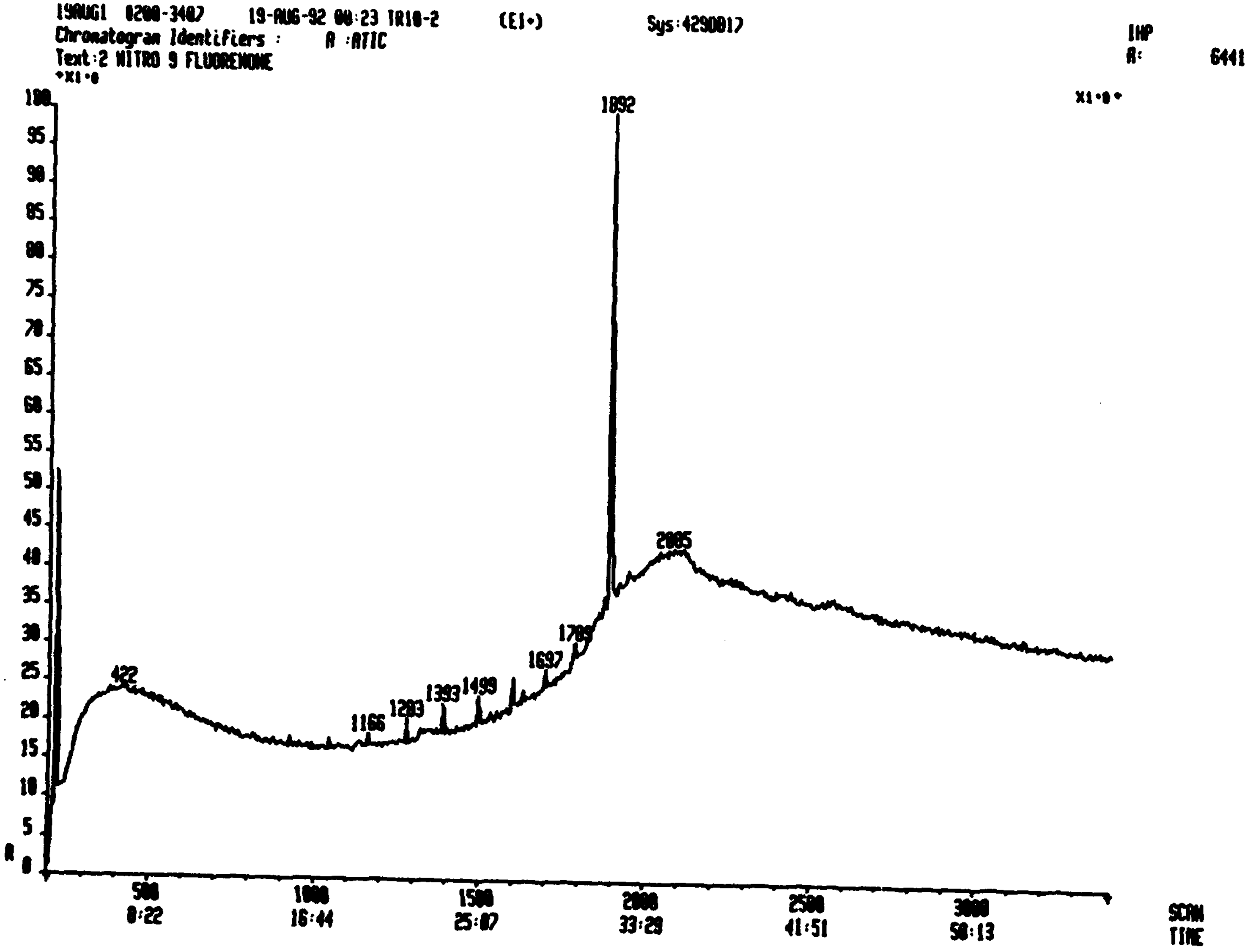
19AUG1 0200-3407
19-AUG-92 00:23 TR10-2
(EI+)
Sys:4290017
Chromatogram Identifiers : A :ATIC
Text:2 NITRO 9 FLUORENONE
*X1.0
IHP
A: 6441
X1.0*
100
95
90
85
80
75
70
65
60
55
50
45
40
35
30
25
20
15
10
5
A 0
422
1166
1203
1393
1499
1697
1789
1892
2005
500
8:22
1000
16:44
1500
25:07
2000
33:29
2500
41:51
3000
50:13
SCAN
TIME

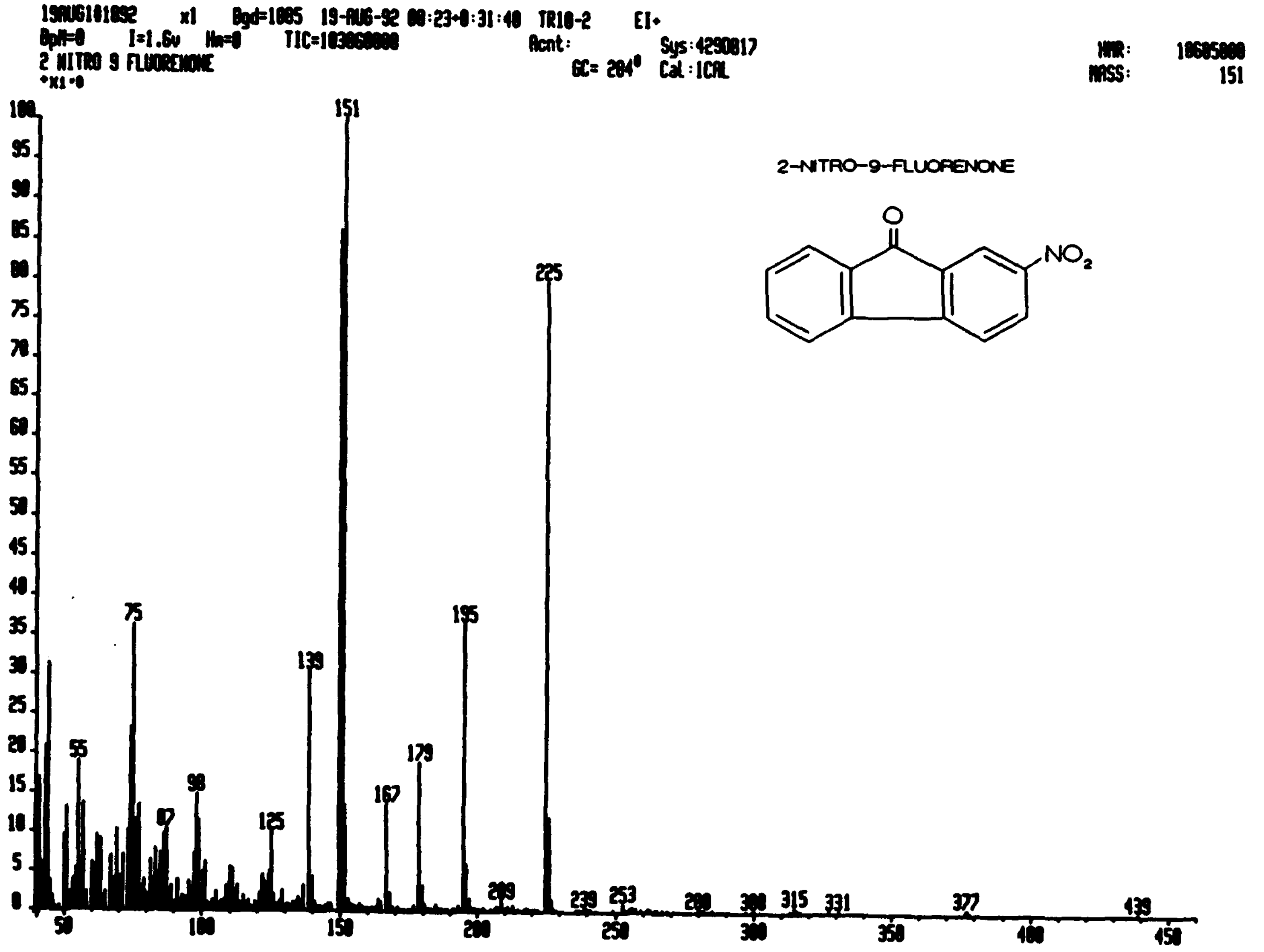
19AUG101092 x1 Bgd=1005 19-AUG-92 00:23+0:31:40 TR10-2 EI+
BpM=0 I=1.6v Hm=0 TIC=103060000 Acnt: Sys:4290817
2 NITRO 9 FLUORENONE GC= 204° Cal:ICAL
*X1.0
HMR: 10605000
MASS: 151
2-NITRO-9-FLUORENONE
O
$NO_2$
151
225
195
139
75
179
55
98
167
125
87
209
239
253
280
300
315
331
377
439
100
95
90
85
80
75
70
65
60
55
50
45
40
35
30
25
20
15
10
5
0
50
100
150
200
250
300
350
400
450

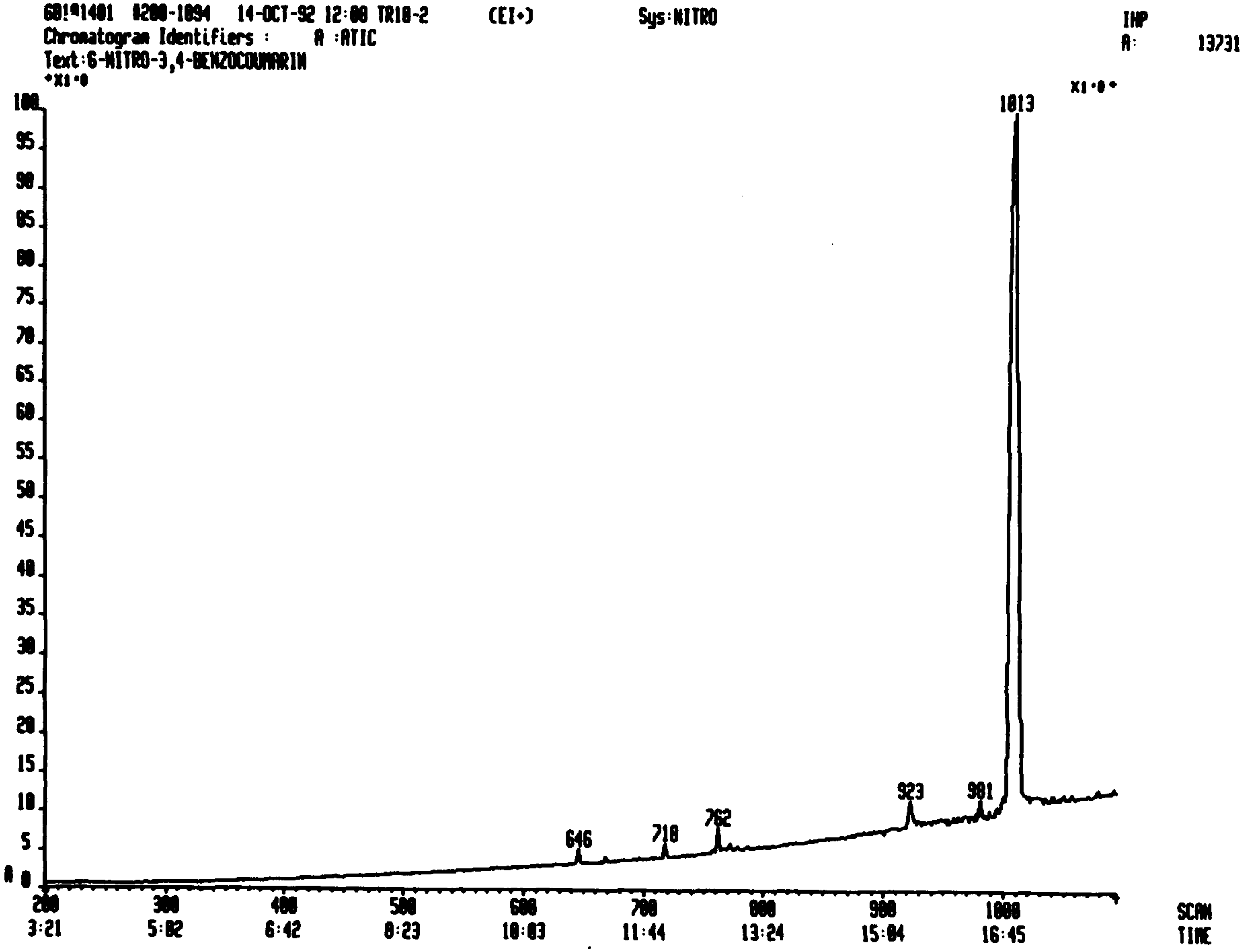
60!ª1401 #200-1094 14-OCT-92 12:00 TR10-2 (EI+) Sys:NITRO
Chromatogram Identifiers : A :ATIC
Text:6-NITRO-3,4-BENZOCOUMARIN
*X1·0
IHP
A: 13731
X1·0*
1013
981
923
762
718
646
100
95
90
85
80
75
70
65
60
55
50
45
40
35
30
25
20
15
10
5
0
A
200
3:21
300
5:02
400
6:42
500
8:23
600
10:03
700
11:44
800
13:24
900
15:04
1000
16:45
SCAN
TIME

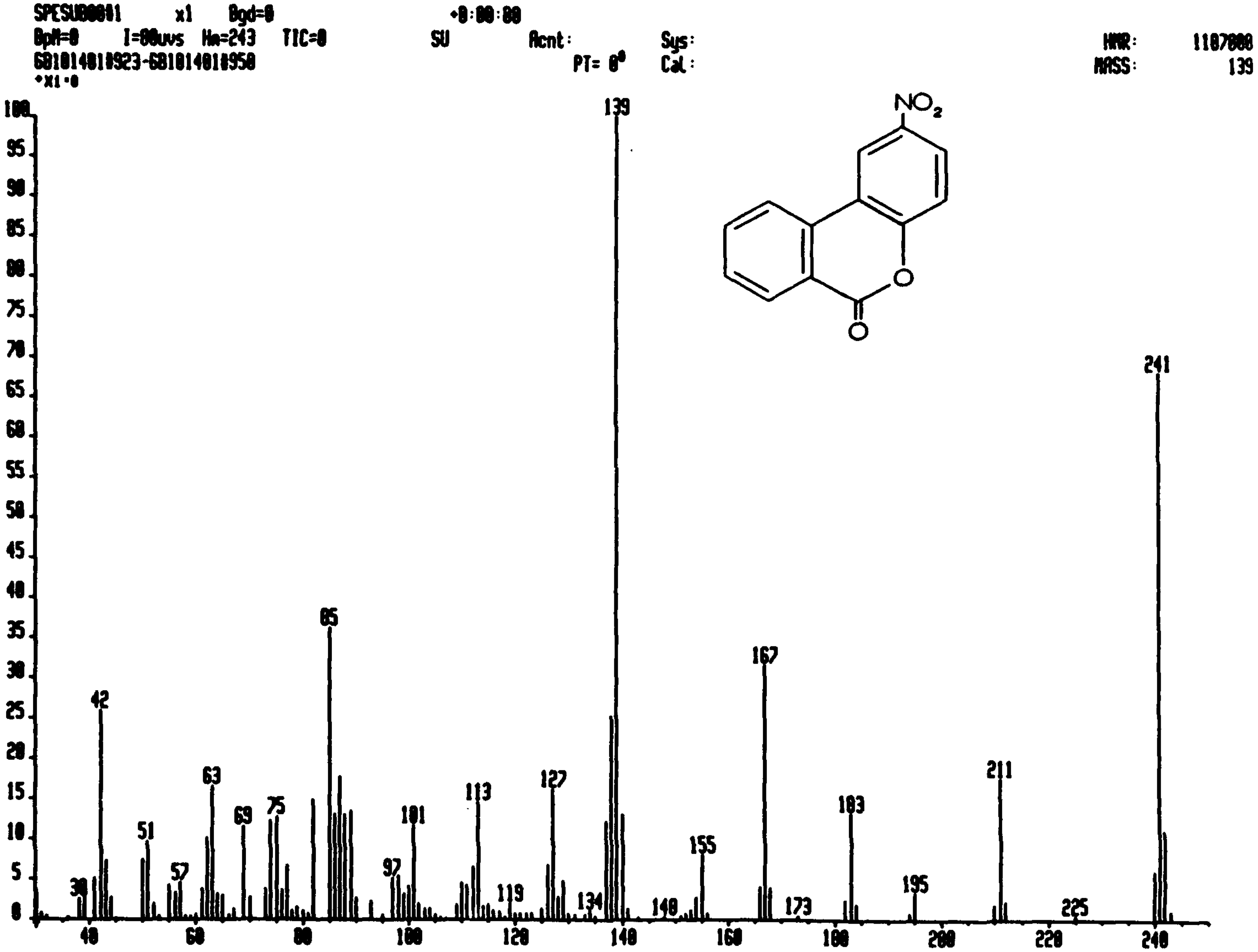
SPESUB0001 x1 Bgd=0
+0:00:00
BpM=0 I=00uvs Hm=243 TIC=0
SU
Acnt:
Sys:
6B1014010923-6B1014010950
PT= 0°
Cal:
*X1·0
HMR: 1107000
MASS: 139
$NO_2$
O
O
100
95
90
85
80
75
70
65
60
55
50
45
40
35
30
25
20
15
10
5
0
40
60
80
100
120
140
160
180
200
220
240
38
42
51
57
63
69
75
85
97
101
113
119
127
134
139
148
155
167
173
183
195
211
225
241

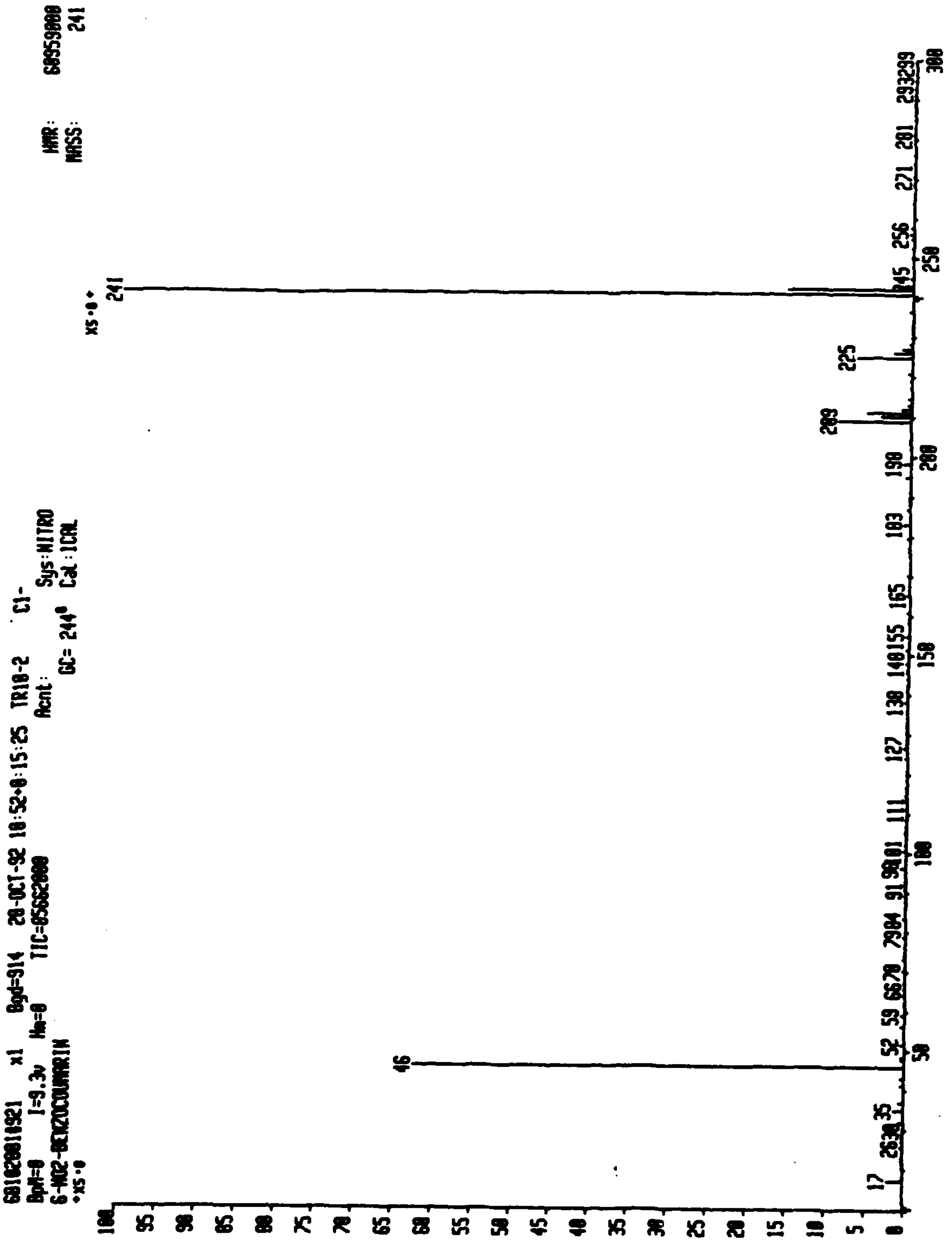
GB1020B01I921 x1 Bgd=914 20-OCT-92 10:52+0:15:25 TR10-2 CI-
BpM=0 I=9.3v Hm=0 TIC=85662000 Acnt: Sys:NITRO
6-NO2-BENZOCOUMARIN GC= 244° Cal:ICAL
*XS-0
HMR: 68059000
MASS: 241
XS-0*
241
46
209
225
17
2630
35
52
59
6670
7984
9198101
111
127
138
140155
165
183
198
245
256
271
281
293299
0
5
10
15
20
25
30
35
40
45
50
55
60
65
70
75
80
85
90
95
100
50
100
150
200
250
300

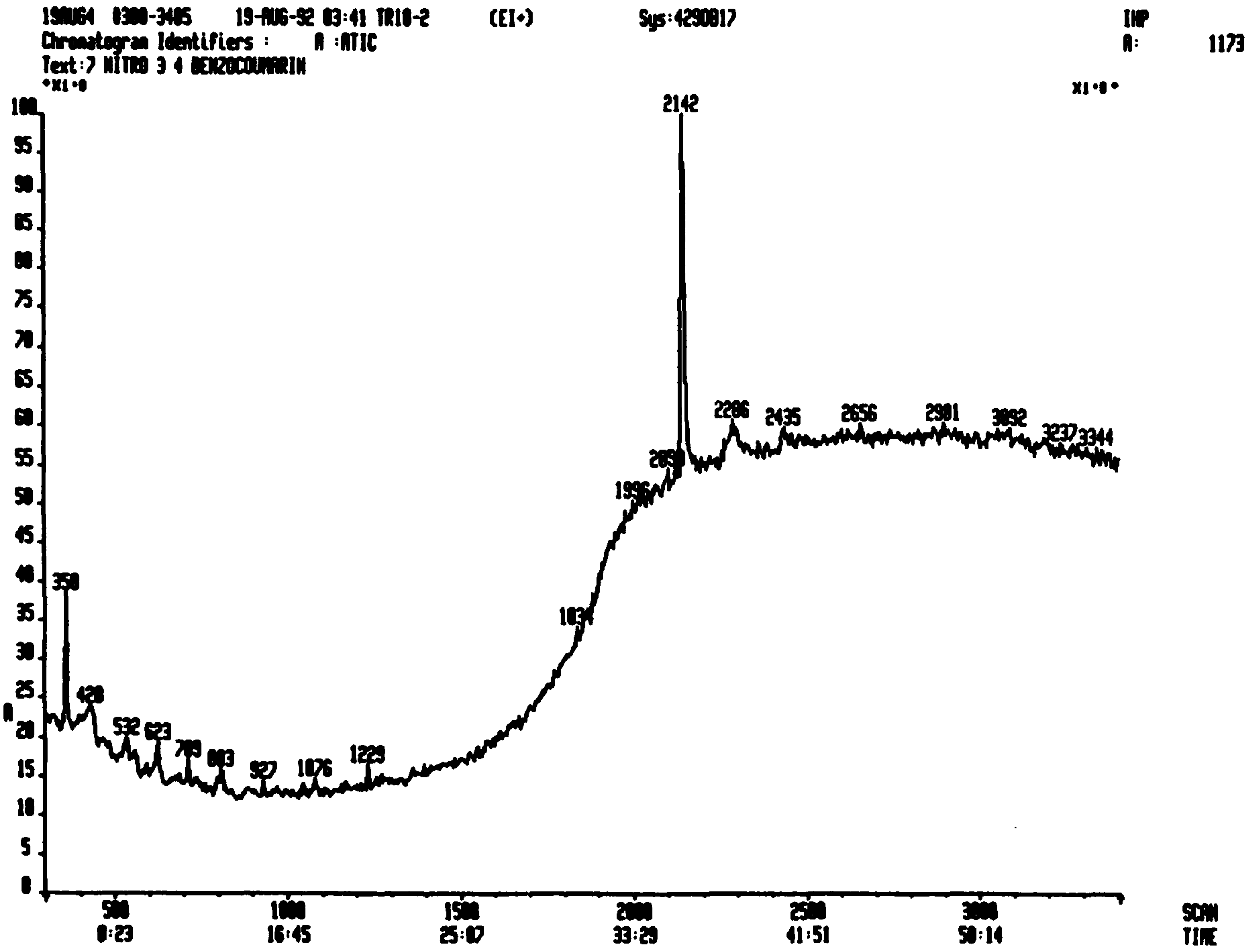
19AUG64 0300-3405 19-AUG-92 03:41 TR10-2 (EI+) Sys:4290817
Chromatogram Identifiers : A :ATIC
Text:7 NITRO 3 4 BENZOCOUMARIN
*X1.0
INP
A: 1173
X1.0*
A
100
95
90
85
80
75
70
65
60
55
50
45
40
35
30
25
20
15
10
5
0
358
428
532
623
709
803
927
1076
1229
1834
1996
2090
2142
2286
2435
2656
2901
3092
3237
3344
500
8:23
1000
16:45
1500
25:07
2000
33:29
2500
41:51
3000
50:14
SCAN
TIME

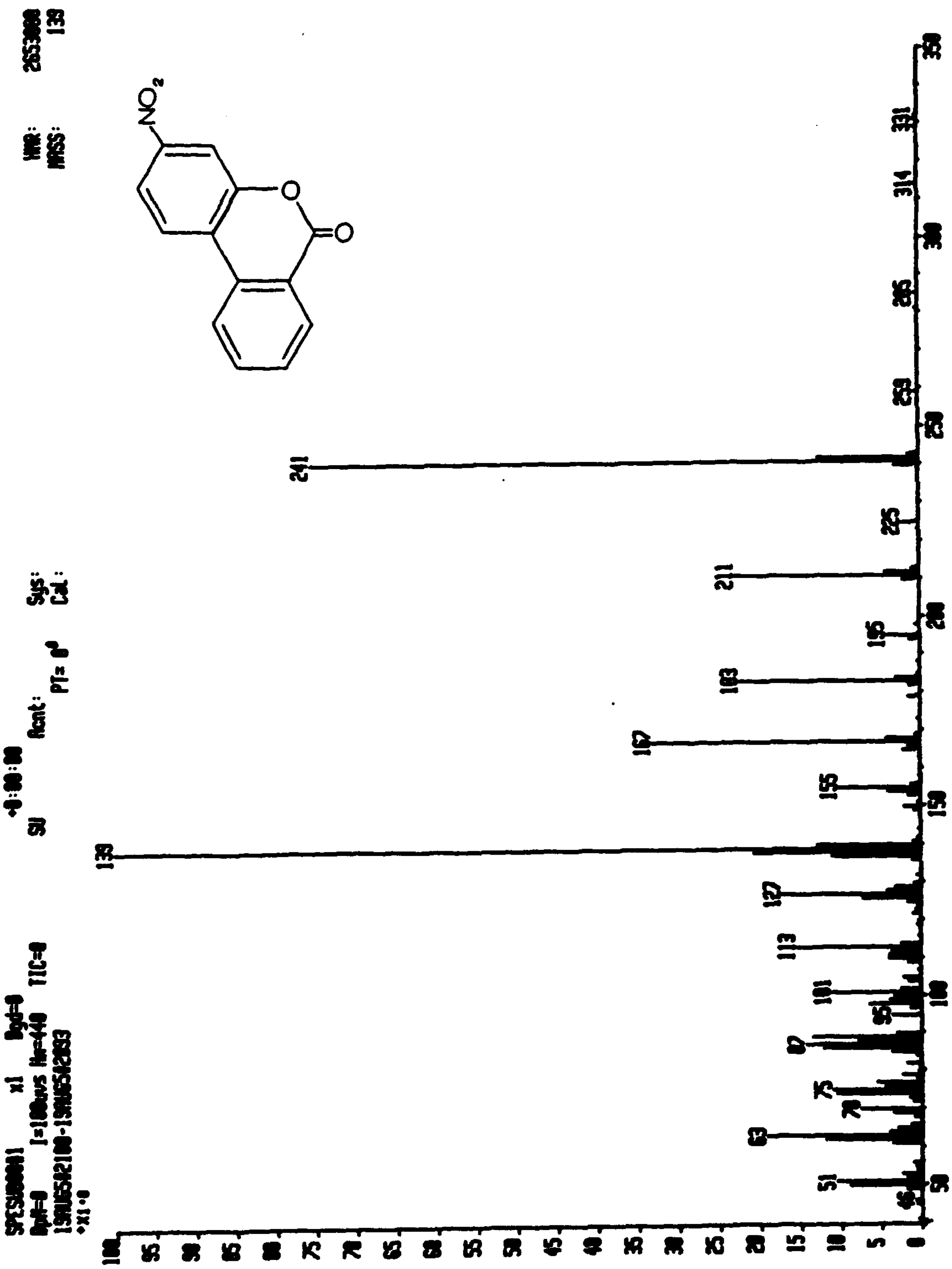
SU +0:00:00
Acnt:
PT= 0°
Sys:
Cal:
MAR: 2653000
MASS: 139
NO2
O
O
139
241
167
183
211
63
127
113
101
87
75
70
95
51
155
195
225
259
285
300
314
331
46
50
100
150
200
250
350
0
5
10
15
20
25
30
35
40
45
50
55
60
65
70
75
80
85
90
95
100

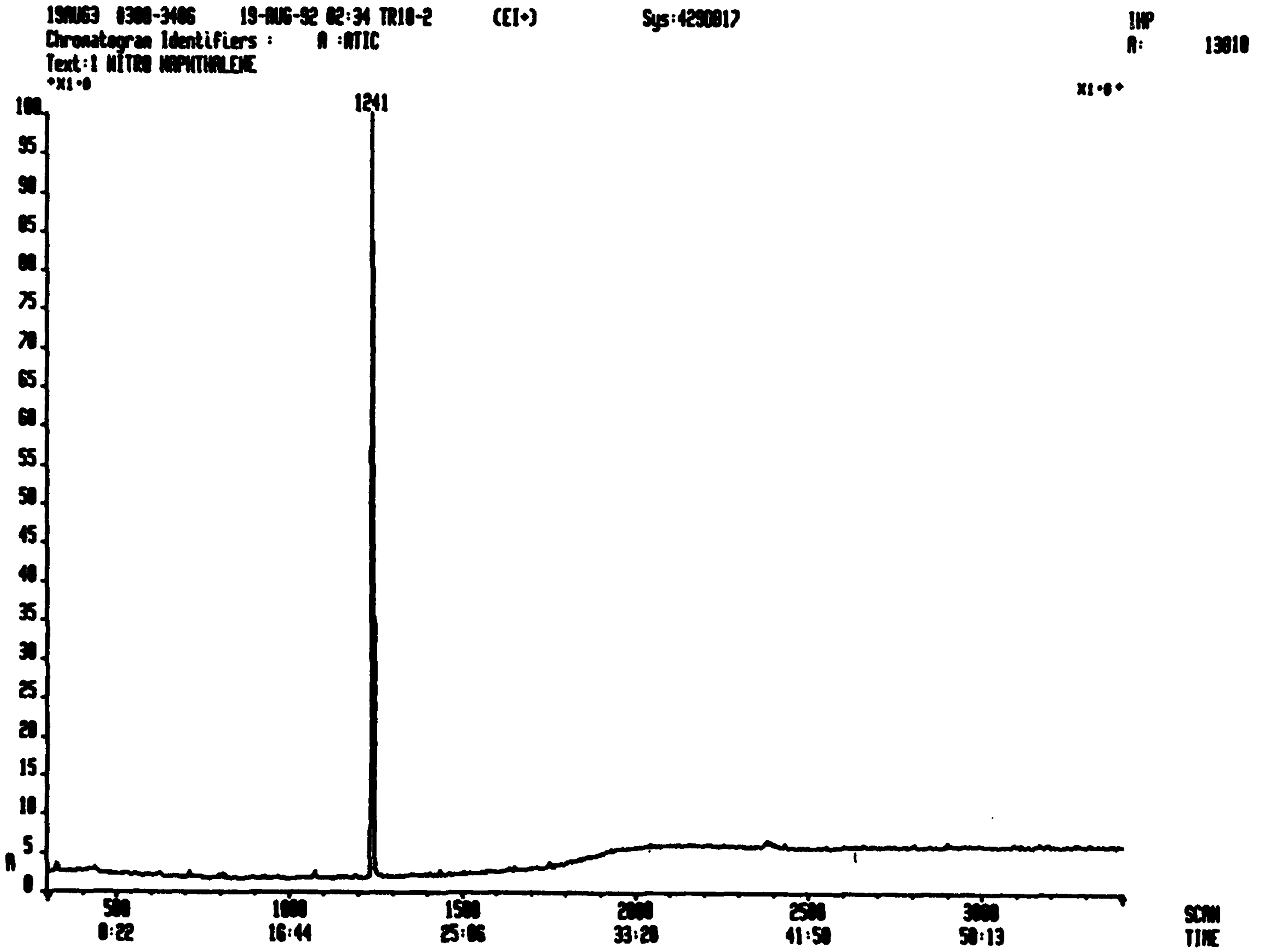
19AUG63 0300-3406 19-AUG-92 02:34 TR10-2 (EI+) Sys:4290817
Chromatogram Identifiers : A :ATIC
Text:1 NITRO NAPHTHALENE
*X1·0
!HP
A: 13010
X1·0*
1241
100
95
90
85
80
75
70
65
60
55
50
45
40
35
30
25
20
15
10
5
A
0
500
8:22
1000
16:44
1500
25:06
2000
33:28
2500
41:50
3000
50:13
SCAN
TIME

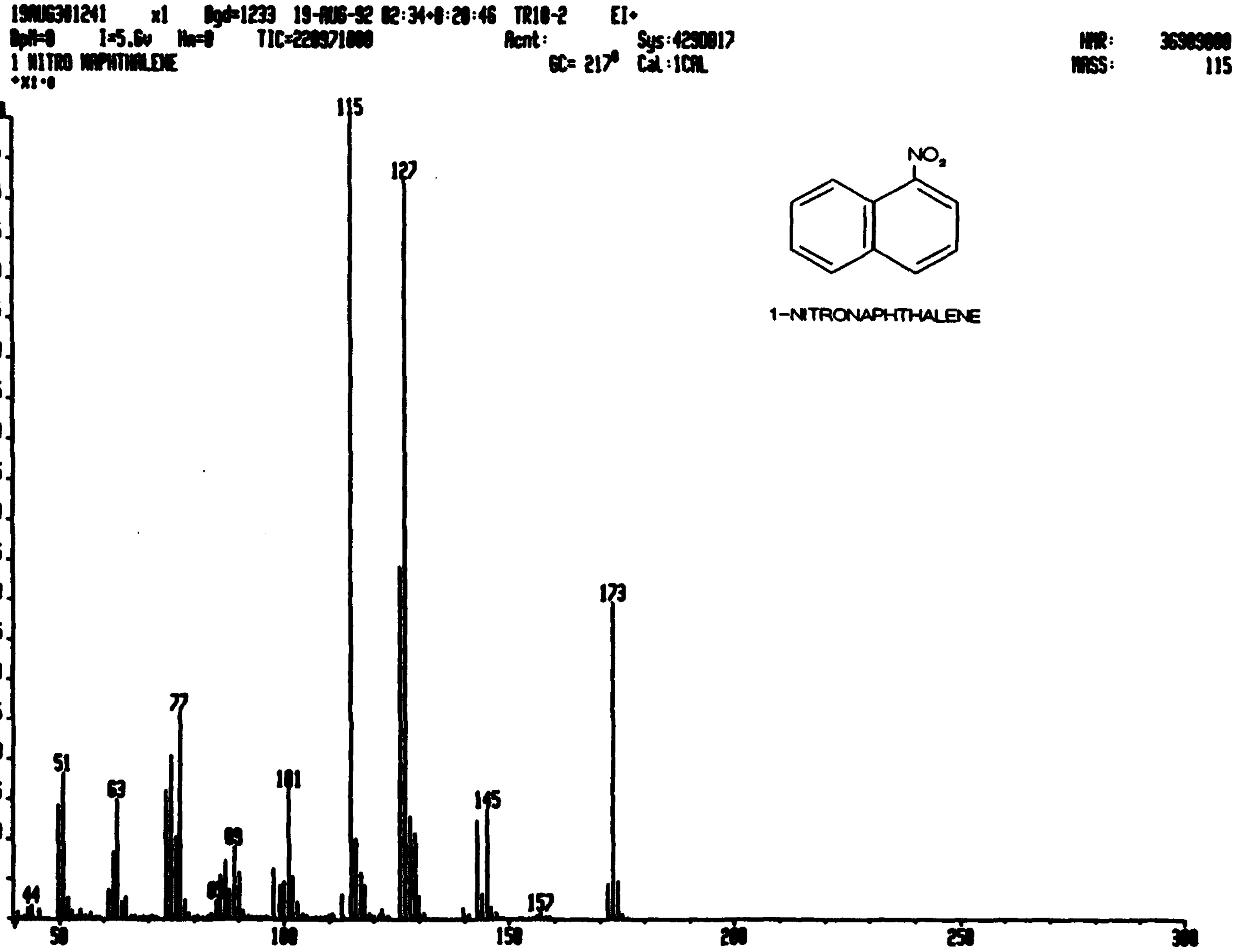

19AUG301241 x1 Bgd=1233 19-AUG-92 02:34+0:20:46 TR10-2 EI+
BpM=0 I=5.6v Hm=0 TIC=220971000 Acnt: Sys:4290017
1 NITRO NAPHTHALENE GC= 217° Cal:1CAL
*X1·0
HMR: 36909000
MASS: 115
NO2
1-NITRONAPHTHALENE
100
95
90
85
80
75
70
65
60
55
50
45
40
35
30
25
20
15
10
5
0
44
51
63
77
89
101
115
127
145
157
173
50
100
150
200
250
300

# APPENDIX D

## FAB Spectra of Nitro-PAH and Nitrobenzocoumarin Standards

| Spectra Titles | Page |
|---|---|
| 1. 9-nitroanthracene, bare probe | 226 |
| 2. 9-nitroanthracene, bare probe, expansion (150-250) | 227 |
| 3. 1-nitropyrene, bare probe | 228 |
| 4. 2-nitrofluorene, bare probe | 229 |
| 5. 2-nitrofluorene, bare probe, expansion (80-250) | 230 |
| 6. 2-nitrofluorene, 3-nitrobenzylalcohol (3-NBA) matrix, MIKES Spectrum | 231 |
| 7. 2-nitrofluorene, 3-NBA matrix, histogram,daughters of 211 | 232 |
| 8. 2-nitrofluorene, 3-NBA matrix, MIKES Spectrum | 233 |
| 9. 2-nitrofluorene, 3-NBA matrix, histogram, daughters of 212 | 234 |
| 10. 2-nitrofluorene, 3-NBA matrix, expansion (160-220) | 235 |
| 11. 2-nitro-9-fluorenone, bare probe | 236 |
| 12. 2-nitro-9-fluorenone, glycerol matrix, expansion (190-270) | 237 |
| 13. 2-nitro-9-fluorenone, 3-NBA matrix, expansion (160-250) | 238 |
| 14. 6-nitro-3,4-benzocoumarin, bare probe | 239 |
| 15. 6-nitro-3,4-benzocoumarin, 3-NBA matrix, MIKES Spectrum | 240 |
| 16. 6-nitro-3,4-benzocoumarin, 3-NBA, histogram, daughters of 242 | 241 |
| 17. 6-nitro-3,4-benzocoumarin, 3-NBA matrix, expansion (200-280) | 242 |
| 18. 7-nitro-3,4-benzocoumarin, bare probe | 243 |

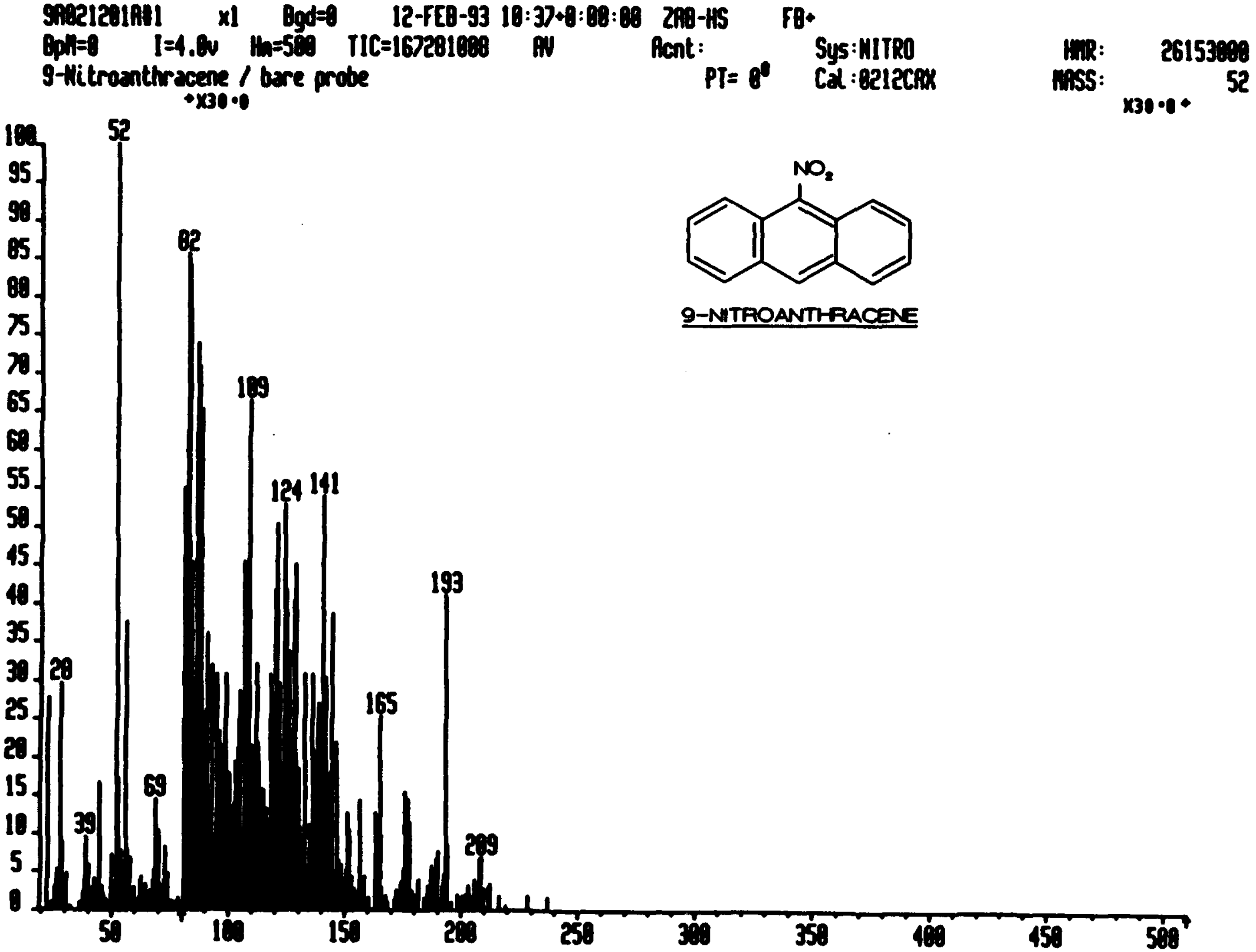
9A021201A01 x1 Bgd=0 12-FEB-93 10:37+0:00:00 ZAB-HS FB+
BpM=0 I=4.0v Hm=500 TIC=167201000 AV Acnt: Sys:NITRO HMR: 26153000
9-Nitroanthracene / bare probe PT= 0° Cal:0212CAX MASS: 52
+X30·0
X30·0+
NO2
9-NITROANTHRACENE
52
82
109
124
141
193
165
28
39
69
209
100
95
90
85
80
75
70
65
60
55
50
45
40
35
30
25
20
15
10
5
0
50
100
150
200
250
300
350
400
450
500

```
9A021201A#1     x1    Bgd=0      12-FEB-93 10:37+0:00:00  ZAB-HS     FB+
BpM=0     I=4.0v   Hm=500   TIC=167201000     AV          Acnt:              Sys:NITRO            HMR:      356000
9-Nitroanthracene / bare probe                                      PT= 0°    Cal:0212CAX          MASS:        193
*X1·0
```

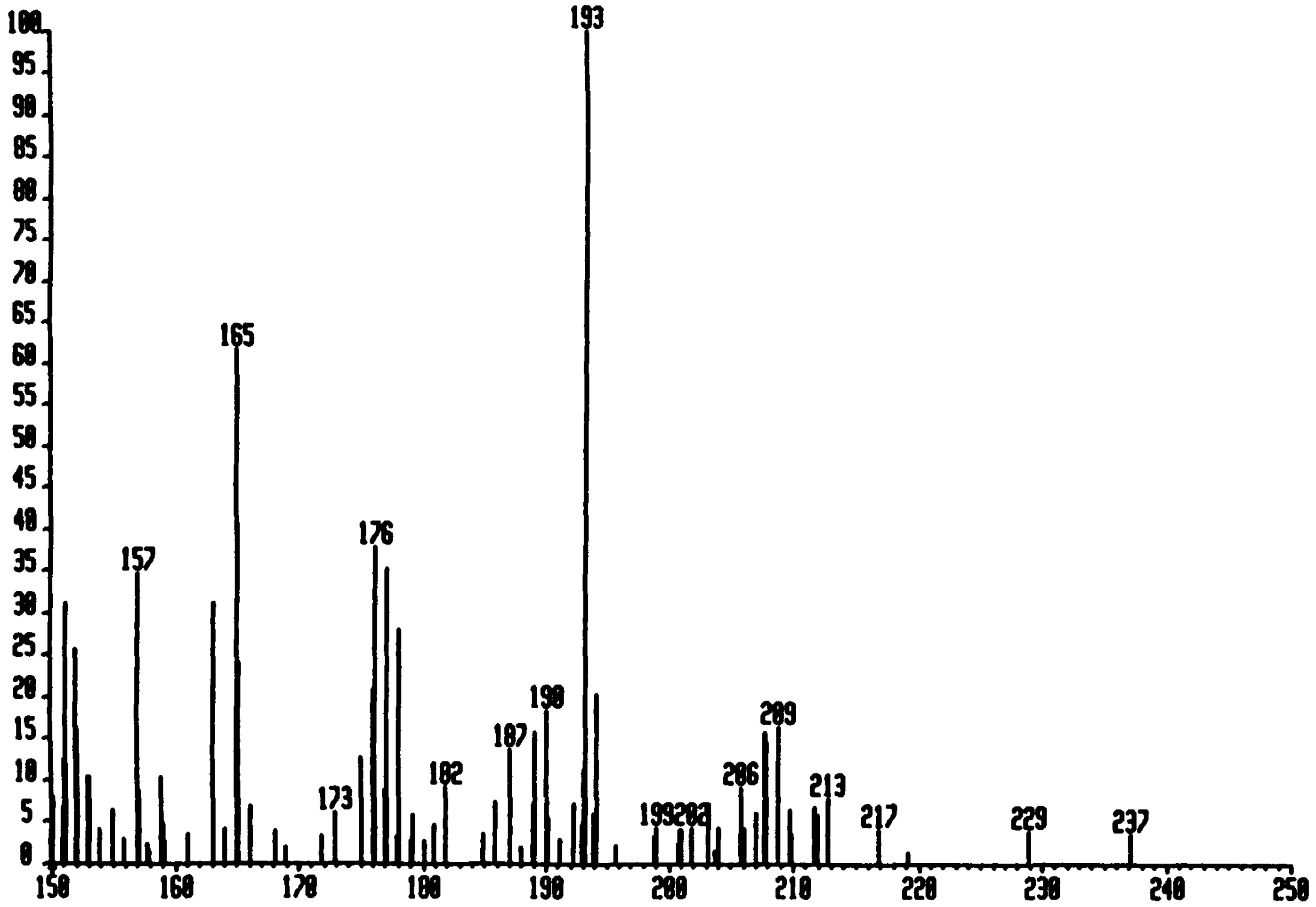

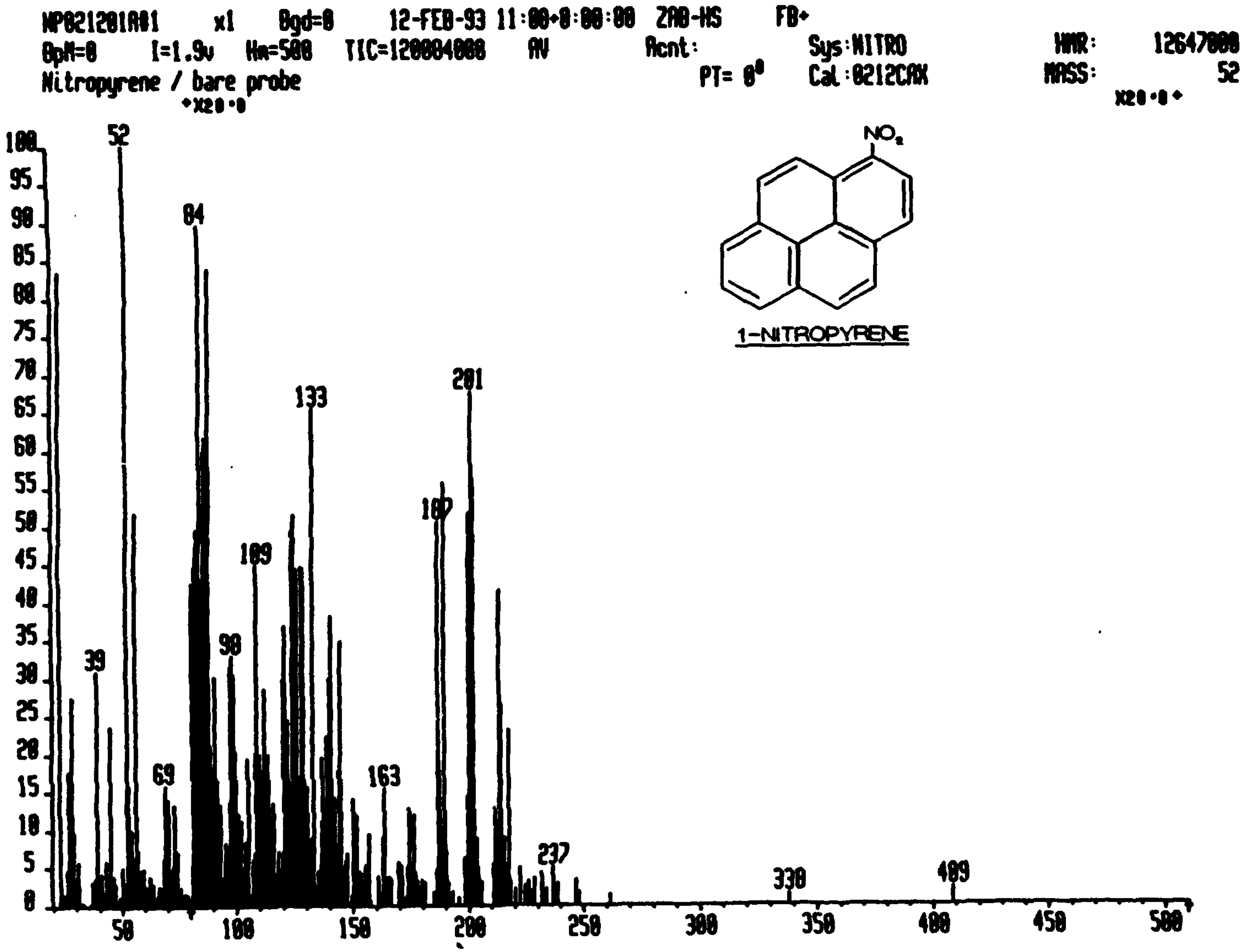
NP021201A01 x1 Bgd=0 12-FEB-93 11:00+0:00:00 ZAB-HS FB+
BpM=0 I=1.9v Hm=500 TIC=120004000 AV Acnt: Sys:NITRO HMR: 12647000
Nitropyrene / bare probe PT= 0⁰ Cal:0212CAX MASS: 52
*X20·0
X20·0*
NO₂
1-NITROPYRENE
100
95
90
85
80
75
70
65
60
55
50
45
40
35
30
25
20
15
10
5
0
52
84
133
201
187
109
98
39
69
163
237
330
409
50
100
150
200
250
300
350
400
450
500

2N021201A01 x1 Bgd=0 12-FEB-93 10:50+0:00:00 ZAB-HS FB+
BpM=0 I=2.3v Hm=500 TIC=92576000 AV Acnt: Sys:NITRO HMR: 14003000
2-Nitrofluorene / bare probe PT= 0° Cal:0212CAX MASS: 52

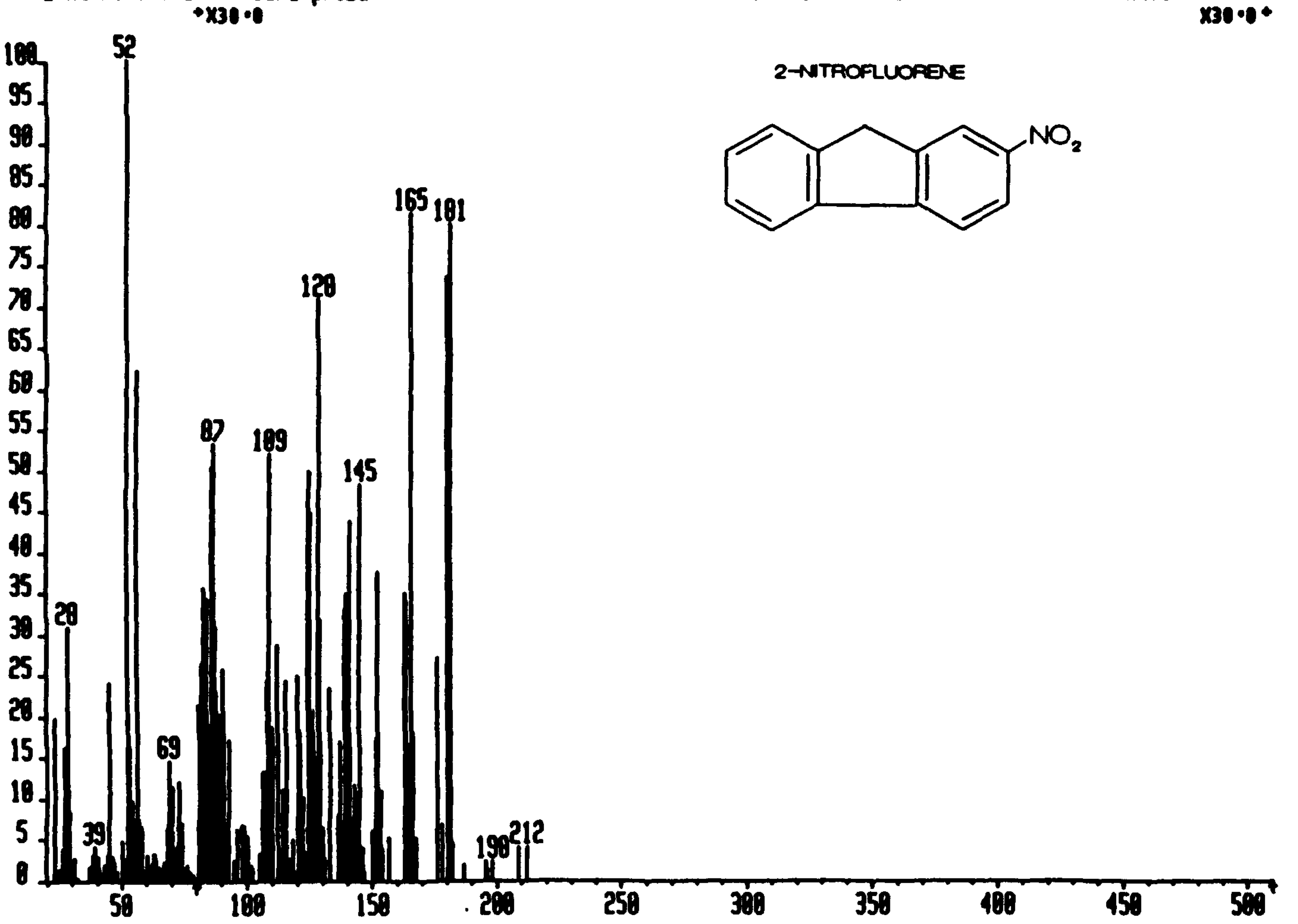

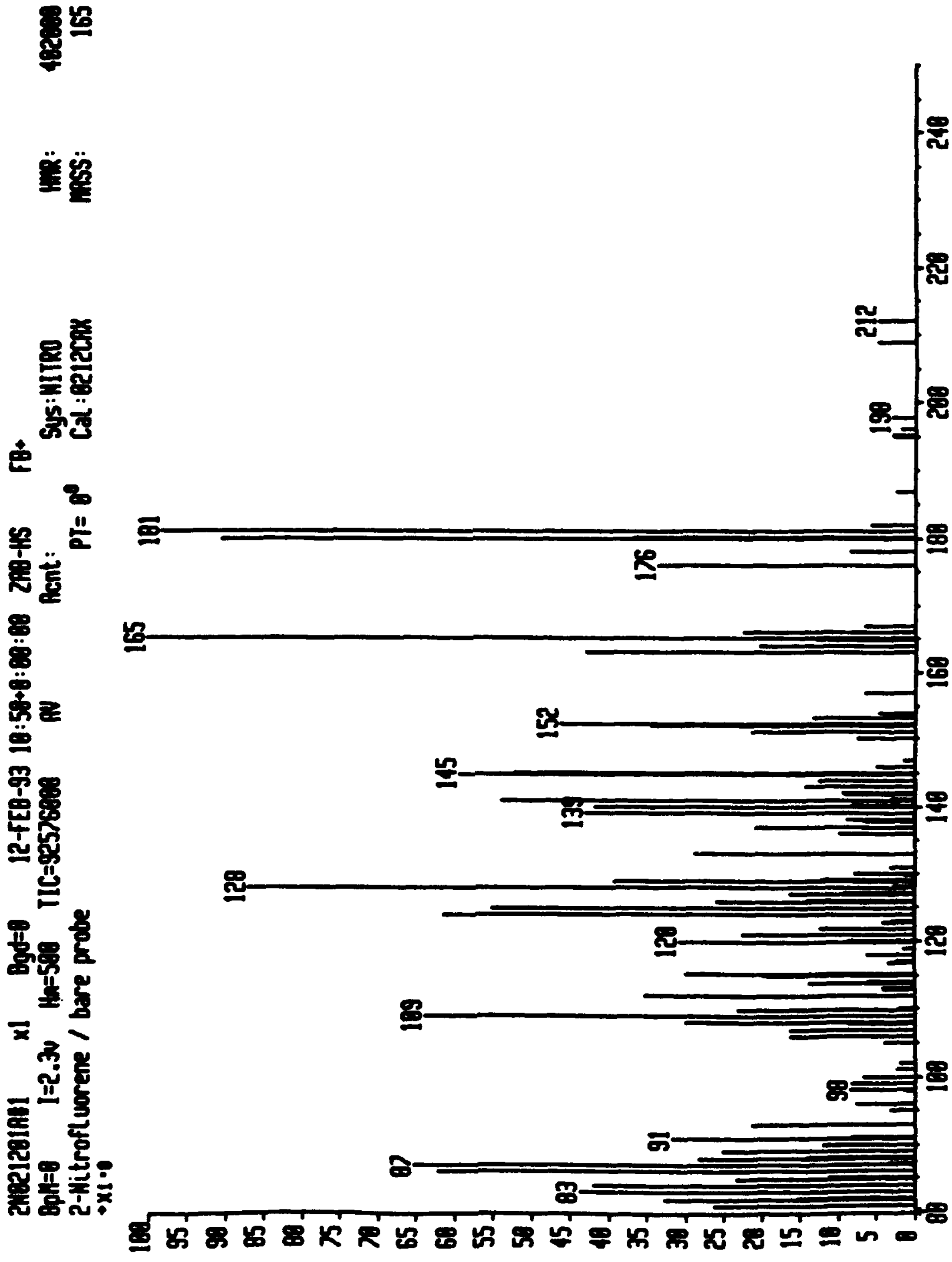
2N0212D1A01 x1 Bgd=0 12-FEB-93 10:58+0:00:00 ZAB-HS FB+
BpM=0 I=2.3v Ha=500 TIC=92576000 AV Acnt: Sys:NITRO HAR: 402000
2-Nitrofluorene / bare probe PT= 0° Cal:0212CMX MASS: 165
*X1·0
100
95
90
85
80
75
70
65
60
55
50
45
40
35
30
25
20
15
10
5
0
80
100
120
140
160
180
200
220
240
83
87
91
98
109
120
128
139
145
152
165
176
181
198
212

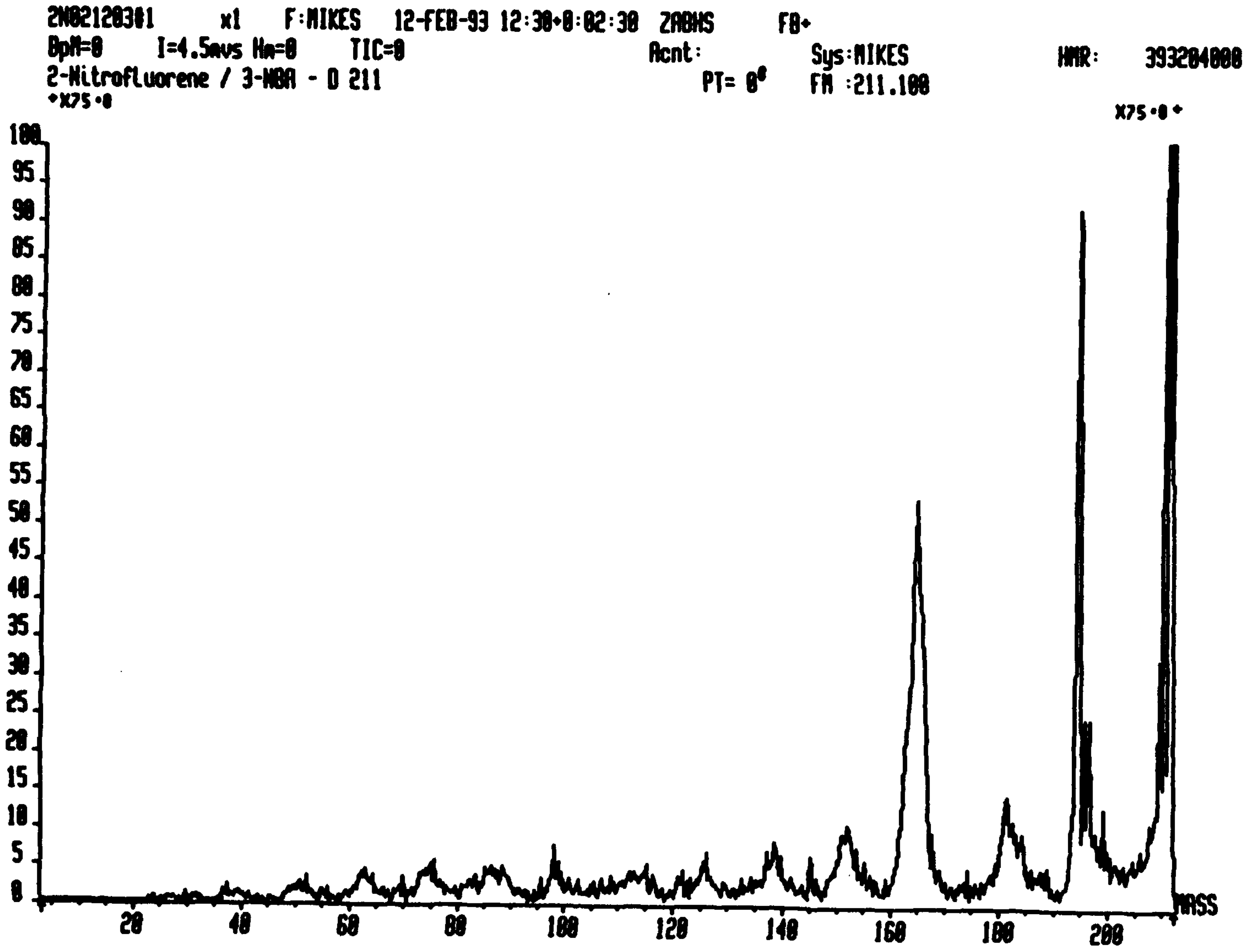
2N02120301 x1 F:MIKES 12-FEB-93 12:30+0:02:30 ZABHS FB+
BpM=0 I=4.5mvs Hm=0 TIC=0 Acnt: Sys:MIKES HMR: 393204000
2-Nitrofluorene / 3-NBA - D 211 PT= 0° FM :211.100
*X75·0
X75·0*
100
95
90
85
80
75
70
65
60
55
50
45
40
35
30
25
20
15
10
5
0
20
40
60
80
100
120
140
160
180
200
MASS

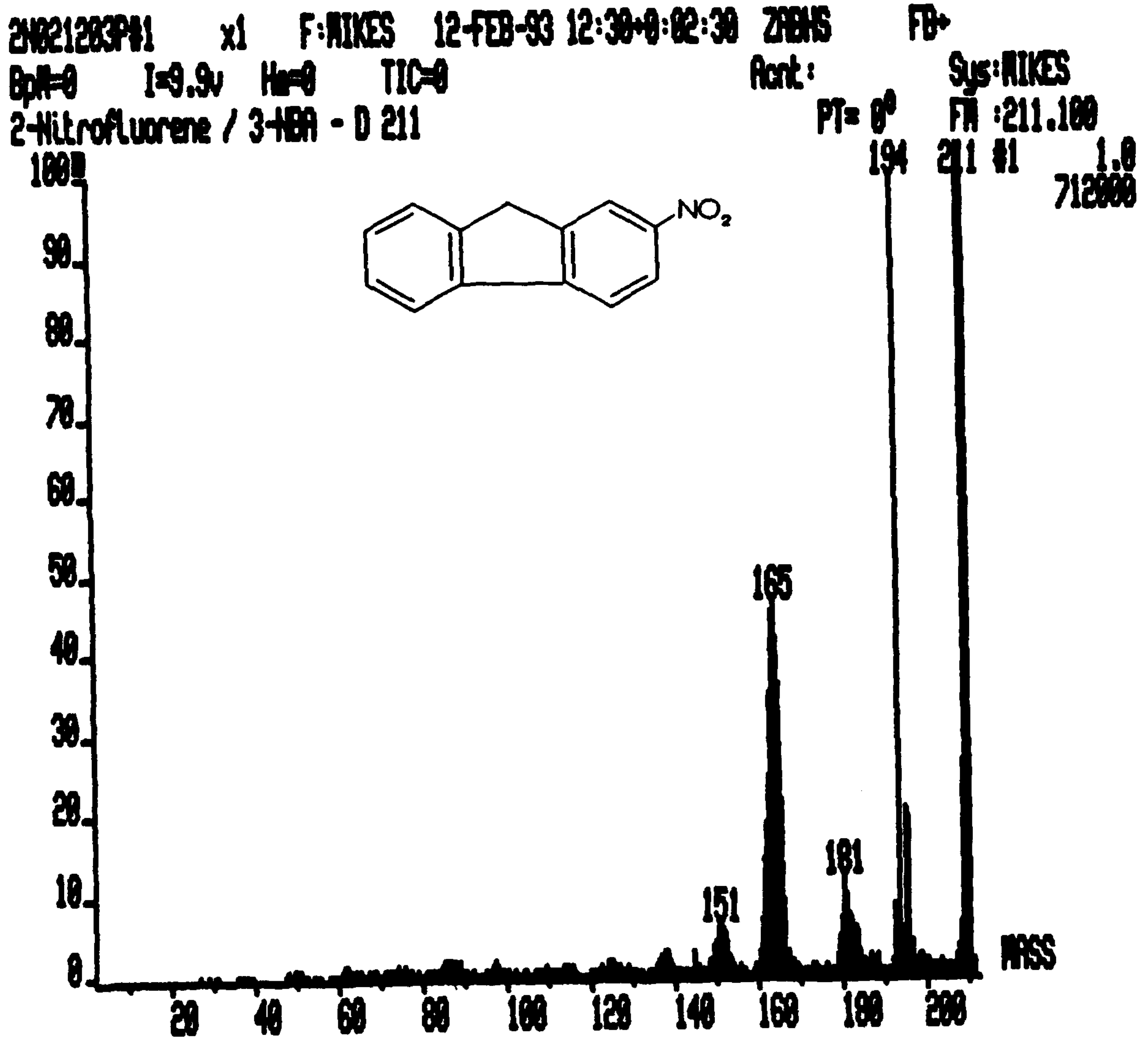
2N021283P#1 x1 F:MIKES 12-FEB-93 12:30+0:02:30 ZABMS FB+
BpM=0 I=9.9v Hm=0 TIC=0
Acnt:
Sys:MIKES
2-Nitrofluorene / 3-NBA - D 211
PT= 0°
FM :211.100
194 211 #1 1.0
712000
NO2
100
90
80
70
60
50
40
30
20
10
0
151
165
181
MASS
20
40
60
80
100
120
140
160
180
200

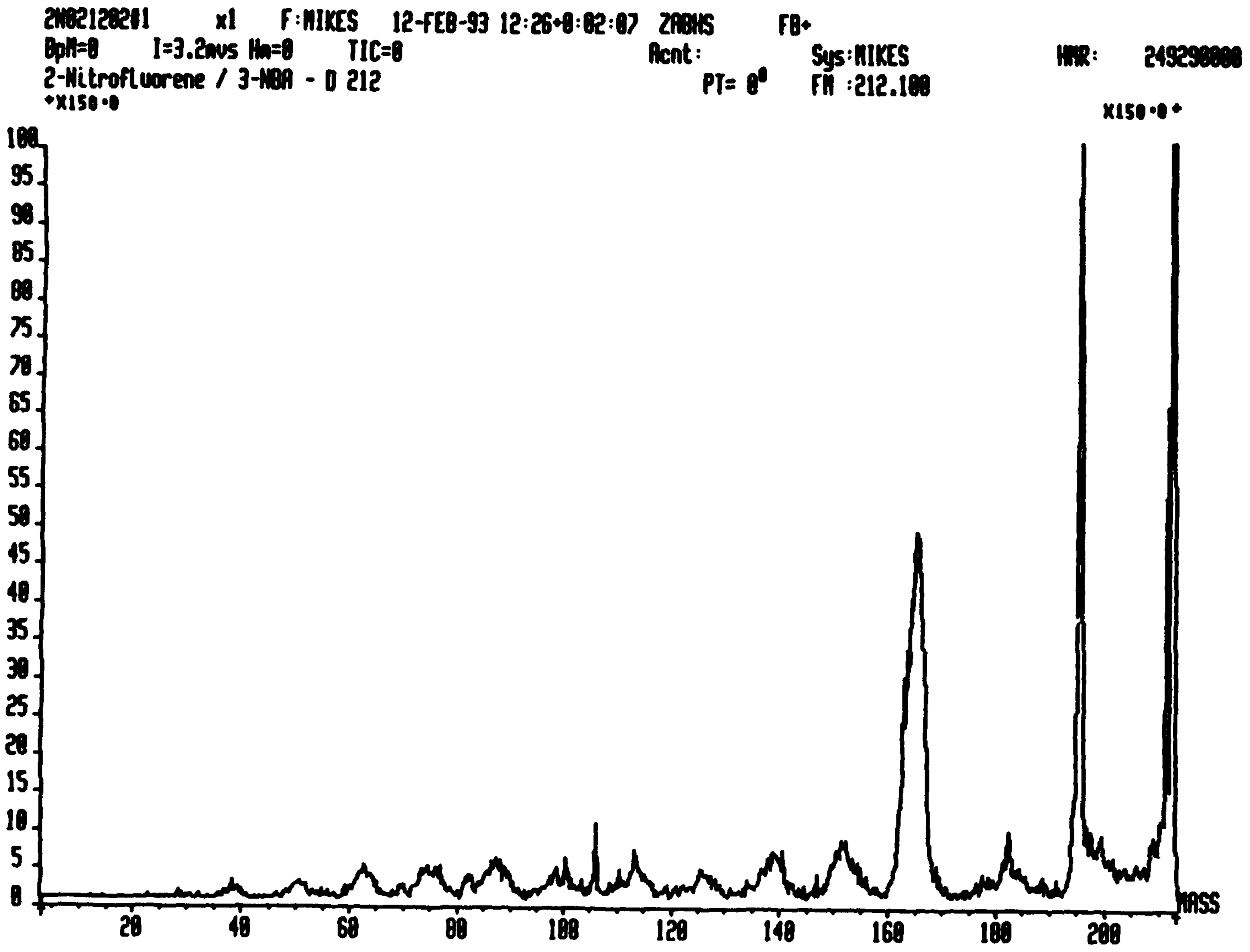
2N0212020I x1 F:MIKES 12-FEB-93 12:26+0:02:07 ZABHS FB+
BpM=0 I=3.2mvs Hm=0 TIC=0 Acnt: Sys:MIKES HMR: 249290000
2-Nitrofluorene / 3-NBA - D 212 PT= 0⁰ FM :212.100
*X150·0
X150·0*
100
95
90
85
80
75
70
65
60
55
50
45
40
35
30
25
20
15
10
5
0
20
40
60
80
100
120
140
160
180
200
MASS

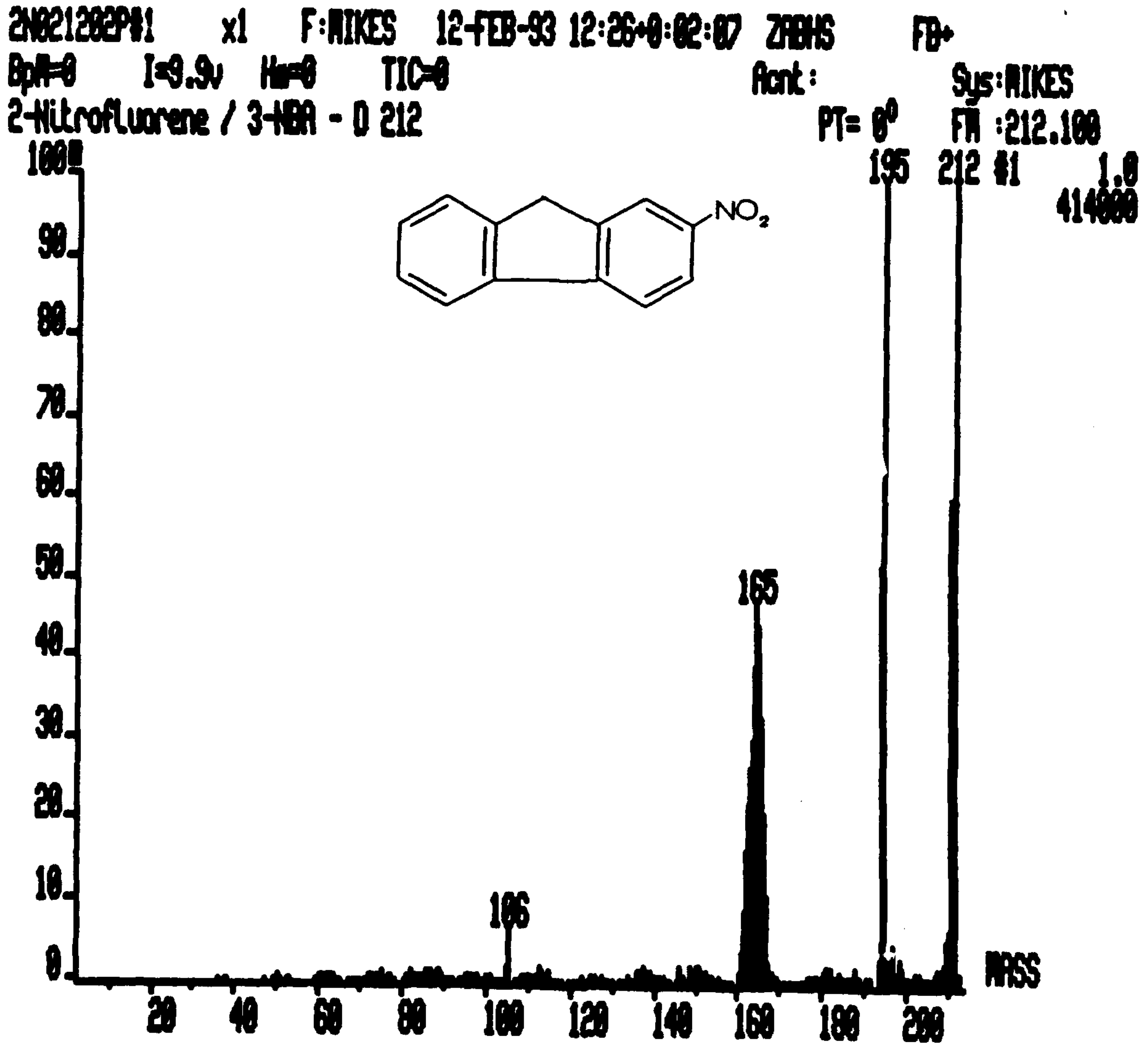
2N021202P#1 x1 F:MIKES 12-FEB-93 12:26+0:02:07 ZABHS FB+
BpM=0 I=9.9v Hm=0 TIC=0 Acnt: Sys:MIKES
2-Nitrofluorene / 3-NBA - D 212 PT= 0⁰ FM :212.100
NO2
195
212 #1
1.0
414000
165
106
100
90
80
70
60
50
40
30
20
10
0
20
40
60
80
100
120
140
160
180
200
MASS

```
2N021204#1      x1    Bgd=1     12-FEB-93 12:36+0:00:23  ZAB-MS     FB+
BpM=0    I=10v    Hm=0    TIC=2992914944             Acnt:           Sys:NITRO             HMR:    20910000
2-Nitrofluorene / 3-NBA                                      PT= 0°    Cal:0212CAX           MASS:        165
+X1.0
```

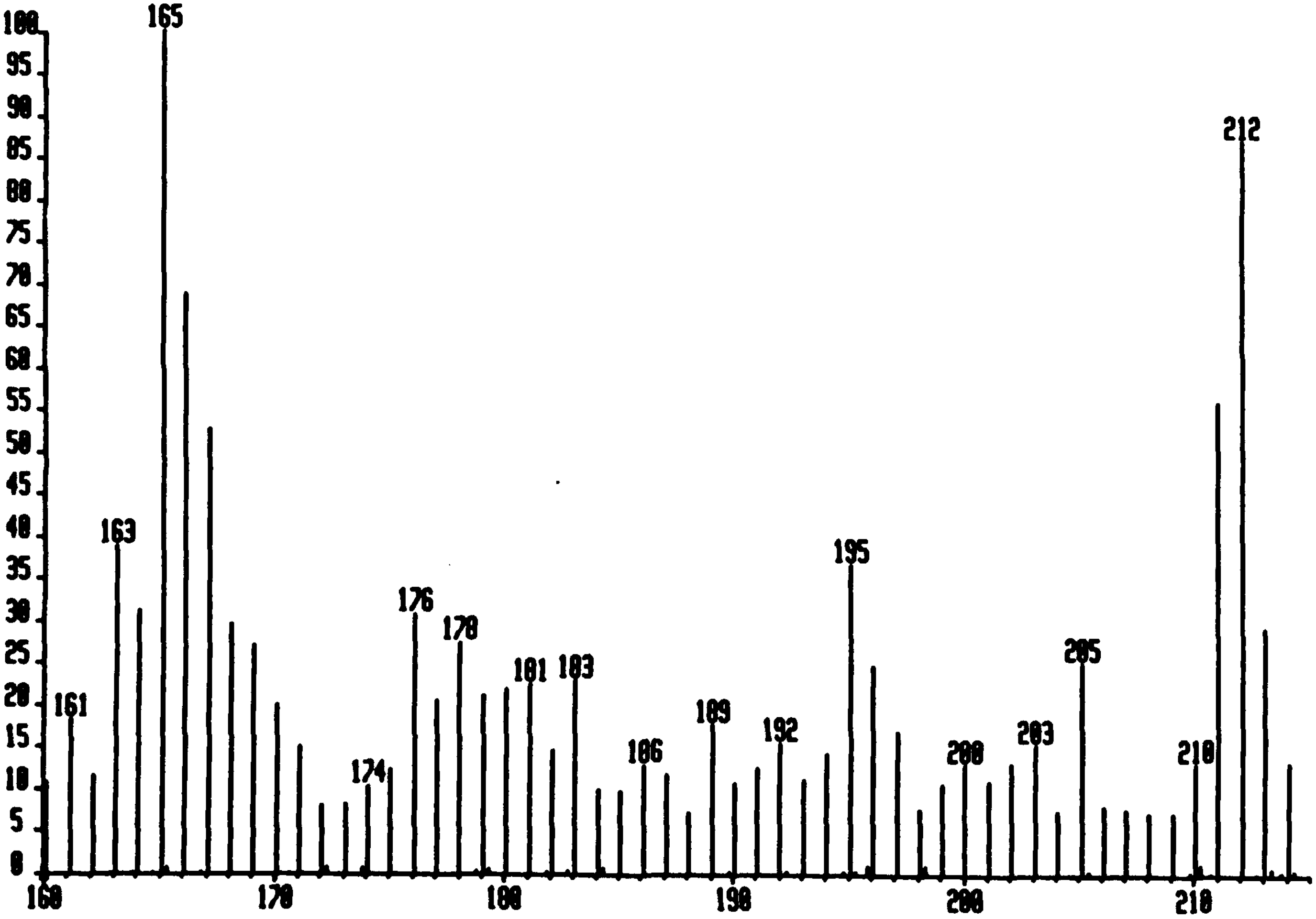

```
2F021201A01      x1     Bgd=0      12-FEB-93 11:32+0:00:00  ZAB-HS     FB+
BpM=0     I=590mv  Hm=500   TIC=65707000     AV         Acnt:          Sys:NITRO             HMR:        3071000
2-Nitro-9-fluorenone / bare probe                                 PT= 0°    Cal:0212CAX           MASS:            52
                 *X15*0                                                                                    X15*0*
```

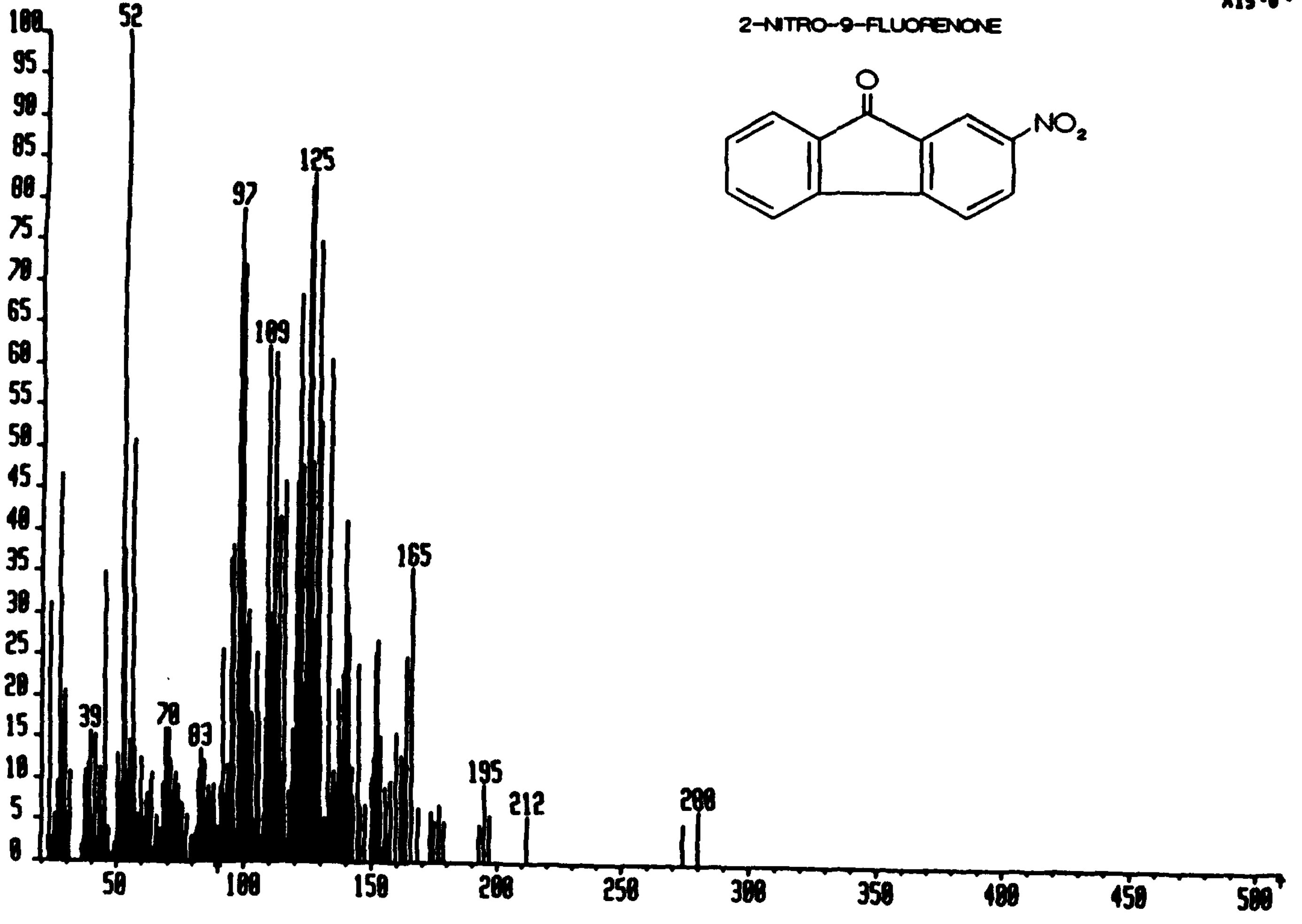

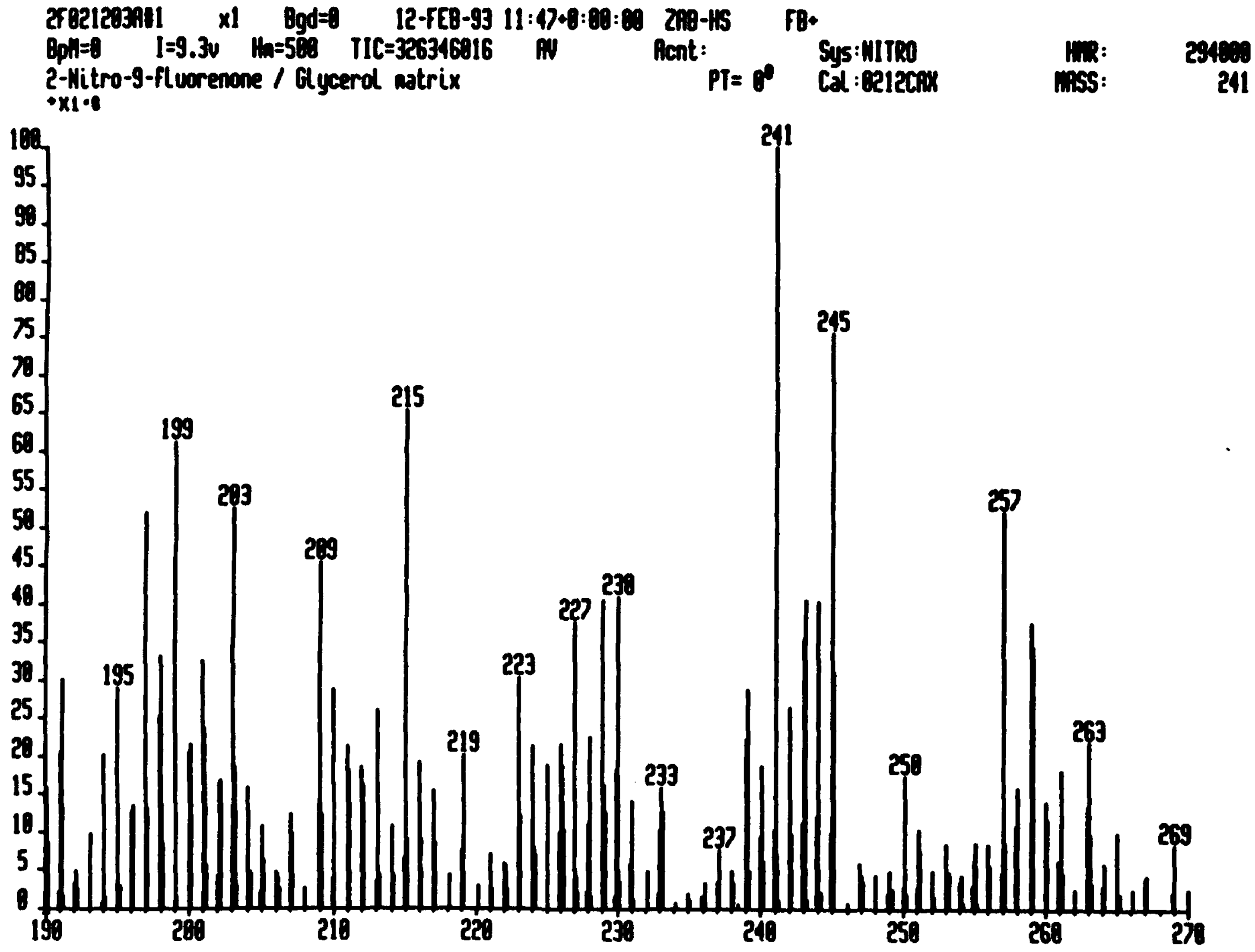
2F021203A01 x1 Bgd=0 12-FEB-93 11:47+0:00:00 ZAB-HS FB+
BpM=0 I=9.3v Hm=500 TIC=326346016 AV Acnt: Sys:NITRO HMR: 294000
2-Nitro-9-fluorenone / Glycerol matrix PT= 0⁰ Cal:0212CAX MASS: 241
*x1.0
100
95
90
85
80
75
70
65
60
55
50
45
40
35
30
25
20
15
10
5
0
190
200
210
220
230
240
250
260
270
195
199
203
209
215
219
223
227
230
233
237
241
245
250
257
263
269

```
2F02120209     x1    Bgd=5     12-FEB-93 11:35+0:02:23  ZAB-HS      FB+
BpM=0     I=5.4v   Hm=0     TIC=370047000             Acnt:        Sys:NITRO           HMR:      2326000
2-Nitro-9-fluorenone / 3-Nitrobenzyl alcohol matrix         PT= 0°   Cal:0212CAX         MASS:         219
*X1.0
```

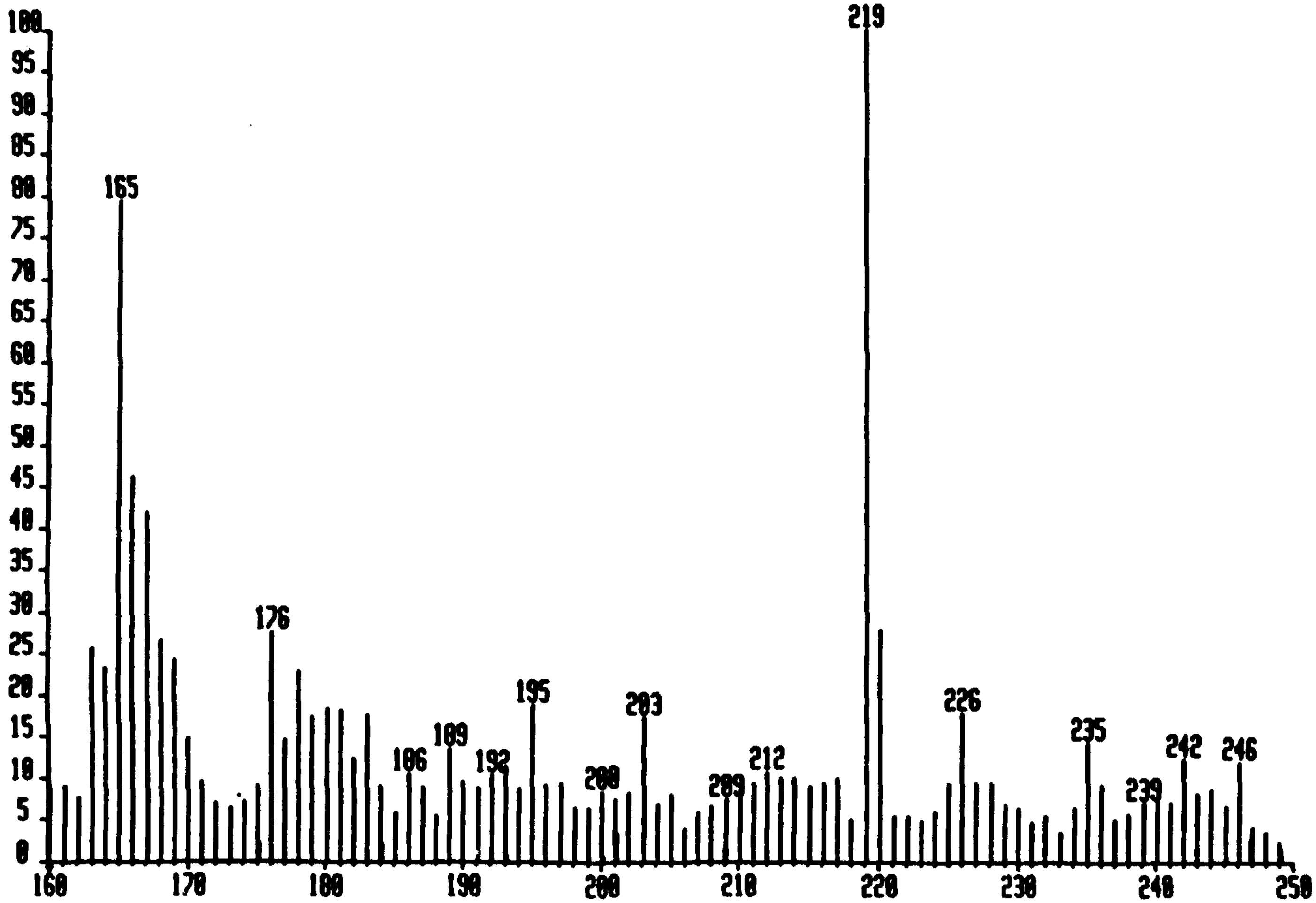

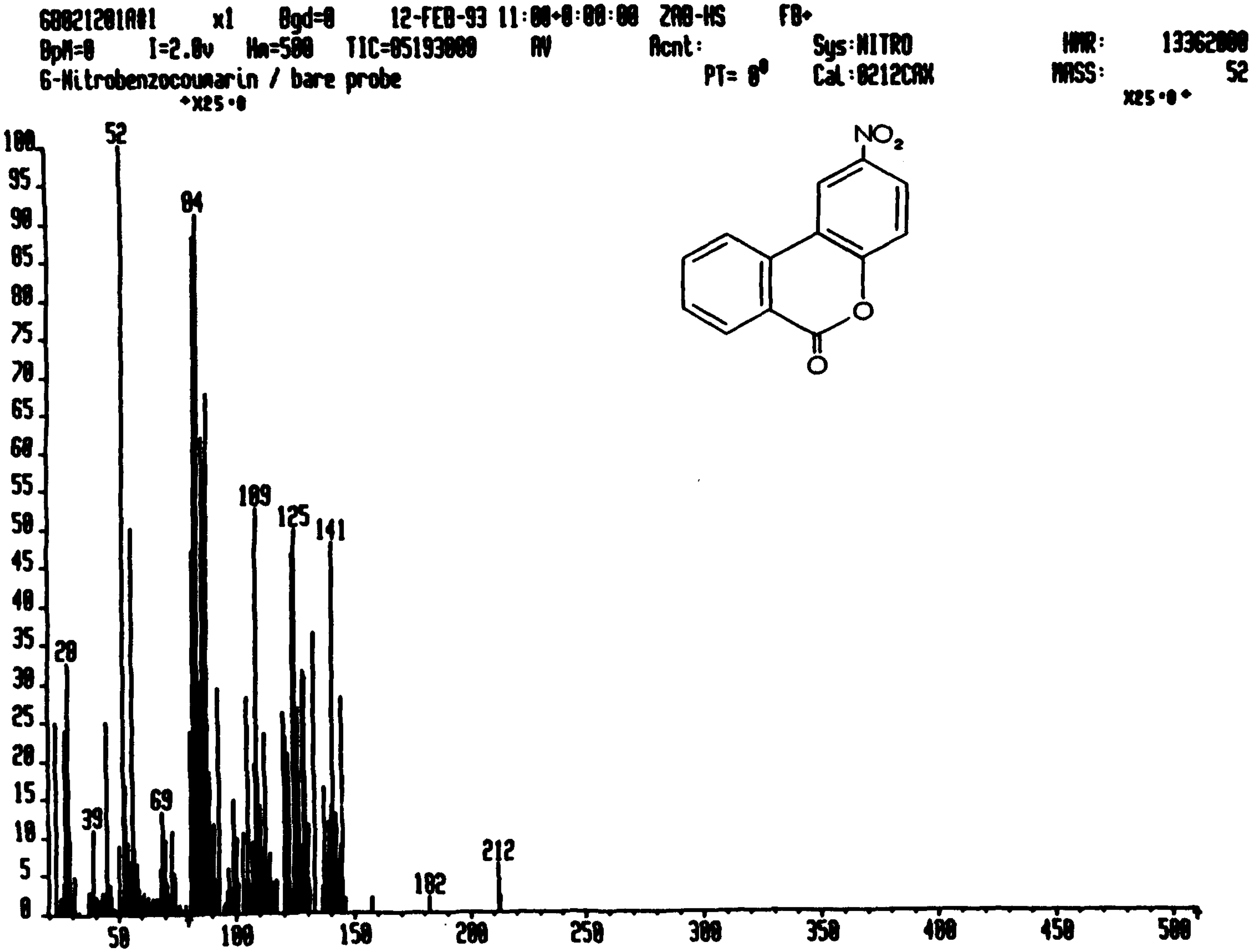
68021201A01 x1 Bgd=0 12-FEB-93 11:00+0:00:00 ZAB-HS FB+
BpM=0 I=2.0v Hm=500 TIC=05193000 AV Acnt: Sys:NITRO HMR: 13362000
6-Nitrobenzocoumarin / bare probe PT= 0° Cal:0212CAX MASS: 52
*X25*0
X25*0*
NO2
O
O
100
95
90
85
80
75
70
65
60
55
50
45
40
35
30
25
20
15
10
5
0
28
39
52
69
84
109
125
141
182
212
50
100
150
200
250
300
350
400
450
500

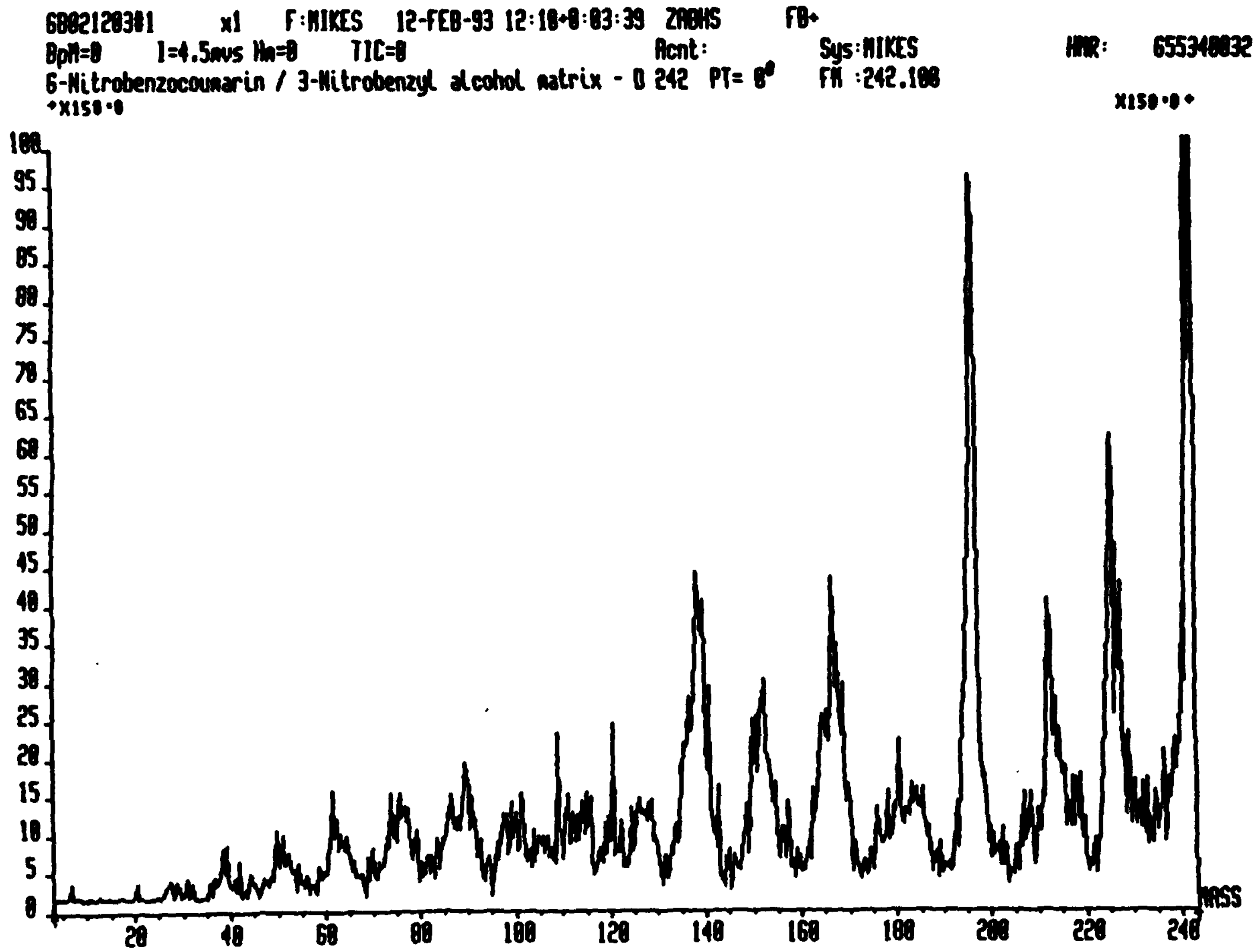
6802120301 x1 F:MIKES 12-FEB-93 12:10+0:03:39 ZABHS FB+
BpM=0 I=4.5mvs Hm=0 TIC=0 Acnt: Sys:MIKES HMR: 655340032
6-Nitrobenzocoumarin / 3-Nitrobenzyl alcohol matrix - D 242 PT= 0°  FM :242.100
+X150·0
X150·0+
100
95
90
85
80
75
70
65
60
55
50
45
40
35
30
25
20
15
10
5
0
20
40
60
80
100
120
140
160
180
200
220
240
MASS

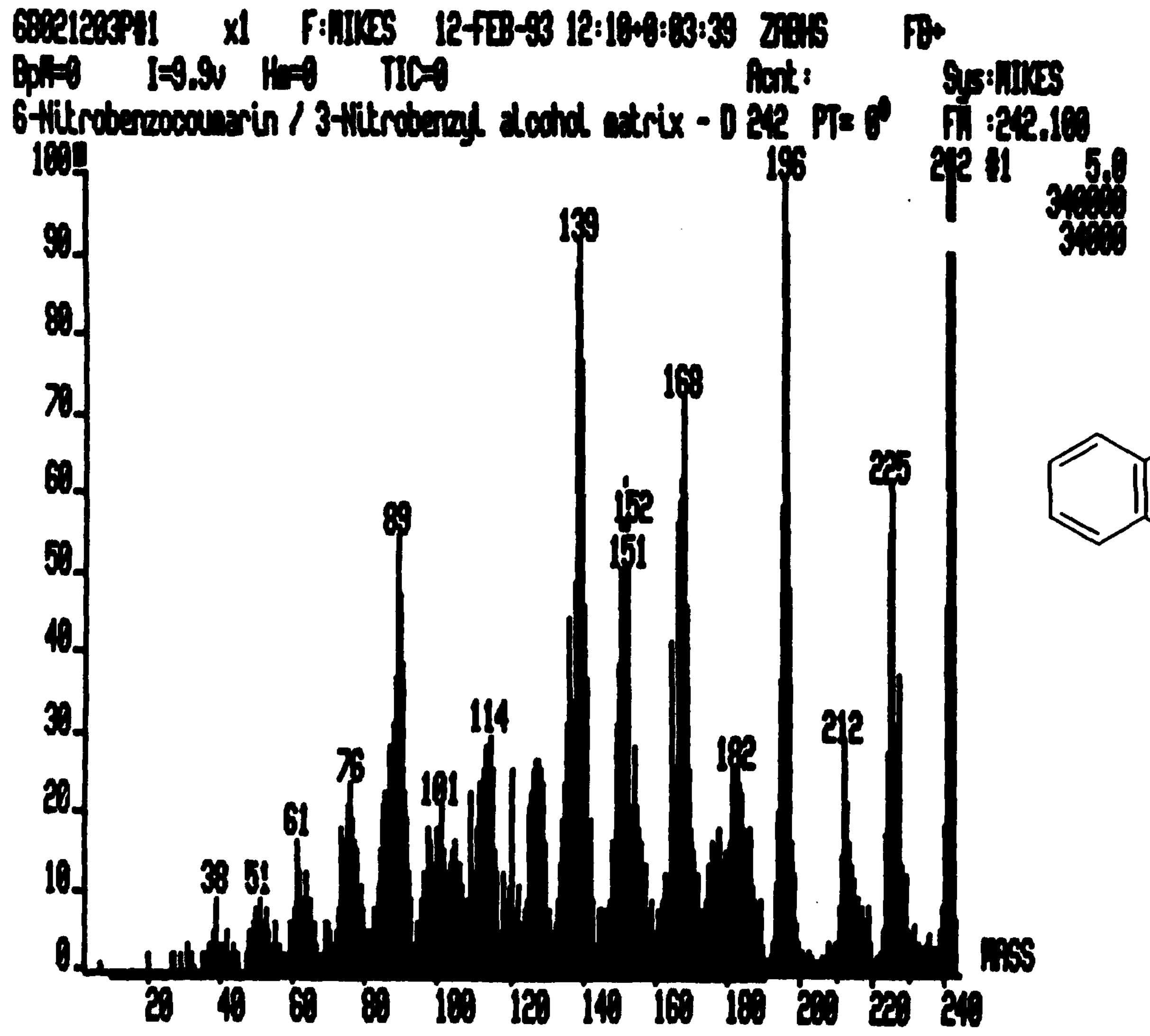
6B021203P01 x1 F:MIKES 12-FEB-93 12:10+0:03:39 ZABHS FB+
BpM=0 I=9.9v Hm=0 TIC=0 Acnt: Sys:MIKES
6-Nitrobenzocoumarin / 3-Nitrobenzyl alcohol matrix - D 242 PT= 0° FM :242.100
242 #1
5.0
340000
34000
100
90
80
70
60
50
40
30
20
10
0
196
139
168
225
152
151
89
114
212
182
76
101
61
38
51
20
40
60
80
100
120
140
160
180
200
220
240
MASS

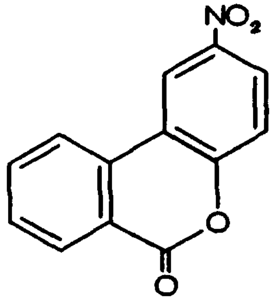
NO₂
O
O

```
6002120206      x1    Bgd=1     12-FEB-93 11:56+0:01:45  ZAB-HS     FB+
BpM=0     I=10v    Hm=0     TIC=1242393904             Acnt:          Sys:NITRO           HMR:      0295000
6-Nitrobenzocoumarin / 3-Nitrobenzyl alcohol matrix          PT= 0°    Cal:0212CAX         MASS:         219
*X1.0
```

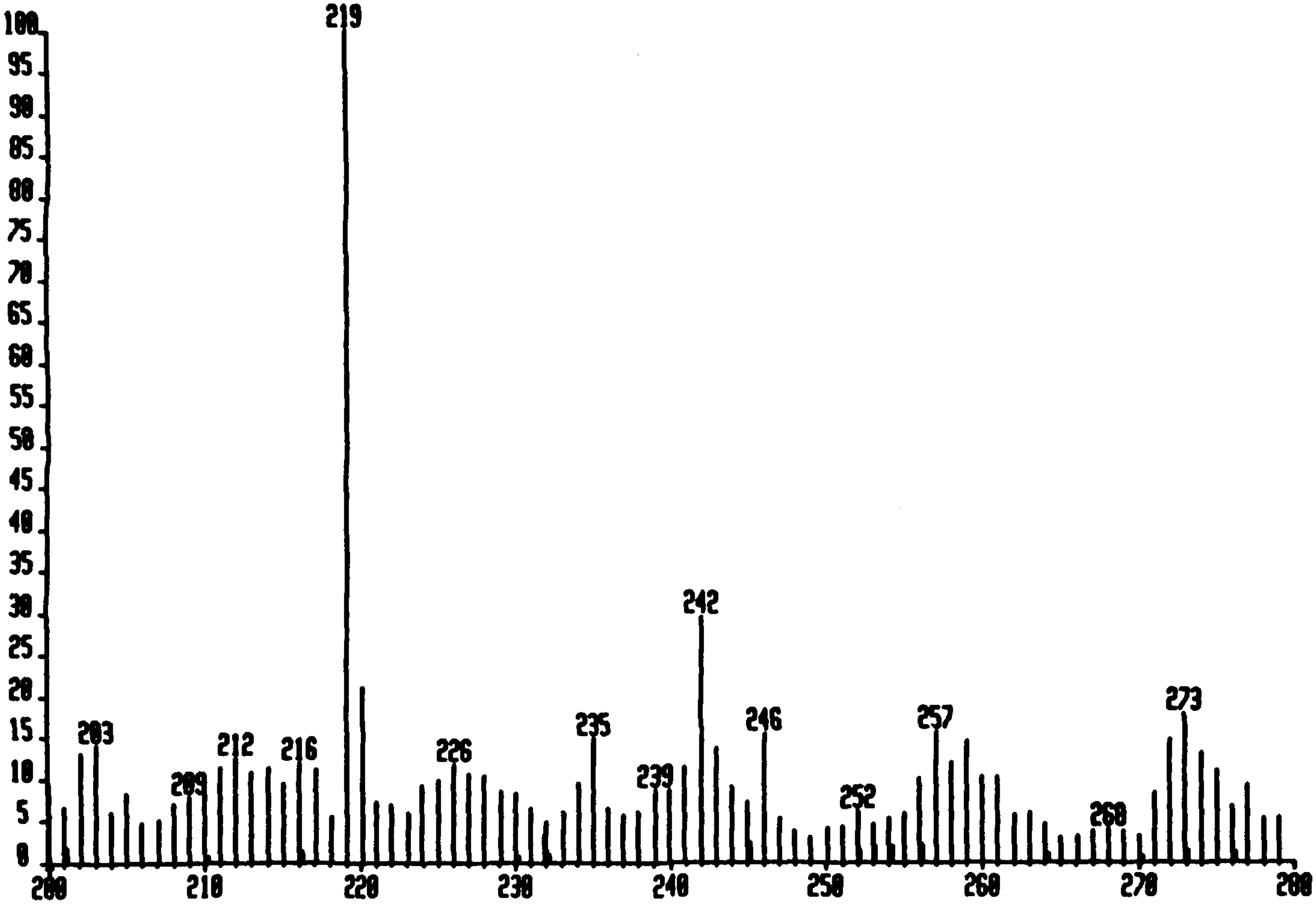

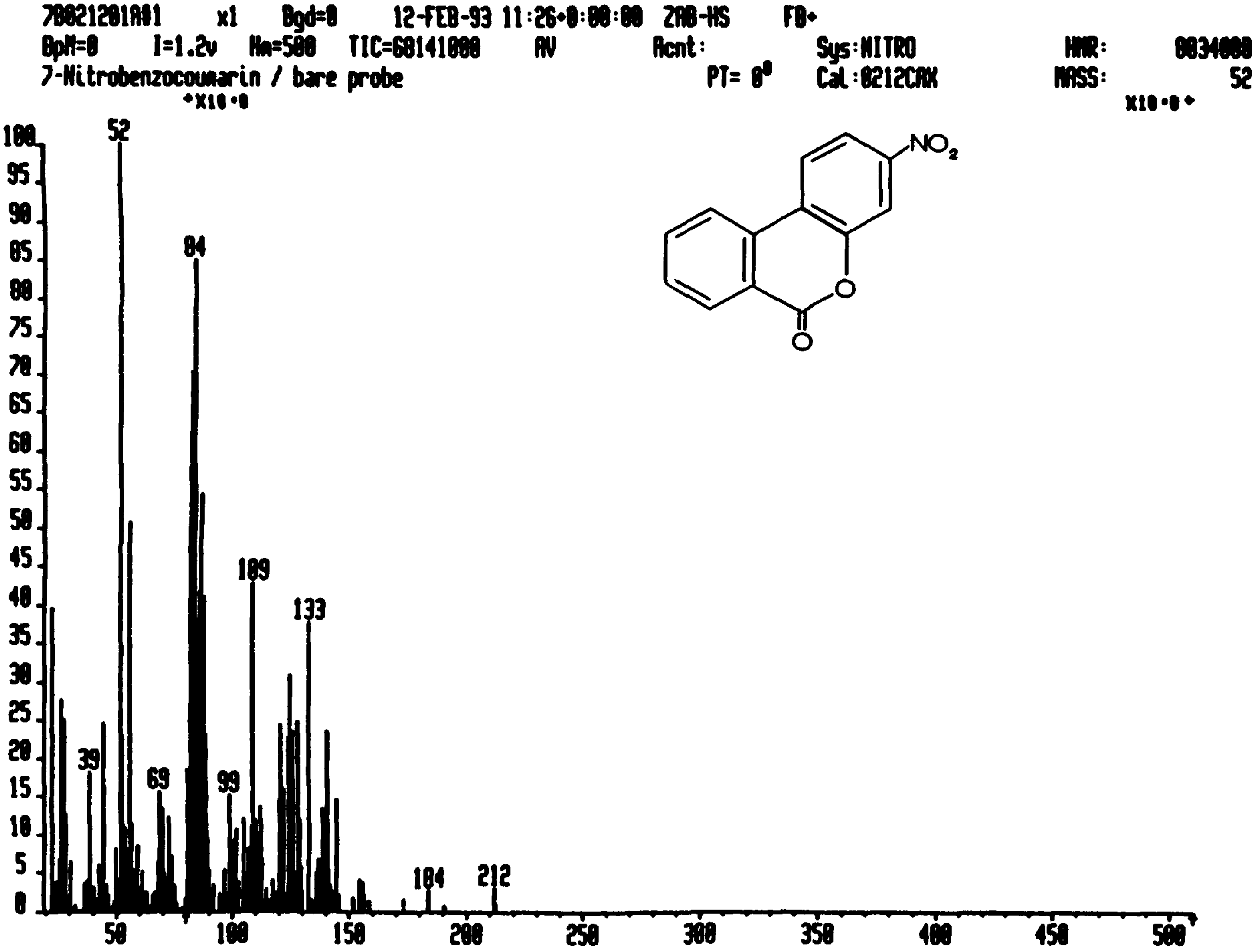

```
70021201A01     x1    Bgd=0     12-FEB-93 11:26+0:00:00  ZAB-HS     FB+
BpM=0     I=1.2v   Hm=500   TIC=60141000    AV        Rcnt:          Sys:NITRO          HMR:       0034000
7-Nitrobenzocoumarin / bare probe                        PT= 0⁰    Cal:0212CAX          MASS:           52
```

# APPENDIX E

## EI MS/MS Spectra of Selected Nitro-Standards

**Spectra Titles** **Page**

1. 7-nitro-3,4-benzocoumarin, daughters of 241 . . . . . . . . . . . . . . . . . . . . . . . . . . 246
2. 7-nitro-3,4-benzocoumarin, neutral loss of 30, (NO) . . . . . . . . . . . . . . . . . . . . 247
3. 7-nitro-3,4-benzocoumarin, daughters of 200 . . . . . . . . . . . . . . . . . . . . . . . . . . 248
4. 7-nitro-3,4-benzocoumarin, daughters of 183 . . . . . . . . . . . . . . . . . . . . . . . . . . 249
5. 7-nitro-3,4-benzocoumarin, parents of 139 . . . . . . . . . . . . . . . . . . . . . . . . . . . 250
6. 7-nitro-3,4-benzocoumarin, daughters of 139 . . . . . . . . . . . . . . . . . . . . . . . . . . 251
7. 2-nitrofluorene, electron ionization spectrum . . . . . . . . . . . . . . . . . . . . . . . . . . 252
8. 2-nitrofluorene, neutral loss of 28, (CO) . . . . . . . . . . . . . . . . . . . . . . . . . . . . 253
9. 2-nitrofluorene, neutral loss of 42, (CNO) . . . . . . . . . . . . . . . . . . . . . . . . . . . 254
10. 2-nitrofluorene, neutral loss of 58, (-NO -CO) . . . . . . . . . . . . . . . . . . . . . . . 255
11. 2-nitrofluorene, daughters of 211 . . . . . . . . . . . . . . . . . . . . . . . . . . . . . . . . 256
12. 2-nitrofluorene, daughters of 194 . . . . . . . . . . . . . . . . . . . . . . . . . . . . . . . . 257
13. 2-nitrofluorene, daughters of 181 . . . . . . . . . . . . . . . . . . . . . . . . . . . . . . . . 258
14. 2-nitrofluorene, daughters of 165 . . . . . . . . . . . . . . . . . . . . . . . . . . . . . . . . 259
15. 2-nitrofluorene, daughters of 153 . . . . . . . . . . . . . . . . . . . . . . . . . . . . . . . . 260
16. 2-nitrofluorene, daughters of 139 . . . . . . . . . . . . . . . . . . . . . . . . . . . . . . . . 261
17. 1-nitropyrene, daughters of 247 . . . . . . . . . . . . . . . . . . . . . . . . . . . . . . . . . 262
18. 1-nitropyrene, daughters of 231 . . . . . . . . . . . . . . . . . . . . . . . . . . . . . . . . . 263

19. 1-nitropyrene, daughters of 217 . . . . . . . . . . . . . . . . . . . . . . . . . . . . . 264

20. 1-nitropyrene, daughters of 201 . . . . . . . . . . . . . . . . . . . . . . . . . . . . . 265

21. 1-nitropyrene, daughters of 189 . . . . . . . . . . . . . . . . . . . . . . . . . . . . . 266

22. 1-nitropyrene, daughters of 174 . . . . . . . . . . . . . . . . . . . . . . . . . . . . . 267

23. 1-nitropyrene, daughters of 163 . . . . . . . . . . . . . . . . . . . . . . . . . . . . . 268

24. 1-nitropyrene, daughters of 150 . . . . . . . . . . . . . . . . . . . . . . . . . . . . . 269

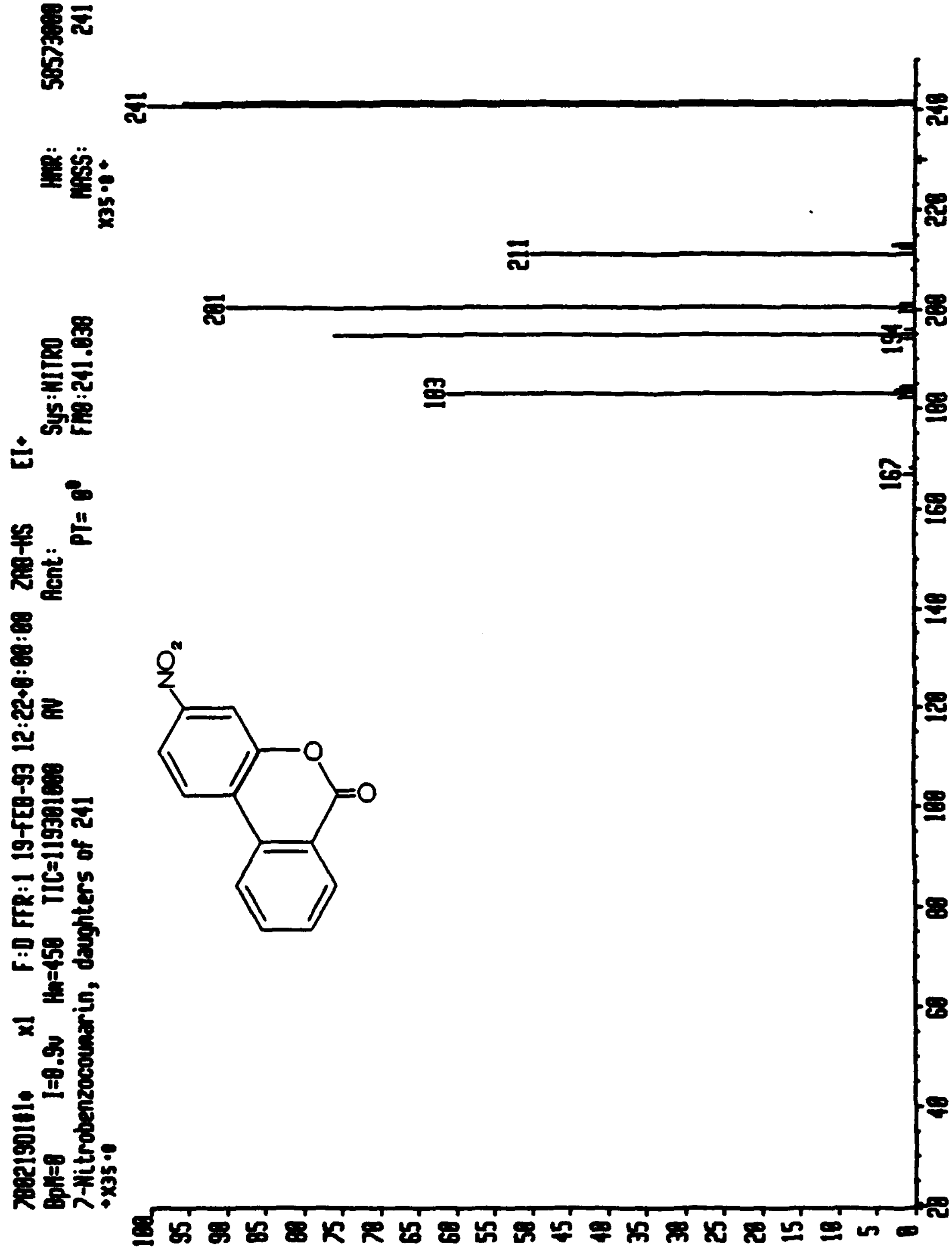
7002190181+ x1 F:D FFR:1 19-FEB-93 12:22+0:00:00 ZAB-HS EI+
BpM=0 I=0.9v Hm=450 TIC=119301000 AV
Acnt: Sys:NITRO HMR: 50573000
7-Nitrobenzocoumarin, daughters of 241
PT= 0° FMA:241.030 MASS: 241
+X35·0
X35·0+
NO2
O
O
241
211
201
194
183
167
100
95
90
85
80
75
70
65
60
55
50
45
40
35
30
25
20
15
10
5
0
20
40
60
80
100
120
140
160
180
200
220
240

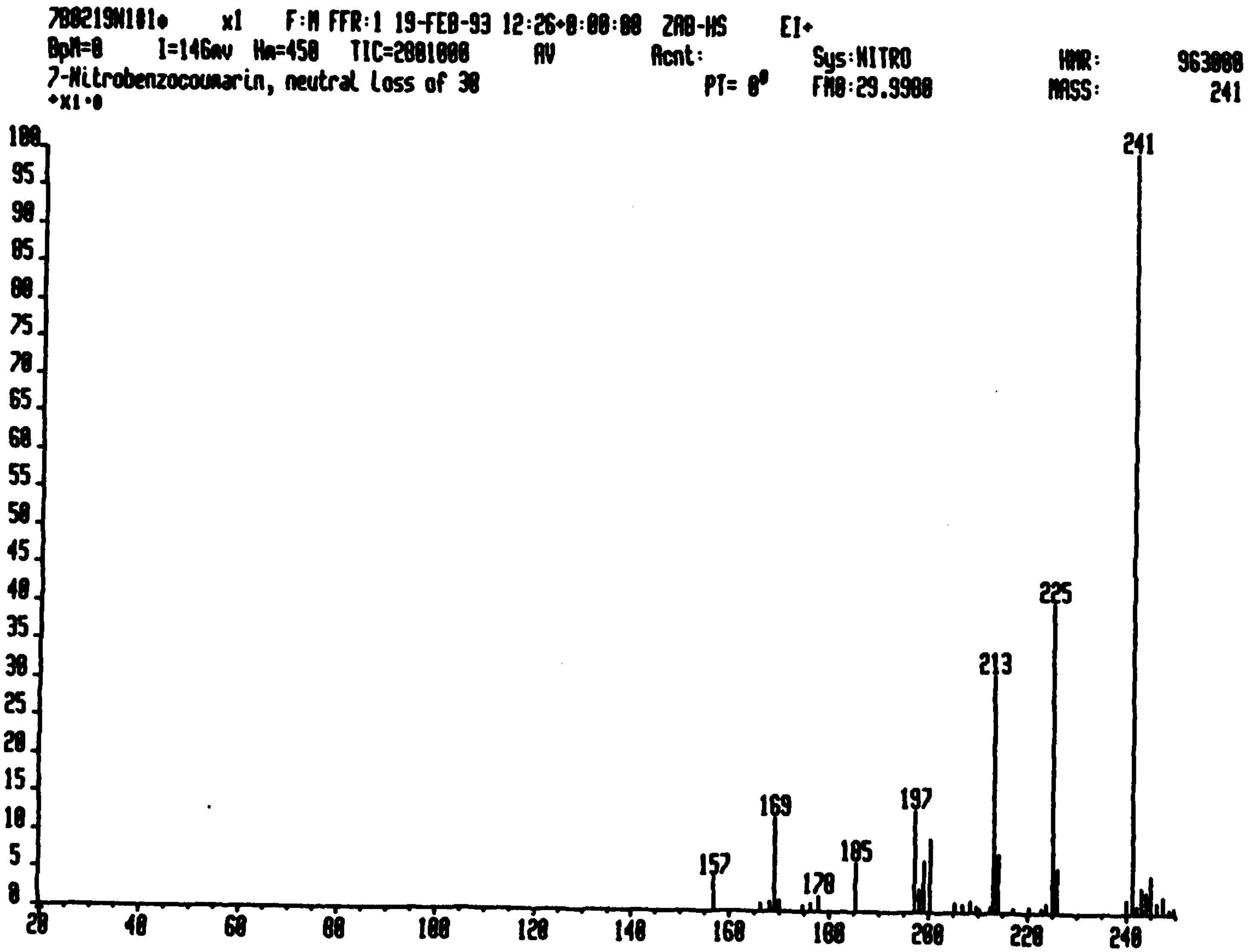
700219N101+ x1 F:M FFR:1 19-FEB-93 12:26+0:00:00 ZAB-HS EI+
BpM=0 I=146mv Hm=450 TIC=2001000 AV Acnt: Sys:NITRO HMR: 963000
7-Nitrobenzocoumarin, neutral Loss of 30 PT= 0° FM0:29.9900 MASS: 241
+x1.0
100
95
90
85
80
75
70
65
60
55
50
45
40
35
30
25
20
15
10
5
0
20
40
60
80
100
120
140
160
180
200
220
240
241
225
213
197
185
178
169
157

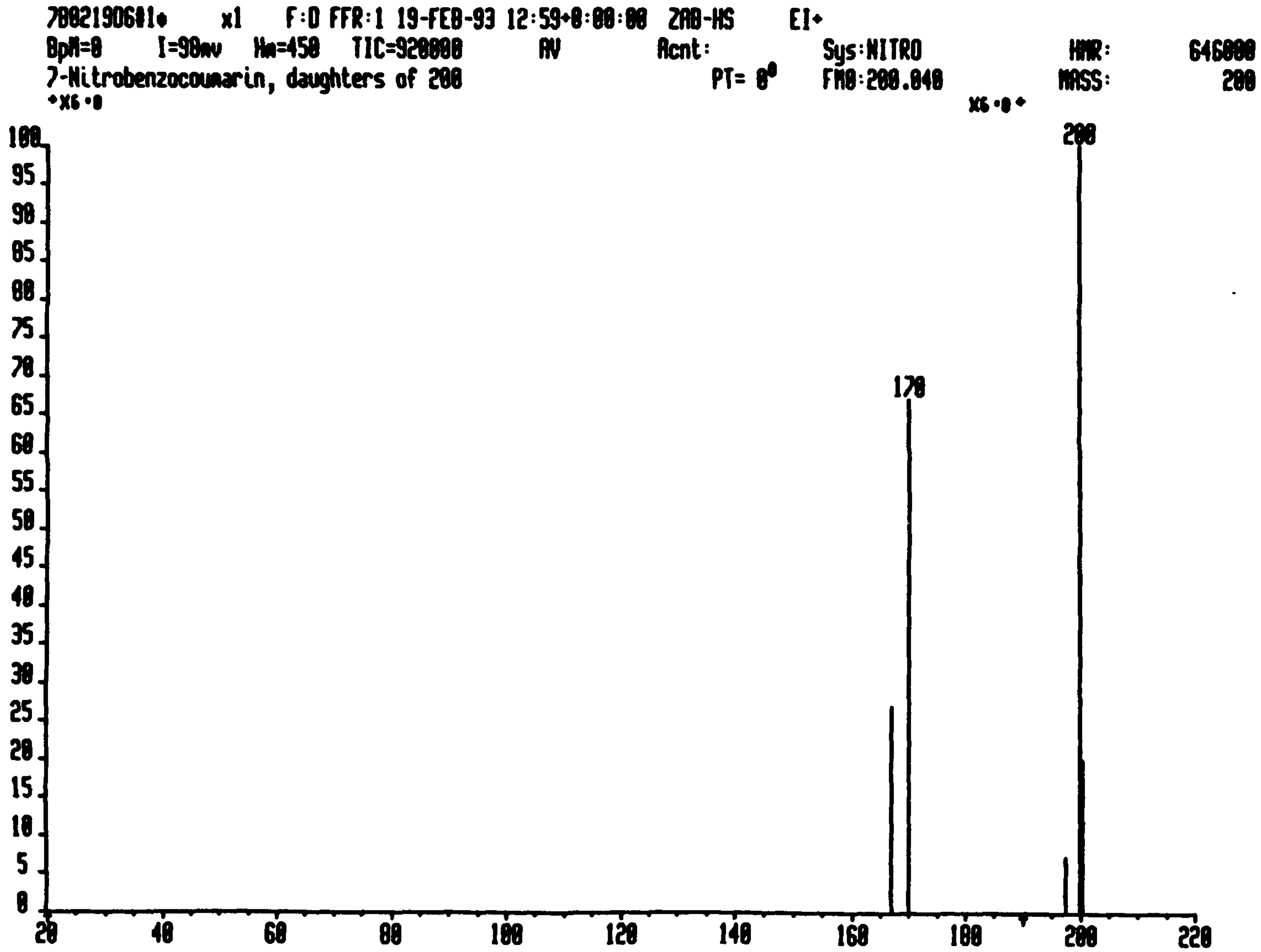
7002190601● x1 F:D FFR:1 19-FEB-93 12:59+0:00:00 ZAB-HS EI+
BpM=0 I=90mv Hm=450 TIC=920000 AV Acnt: Sys:NITRO HMR: 646000
7-Nitrobenzocoumarin, daughters of 200 PT= 0⁰ FM0:200.040 MASS: 200
*X6·0
X6·0*
200
170
100
95
90
85
80
75
70
65
60
55
50
45
40
35
30
25
20
15
10
5
0
20
40
60
80
100
120
140
160
180
200
220

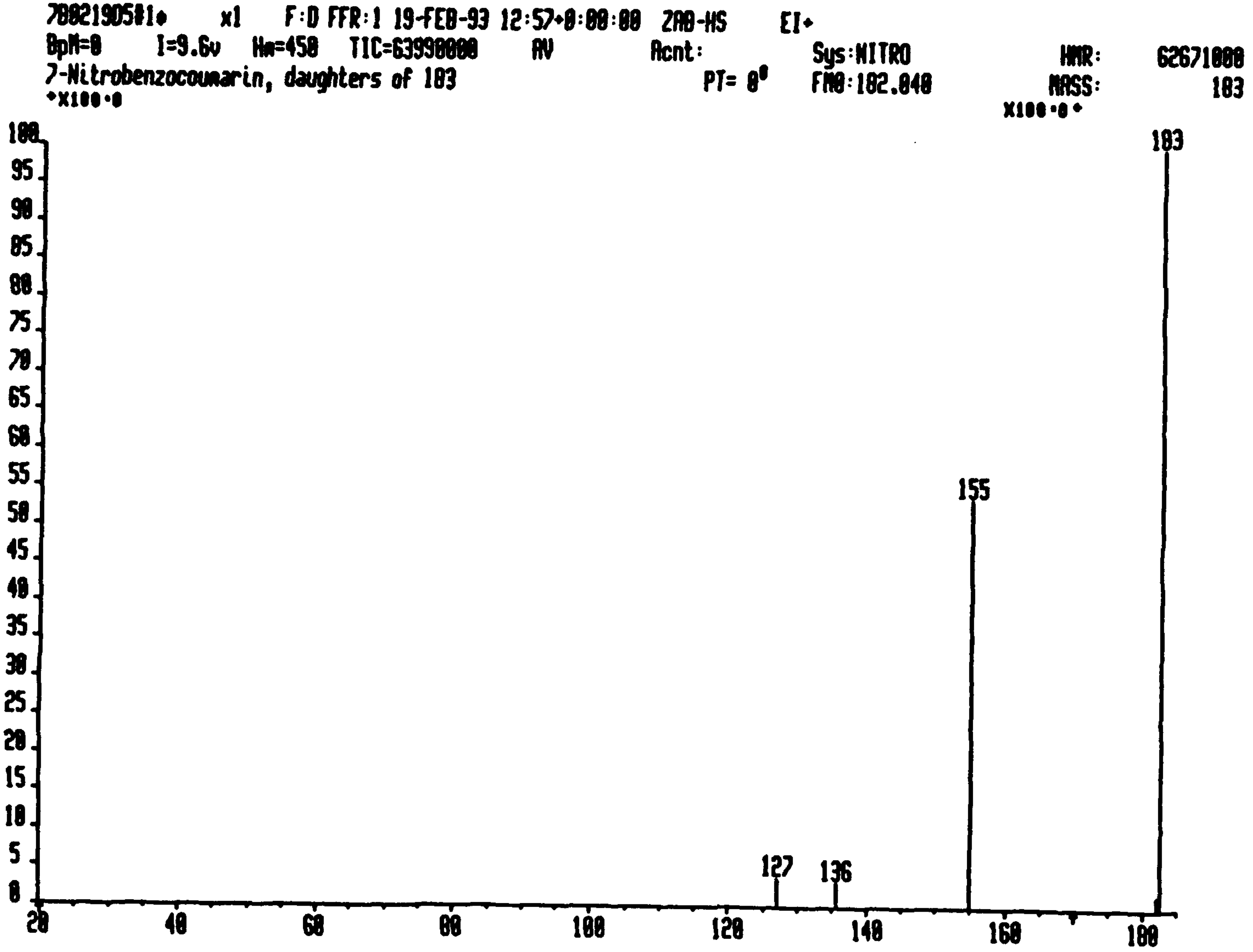

```
70021905#1◆     x1    F:D FFR:1 19-FEB-93 12:57+0:00:00  ZAB-HS      EI+
BpM=0     I=9.6v   Hm=450   TIC=63990000      AV          Acnt:          Sys:NITRO           HMR:       62671000
7-Nitrobenzocoumarin, daughters of 183                       PT= 0°    FM0:182.040         MASS:           183
*X100*0                                                                               X100*0*
```

7B0219P101+ x1 F:P FFR:1 19-FEB-93 12:20+0:00:00 ZAB-HS EI+
BpM=0 I=5.7v Ha=450 TIC=66557000 AV Acnt: Sys:NITRO HMR: 37503000
7-Benzocoumarin / parents of 139 PT= 0° FM0:139.030 MASS: 139

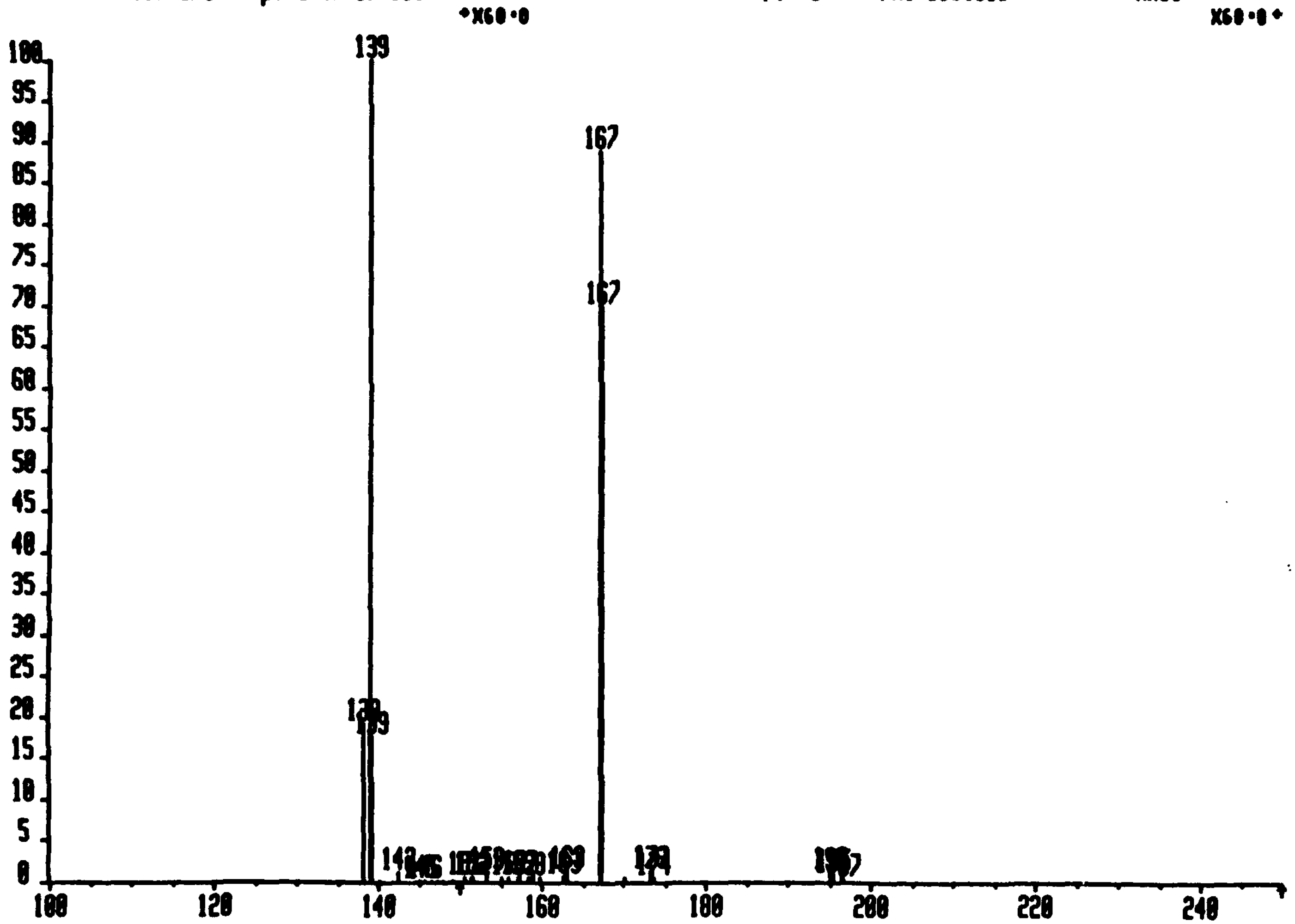

```
7802190301*     x1    F:D FFR:1 19-FEB-93 12:52+0:00:00  ZAB-HS     EI+
BpM=0     I=10v    Ha=450   TIC=92105000     AV        Acnt:          Sys:NITRO            HMR:     65534000
7-Nitrobenzocoumarin, daughters of 139                    PT= 0°    FM0:139.030          MASS:         139
```

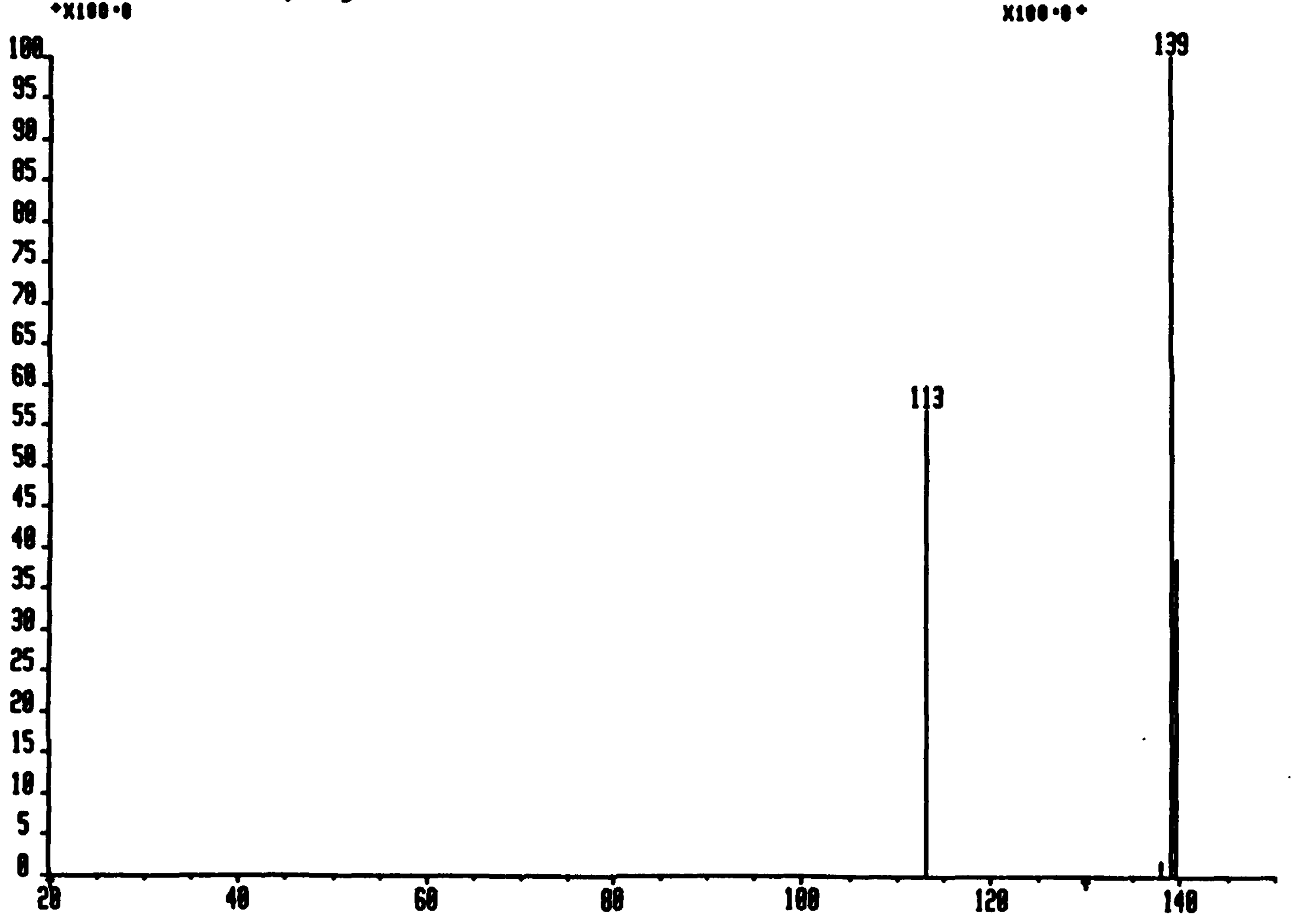

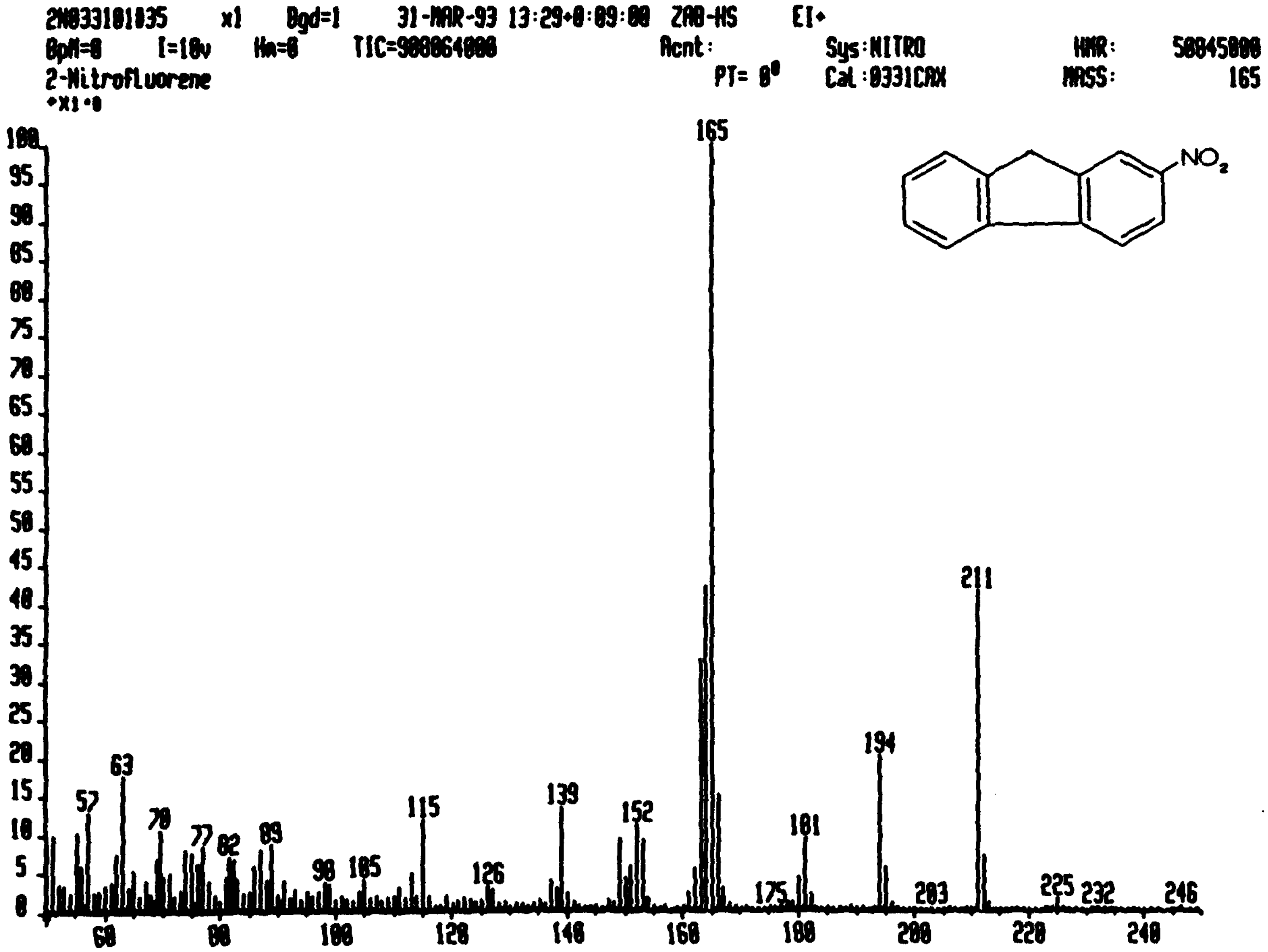
2N033101035 x1 Bgd=1 31-MAR-93 13:29+0:09:00 ZAB-HS EI+
BpM=0 I=10v Hm=0 TIC=900064000 Acnt: Sys:NITRO HMR: 50045000
2-Nitrofluorene PT= 0° Cal:0331CAX MASS: 165
+X1·0
$NO_2$
100
95
90
85
80
75
70
65
60
55
50
45
40
35
30
25
20
15
10
5
0
57
63
70
77
82
89
98
105
115
126
139
152
165
175
181
194
203
211
225
232
246
60
80
100
120
140
160
180
200
220
240

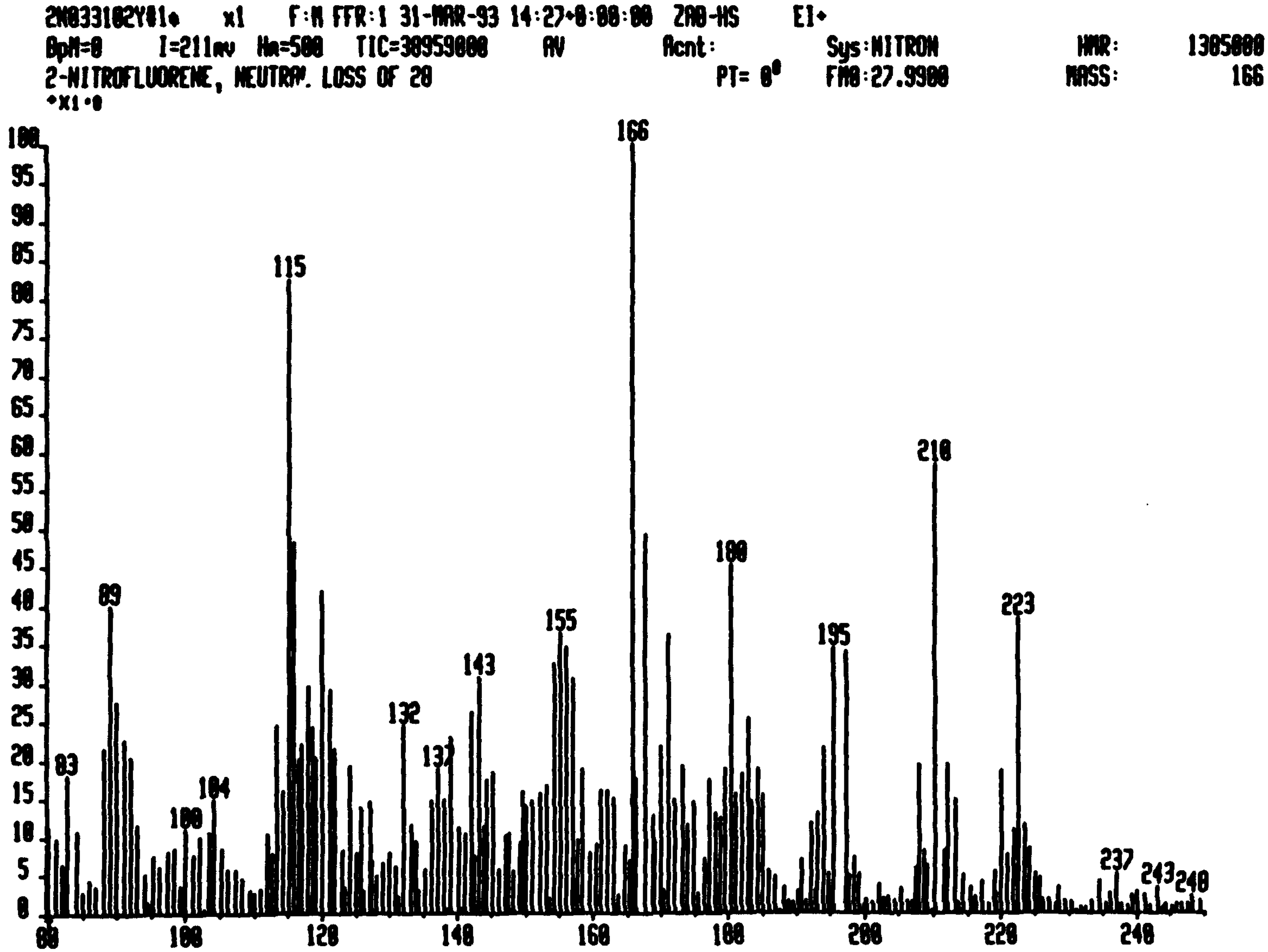

2N033102Y01+ x1 F:M FFR:1 31-MAR-93 14:27+0:00:00 ZAB-HS EI+
BpM=0 I=211mv Hm=500 TIC=30959000 AV Acnt: Sys:NITRON HMR: 1305000
2-NITROFLUORENE, NEUTRAL. LOSS OF 28 PT= 0° FM0:27.9900 MASS: 166
*X1.0

```
2N033102201+    x1    F:M FFR:1 31-MAR-93 14:25+0:00:00  ZAB-HS     EI+
BpM=0     I=241mv  Hm=500   TIC=39012000     AV        Acnt:           Sys:NITRON            HMR:      1400000
2-NITROFLUORENE, NEUTRAL LOSS OF 42                          PT= 0°   FM0:42.0300           MASS:         164
*X1*0
```

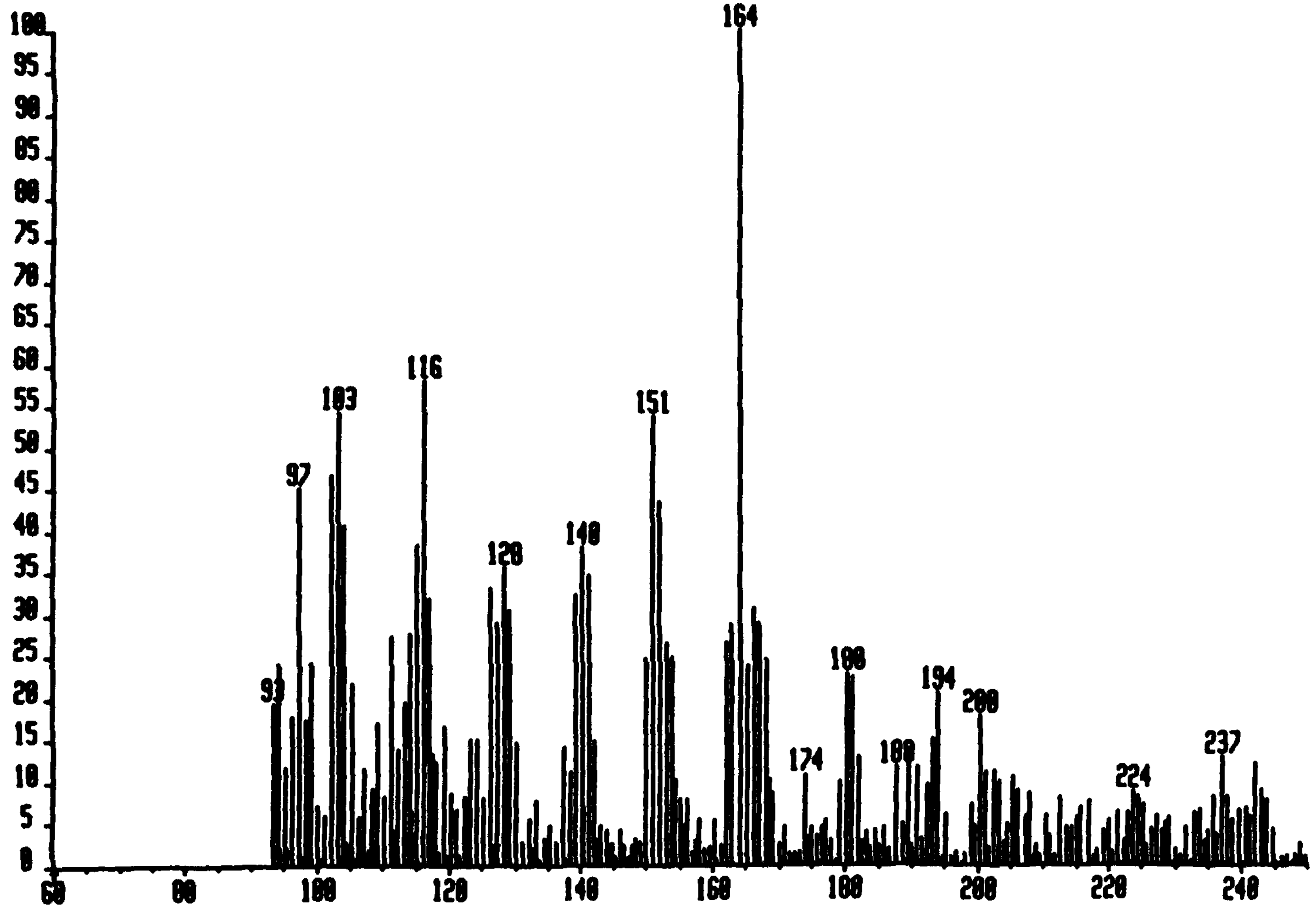

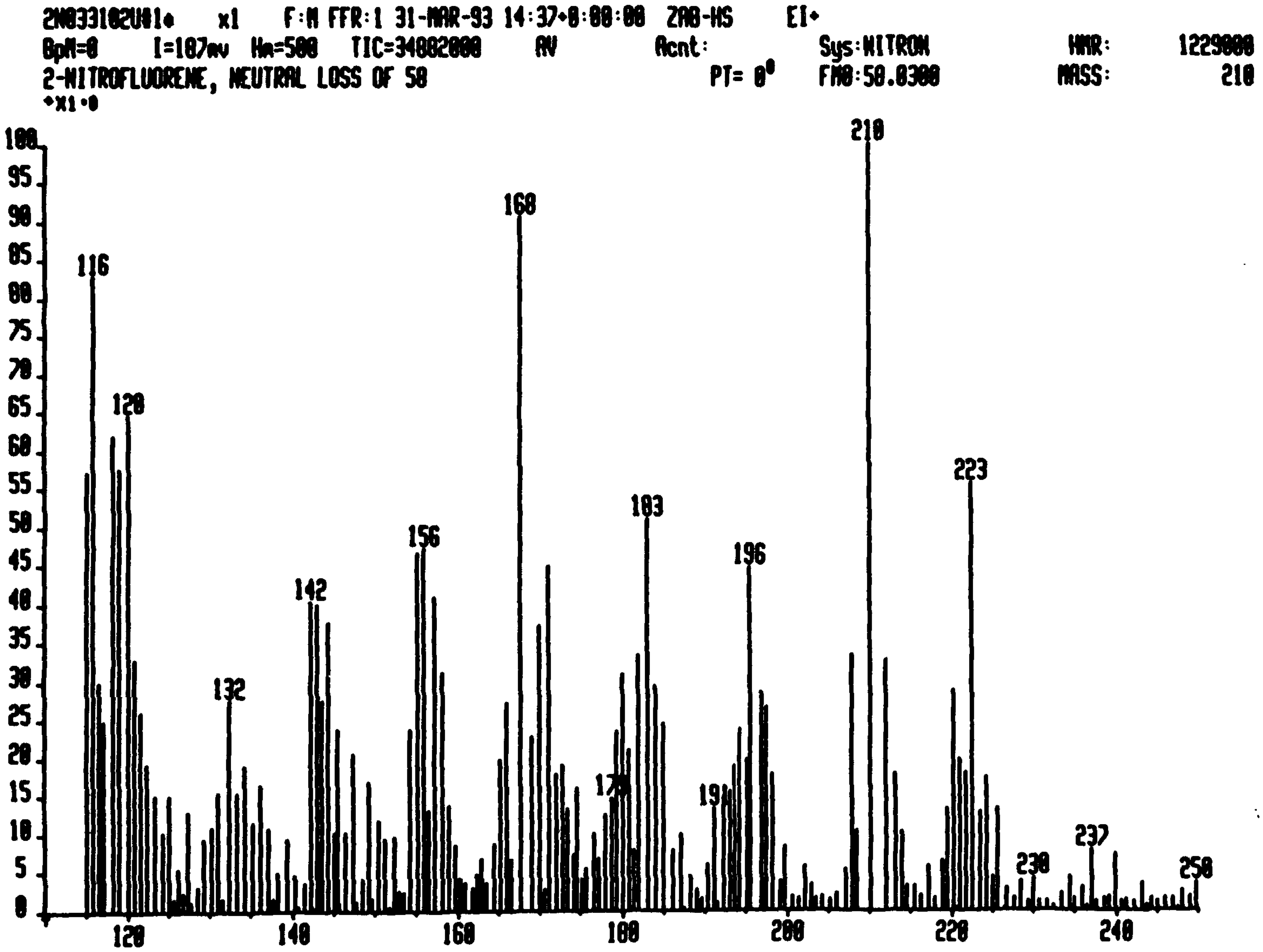
2N033102U01+ x1 F:M FFR:1 31-MAR-93 14:37+0:00:00 ZAB-HS EI+
BpM=0 I=107mv Hm=500 TIC=34002000 AV Acnt: Sys:NITRON HAR: 1229000
2-NITROFLUORENE, NEUTRAL LOSS OF 58 PT= 0⁰ FM0:50.0300 MASS: 210
+X1.0
100
95
90
85
80
75
70
65
60
55
50
45
40
35
30
25
20
15
10
5
0
116
120
132
142
156
168
178
183
19
196
210
223
230
237
250
120
140
160
180
200
220
240

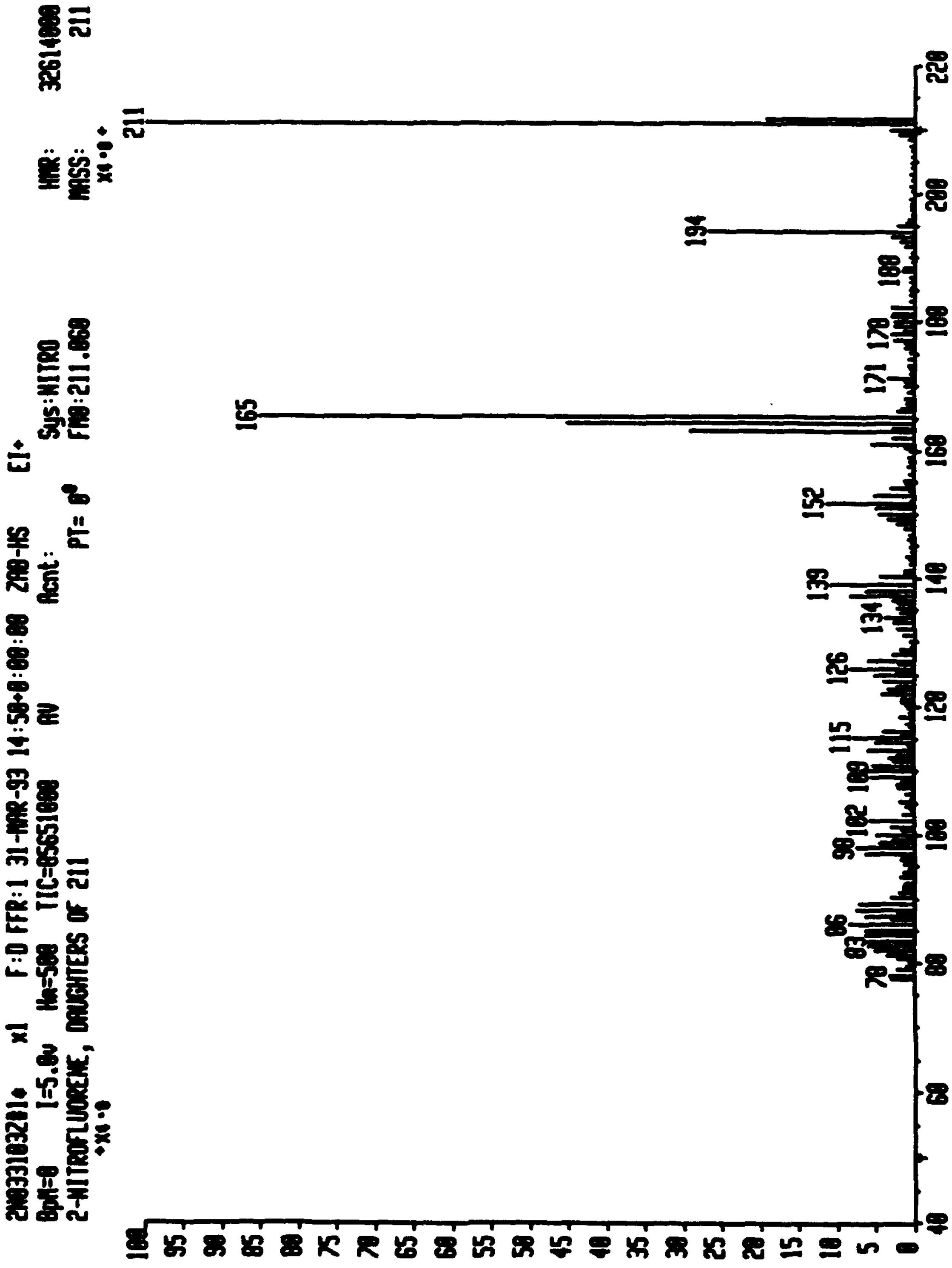
2N0331032B1+ x1 F:D FFR:1 31-MAR-93 14:58+0:00:00 ZAB-HS EI+
BpM=0 I=5.0v Hm=500 TIC=05651008 AV
Acnt:
Sys:NITRO
HMR: 32614000
2-NITROFLUORENE, DAUGHTERS OF 211
PT= 0°
FMB:211.060
MASS: 211
+X4.0
X4.0+
211
194
180
178
171
165
152
139
134
126
115
109
102
98
86
83
78
100
95
90
85
80
75
70
65
60
55
50
45
40
35
30
25
20
15
10
5
0
40
60
80
100
120
140
160
180
200
220

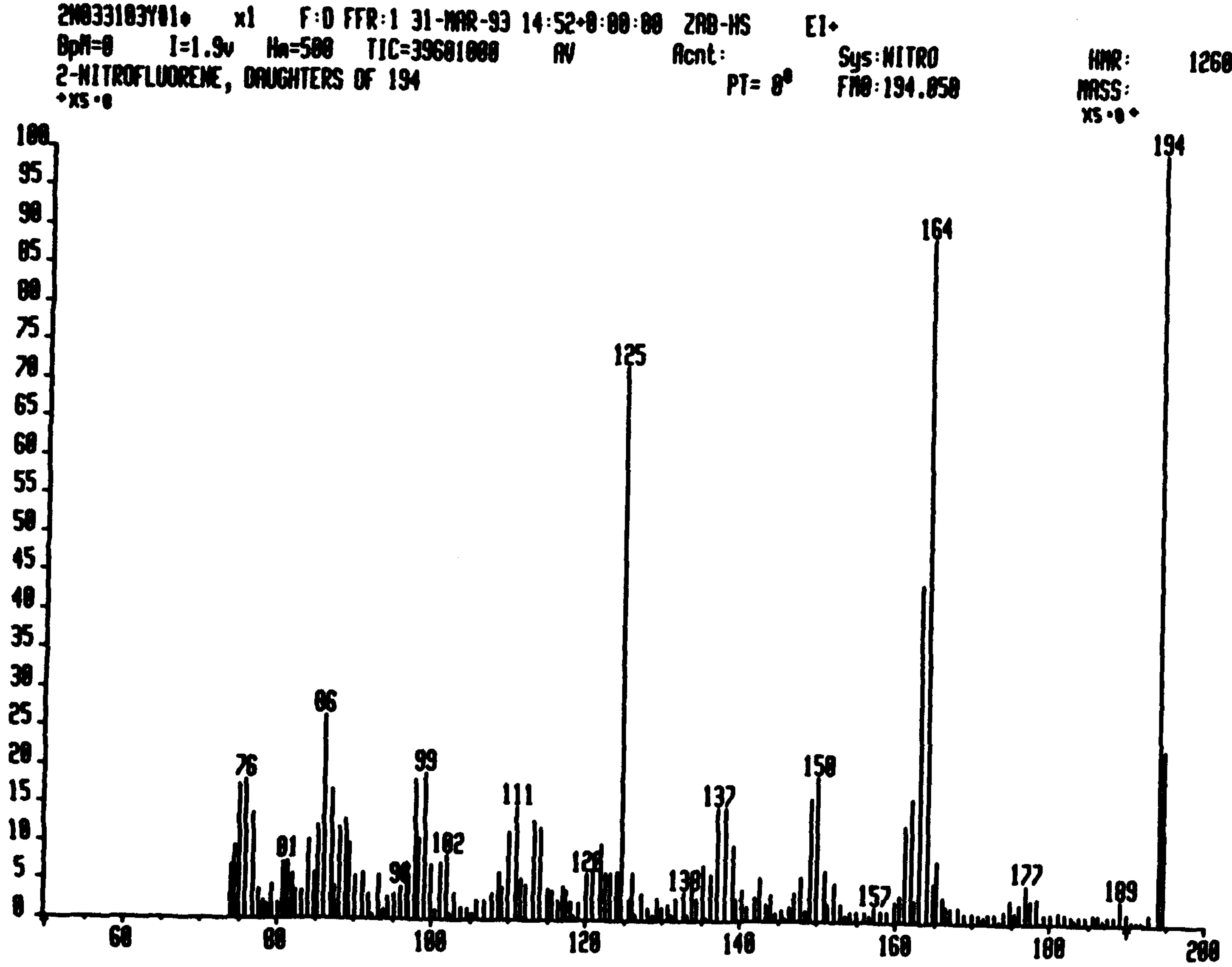
2M033103Y01+ x1 F:0 FFR:1 31-MAR-93 14:52+0:00:00 ZAB-HS EI+
BpM=0 I=1.9v Hm=500 TIC=39601000 AV Acnt: Sys:NITRO HMR: 12609000
2-NITROFLUORENE, DAUGHTERS OF 194 PT= 0° FM0:194.050 MASS: 194
+xS·0
xS·0+
100
95
90
85
80
75
70
65
60
55
50
45
40
35
30
25
20
15
10
5
0
60
80
100
120
140
160
180
200
76
81
86
96
99
102
111
125
137
150
157
164
177
189
194

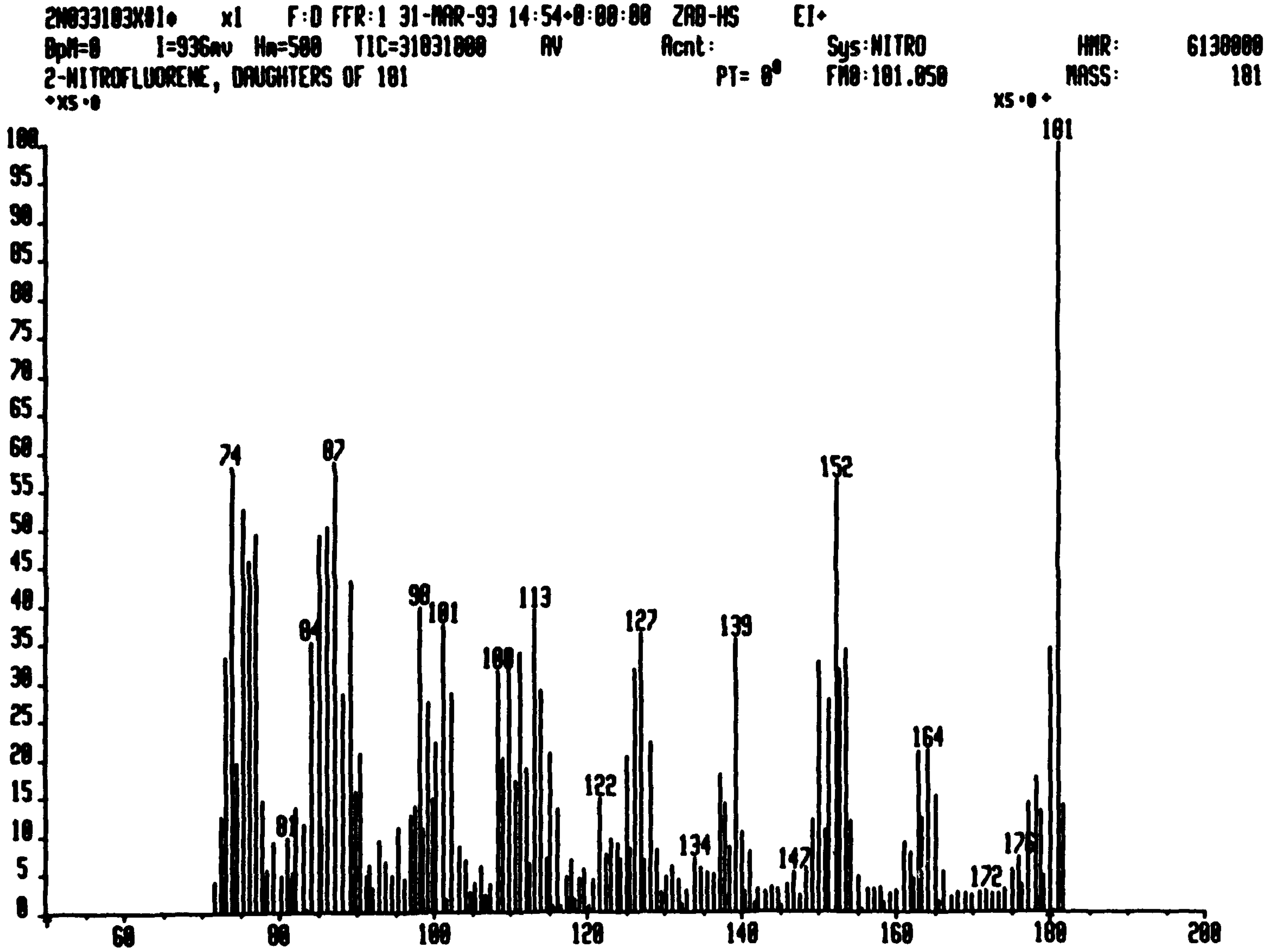
2N033103X01+ x1 F:D FFR:1 31-MAR-93 14:54+0:00:00 ZAB-HS EI+
BpM=0 I=936mv Hm=500 TIC=31031000 AV Acnt: Sys:NITRO HMR: 6130000
2-NITROFLUORENE, DAUGHTERS OF 181 PT= 0° FM0:181.050 MASS: 181
*X5.0
X5.0*
100
95
90
85
80
75
70
65
60
55
50
45
40
35
30
25
20
15
10
5
0
60
80
100
120
140
160
180
200
74
87
84
81
98
101
108
113
122
127
134
139
147
152
164
172
176
181

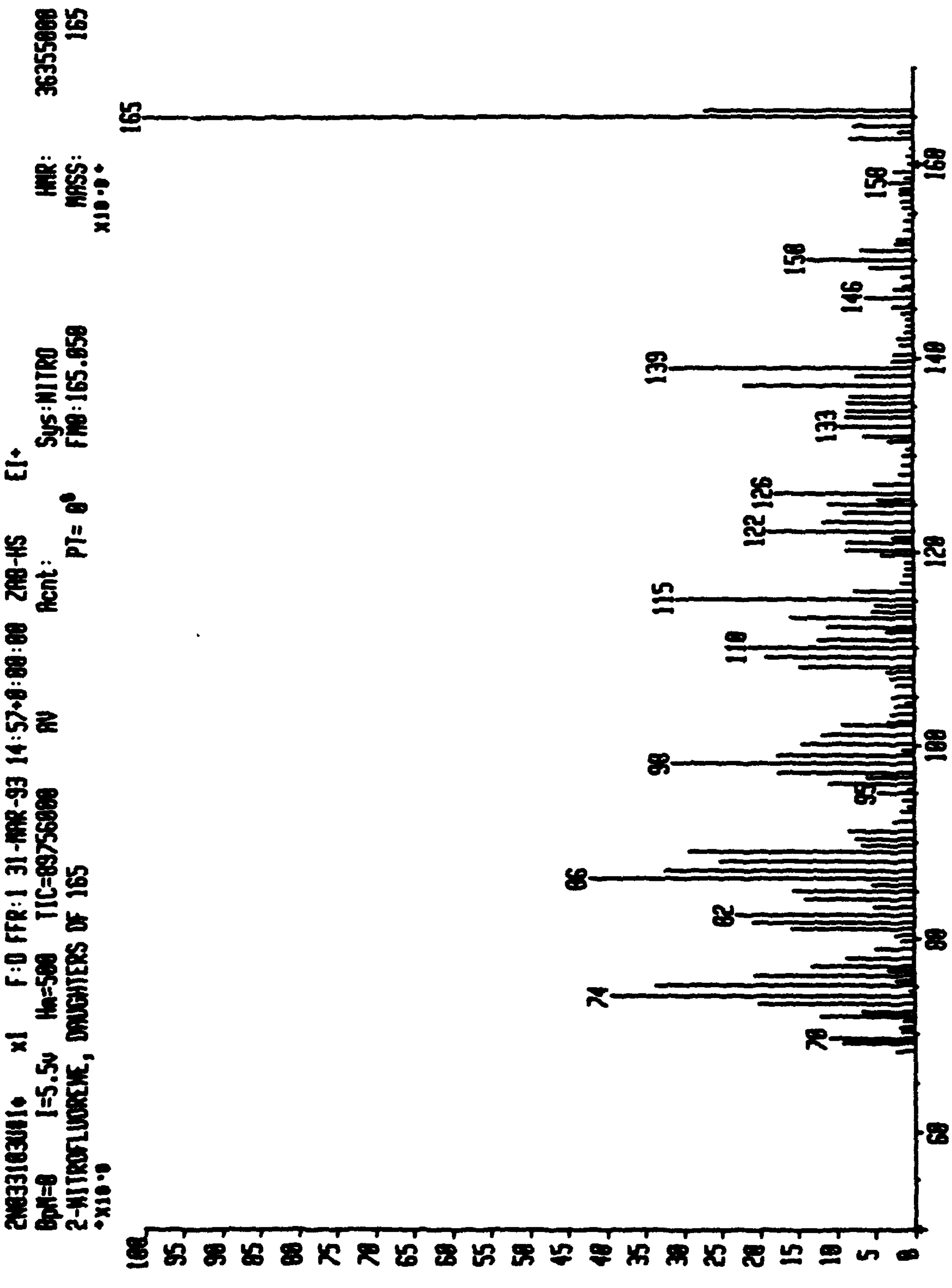
2NB331B3U01+ x1 F:D FFR:1 31-MAR-93 14:57+0:00:00 ZAB-HS EI+
BpM=0 I=5.5v Hm=500 TIC=89756000 AV Acnt: Sys:NITRO
2-NITROFLUORENE, DAUGHTERS OF 165 PT= 0° FM0:165.050
*X10*0
HMR: 36355000
MASS: 165
X10*0*
165
139
115
98
86
74
82
110
122
126
133
146
150
158
70
95
60
80
100
120
140
160
100
95
90
85
80
75
70
65
60
55
50
45
40
35
30
25
20
15
10
5
0

```
2N033103V01+     x1     F:0 FFR:1 31-MAR-93 14:50+0:00:00  ZAB-HS      EI+
BpM=0      I=1.4v   Hm=500   TIC=35590000      AV          Acnt:           Sys:NITRO             HMR:       9470000
2-NITROFLUORENE, DAUGHTERS OF 153                          PT= 0°    FM0:153.050           MASS:          153
+XS•0                                                                                   XS•0+
```

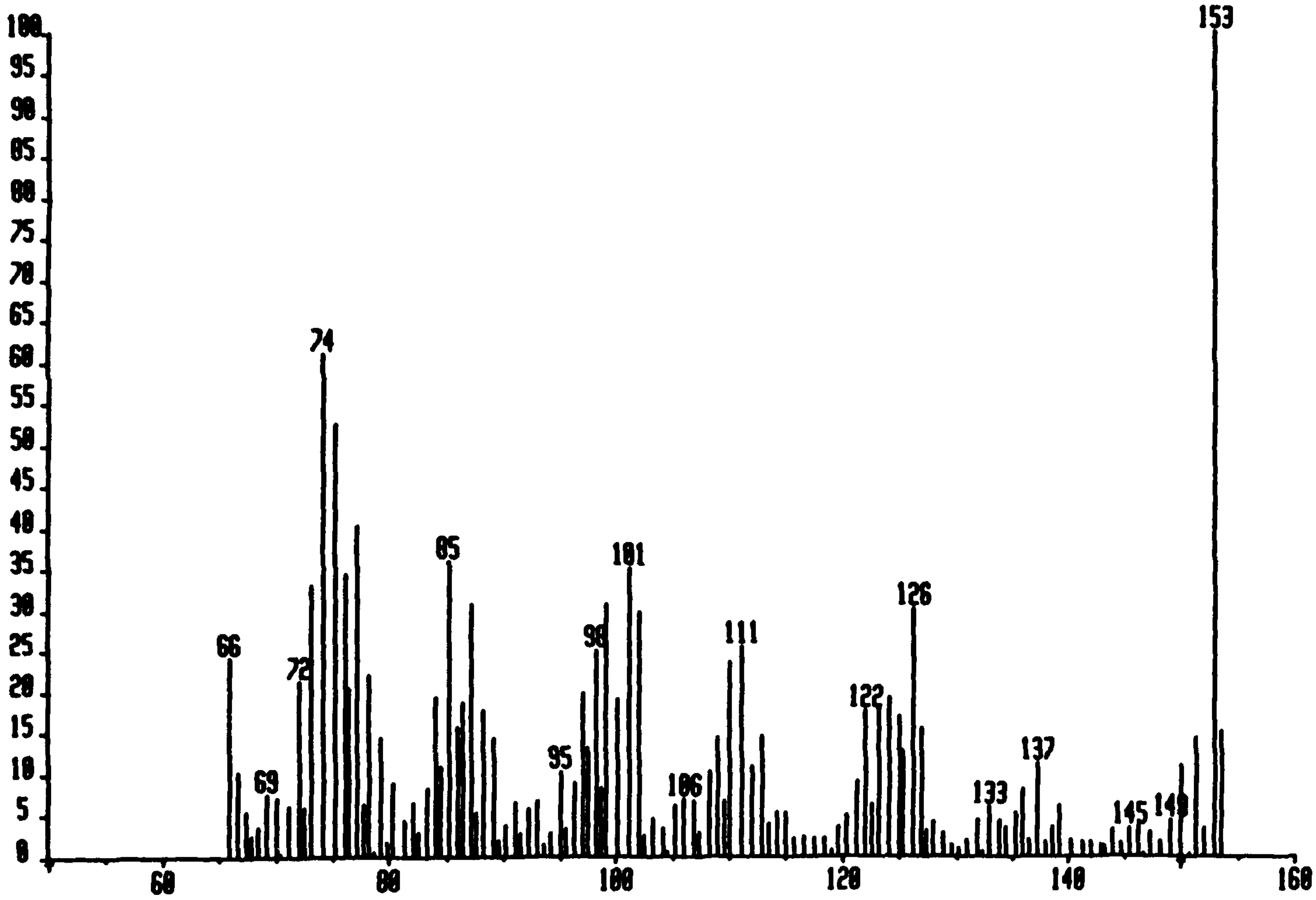

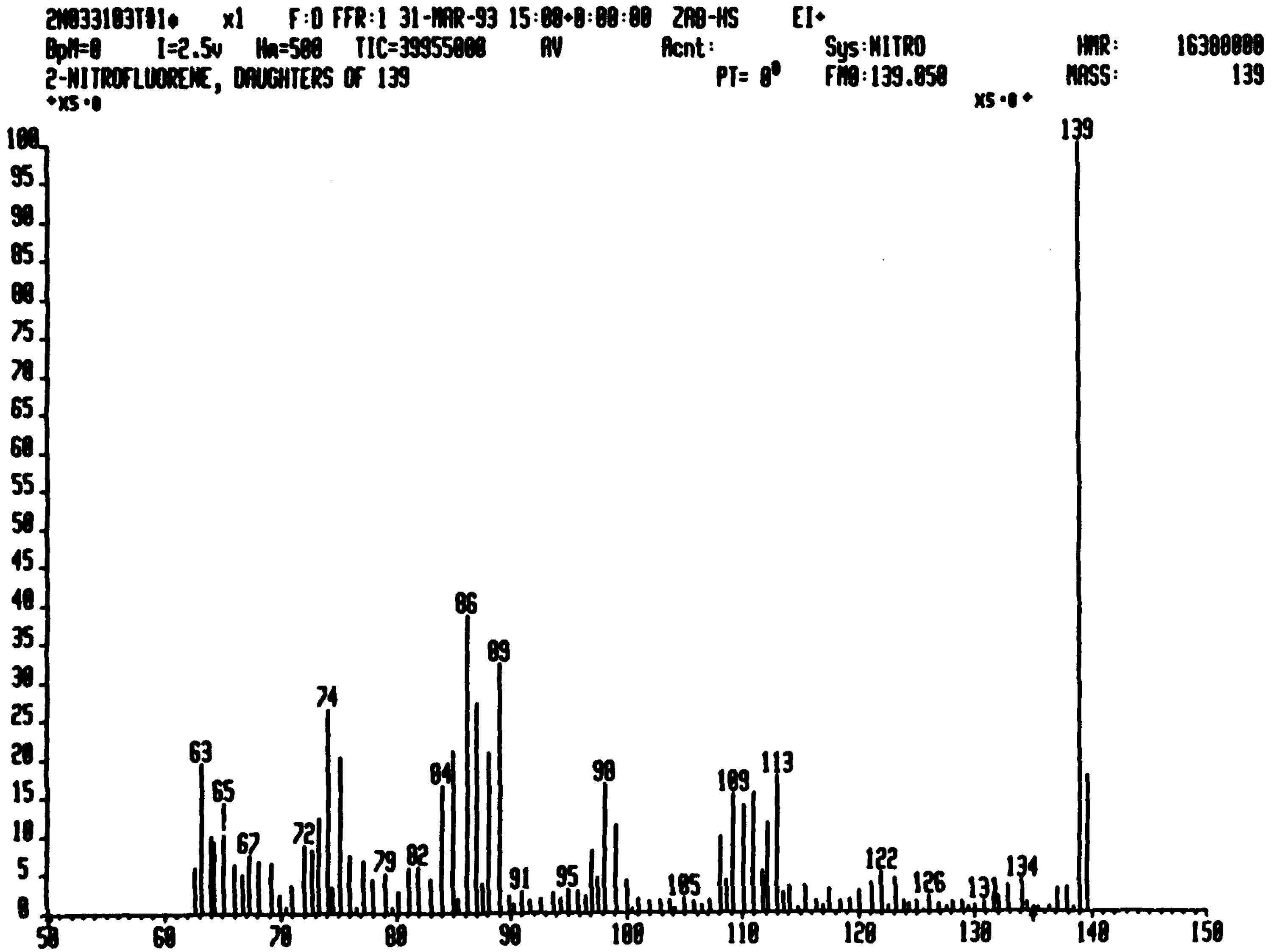

```
2N033103T01♦    x1    F:D FFR:1 31-MAR-93 15:00+0:00:00  ZAB-HS     EI+
BpM=0    I=2.5v   Hm=500   TIC=39955000    AV        Acnt:          Sys:NITRO          HMR:      16300000
2-NITROFLUORENE, DAUGHTERS OF 139                    PT= 0°    FM0:139.050        MASS:          139
*XS•0                                                                  XS•0*
```

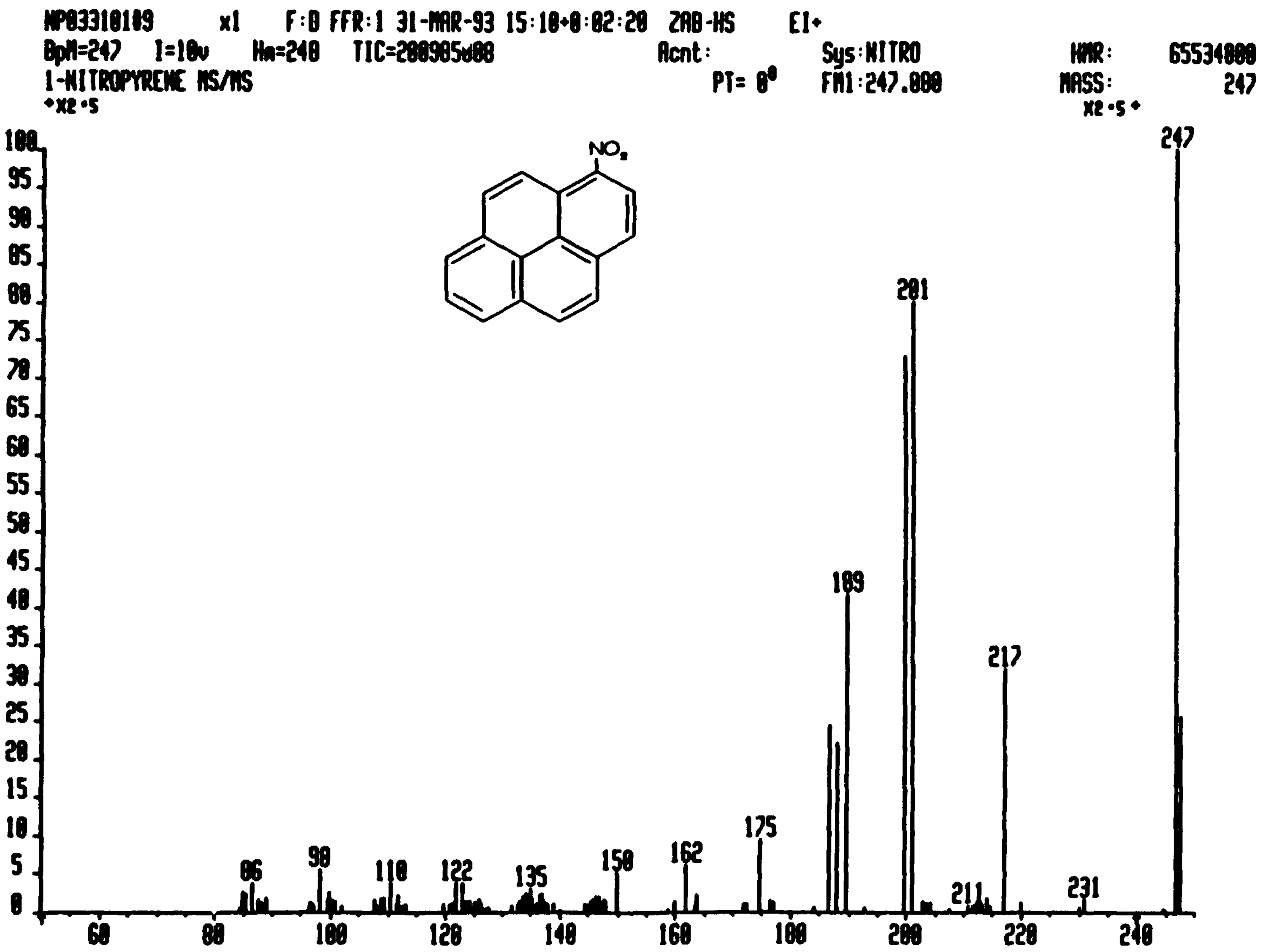
NP03310109 x1 F:0 FFR:1 31-MAR-93 15:10+0:02:20 ZAB-HS EI+
BpM=247 I=10v Hm=240 TIC=200985u00 Acnt: Sys:NITRO HMR: 65534000
1-NITROPYRENE MS/MS PT= 0° FM1:247.000 MASS: 247
*X2·5
X2·5*
NO2
247
201
189
217
175
162
150
135
122
110
98
86
211
231
100
95
90
85
80
75
70
65
60
55
50
45
40
35
30
25
20
15
10
5
0
60
80
100
120
140
160
180
200
220
240

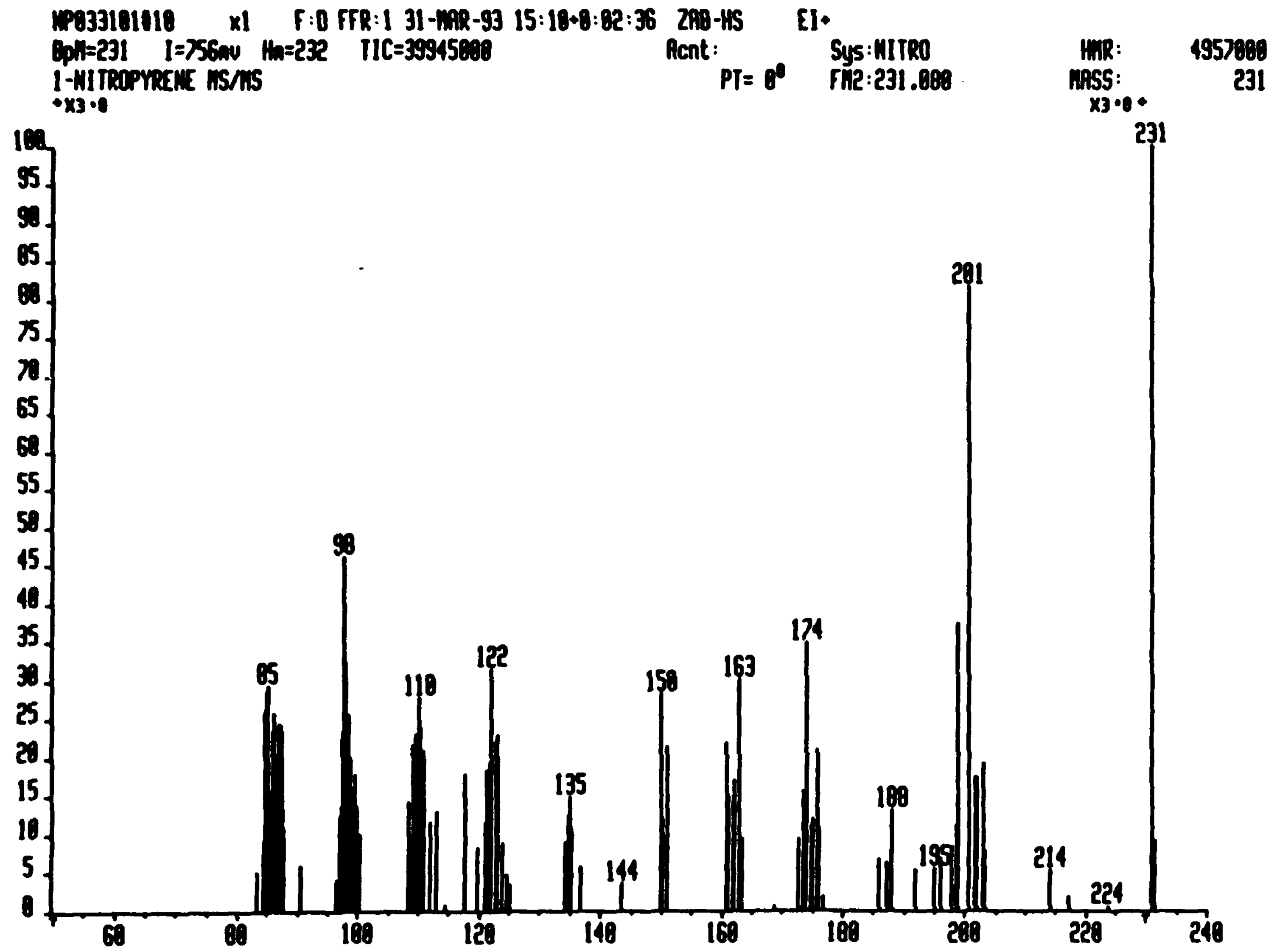
MP033101010 x1 F:0 FFR:1 31-MAR-93 15:10+0:02:36 ZAB-HS EI+
BpM=231 I=756mv Hm=232 TIC=39945000 Acnt: Sys:NITRO HMR: 4957000
1-NITROPYRENE MS/MS PT= 0° FM2:231.000 MASS: 231
*X3*0
X3*0*
100
95
90
85
80
75
70
65
60
55
50
45
40
35
30
25
20
15
10
5
0
60
80
100
120
140
160
180
200
220
240
85
98
110
122
135
144
150
163
174
188
195
201
214
224
231

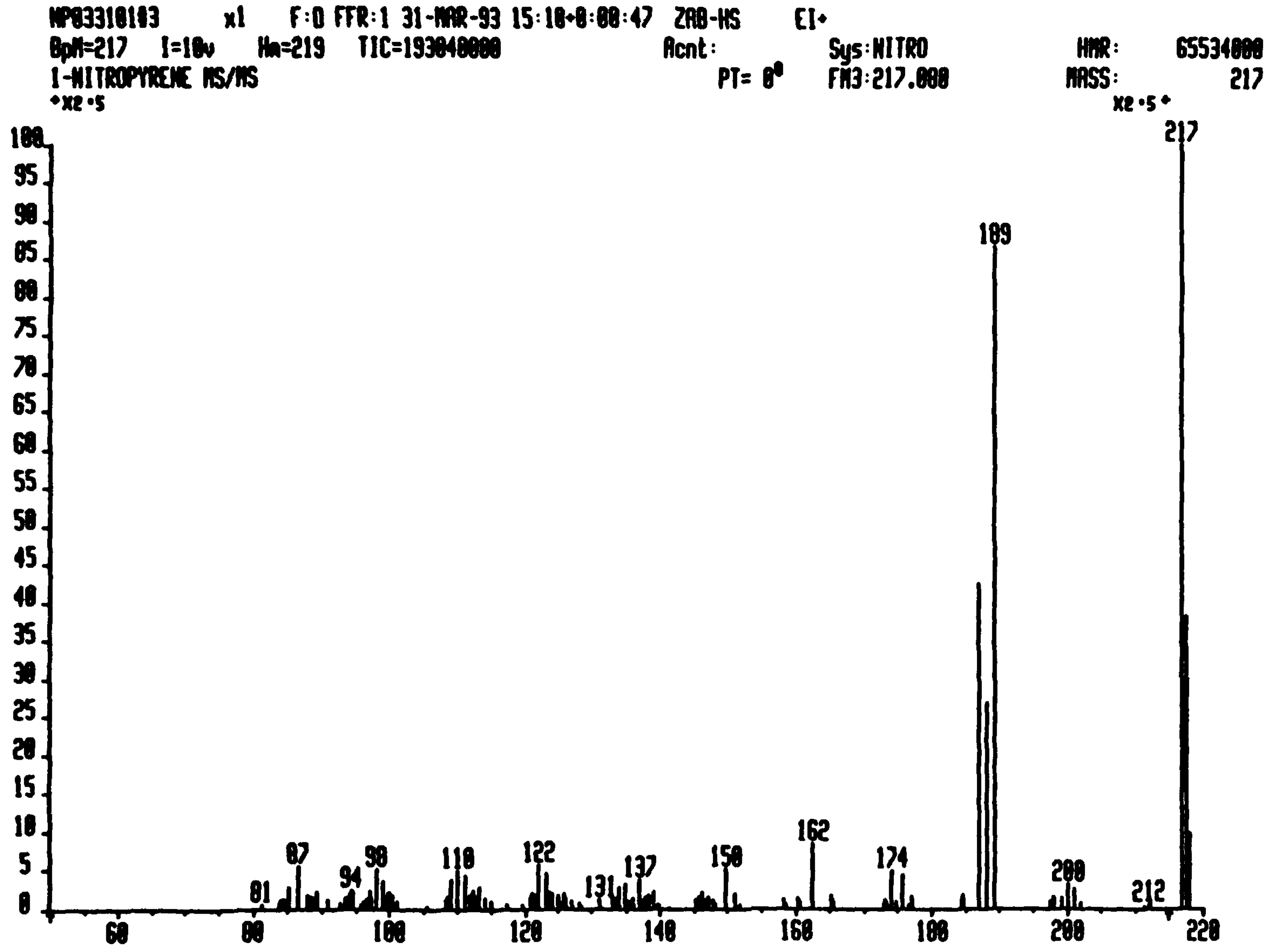
NP03310103 x1 F:0 FFR:1 31-MAR-93 15:10+0:00:47 ZAB-HS EI+
BpM=217 I=10v Hm=219 TIC=193040000 Acnt: Sys:NITRO HMR: 65534000
1-NITROPYRENE MS/MS PT= 0° FM3:217.000 MASS: 217
*x2.5
x2.5*
100
95
90
85
80
75
70
65
60
55
50
45
40
35
30
25
20
15
10
5
0
60
80
100
120
140
160
180
200
220
81
87
94
98
110
122
131
137
150
162
174
189
200
212
217

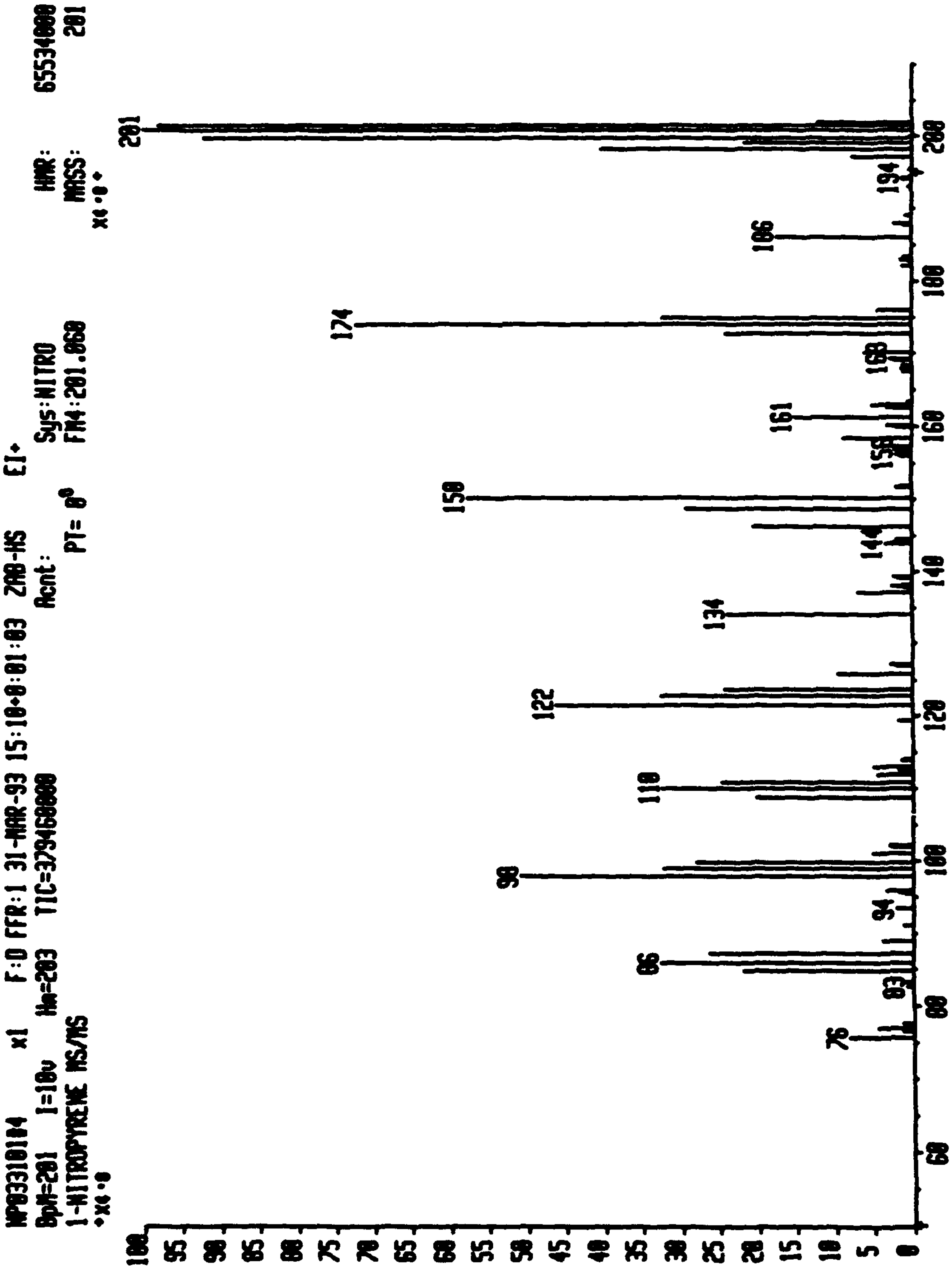
NPB3310104 x1 F:D FFR:1 31-MAR-93 15:10+0:01:03 ZAB-HS EI+
BpM=201 I=10v Hm=203 TIC=379460000 Acnt: Sys:NITRO
1-NITROPYRENE MS/MS PT= 0° FM4:201.060
•x4•0
HMR: 65534000
MASS: 201
x4•0•
201
194
186
174
168
161
158
150
144
134
122
110
98
94
86
83
76
60
80
100
120
140
160
180
200
100
95
90
85
80
75
70
65
60
55
50
45
40
35
30
25
20
15
10
5
0

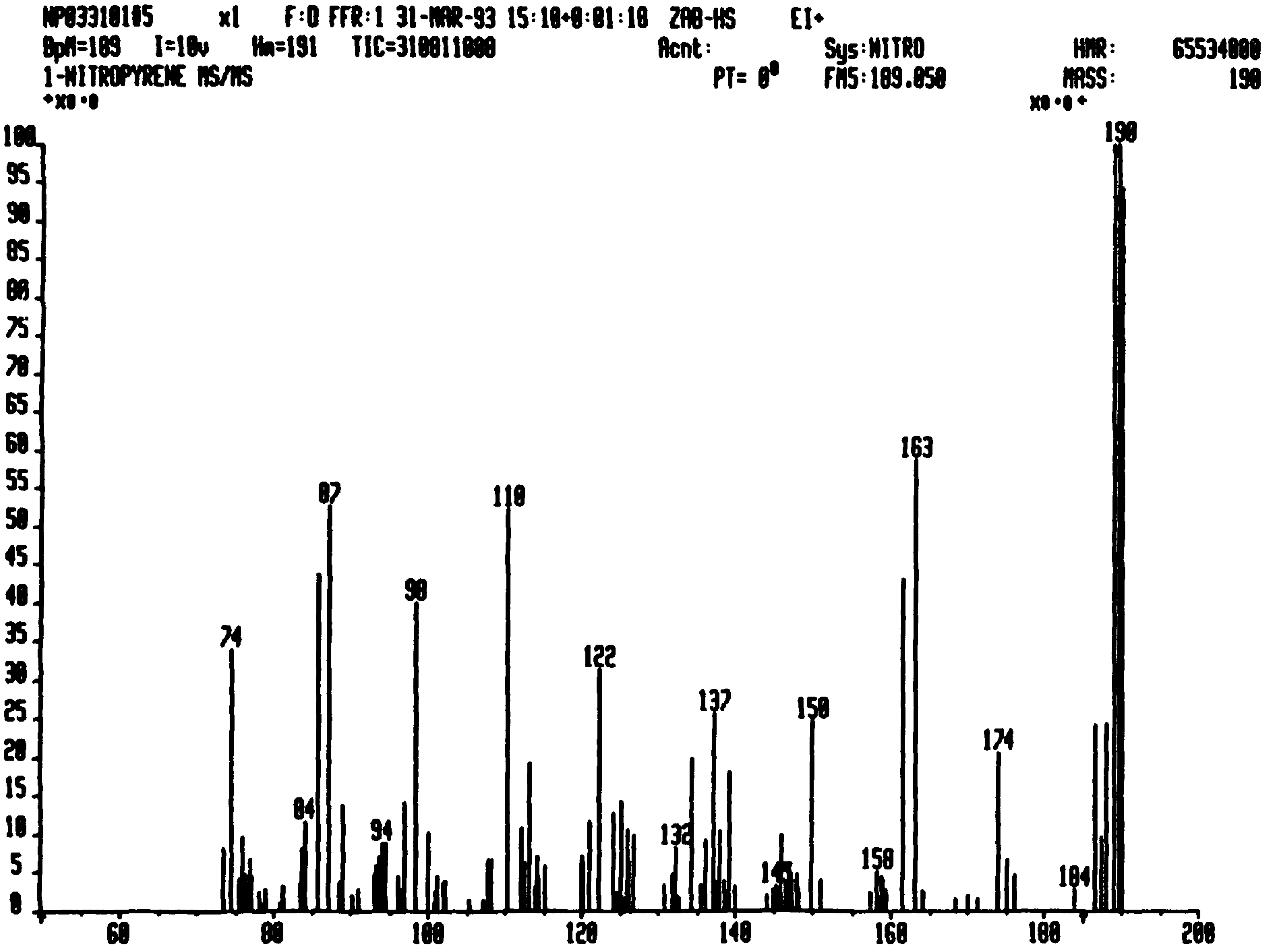
NP03310105 x1 F:D FFR:1 31-MAR-93 15:10+0:01:10 ZAB-HS EI+
BpM=189 I=10v Hm=191 TIC=310011000 Acnt: Sys:NITRO HMR: 65534000
1-NITROPYRENE MS/MS PT= 0° FMS:189.050 MASS: 190
*x0·0
x0·0*
190
163
87
110
98
74
122
137
150
174
84
94
132
145
158
184
100
95
90
85
80
75
70
65
60
55
50
45
40
35
30
25
20
15
10
5
0
60
80
100
120
140
160
180
200

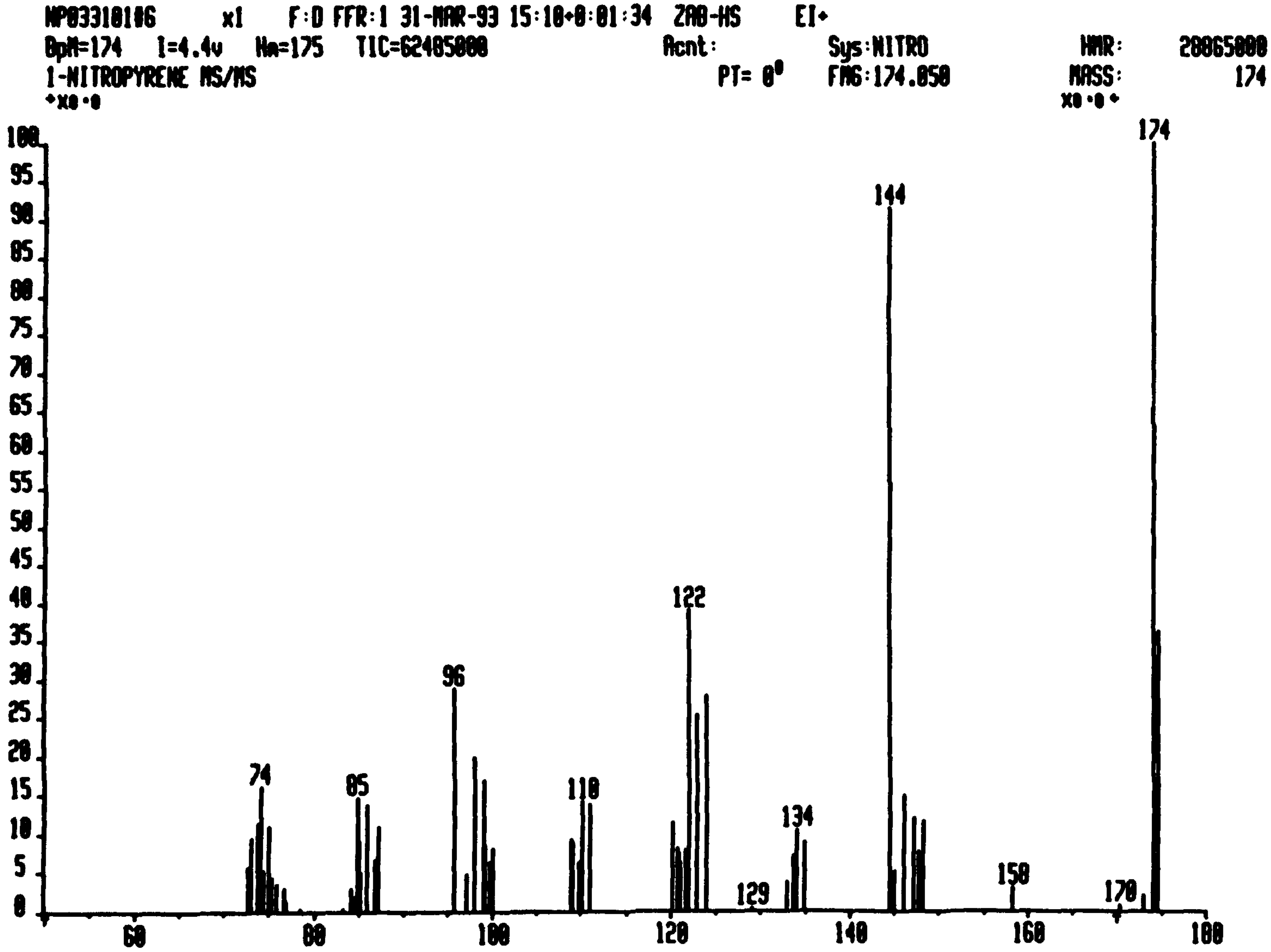
NP03310106 x1 F:D FFR:1 31-MAR-93 15:10+0:01:34 ZAB-HS EI+
BpM=174 I=4.4v Hm=175 TIC=62405000 Acnt: Sys:NITRO HMR: 20065000
1-NITROPYRENE MS/MS PT= 0⁰ FMG:174.050 MASS: 174
+x0·0
x0·0+
174
144
122
96
74
85
110
134
129
158
170
100
95
90
85
80
75
70
65
60
55
50
45
40
35
30
25
20
15
10
5
0
60
80
100
120
140
160
180

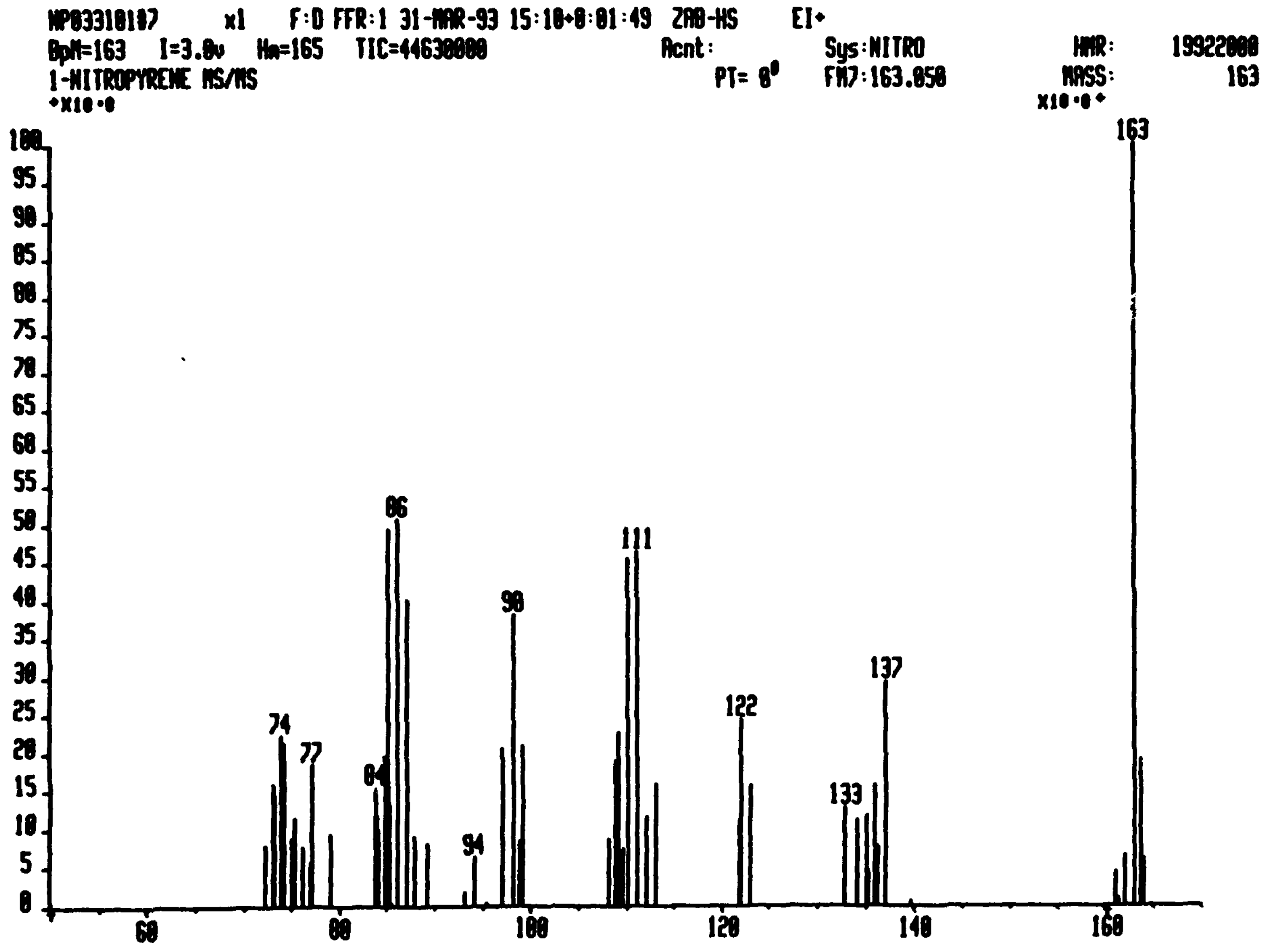
NP03310187 x1 F:D FFR:1 31-MAR-93 15:10+0:01:49 ZAB-HS EI+
BpM=163 I=3.0v Hm=165 TIC=44630000 Acnt: Sys:NITRO HMR: 19922000
1-NITROPYRENE MS/MS PT= 0° FM7:163.058 MASS: 163
*X10·0
X10·0*
100
95
90
85
80
75
70
65
60
55
50
45
40
35
30
25
20
15
10
5
0
60
80
100
120
140
160
74
77
84
86
94
98
111
122
133
137
163

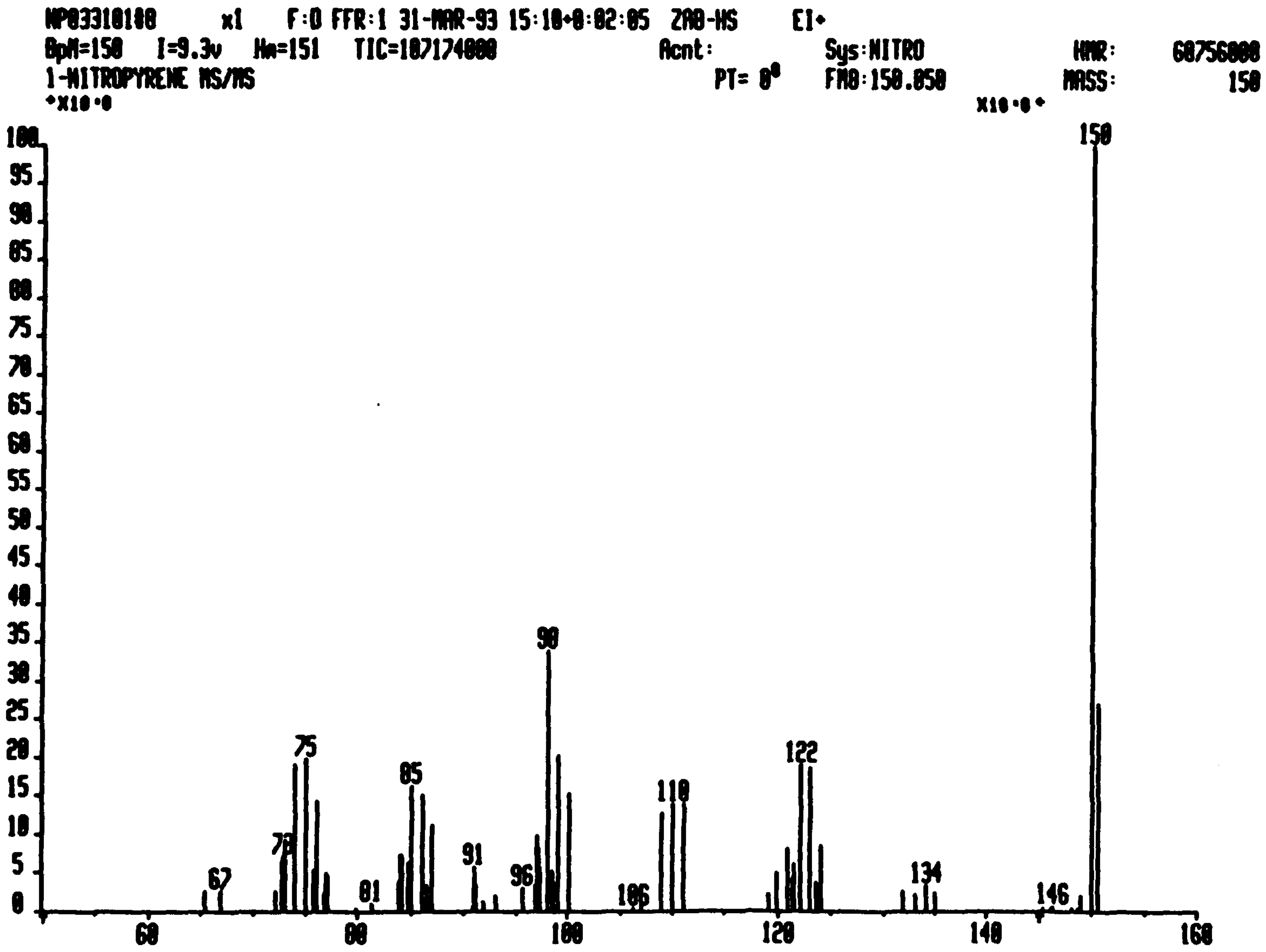
NP03310100 x1 F:0 FFR:1 31-MAR-93 15:10+0:02:05 ZAB-HS EI+
BpM=150 I=9.3v Hm=151 TIC=107174000 Acnt: Sys:NITRO HMR: 68756000
1-NITROPYRENE MS/MS PT= 0⁰ FMB:150.050 MASS: 150
*X10·0
X10·0*
100
95
90
85
80
75
70
65
60
55
50
45
40
35
30
25
20
15
10
5
0
150
98
75
122
85
110
70
91
96
134
67
81
106
146
60
80
100
120
140
160